Oxidative Medicine and Cellular Longevity

Interplay of Oxidative Stress, Inflammation, and Autophagy: Their Role in Tissue Injury of Heart, Liver, and Kidney

Lead Guest Editor: Partha Mukhopadhyay
Guest Editors: Nabil A. S. Eid, Mohamed A. Abdelmegeed, and Aditya Sen

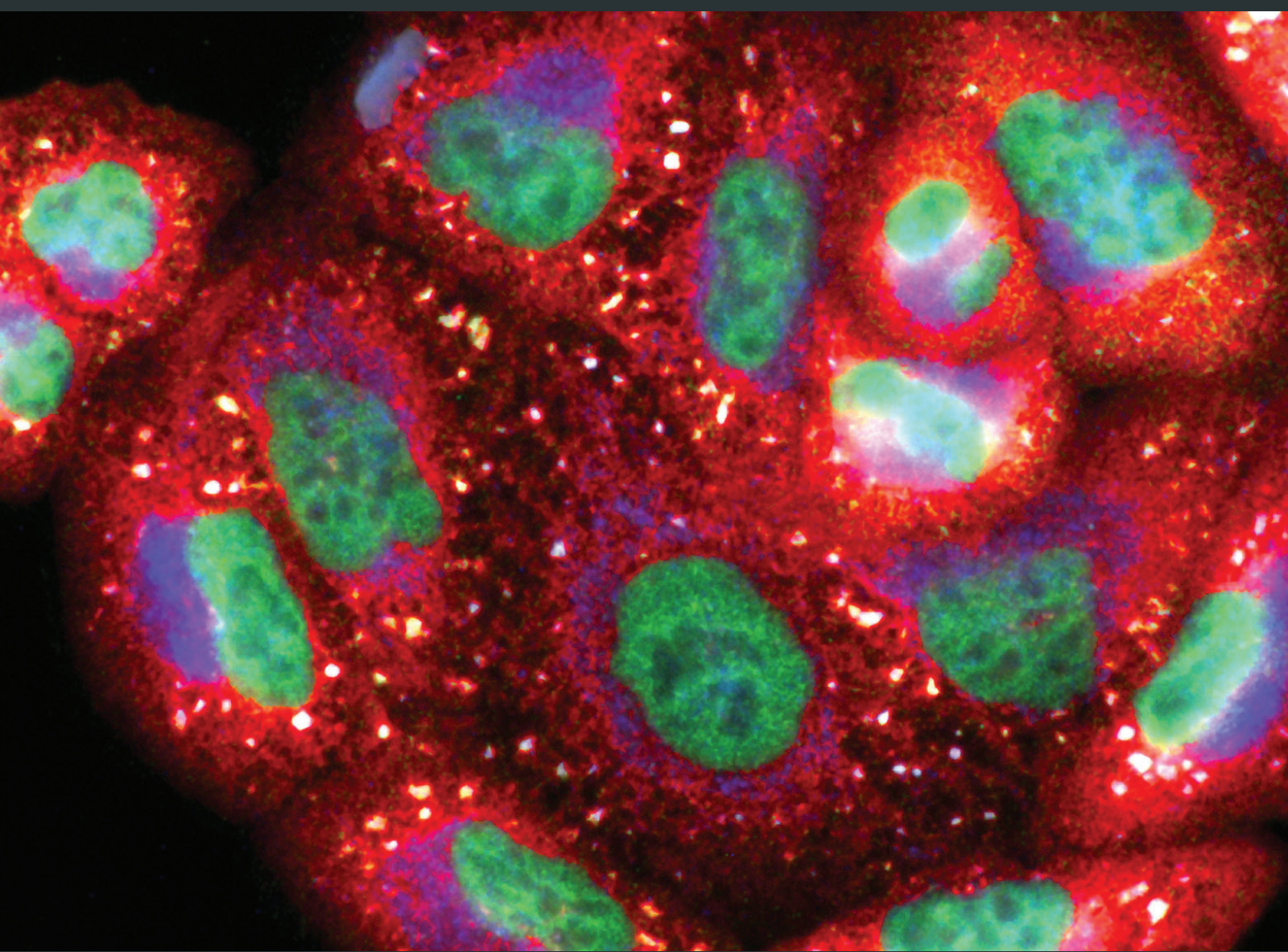

Interplay of Oxidative Stress, Inflammation, and Autophagy: Their Role in Tissue Injury of Heart, Liver, and Kidney

Oxidative Medicine and Cellular Longevity

Interplay of Oxidative Stress, Inflammation, and Autophagy: Their Role in Tissue Injury of Heart, Liver, and Kidney

Lead Guest Editor: Partha Mukhopadhyay
Guest Editors: Nabil A. S. Eid, Mohamed A. Abdelmegeed, and Aditya Sen

Editorial Board

Contents

Hindawi
Oxidative Medicine and Cellular Longevity
Volume 2018, Article ID 2090813, 3 pages
https://doi.org/10.1155/2018/2090813

Editorial

Interplay of Oxidative Stress, Inflammation, and Autophagy: Their Role in Tissue Injury of the Heart, Liver, and Kidney

Partha Mukhopadhyay,[1] **Nabil Eid**,[2] **Mohamed A. Abdelmegeed**,[3] **and Aditya Sen**[4]

[1]*Laboratory of Cardiovascular Physiology and Tissue Injury, NIAAA, National Institutes of Health, Bethesda, MD 20852, USA*
[2]*Division of Life Sciences, Department of Anatomy and Cell Biology, Osaka Medical College, Takatsuki, Osaka 569-8686, Japan*
[3]*Section of Molecular Pharmacology and Toxicology, Laboratory of Membrane Biochemistry and Biophysics, National Institute on Alcohol Abuse and Alcoholism, Bethesda, MD, USA*
[4]*Department of Biochemistry and Molecular Biology, Uniformed Services University, Bethesda, MD 20814, USA*

Correspondence should be addressed to Partha Mukhopadhyay; mpartha@mail.nih.gov
and Mohamed A. Abdelmegeed; abdelmegeedm@mail.nih.gov

Received 5 February 2018; Accepted 5 February 2018; Published 22 March 2018

Oxidative/nitrosative stress, inflammation, and autophagy roles have been described in many studies as prominent factors in mediating many pathological alterations, in response to toxic agents or in disease states [1]; however, it is not well characterized whether there is an interplay between these three factors or any combination of them, in addition to their sole effect, in mediating the harmful mechanisms of pathological alterations particularly in the heart, liver, and kidney. These harmful mechanisms might be identified directly via exposure to various insults or indirectly via evaluating the mechanism(s) of the prevention of these pathological alterations or by both methods. It was our intention in this special issue to invite new insights and to shed a light on this very interesting topic that would encourage scientists to identify new therapeutic targets for various diseases, in the context of oxidative stress, inflammation, and autophagy, and to tackle them in hope of developing better treatments.

It is well established that there is a balance between reactive oxygen and nitrogen species (ROS and RNS, resp.) production and removal in the body under normal physiological conditions and that basal low levels of ROS/RNS is vital for cell signaling and cell survival [2]. However, upon exposure to chemicals or toxic agents such as alcohol, acetaminophen, and cisplatin, or under disease state such as diabetes, cancer, inflammatory diseases, and ischemia reperfusion, to name a few, ROS/RNS may be produced in excessive amounts, beyond the antioxidant cell defense capacity, from many sources within the cell such as cytochromes P450 2E1 and 4A, nicotinamide adenine dinucleotide phosphate-oxidase (NADPH oxidase), xanthine oxidase, and mitochondrial electron transport chain [3–5]. ROS/RNS can also be produced in response to inflammation and immune cell activation [6]. The increased levels of ROS/RNS may induce their deleterious effects in the cells by damaging and/or modifying proteins, DNA, lipids, and vitamins, contributing to disturbance of their normal functions, which might be essential for cell survival, leading to the development and/or progression of tissue injury.

Although oxidative stress might be induced by inflammation, inflammation is also one of the most common outcomes of oxidative stress. It has been suggested that increased oxidative stress levels might stimulate the expression of chemokines and cytokines leading to increased inflammation [7]. As with oxidative stress, inflammation is also part of the host defense mechanism and might be important for maintain vital functions; however, excessive inflammation might cause cellular damage and/or death.

Autophagy is an essential process for normal cell homeostasis. Many forms of autophagy have been identified such as macroautophagy, microautophagy, and chaperone-mediated autophagy. Autophagy is being considered as one of the cellular defense against increased oxidative stress as well as

other diverse cell stress conditions [8]. Intriguingly, autophagy has been reported to regulate oxidative stress and inflammation signaling and formation [9].

Thus, it seems that there might be an interplay between oxidative stress, inflammation, and autophagy and that unchecked oxidative stress, unresolved inflammation, and disturbed autophagy are common features in many diseases, upon exposure to toxic chemicals, and even exposure to unhealthy dietary habits. The use of antioxidant and anti-inflammatory whether naturals or chemicals, particularly naturals, might be an easy and effective method to prevent disease development and/or progression, as these agents might consequently prevent disruption of autophagy process.

The articles included in this special issue review addressed many of the goals of this issue as they provide better understanding in some of the underlying mechanisms of some of the important pathological changes that occur during tissue injury upon exposure to injurious insults as well as providing some potential preventive and/or therapeutic approaches to prevent tissue injury, particularly by natural compounds. There are two articles involving the beneficial effects of baicalin, which is a main bioactive component of *Scutellaria baicalensis* Georgi (*S. baicalensis*), used as a traditional Chinese herbal medicine, and has been recently a focus of many studies due to its seemingly beneficial effects. The first article, by using in vivo and in vitro models, suggested that baicalin ameliorates biliary duct ligation-induced experimental liver fibrosis alleviating inflammation, oxidative stress, and apoptosis. Another study reported that baicalin attenuated subarachnoid hemorrhage in mice via decreasing inflammation (inhibited microglial activation), oxidative damage, and brain edema. Apigenin, an abundant dietary flavonoid that can be found in many fruits and vegetables, was reported by one of the articles to alleviate myocardial toxicity in a mouse model induced by endotoxin via the modulation of oxidative stress, inflammation, and autophagy. Daidzein, another naturally occurring compound belong to isoflavones that can be found in soybeans and other legumes, by using both in vivo and in vitro models, was shown to improve kidney regeneration in a cisplatin-induced nephrotoxicity model through decreased levels of nitroxidative stress, inflammation, and apoptosis. In another article related to heart diseases, ischemia preconditioning was suggested to alleviate cardiac infarction via the increased expression of immediate early response gene (IEX-1), which might decrease cardiac apoptosis and necrosis via decreased intracellular ROS accumulation. Rhodiola sacra, a genotype of Rhodiola species, a famous genus of Chinese medicinal herb, when combined with exercise was shown by one of the articles of this issue to enhance mitochondrial quality control leading to improvement of exercise capacity and decrease exhaustive exercise-induced skeletal and cardiac muscle damage. Another article suggested a potentially protective role of granulocyte colony-stimulating factor (G-CSF) against neonatal brain suffering from bacteria-induced meningitis, possibly via a selective therapeutic action site of G-CSF through epigenetic histone modification particularly in the *TNFA* gene promotor. There was also an article suggesting a protective role of exogenous hydrogen sulfide against the development of acute kidney injury in response to LPS via the inhibition of inflammation and oxidative stress in a mouse model and blood samples from patients. An interesting study reported that bone marrow-derived mesenchymal stem cells (BMSCs) may have a therapeutic potential against sepsis by increasing Parkin-related mitophagy and decreasing mitochondrial oxidative stress leading to restriction of inflammasome activation in macrophages in a cecal ligation and puncture (CLP) mouse model. This might be a crucial mechanism for MSCs to combat sepsis in various models. Finally, the last article presented the development of cardiac autonomic neuropathy (CAN) and the early signaling changes in the myocardium as early consequences of mild metabolic challenge without significant changes on gross cardiac structure/function and the absence of signs of diabetes or impaired glucose tolerance. They also highlighted a potential corrective role for metformin and pioglitazone, which are not related to their blood glucose lowering effect and evaluated the effect of dietary interventions after a period of high caloric diet.

Taken together, we believe that these contributions advance the current knowledge about the pathophysiology of tissue injury with emphasis on the role of oxidative stress, inflammation, and autophagy and thus might help developing novel pharmacotherapeutic strategies for disease control and management.

Finally, we would like to thank all the contributors to this special issue for their participation and interest and many others who submitted but we could not accommodate.

Partha Mukhopadhyay
Nabil Eid
Mohamed A. Abdelmegeed
Aditya Sen

References

[1] K. F. Ayoub, N. V. K. Pothineni, J. Rutland, Z. Ding, and J. L. Mehta, "Immunity, inflammation, and oxidative stress in heart failure: emerging molecular targets," *Cardiovascular Drugs and Therapy*, vol. 31, no. 5-6, pp. 593–608, 2017.

[2] R. B. Hamanaka and N. S. Chandel, "Mitochondrial reactive oxygen species regulate cellular signaling and dictate biological outcomes," *Trends in Biochemical Sciences*, vol. 35, no. 9, pp. 505–513, 2010.

[3] M. A. Abdelmegeed and B. J. Song, "Functional roles of protein nitration in acute and chronic liver diseases," *Oxidative Medicine and Cellular Longevity*, vol. 2014, Article ID 149627, 21 pages, 2014.

[4] P. Mukhopadhyay, B. Horvath, M. Rajesh et al., "PARP inhibition protects against alcoholic and non-alcoholic steatohepatitis," *Journal of Hepatology*, vol. 66, no. 3, pp. 589–600, 2017.

[5] P. Mukhopadhyay, B. Horvath, Z. Zsengeller et al., "Mitochondrial-targeted antioxidants represent a promising approach for prevention of cisplatin-induced nephropathy," *Free Radical Biology & Medicine*, vol. 52, no. 2, pp. 497–506, 2012.

[6] M. B. Hampton, A. J. Kettle, and C. C. Winterbourn, "Inside the neutrophil phagosome: oxidants, myeloperoxidase, and bacterial killing," *Blood*, vol. 92, no. 9, pp. 3007–3017, 1998.

[7] S. Reuter, S. C. Gupta, M. M. Chaturvedi, and B. B. Aggarwal, "Oxidative stress, inflammation, and cancer: how are they linked?," *Free Radical Biology & Medicine*, vol. 49, no. 11, pp. 1603–1616, 2010.

[8] S. A. Tooze, H. C. Dooley, H. B. J. Jefferies et al., "Assessing mammalian autophagy," *Methods in Molecular Biology*, vol. 1270, pp. 155–165, 2015.

[9] A. Sureshbabu, S. W. Ryter, and M. E. Choi, "Oxidative stress and autophagy: crucial modulators of kidney injury," *Redox Biology*, vol. 4, pp. 208–214, 2015.

Hindawi
Oxidative Medicine and Cellular Longevity
Volume 2018, Article ID 3537609, 15 pages
https://doi.org/10.1155/2018/3537609

Research Article

A Novel Mechanism of Mesenchymal Stromal Cell-Mediated Protection against Sepsis: Restricting Inflammasome Activation in Macrophages by Increasing Mitophagy and Decreasing Mitochondrial ROS

Shuang Li,[1,2] Hao Wu,[3] Dong Han,[4] Sai Ma,[4] Wensi Fan,[4] Yabin Wang,[1] Ran Zhang,[1] Miaomiao Fan,[4] Yuesheng Huang,[5] Xiaobing Fu,[1] and Feng Cao[1]

[1]*Department of Cardiology & National Clinical Research Center of Geriatrics Disease, Chinese PLA General Hospital, Beijing 100853, China*
[2]*Department of Cardiology, Chengdu Military General Hospital, Chengdu 610083, China*
[3]*Department of Toxicology, School of Public Health, Fourth Military Medical University, Xi'an, Shaanxi 710032, China*
[4]*Department of Cardiology, Xijing Hospital, Fourth Military Medical University, Xi'an, Shaanxi 710032, China*
[5]*Institute of Burn Research, State Key Laboratory of Trauma, Burn and Combined Injury, Southwest Hospital, Third Military Medical University, Chongqing 400038, China*

Correspondence should be addressed to Feng Cao; fengcao8828@163.com

Received 30 July 2017; Revised 2 November 2017; Accepted 4 December 2017; Published 13 February 2018

Academic Editor: Nabil Eid

Sepsis, a systemic inflammatory response to infection, is the leading cause of death in the intensive care unit (ICU). Previous studies indicated that mesenchymal stromal cells (MSCs) might have therapeutic potential against sepsis. The current study was designed to investigate the effects of MSCs on sepsis and the underlying mechanisms focusing on inflammasome activation in macrophages. The results demonstrated that the bone marrow-derived mesenchymal stem cells (BMSCs) significantly increased the survival rate and organ function in cecal ligation and puncture (CLP) mice compared with the control-grouped mice. BMSCs significantly restricted NLRP3 inflammasome activation, suppressed the generation of mitochondrial ROS, and decreased caspase-1 and IL-1β activation when cocultured with bone marrow-derived macrophages (BMDMs), the effects of which could be abolished by Mito-TEMPO. Furthermore, the expression levels of caspase-1, IL-1β, and IL-18 in BMDMs were elevated after treatment with mitophagy inhibitor 3-MA. Thus, BMSCs exert beneficial effects on inhibiting NLRP3 inflammasome activation in macrophages primarily via both enhancing mitophagy and decreasing mitochondrial ROS. These findings suggest that restricting inflammasome activation in macrophages by increasing mitophagy and decreasing mitochondrial ROS might be a crucial mechanism for MSCs to combat sepsis.

1. Introduction

Sepsis syndrome, the inflammatory response to infection, is one of the leading causes for death in hospitalized patients [1]. Complications of sepsis, such as acute respiratory distress syndrome (ARDS) and multiple organ dysfunction syndrome (MODS), are major causes for morbidity and mortality in critical patients. Sepsis-associated mortality in the intensive care unit (ICU) is extremely high, with rates of 20% for sepsis, 35% to 45% for severe sepsis, and 60% for septic shock [2]. Therefore, it is essential to identify effective therapeutic strategies for sepsis.

The pathophysiologic process for sepsis is complicated, including invading microorganisms, proinflammatory response, anti-inflammation, and associated immunoparalysis [3, 4]. Extensive data have demonstrated that mesenchymal stromal cells (MSCs), a type of adult stem-like cells, are capable of inhibiting inflammation and immunity responses

[5]. Therefore, stem cells have drawn growing interest in the treatment of inflammatory diseases. Of note, it has been reported that MSCs can improve organ function and decrease mortality [6, 7] as well as reduce sepsis-induced inflammation in an animal sepsis model induced by cecal ligation and puncture (CLP) [8]. However, the underlying mechanism is poorly understood, which vastly limits the therapeutic potential of cytotherapy. Previous studies have shown that mitophagy is a prosurvival mechanism associated with cellular exposure to various mitochondrial stressors [9]. Recent studies have indicated that excessive reactive oxygen species (ROS) production is involved in activating mitophagy [10, 11]. It is also well established that the cytosolic E3 ubiquitin ligase, Parkin, and the outer mitochondrial membrane kinase, PTEN-induced putative kinase 1 (PINK1), are two main regulators of mitophagy in mammalian cells [9, 12, 13].

Based on previous reports, we hypothesized that bone marrow-derived mesenchymal stem cells (BMSCs) could reduce sepsis-associated inflammation and organ dysfunction in CLP-induced sepsis. We further investigated the immune-modulatory effects of BMSCs on bone marrow-derived macrophages (BMDMs) to determine the mechanisms for the beneficial effects of BMSCs against sepsis.

2. Materials and Methods

2.1. Ethics. All animal procedures were conducted in conformity with the National Institutes of Health Guide for the Care and Use of Laboratory Animals. The experimental protocol was approved by the Chinese PLA General Hospital and Fourth Military Medical University Committee on Animal Care.

2.2. Animal Study Protocol and CLP Procedures. Transgenic C57BL/6-Tg (CAG-EGFP)1Osb/J mice (C57BL/6, 8–10 weeks, 20–24 g), which continuously express eGFP in all tissues and organs, were commercially purchased from Jackson Laboratory (stock number 003291). Wild-type C57BL/6 mice (8–10 weeks, 20–24 g) were from Animal Laboratory of Fourth Military Medical University. All animals had free access to water and food during the experiment. C57BL/6 mice that underwent the CLP operation were randomly divided into three groups depending on the intravenously injected solution at 1 h postoperation ($n = 20$ in each group), the CLP + saline group (injected with 100 μl of saline); CLP + Fbs group (injected with 2.5×10^5 fibroblasts in 100 μl); and CLP + BMSC group (injected with 2.5×10^5 BMSCs in 100 μl). The fate of BMSCs and myocardial function were detected 24 h after the operation. Visualization of BMSCs in C57BL/6 mice liver tissue at 1–6 h after intravenous injection was shown in supplemental Figure S1C. The survival rate was analyzed every 6 h after the operation until 96 h.

CLP was performed according to the protocol proposed by Rittirsch et al. [14]. Briefly, C57BL/6 mice were anesthetized with persistently inhaled 2% isoflurane during the operation. The abdominal zone was shaved and prepared with 70% ethanol. A ventral midline incision (approximately 1 cm) was made, and the cecum was exteriorized. The cecum was ligated at the designated position with silk suture and penetrated through-and-through with a 22 G needle. Then, the abdominal incision was closed. In the sham group, the cecum was exteriorized, without being ligated or punctured. Immediately after surgery, animals were subcutaneously injected with 1 ml/30 g saline and imipenem-cilastatin for fluid resuscitation and infection prevention.

2.3. Cardiac Function Evaluation by Echocardiography. Echocardiography was performed using the Vevo 2100 ultrasound system (Visual-Sonics, Toronto, Canada) with a 30 MHz linear transducer. Anesthesia was conducted with persistently inhaled 1.0% isoflurane. Data of the left ventricular end-diastolic diameter (LVEDd), left ventricular end-systolic diameter (LVESd), and left ventricle (LV) internal dimension in diastole (LVID, d) and systole (LVID, s) were measured. The left ventricular ejection fraction (LVEF) and fractional shortening (FS) were calculated accordingly. The whole procedure was performed by two blinded investigators.

2.4. Isolation, Culturing, and Characterization of BMSCs and Preparation of BMDMs. BMSCs^{eGFP+} continuously expressing eGFP were isolated from transgenic C57BL/6-Tg(CAG-EGFP)1Osb/J mice and cultured as previously described [15]. Isolated BMSCs were uniformly negative for CD34, CD45, and Sca-1; were positive for CD29, CD44, and CD90; and had multidifferentiation potential for adipogenesis and osteogenesis (shown in supplemental Figure S1A and B).

Mice were sacrificed, and femurs were removed and cleansed of tissue. Marrows were flushed from the femurs with PBS and collected by centrifugation (200g, 5 min). Cells were cultured at the density of 5×10^5/ml in culture dishes with DMEM medium supplemented with 10% (vol/vol) FBS, 1% (vol/vol) penicillin and streptomycin. Following 6 h of incubation at 37°C in 5% CO_2, nonadherent cells (primary bone marrow-derived macrophages) were decanted and seeded in plates and incubated in complete medium with 25% (vol/vol) conditioned medium from L929 mouse fibroblasts for 7 days (over 90% cells are positive for the cell type surface marker CD11b) to form proliferative nonactivated cells (M0 macrophages) [16, 17].

The *in vitro* cell study was divided into the following six groups: (1) control group (control); (2) LPS-treated group (LPS), BMDMs were primed with LPS (2 μg/ml) for 4 hours; (3) LPS + ATP-treated group (LPS + ATP-stimulated), BMDMs were primed with LPS (2 μg/ml) for 4 hours followed by incubation with ATP (5 mM) for 0.5 h; (4) BMSC coculture group (BMSCs); (5) BMSC coculture and LPS-treated group (BMSC-LPS); and (6) BMSC coculture and LPS + ATP-treated group (BMSC-treated), BMDMs were primed with LPS (2 μg/ml) for 4 hours followed by incubation with ATP (5 mM) for 0.5 h. BMSCs, in transwell coculture, were added to BMDMs in the ATP stimulation step.

2.5. Evaluation of Inflammatory Cytokines and Organ Injury Markers. Inflammatory cytokines (IL-1β, TNF-α, IL-6, and IL-10) and serum biomarkers (cTnI, CK, LDH, ALT, AST, Amylase, Scr, and BUN) were measured with spectrophotometrically commercial ELISA assay kits (R&D Systems, USA) according to the manufacturers' instructions.

2.6. Immunohistochemical Staining. Immunohistochemical staining was performed to detect inflammatory cell infiltration. Tissue sections were blocked with 5–10% normal goat serum for 30 min and then incubated with monoclonal antibodies of anti-Ly-6G and anti-Mac-3 (from Biolegend, San Diego, CA, USA) overnight at 4°C. Then, sections were washed and incubated with secondary horseradish peroxidase-conjugated goat anti-rabbit antibodies (from Zhongshan Biotechnology Co. Ltd., Beijing, China) at 37°C for 1 h. Sections were randomly selected, and images were visualized and photographed with inverted or confocal microscopy (Olympus, Japan).

2.7. Western Blot. Western blot was performed as previously described [18]. Briefly, proteins were harvested from cells or tissues with RIPA Lysis Buffer (Beyotime Biotechnology, Beijing, China). Total proteins were loaded onto SDS-PAGE gels and transferred electrophoretically to PVDF membranes (Millipore, Billerica, MA). After blocking with 5% skim milk for 1 h, the membranes were incubated with primary antibody at 4°C overnight. Afterwards, membranes were washed and incubated with corresponding secondary antibody at 37°C for 1 h. The blots were developed with enhanced chemiluminescence (ECL) reagent (Millipore) and visualized using UVP Bio-Imaging Systems. Blot densities were analyzed with Quantity One System Software.

Primary antibodies are as follows: procaspase-1, caspase-1, pro-IL-1β, P2X7, ASC, NLRP3, PINK1, Parkin, LC3, and β-actin (all from Abcam, Cambridge, MA, USA). Secondary antibodies are as follows: horseradish peroxidase-conjugated goat anti-rabbit and goat anti-rat (Zhongshan Biotechnology Co. Ltd.).

2.8. Transmission Electron Microscopy (TEM). TEM was performed to observe the mitochondrial morphology. Briefly, collected BMDMs underwent the procedures of fixation, stepwise alcohol dehydration, embedding, polymerization, sectioning, and staining. Images were observed with an electron microscope (JEM-2000EX TEM, JEOL Ltd., Tokyo, Japan). Random sections were visualized by a blinded technician.

2.9. Mitochondrial ROS Production Detection. Mitochondrial ROS production was detected using MitoSOX™ (Ex/Em: 510/580 nm), MitoTracker® Deep Red FM (Ex/Em: 640/662 nm), and MitoTracker Green FM (Ex/Em: 490/516 nm) fluorescent dye (all from Invitrogen, Invitrogen Corporation, USA) by flow cytometry.

2.10. Statistical Analysis. Data were expressed as the mean ± SD and were analyzed using ANOVA followed by a Bonferroni correction for the post hoc *t*-test. The survival rate was analyzed with the Kaplan-Meier test followed by the log-rank post hoc test. All statistical tests were performed using SPSS software version 17.0 (IBM, Armonk, NY, USA) and GraphPad Prism software version 5.0 (GraphPad Software, San Diego, CA). A value of $p < 0.05$ was considered statistically significant.

3. Results

3.1. BMSC Treatment Improved Survival Rate and Multiorgan Functions after CLP. Figure 1(a) shows the survival curve of C57BL/6 mice after CLP. Compared with the CLP + saline and CLP + Fbs groups, the survival rate was significantly increased in the CLP + BMSC group, with survival rates of 10%, 5%, and 40% in the three groups at the time point of 96 h ($p < 0.05$). As revealed by HE staining, BMSC observably improved morphological changes in vital organs, such as the heart, liver, spleen, lungs, and kidneys, which was manifested by interstitial edema, red blood cell, and inflammatory cell infiltration (Figure 1(b)). In addition, serum biomarkers, including cardiac troponin I (cTnI), creatinine kinase (CK), lactate dehydrogenase (LDH), alanine aminotransferase (ALT), aspartate aminotransferase (AST), amylase, serum creatinine values (SCr), and blood urea nitrogen (BUN), were significantly reduced in the CLP + BMSC group compared with the CLP + Saline and CLP + Fbs groups ($P < 0.05$), indicating that BMSC treatment improved organ functions after CLP (Figure 1(c)).

3.2. BMSCs Improved Myocardial Function after CLP. Figure 1(d) shows representative M-mode echocardiography images in each group. CLP-induced cardiac depression was manifested by a decreased left ventricular ejection fraction (LVEF), left ventricular fractional shortening (LVFS), and maximal velocity increase as well as a decrease in the pressure per second in the left ventricular (±dP/dt) in the CLP + saline group ($p < 0.05$, CLP + saline group versus sham group). In comparison with the CLP + saline and CLP + Fbs group, BMSCs had an increased left ventricular ejection fraction (LVEF), left ventricular fractional shortening (LVFS), and maximal velocity as well as a decrease in pressure per second in the left ventricle (±dP/dt), suggesting that BMSC treatment improved myocardial function after CLP (Figures 1(e) and 1(f)).

3.3. BMSCs Reduced the CLP-Induced Inflammation Level. Inflammatory cell infiltration in the heart and lung tissue was determined by the immunohistochemistry for Ly-6G and MAC-3, which are well-recognized biomarkers for neutrophils and macrophages. It could be inferred that BMSC treatment inhibited inflammatory cell infiltration, as evidenced by decreased macrophage (Mac-3) (Figures 2(a) and 2(c)) and neutrophil (Ly6G) infiltration (Figures 2(b) and 2(c)) in the lung and liver tissues. Furthermore, BMSCs decreased the proinflammatory cytokine levels of IL-6, IL-1β, and TNF-α, while increasing anti-inflammatory cytokine IL-10 in the serum (Figure 2(d), $p < 0.05$, CLP + BMSC group versus CLP + saline group; $p < 0.05$, CLP + BMSC group versus CLP + Fbs group).

3.4. BMSCs Inhibited NLRP3 Inflammasome-Mediated Caspase-1 and IL-1β Activation. Figure 3(a) shows representative blots of NLRP3, ASC, procaspase-1, caspase-1 p20, pro-IL-1β, and IL-1β in liver tissue. NLRP3 inflammasome expression was decreased after BMSC treatment as compared with the CLP + saline and CLP + Fbs groups (Figures 3(a) and 3(b)). Moreover, caspase-1 cleavage and activation, leading

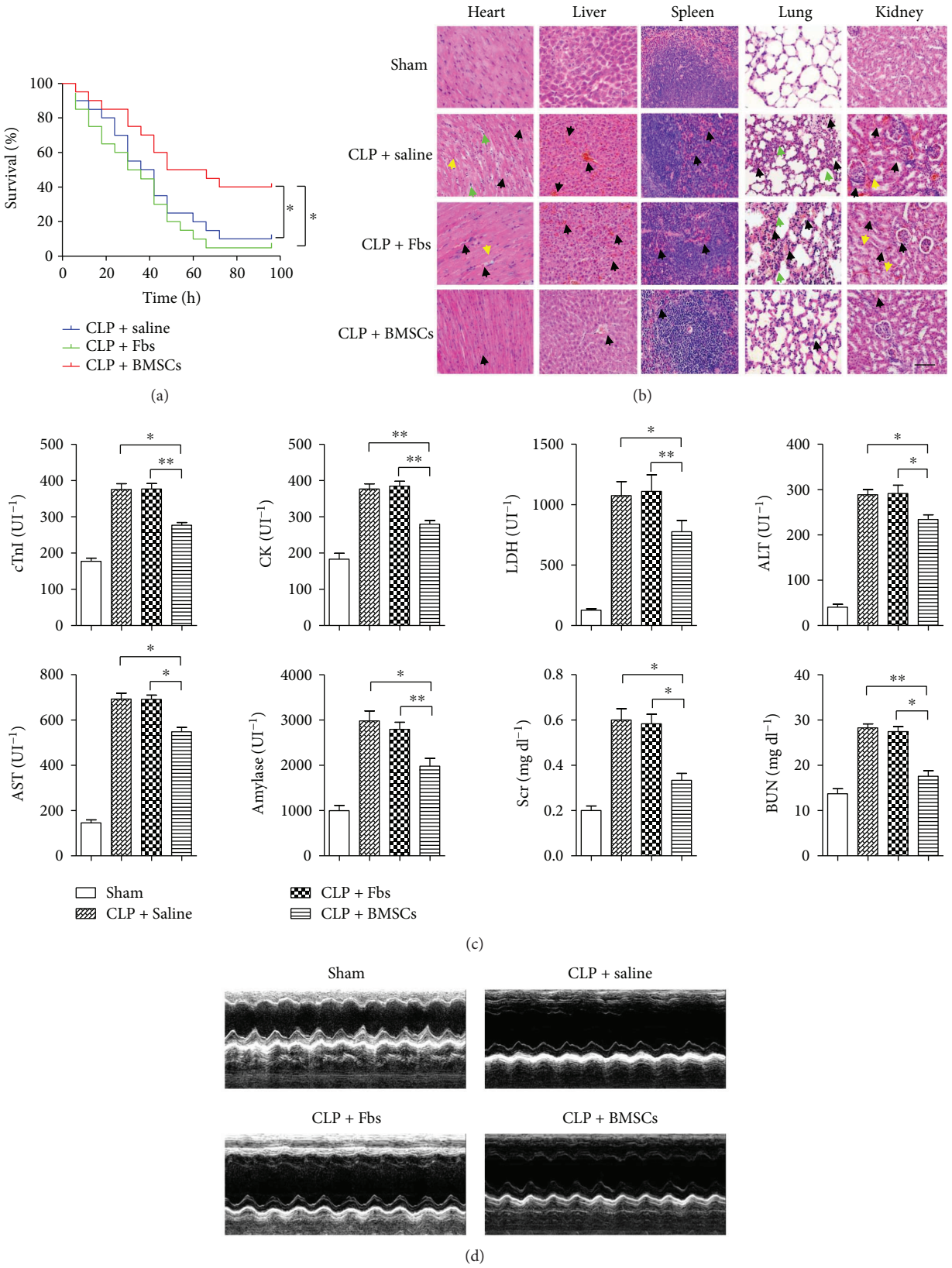

Figure 1: Continued.

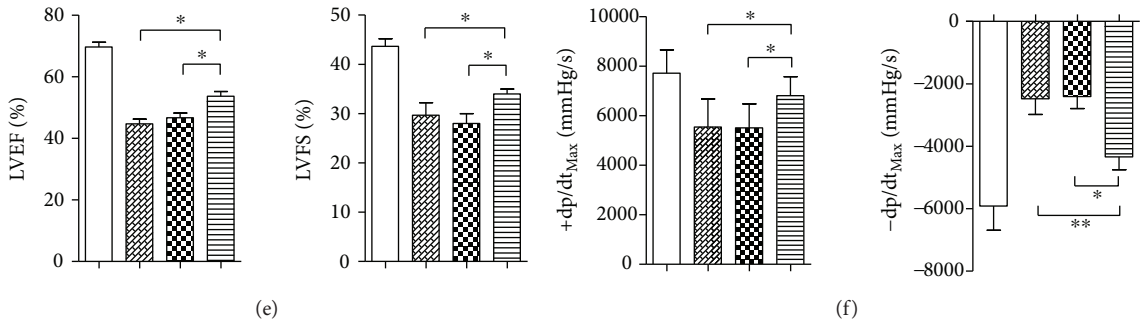

Figure 1: Effect of intravenous injection of BMSCs on the course of sepsis after CLP. (a) Survival curves of C57BL/6 mice after CLP and treatment using BMSCs as well as fibroblasts. (b) Representative images of organs from mice that received saline or BMSCs after CLP surgery. The arrows point to interstitial edema (yellow arrows), red blood cell infiltration (black arrows), and inflammatory cell infiltration (green arrows). Scale bar, 200 μm. (c) Effect of BMSC treatments on CLP-induced multiorgan injury. Serum biomarkers, including cardiac troponin I (cTnI), creatinine kinase (CK), lactate dehydrogenase (LDH), alanine aminotransferase (ALT), aspartate aminotransferase (AST), amylase, serum creatinine values (SCr), and blood urea nitrogen (BUN), were measured in serum by ELISA. (d) Representative M-mode echocardiography images of mice. (e) Measurement of the left ventricular ejection fraction (LVEF) and left ventricular fractional shortening (LVFS). (f) Measurement of the maximal velocity increase and decrease in the pressure per second in the left ventricle (±dP/dt). Error bars represent the means ± s.e.m. $n = 10$–15 per group. $^{*}p < 0.05$ and $^{**}p < 0.01$. The data are representative of three independent experiments.

to maturation and secretion of IL-1β, revealed by caspase-1 p20 and IL-1β p17 expression, were more suppressed in liver tissues of mice with BMSC treatment than that with single saline or Fbs treatment.

3.5. BMSCs Inhibited Caspase-1 and IL-1β Activation in BMDMs. Briefly, BMDMs were primed with LPS (2 μg/ml) for 4 hours, which was followed by incubation with ATP (5 mM) for 0.5 h. BMSCs, in transwell coculture, were added to BMDMs at the ATP stimulation step. Then, 18 hours later, caspase-1 and IL-1β activation were analyzed in macrophage lysates by Western blot (shown in Figure 4(a)). Both LPS and ATP stimulation induced caspase-1 and IL-1β activation, as evidenced by increased caspase-1 p20 and IL-1β p17 expression. Furthermore, BMSC coculturing suppressed LPS and ATP stimulation induced caspase-1 and IL-1β activation in BMDMs ($p < 0.01$, $p < 0.05$, BMSC-treated group versus LPS + ATP-stimulated group) (Figure 4(b)). Similarly, the levels of IL-1β and IL-18 in the supernatants were reduced in the BMSC-treated group compared with the LPS + ATP-stimulated group (Figure 4(c)). In addition, there was no significant difference in the expression levels of P2X7, procaspase-1, and pro-IL-1β among the groups (Figure 4(b)).

3.6. BMSCs Inhibited NLRP3 Inflammasome Activation in BMDMs by Decreasing Mitochondrial ROS. Compared with the LPS + ATP-stimulated group, BMSC coculturing reduced the mitochondrial ROS (mtROS) level in BMDMs (Figure 5(a)). The flow cytometry analysis of MitoTracker Deep Red-MitoTracker Green (Figure 5(b)) indicated that BMSCs alleviated LPS + ATP stimulation-induced mitochondrial damage in BMDMs. Antioxidant Mito-TEMPO was used to inhibit mtROS generation. Figure 5(c) shows the colocalization of NLRP3 (green), mitochondria (red), and nucleus (blue) by immunofluorescence staining. In control BMDMs, very little NLRP3 cosedimented with mitochondria. However, much more NLRP3 was colocalized with or adjacent to mitochondria after LPS-ATP stimulation. Both BMSCs and Mito-TEMPO resulted in less colocalization of NLRP3 and mitochondria. After LPS and ATP stimulation, Mito-TEMPO treatment decreased the expression levels of caspase-1 p20 and IL-1β p17 ($p < 0.01$, $p < 0.05$), suggesting that NLRP3 activation was associated with mtROS level. Additionally, the expression levels of caspase-1 p20 and IL-1β p17 were also reduced in the BMSC-treated group ($p < 0.01$, $p < 0.01$), indicating that the effect of BMSCs on BMDMs could be attributed to mtROS scavenge (Figures 5(d) and 5(e)). Moreover, both BMSCs and Mito-TEMPO decreased the cytokine secretions of IL-1β and IL-18 (Figure 5(f), $P < 0.05$).

3.7. BMSCs Inhibited NLRP3 Inflammasome Activation by Increasing BMDM Mitophagy. Using electron microscopy (EM), we directly assessed the mitochondrial integrity and state. We observed more mitophagy (indicated by red arrows) and fewer swollen mitochondria in the BMSC-treated group than for treatment with LPS and ATP in BMDMs (Figure 6(a)). In addition, autophagy-associated LC3 puncta were found to accumulate around the mitochondria in BMDMs when coculturing with BMSCs after stimulation by LPS and ATP (Figure 6(b)). As was shown by the Western blot results in Figures 6(c) and 6(d), treatment of BMDMs with the mitophagy/autophagy inhibitor 3-methyladenine (3-MA) enhanced the activation of caspase-1 and IL-1β, as well as the secretion of IL-1β and IL-18 in BMDMs when coculturing with BMSCs after LPS and ATP stimulation (Figure 6(e)).

3.8. BMSCs Increased Parkin-Mediated Mitophagy in BMDMs. Both BMSCs and Mito-TEMPO significantly elevated the expression of PINK1, Parkin, and LC3BII/I ratio (Figures 7(a) and 7(b)). MitoSOX flow cytometry revealed that BMSCs significantly decreased mtROS generation, while mitophagy inhibition by 3-MA diminished this effect,

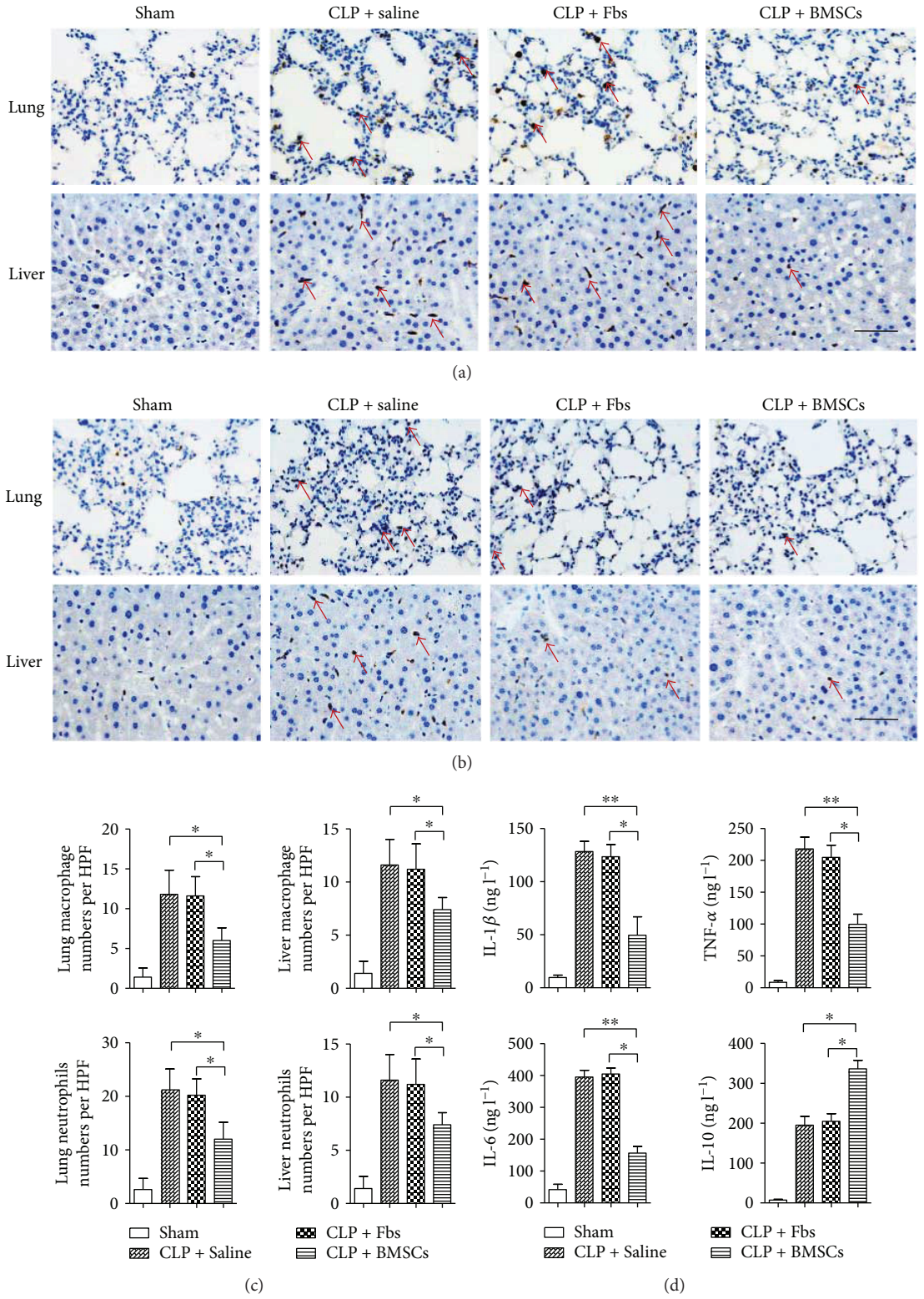

FIGURE 2: Treatment with BMSCs reduced the levels of sepsis-induced inflammation. (a-b) Treatment with BMSCs attenuated sepsis-induced inflammatory cell infiltration in organs. Inflammatory cell infiltration was determined by immunohistochemistry staining. Red arrows indicate inflammatory cells. (a) The sections were immunohistochemically analyzed using antibodies against Mac-3 for macrophages (red arrows). Scale bar, 100 μm. (b) The sections were immunohistochemically analyzed using antibodies against Ly6G for neutrophils (red arrows). Scale bar, 100 μm. (c) Quantitative analysis of positive cell numbers per five different HPFs (high magnification fields). (d) Levels of the proinflammatory cytokines IL-6, IL-1β, and TNF-α and anti-inflammatory cytokine IL-10 in serum were measured by ELISA. Error bars represent the means ± s.e.m. $n = 10$–15 per group. $^{*}p < 0.05$ and $^{**}p < 0.01$. Data are representative of three independent experiments.

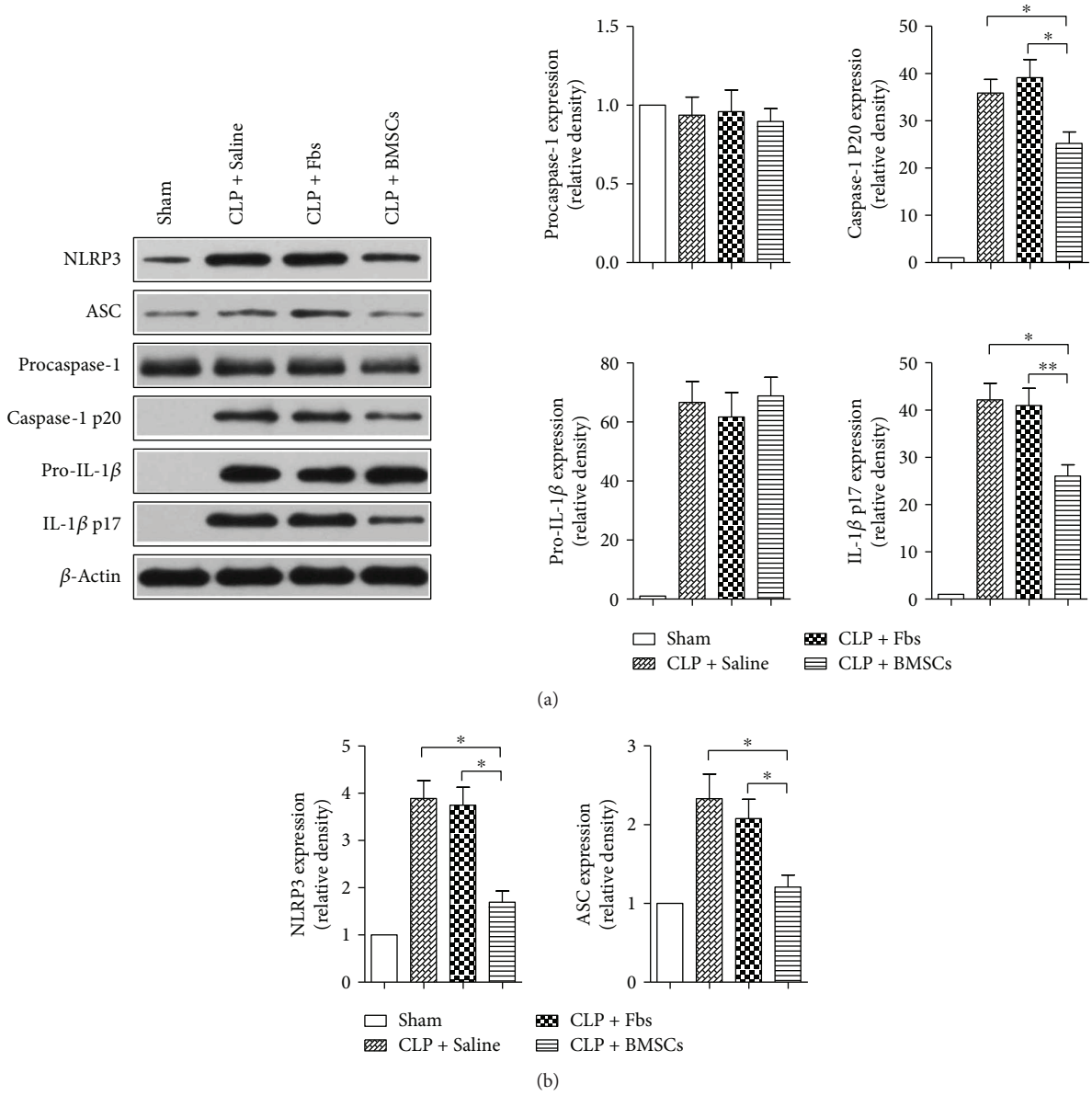

Figure 3: BMSC treatment inhibited NLRP3 inflammasome-mediated and IL-1β activation in liver tissues of C57BL/6 mice. (a) Representative blots of P2X7, NLRP3, ASC, procaspase-1, pro-IL-1β, caspase-1, and IL-1β in livers subjected to CLP. (b) Semiquantitative analysis of the Western blots. $^{*}p < 0.05$ and $^{**}p < 0.01$. $n = 5$–10. Data are representative of three or more independent experiments.

indicating that the inhibitory effects of BMSCs on mtROS generation were mediated by mitophagy (Figure 7(c)).

4. Discussion

Several studies have indicated the beneficial effects of MSCs against sepsis, but the underlying mechanisms remain unclear. In the present study, we demonstrate that BMSCs exert beneficial effects on experimental sepsis *via* inhibiting NLRP3 inflammasome activation in macrophages. Furthermore, one important finding in the present study was that BMSCs restricted NLRP3 inflammasome activation through increasing mitophagy activation and decreasing mitochondrial ROS in macrophages.

The antisepsis efficacy of MSCs may be attributed to their ability to home injured tissue, secrete paracrine cytokines, decrease apoptosis in injured tissues, and modulate immune cells [19, 20]. It was reported that MSCs attenuated septic injury by reducing the infiltration of inflammatory cells and cell death in various targeted organs [21]. However, Krasnodembskaya et al. determined that human BMSCs attenuated live bacteria-induced injury due to direct antimicrobial activity [22]. Moreover, the same group has published a study on therapeutic potential of human MSC in the model of sepsis, in which they found that MSC effect was associated with increased phagocytic activity of blood monocytes and M2 polarization of monocytes/macrophages in the spleen [23]. Although complex, the acquisition of a

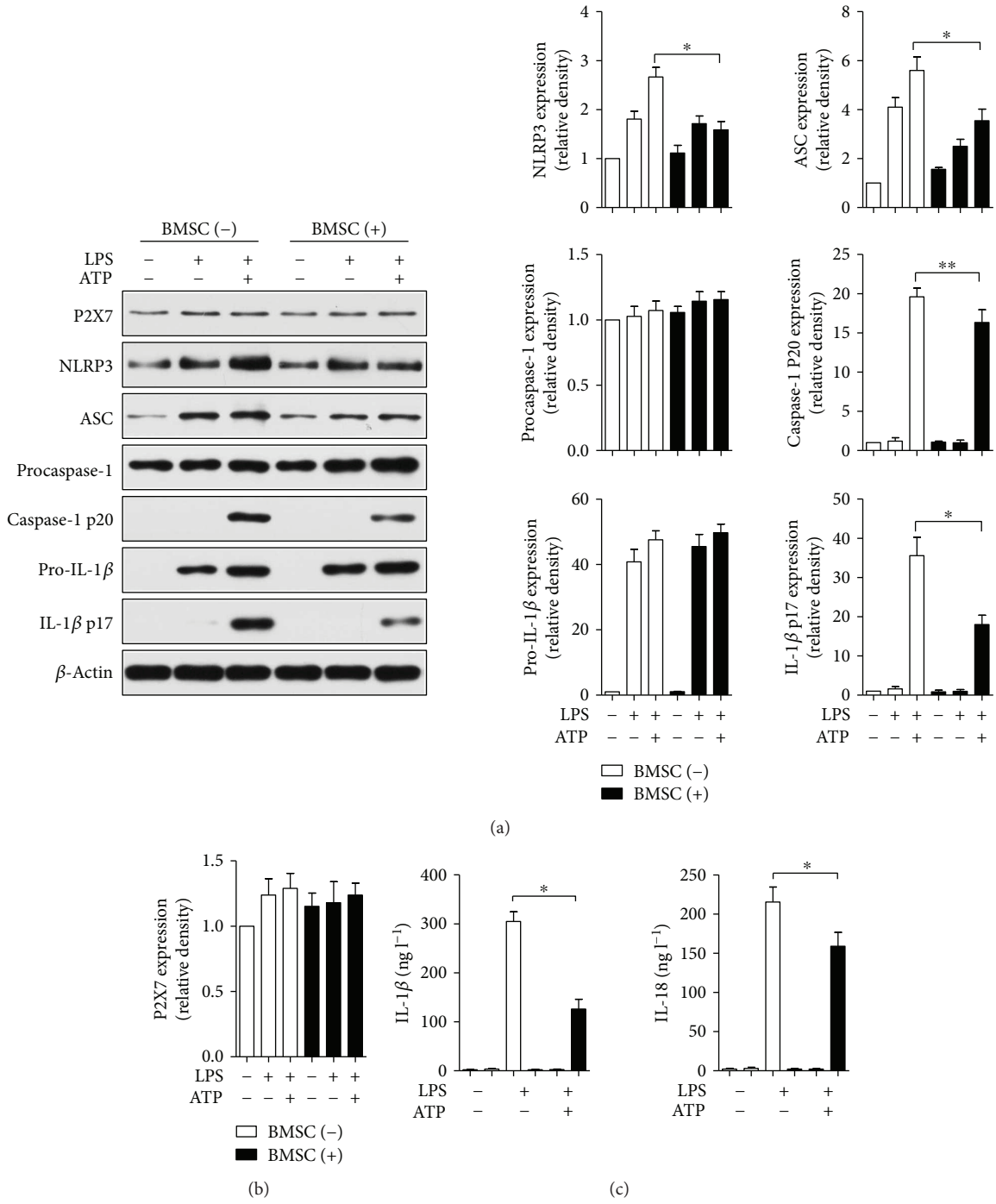

FIGURE 4: BMSCs inhibited NLRP3 inflammasome-mediated caspase-1 activation and IL-1β and IL-18 secretion in bone marrow-derived macrophages (BMDMs). BMDMs were primed with LPS (2 μg/ml) for 4 hours, which was followed by incubation with ATP (5 mM) for 0.5 h. BMSCs, in transwell coculture, were added to BMDMs at the ATP stimulation step. At 18 hours, caspase-1 and IL-1β activation was analyzed in lysates of macrophages by Western blot (a, b), and IL-1β and IL-18 secretion in the supernatants was quantified by ELISA (c). Error bars represent the means ± s.e.m. $^{*}p < 0.05$ and $^{**}p < 0.01$. $n = 5$–10. The data are representative of three or more independent experiments.

mechanistic knowledge is essential for developing BMSC cell therapy against sepsis injury. In the present study, our data showed that BMSCs increased the CLP murine survival rate and alleviated organ injury via improving organ function and alleviating proinflammatory cytokines.

Cardiac function is crucial to the clinical outcomes of sepsis. Therefore, myocardial dysfunction has been gaining increasing attention in recent years [24, 25]. In the current study, we observed impaired cardiac function in septic mice by echocardiography and hemodynamic measurements.

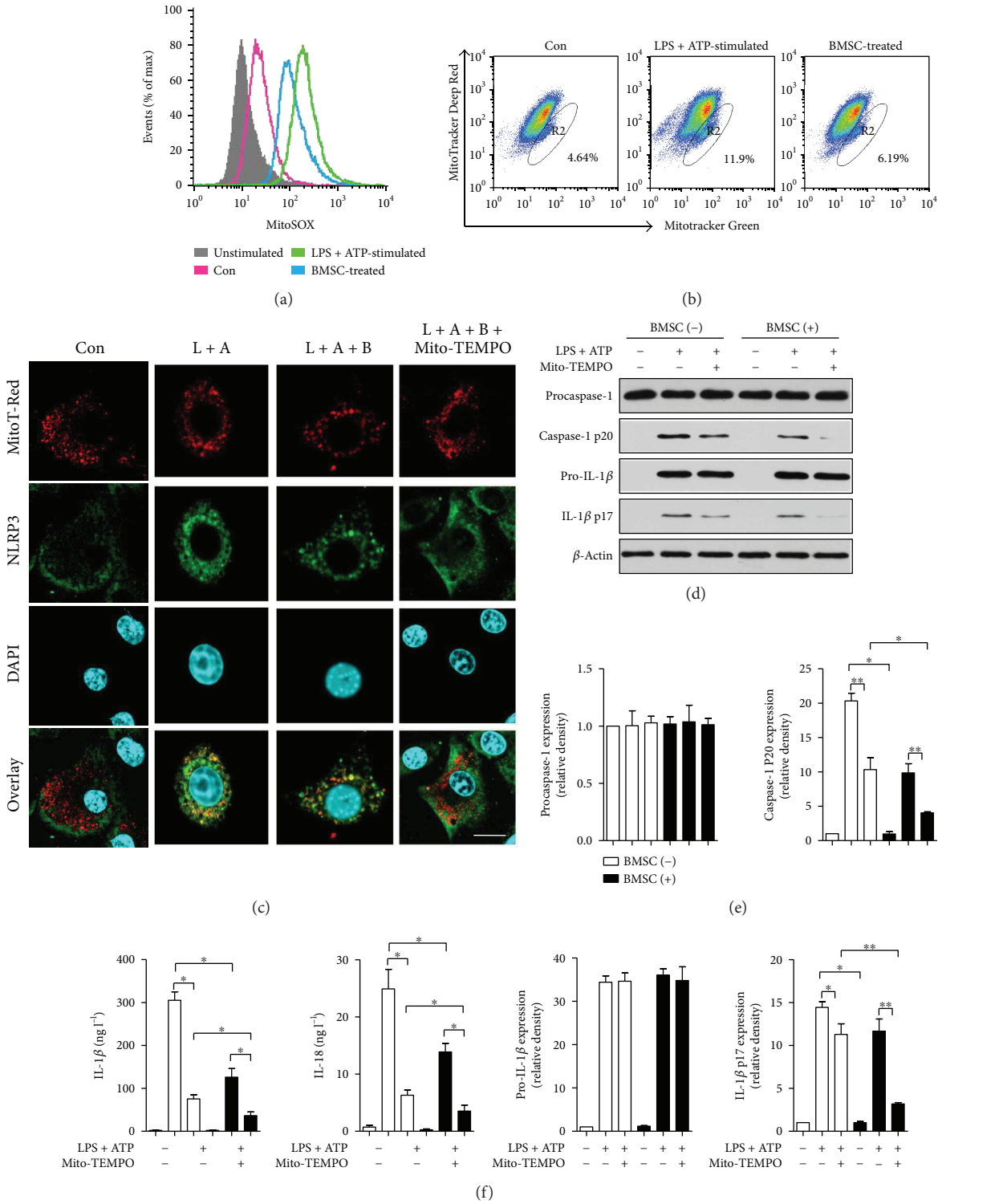

FIGURE 5: BMSCs negatively regulate the NLRP3 inflammasome in BMDMs by decreasing mitochondrial ROS (mt ROS). (a), (b) BMDMs were treated with LPS (2 μg/ml, 4 hours) and ATP (5 mM, 0.5 h) (L + A). BMSCs were cocultured with BMDMs in transwell from ATP licensing for 2 h (L + A + B). BMDMs were stained with MitoSOX (5 μM) (a) or MitoTracker Deep Red (500 nM) and MitoTracker Green (200 nM) (c) for the final 30 min and then analyzed by flow cytometry. (c) Colocalization of the NLRP3 and mitochondria. BMDMs expressing NLRP3 (green) were analyzed for the colocalization of NLRP3 with the mitochondria (red) using confocal microscopy. Scale bar, 20 μm. (d–f) Inhibition of mtROS generation abolished caspase-1 activation. Western blot analysis for caspase-1 and IL-1β in lysates (d, e) and cytokine secretion (f) of BMDMs incubated for 1 h with Mito-TEMPO (500 μM), which was followed by LPS and ATP. Error bars represent the means ± s.e.m. $^{*}p < 0.05$ and $^{**}p < 0.01$. $n = 5$–10. The data are representative of three or more independent experiments.

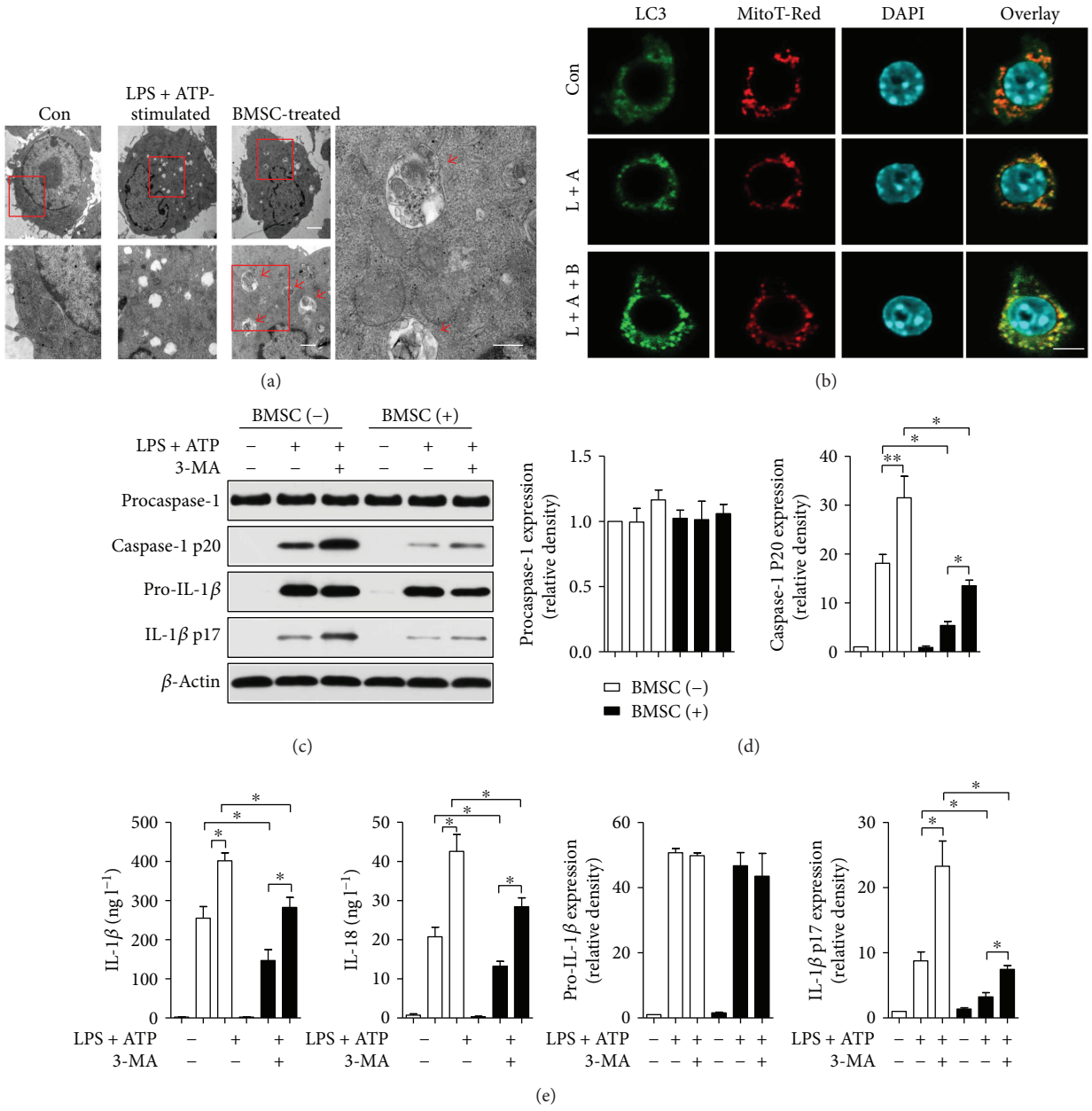

Figure 6: BMSCs inhibited NLRP3 inflammasome activation in BMDMs by increasing the mitophagy of BMDMs. (a) Electron microscopy images of BMDMs showing mitochondrial morphologic changes. Red arrows indicate mitophagy. Scale bar, 2 μm (top row), 600 nm (bottom row, left), and 400 nm (bottom row, right). (b) Confocal microscopy analysis of BMDMs stained for LC3 (green) and mitochondria (red) for colocalization as an indicator of mitophagy. Scale bar, 20 μm. (c–e) Inhibition of mitophagy results in caspase-1 activation. Western blot analysis for caspase-1 and IL-1β in lysates (c, d) and cytokine secretion (e) of BMDMs incubated for 6 h with 3-methyladenine (3-MA) (10 mM), which was followed by LPS and ATP. Error bars represent the means ± s.e.m. $^{*}p < 0.05$ and $^{**}p < 0.01$. $n = 5$–10. The data are representative of three or more independent experiments.

BMSC treatment effectively improved cardiac function induced by CLP. Similarly, the results of Weil et al. suggested that intravenous infusion of MSCs improved myocardial function in the endotoxemia model [26]. However, the precise mechanism of MSCs' beneficial function in cardiac recovery is far from clear. Data from Rogers et al. revealed that MSCs exerted reparative effects on myocardium through molecular reprogramming of the cardiomyocytes themselves [27]. Notably, studies on sepsis indicate that mitochondria could mediate organ dysfunction, including heart function depression. Considering our data, mitochondrial dysfunction may be a fundamental contributor to cardiac depression in sepsis. However, further studies are still needed to clarify this.

According to previous studies, sepsis is initiated when well-conserved microbial structures (also known as pathogen-associated molecular patterns, PAMPs) bind to receptors embedded either on the cell membranes or inside the cell cytoplasm of cells of the innate immune system, namely, blood monocytes and tissue macrophages. The characteristic of the first phase of sepsis is the production

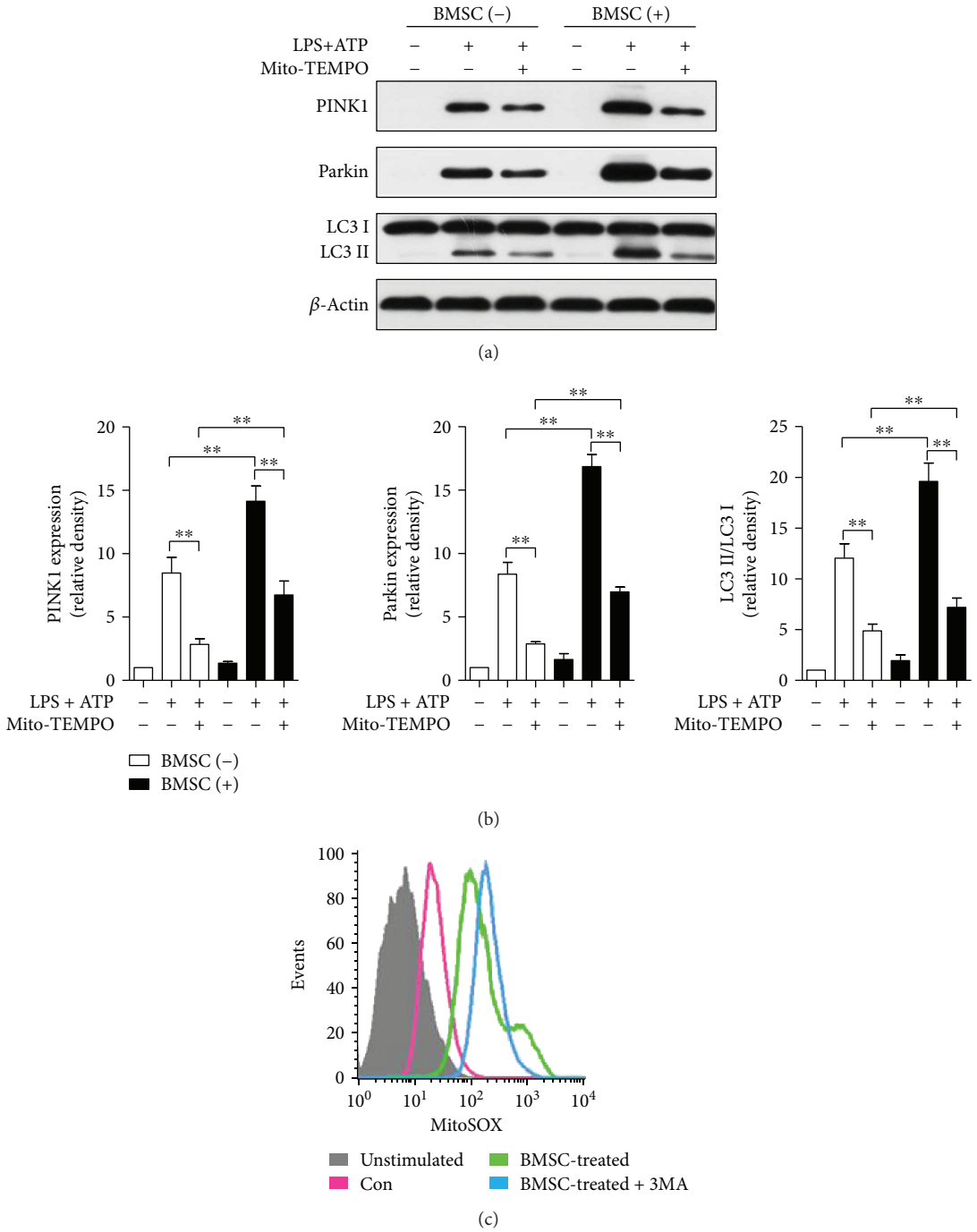

Figure 7: BMSCs increased Parkin-mediated mitophagy and decreased mtROS generation of BMDMs. (a-b) Western blot analysis for caspase-1 and IL-1β in lysates (a, b) of BMDMs incubated for 1 h with Mito-TEMPO (500 μM), which was followed by LPS and ATP. (c) BMDMs stimulated with 3-MA (10 mM) for 6 h were stained with MitoSOX (5 μM) for 30 min and were then analyzed by flow cytometry. Error bars represent the means ± s.e.m. $^{**}p < 0.01$. $n = 5$–10. The data are representative of three or more independent experiments.

of proinflammatory cytokines, including tumor necrosis factor-alpha (TNF-α), interleukin- (IL-) 1β, IL-6, and IL-8. These proinflammatory mediators orchestrate septic reaction of the host. Soon after this first phase of hyperproduction of proinflammatory mediators, a second phase ensues during which Th2 cells, monocytes, and macrophages stimulated by PAMPs secrete a large amount of anti-inflammatory mediators like IL-10. This phase is considered a state of immunosuppression or immunoparalysis of the host when multiple organ dysfunctions take place [28]. Consistent with previous reports, we found that the inflammatory biomarkers (IL-1β, TNF-α, IL-6, and IL-10), serum markers (cTnI, CK, LDH, ALT, AST, Amylase, Scr, and BUN), and inflammatory cell infiltration were increased in CLP mice compared with those in control mice [7, 26, 29]. In addition, mitochondrial ROS generation was also elevated in CLP-induced septic

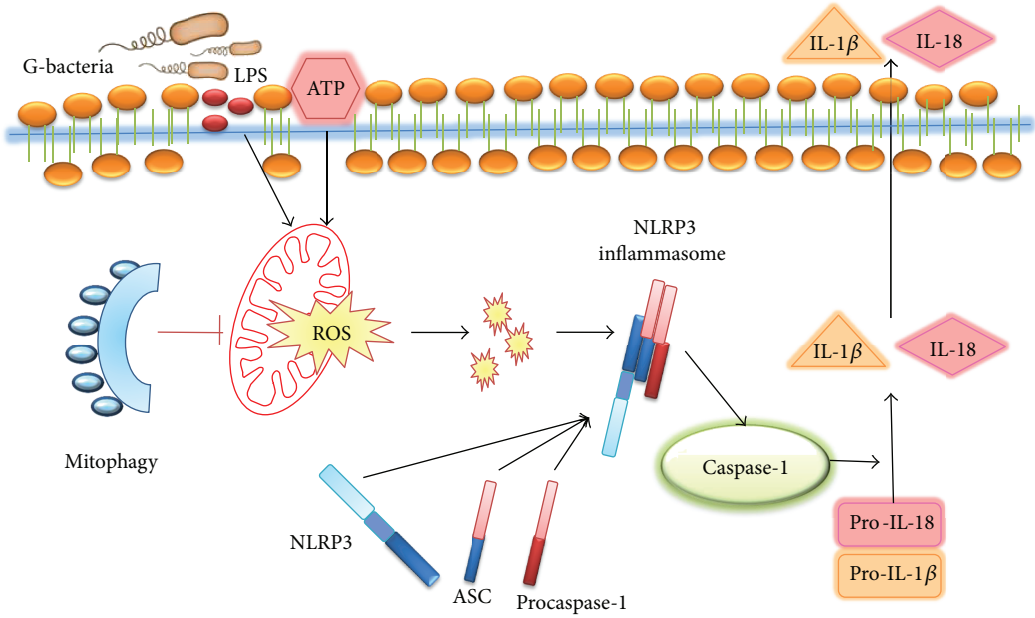

Figure 8: Proposed scheme for the mechanism of mesenchymal stromal cell-mediated protection against sepsis. A summary of our current hypothesis about the mechanisms that underlie the interactions between BMSCs and BMDMs in the CLP sepsis model. BMSCs negatively regulate the NLRP3 inflammasome in BMDMs primarily by increasing mitophagy of BMDMs in response to crosstalk with activated BMDMs and thus by decreasing mitochondrial ROS.

mice. These results were consistent with the findings by Chang et al., who proposed that CLP-induced sepsis triggered a rigorous inflammatory response with the generation of ROS [30]. Sepsis is characterized by overwhelming activation of inflammatory and immune responses. An interesting finding in the present study was that BMSCs restricted the inflammatory responses and ROS generation in CLP animals. This is comparable to previous reports. Yip and his colleagues reported that combined therapy with melatonin and apoptotic adipose-derived mesenchymal stem cells alleviated sepsis-induced organ injury through attenuating inflammatory reactions and oxidative stress [2, 31]. Notably, the inflammatory cytokines were produced by macrophages rather than injected BMSCs, suggesting that the therapeutic effect of BMSCs against excessive inflammatory responses was mediated by an interaction between BMSCs and macrophages. The *in vitro* coculture experiments further confirmed this finding.

Inflammasomes are a variety of protein complexes that could recognize inflammation-inducing stimuli and control inflammatory cytokine production [32]. Among them, the NLRP3 (nucleotide-binding domain, leucine-rich-repeat-containing family, and pyrin domain-containing 3) inflammasome is one of the most widely studied inflammasomes. The NLRP3 inflammasome, consisting of the regulatory subunit NLRP3, adaptor ASC, and effector caspase-1, is a molecular complex that could be activated to trigger immune defenses through secreting inflammatory cytokines such as IL-1β or IL-18 [33, 34]. Previous researches showed that the NLRP3 inflammasome was upregulated and activated in the liver during sepsis [35, 36]. Our data revealed that NLRP3 inflammasome-mediated and IL-1β activation in septic liver tissue, and BMSCs inhibited NLRP3 activation and resultant IL-1β activation. Although the level of NLRP3 or its adaptor ASC did not reveal a significant alteration, its cellular localization changed. As inferred by our immunofluorescence results, the resting NLRP3 was localized in the endoplasmic reticulum, while under the condition of inflammasome activation, NLRP3 colocalized with endoplasmic reticulum and mitochondrion structures. Mitochondrial ROS was capable of inducing NLRP3 inflammasome activation [37]. As revealed in our data, with the addition of Mito-TEMPO (a mitochondria-targeted antioxidant), the relocalization of NLRP3 inflammasome was further attenuated, in combination with subsequent decreased activation of caspase-1 and IL-1β. Similar to the previous results, we observed that N-acetylcysteine (NAC, a general reactive oxygen inhibitor) abrogated the apparent increase in caspase-1 activation and IL-1β expression in BMDMs in response to LPS and ATP. These results suggested that the protective effect of BMSCs on the NLRP3 inflammasome was mediated by regulating mitochondrial ROS generation.

Maintaining a healthy mitochondrion population is important for cells. Autophagic clearance is the major pathway in mitochondrial turnover, termed as mitophagy [38]. Recently, Mahrouf-Yorgov et al. found that MSCs that engrafted into infarcted hearts of mice could reduce damage via upregulating HO-1 and increasing mitochondrial biogenesis, and inhibition of mitophagy or HO-1 failed to protect against cardiac apoptosis [39]. Activation of the autophagy process has been reported to attenuate cardiac dysfunction and liver injury in septic mice [40–42]. Similarly, Carchman et al. demonstrated that mitophagy was necessary to prevent organ injury in sepsis, but the authors attributed this protective process to the activation of TLR9 signaling [43]. Parkin, an E3 ubiquitin ligase, promotes dysfunctional

mitochondrion clearance by autophagy [44]. In our current study, the results indicated that BMSCs increased Parkin-mediated mitophagy and decreased mtROS generation of BMDMs. Furthermore, inhibition of mitophagy with 3-MA agent blocked the inhibitory role of BMSCs in IL-1β activation and mitochondrial ROS production, indicating that the effect of BMSCs on inflammatory regulation and mitochondrial ROS generation was mainly mediated by mitophagy.

Although the data from our study bear some clinical relevance, several limitations remain. First, cardiac function depression in sepsis may be detoxified by various factors, such as inflammatory factors, which may not represent all contributors. We only observed the effects of MSCs, but the underlying mechanisms are still unclear. Second, the data were based on a murine CLP model, and the dose of BMSCs may be different in a clinical setting. Besides, as the *in vitro* cell study cannot fully simulate the *in vivo* circumstances, the weak link between *in vivo* and *in vitro* studies should be taken into consideration. Although the mechanisms of inflammasome inhibition by MSCs were dissected *in vitro*, it was less well confirmed *in vivo*. Therefore, more studies are warranted to confirm if our current findings are true for human MSCs in clinical settings.

5. Conclusion

BMSCs improved the murine survival rate and alleviated organ injury in experimental sepsis induced by CLP. BMSCs' beneficial effects were mediated by inhibiting NLRP3 inflammasome activation in macrophages, which was primarily through increasing the mitophagy of macrophages and decreasing mitochondrial ROS generation (Figure 8). Taken together, MSCs can act as promising cellular therapy, as an immune-modulator, for fighting against sepsis.

Conflicts of Interest

The authors have declared that no competing interest exists.

Authors' Contributions

Shuang Li, Hao Wu, and Dong Han contributed equally to this work.

Acknowledgments

This work was supported by the National Key Research Program of China (2016YFA0100903), National Funds for Distinguished Young Scientists of China (81325009), National Nature Science Foundation of China (81530058), (FCao BWS12J037), Innovation Team Grant of Shannxi Province (no. 2014KCT-20), and General Financial Grant from the China Postdoctoral Science Foundation (2017M613337).

Supplementary Materials

Supplementary 1. Figure S1: characterization and fate of injected of BMSCseGFP+. A. Differentiation potential of BMSCseGFP+. Fibroblast-like-shaped BMSCseGFP+ were GFP positive. Adipogenesis of BMSCseGFP+ under the adipogenic differentiation conditions was detected by oil red O staining. Osteogenesis was evaluated by Alizarin red S staining. Scale bar, 100 μm. B. Flow cytometry results show that BMSCseGFP+ were uniformly negative for CD34, CD45, and Sca-1 and positive for CD29, CD44, and CD90. C. Visualization of BMSCseGFP+ (red arrows) in C57BL/6 mice liver tissue at 1–6 h after intravenous injection. Scale bar, 100 μm. Data shown are representative of two (A, B) or three (C) independent experiments.

Supplementary 2. Figure S2: inhibition of ROS generation abolished caspase-1 activation. A. Western blot analysis for caspase-1 and IL-1β in lysates of BMDMs incubated for 1 h with NAC (Sigma-Aldrich, USA) (10 mM), which was followed by LPS and ATP. B. Semiquantitative analysis of the Western blots. Error bars represent the means ± s.e.m. $^{*}p < 0.05$ and $^{**}p < 0.01$. $n = 5$–10. The data are representative of at least three independent experiments.

Supplementary 3. Figure S3: confocal microscopy analysis of BMDMs stained for LC3 (green) and mitochondria (red) for colocalization as an indicator of mitophagy. Scale bar, 20 μm.

Supplementary 4. Figure S4: original images of caspase-1 p20 and IL-1β p17 in Figure 4.

Supplementary 5. Figure S5: relative mean fluorescence intensity (MFI) comparisons. A. BMDMs were treated with LPS (2 μg/ml, 4 hours) and ATP (5 mM, 0.5 h) (L + A). BMSCs were cocultured with BMDMs in transwell from ATP licensing for 2 h. BMDMs were stained with MitoSOX (5 μM) for the final 30 min and then analyzed by FlowJo 7.6.1(Becton, Dickinson & Company, USA). B. BMDMs stimulated with 3-MA (10 mM) for 6 h were stained with MitoSOX (5 μM) for 30 min and were then analyzed by FlowJo 7.6.1. The data are representative of three independent experiments.

Supplementary 6. Figure S6: colocalization of the NLRP3 and mitochondria. BMDMs expressing NLRP3 (green) were analyzed for the colocalization of NLRP3 with the mitochondria (red) using confocal microscopy. Scale bar, 20 μm.

References

[1] V. Liu, G. J. Escobar, J. D. Greene et al., "Hospital deaths in patients with sepsis from 2 independent cohorts," *JAMA*, vol. 312, no. 1, pp. 90–92, 2014.

[2] H. H. Chen, K. C. Lin, C. G. Wallace et al., "Additional benefit of combined therapy with melatonin and apoptotic adipose-derived mesenchymal stem cell against sepsis-induced kidney injury," *Journal of Pineal Research*, vol. 57, no. 1, pp. 16–32, 2014.

[3] J. Leentjens, M. Kox, J. G. van der Hoeven, M. G. Netea, and P. Pickkers, "Immunotherapy for the adjunctive treatment of sepsis: from immunosuppression to immunostimulation. Time for a paradigm change?," *American Journal of Respiratory and Critical Care Medicine*, vol. 187, no. 12, pp. 1287–1293, 2013.

[4] D. E. Fry, "Sepsis, systemic inflammatory response, and multiple organ dysfunction: the mystery continues," *The American Surgeon*, vol. 78, no. 1, pp. 1–8, 2012.

[5] K. Le Blanc, L. Tammik, B. Sundberg, S. E. Haynesworth, and O. Ringden, "Mesenchymal stem cells inhibit and stimulate mixed lymphocyte cultures and mitogenic responses independently of the major histocompatibility complex," *Scandinavian Journal of Immunology*, vol. 57, no. 1, pp. 11–20, 2003.

[6] J. E. Gotts and M. A. Matthay, "Mesenchymal stem cells and acute lung injury," *Critical Care Clinics*, vol. 27, no. 3, pp. 719–733, 2011.

[7] K. Németh, A. Leelahavanichkul, P. S. T. Yuen et al., "Bone marrow stromal cells attenuate sepsis via prostaglandin E_2-dependent reprogramming of host macrophages to increase their interleukin-10 production," *Nature Medicine*, vol. 15, no. 1, pp. 42–49, 2009.

[8] S. H. J. Mei, J. J. Haitsma, C. C. Dos Santos et al., "Mesenchymal stem cells reduce inflammation while enhancing bacterial clearance and improving survival in sepsis," *American Journal of Respiratory and Critical Care Medicine*, vol. 182, no. 8, pp. 1047–1057, 2010.

[9] N. Eid, Y. Ito, and Y. Otsuki, "Triggering of Parkin mitochondrial translocation in mitophagy: implications for liver diseases," *Frontiers in Pharmacology*, vol. 7, p. 100, 2016.

[10] Z. Zhong, A. Umemura, E. Sanchez-Lopez et al., "NF-κB restricts inflammasome activation via elimination of damaged mitochondria," *Cell*, vol. 164, no. 5, pp. 896–910, 2016.

[11] Y. Wang, Y. Nartiss, B. Steipe, G. A. McQuibban, and P. K. Kim, "ROS-induced mitochondrial depolarization initiates PARK2/PARKIN-dependent mitochondrial degradation by autophagy," *Autophagy*, vol. 8, no. 10, pp. 1462–1476, 2012.

[12] S. Geisler, K. M. Holmstrom, D. Skujat et al., "PINK1/Parkin-mediated mitophagy is dependent on VDAC1 and p62/SQSTM1," *Nature Cell Biology*, vol. 12, no. 2, pp. 119–131, 2010.

[13] C. Vasquez-Trincado, I. Garcia-Carvajal, C. Pennanen et al., "Mitochondrial dynamics, mitophagy and cardiovascular disease," *The Journal of Physiology*, vol. 594, no. 3, pp. 509–525, 2016.

[14] D. Rittirsch, M. S. Huber-Lang, M. A. Flierl, and P. A. Ward, "Immunodesign of experimental sepsis by cecal ligation and puncture," *Nature Protocols*, vol. 4, no. 1, pp. 31–36, 2009.

[15] Q. Pan, X. Qin, S. Ma et al., "Myocardial protective effect of extracellular superoxide dismutase gene modified bone marrow mesenchymal stromal cells on infarcted mice hearts," *Theranostics*, vol. 4, no. 5, pp. 475–486, 2014.

[16] K. Nakahira, J. A. Haspel, V. A. K. Rathinam et al., "Autophagy proteins regulate innate immune responses by inhibiting the release of mitochondrial DNA mediated by the NALP3 inflammasome," *Nature Immunology*, vol. 12, no. 3, pp. 222–230, 2011.

[17] I. Pineda-Torra, M. Gage, A. de Juan, and O. M. Pello, "Isolation, culture, and polarization of murine bone marrow-derived and peritoneal macrophages," *Methods in Molecular Biology*, vol. 1339, pp. 101–109, 2015.

[18] D. Wang, P. Luo, Y. Wang et al., "Glucagon-like peptide-1 protects against cardiac microvascular injury in diabetes via a cAMP/PKA/Rho-dependent mechanism," *Diabetes*, vol. 62, no. 5, pp. 1697–1708, 2013.

[19] T. J. Wannemuehler, M. C. Manukyan, B. D. Brewster et al., "Advances in mesenchymal stem cell research in sepsis," *Journal of Surgical Research*, vol. 173, no. 1, pp. 113–126, 2012.

[20] J. Walter, L. B. Ware, and M. A. Matthay, "Mesenchymal stem cells: mechanisms of potential therapeutic benefit in ARDS and sepsis," *The Lancet Respiratory Medicine*, vol. 2, no. 12, pp. 1016–1026, 2014.

[21] H. Yagi, A. Soto-Gutierrez, Y. Kitagawa, A. W. Tilles, R. G. Tompkins, and M. L. Yarmush, "Bone marrow mesenchymal stromal cells attenuate organ injury induced by LPS and burn," *Cell Transplantation*, vol. 19, no. 6-7, pp. 823–830, 2010.

[22] A. Krasnodembskaya, Y. Song, X. Fang et al., "Antibacterial effect of human mesenchymal stem cells is mediated in part from secretion of the antimicrobial peptide LL-37," *Stem Cells*, vol. 28, no. 12, pp. 2229–2238, 2010.

[23] A. Krasnodembskaya, G. Samarani, Y. Song et al., "Human mesenchymal stem cells reduce mortality and bacteremia in gram-negative sepsis in mice in part by enhancing the phagocytic activity of blood monocytes," *American Journal of Physiology Lung Cellular and Molecular Physiology*, vol. 302, no. 10, pp. L1003–L1013, 2012.

[24] K. E. Fenton and M. M. Parker, "Cardiac function and dysfunction in sepsis," *Clinics in Chest Medicine*, vol. 37, no. 2, pp. 289–298, 2016.

[25] R. Latini, P. Caironi, and S. Masson, "Cardiac dysfunction and circulating cardiac markers during sepsis," *Minerva Anestesiologica*, vol. 82, no. 6, pp. 697–710, 2016.

[26] B. R. Weil, J. L. Herrmann, A. M. Abarbanell, M. C. Manukyan, J. A. Poynter, and D. R. Meldrum, "Intravenous infusion of mesenchymal stem cells is associated with improved myocardial function during endotoxemia," *Shock*, vol. 36, no. 3, pp. 235–241, 2011.

[27] T. B. Rogers, S. Pati, S. Gaa et al., "Mesenchymal stem cells stimulate protective genetic reprogramming of injured cardiac ventricular myocytes," *Journal of Molecular and Cellular Cardiology*, vol. 50, no. 2, pp. 346–356, 2011.

[28] D. Rittirsch, M. A. Flierl, and P. A. Ward, "Harmful molecular mechanisms in sepsis," *Nature Reviews Immunology*, vol. 8, no. 10, pp. 776–787, 2008.

[29] B. R. Weil, M. C. Manukyan, J. L. Herrmann et al., "Mesenchymal stem cells attenuate myocardial functional depression and reduce systemic and myocardial inflammation during endotoxemia," *Surgery*, vol. 148, no. 2, pp. 444–452, 2010.

[30] C. L. Chang, S. Leu, H. C. Sung et al., "Impact of apoptotic adipose-derived mesenchymal stem cells on attenuating organ damage and reducing mortality in rat sepsis syndrome induced by cecal puncture and ligation," *Journal of Translational Medicine*, vol. 10, no. 1, p. 244, 2012.

[31] H. K. Yip, Y. C. Chang, C. G. Wallace et al., "Melatonin treatment improves adipose-derived mesenchymal stem cell therapy for acute lung ischemia-reperfusion injury," *Journal of Pineal Research*, vol. 54, no. 2, pp. 207–221, 2013.

[32] T. Strowig, J. Henao-Mejia, E. Elinav, and R. Flavell, "Inflammasomes in health and disease," *Nature*, vol. 481, no. 7381, pp. 278–286, 2012.

[33] R. Zhou, A. S. Yazdi, P. Menu, and J. Tschopp, "A role for mitochondria in NLRP3 inflammasome activation," *Nature*, vol. 469, no. 7329, pp. 221–225, 2011.

[34] T. Murakami, J. Ockinger, J. Yu et al., "Critical role for calcium mobilization in activation of the NLRP3 inflammasome," *Proceedings of the National Academy of Sciences of the United States of America*, vol. 109, no. 28, pp. 11282–11287, 2012.

[35] Y. Wu, J. Ren, B. Zhou et al., "Gene silencing of non-obese diabetic receptor family (NLRP3) protects against the sepsis-induced hyper-bile acidaemia in a rat model," *Clinical and Experimental Immunology*, vol. 179, no. 2, pp. 277–293, 2015.

[36] M. Ganz, T. Csak, B. Nath, and G. Szabo, "Lipopolysaccharide induces and activates the Nalp3 inflammasome in the liver," *World Journal of Gastroenterology*, vol. 17, no. 43, pp. 4772–4778, 2011.

[37] M. E. Heid, P. A. Keyel, C. Kamga, S. Shiva, S. C. Watkins, and R. D. Salter, "Mitochondrial reactive oxygen species induces NLRP3-dependent lysosomal damage and inflammasome activation," *The Journal of Immunology*, vol. 191, no. 10, pp. 5230–5238, 2013.

[38] I. Kim, S. Rodriguez-Enriquez, and J. J. Lemasters, "Selective degradation of mitochondria by mitophagy," *Archives of Biochemistry and Biophysics*, vol. 462, no. 2, pp. 245–253, 2007.

[39] M. Mahrouf-Yorgov, L. Augeul, C. C. Da Silva et al., "Mesenchymal stem cells sense mitochondria released from damaged cells as danger signals to activate their rescue properties," *Cell Death and Differentiation*, vol. 24, no. 7, pp. 1224–1238, 2017.

[40] C. H. Hsieh, P. Y. Pai, H. W. Hsueh, S. S. Yuan, and Y. C. Hsieh, "Complete induction of autophagy is essential for cardioprotection in sepsis," *Annals of Surgery*, vol. 253, no. 6, pp. 1190–1200, 2011.

[41] Y. T. Yen, H. R. Yang, H. C. Lo et al., "Enhancing autophagy with activated protein C and rapamycin protects against sepsis-induced acute lung injury," *Surgery*, vol. 153, no. 5, pp. 689–698, 2013.

[42] C. W. Lin, S. Lo, D. S. Perng et al., "Complete activation of autophagic process attenuates liver injury and improves survival in septic mice," *Shock*, vol. 41, no. 3, pp. 241–249, 2014.

[43] E. Carchman and B. Zuckerbraun, "Mitophagy/mitochondrial biogenesis is necessary to prevent organ injury in sepsis and is dependent on TLR9 signaling," *Journal of the American College of Surgeons*, vol. 213, no. 3, article S59, 2011.

[44] N. C. Chan, A. M. Salazar, A. H. Pham et al., "Broad activation of the ubiquitin-proteasome system by Parkin is critical for mitophagy," *Human Molecular Genetics*, vol. 20, no. 9, pp. 1726–1737, 2011.

Hindawi
Oxidative Medicine and Cellular Longevity
Volume 2018, Article ID 9797146, 10 pages
https://doi.org/10.1155/2018/9797146

Research Article

Granulocyte Colony-Stimulating Factor Alleviates Bacterial-Induced Neuronal Apoptotic Damage in the Neonatal Rat Brain through Epigenetic Histone Modification

Yung-Ning Yang,[1,2,3] Yu-Tsun Su,[1,2] Pei-Ling Wu,[1,2,3] Chun-Hwa Yang,[1] Yu-Chen S. H. Yang,[4] Jau-Ling Suen,[3,5,6] and San-Nan Yang[1,2]

[1]*Department of Pediatrics, E-DA Hospital, Kaohsiung, Taiwan*
[2]*School of Medicine, I-Shou University, Kaohsiung, Taiwan*
[3]*Graduate Institute of Medicine, College of Medicine, Kaohsiung Medical University, Kaohsiung, Taiwan*
[4]*Joint Biobank, Office of Human Research, Taipei Medical University, Taipei, Taiwan*
[5]*Research Center for Environmental Medicine, Kaohsiung Medical University, Kaohsiung, Taiwan*
[6]*Department of Medical Research, Kaohsiung Medical University Hospital, Kaohsiung, Taiwan*

Correspondence should be addressed to San-Nan Yang; ancaly2022@gmail.com

Received 30 August 2017; Revised 7 November 2017; Accepted 23 November 2017; Published 1 February 2018

Academic Editor: Partha Mukhopadhyay

Bacterial meningitis during the perinatal period may cause long-term neurological deficits. The study investigated whether bacterial lipopolysaccharide (LPS) derived from *E. coli.* led to neuronal apoptosis with an impaired performance of long-term cognitive function involving the activation of histone modification in the TNF-α gene promoter. Further, we looked into the therapeutic efficacy of granulocyte colony-stimulating factor (G-CSF) in a neonatal brain suffering from perinatal bacterial meningitis. We applied the following research techniques: neurobehavioral tasks, confocal laser microscopy, chromatin immunoprecipitation, and Western blotting. At postnatal day 10, the animals were subjected to LPS and/or G-CSF. The target brain tissues were then collected at P17. Some animals (P45) were studied using neurobehavioral tasks. The LPS-injected group revealed significantly increased expression of NF-κB phosphorylation and trimethylated H3K4 in the *TNFA* gene promoter locus. Furthermore, the caspase-3, neuronal apoptosis expression, and an impaired performance in cognitive functions were also found in our study. Such deleterious outcomes described above were markedly alleviated by G-CSF therapy. This study suggests that selective therapeutic action sites of G-CSF through epigenetic regulation in the *TNFA* gene promoter locus may exert a potentially beneficial role for the neonatal brain suffering from perinatal bacterial-induced meningitis.

1. Introduction

Infectious disease especially meningitis during the neonatal or perinatal period may incur a high risk of causing brain damage and long-term development impairment such as cerebral palsy, schizophrenia, affective disorders, autism, and stroke [1]. Although many researchers had investigated how to prevent neurological sequelae after bacterial meningitis, its incidence does not seem to have significantly decreased over the last decade [2]. Current adjunctive therapeutic options are limited, and therefore ongoing research into the pathophysiology due to bacterial meningitis aims at providing the scientific basis for better adjunctive options [3].

Lipopolysaccharides, a well-known endotoxin and lipoglycans, are a membrane structural constituent of gram-negative bacteria. The immune response caused by lipopolysaccharide (LPS) due to bacterial infection may trigger the production of inflammatory cytokines. LPS stimulates the innate immune system to increase the expression of interleukin 1, NF-κB, and tumor necrosis factor-alpha (TNF-α) [4, 5]. In the brain, LPS was found to bind to toll-like receptor 4 (TLR4), a kind of membrane protein, and then

to trigger the nuclear factor-kappa B (NF-κB) pathway that regulated the immune system [6] and controlled neuroprotection and neurodegeneration [7–9]. The activated NF-κB pathway has been reported to induce the transcription of tumor necrosis factor-alpha (TNF-α) with LPS exposure [9, 10]. Furthermore, this induced TNF-α expression has been associated with acute or chronic inflammatory disease in the central nervous system (CNS) [11]. When it comes to bacterial infection, LPS exposure was reported to induce microglia to increase the secretion of TNF-α that increased neuron apoptosis via the caspase-3 pathway in the developing cerebral cortex [12]. In addition to increased apoptosis, LPS exposure was found to lead to decreased neurogenesis in the brain after [13, 14]. Therefore, bacterial meningitis may cause apoptosis of a neuron cell and decease neurogenesis though the NF-κB and TNF-α pathways. The consequences of neonatal bacterial meningitis have been extensively investigated in the past, but the mechanisms related to long-term neurological dysfunctions have yet to be well documented.

Granulocyte colony-stimulating factor (G-CSF) is a kind of glycoprotein that has been used in patients with neutropenia in the past [15, 16]. Associated with the effects of neurogenesis, antiapoptosis, anti-inflammation, neurotrophy, and angiogenesis, G-CSF has neuroprotective effects on the mammalian adult brain [17–20]. G-CSF can stimulate bone marrow to produce stem cells and mobilize these stem cells from the bone marrow to the brain to induce neurogenesis in adult animals with stroke and improve functional outcomes [17, 18]. Additionally, G-CSF can reduce caspase-3 and thereby decrease apoptosis of cortical neurons [21]. Furthermore, G-CSF can also improve neurogenesis recovery and the decreased performance of long-term cognitive functions caused by perinatal hypoxia in the neonatal rat brain [22]. Moreover, the antiapoptotic effect of G-CSF in treating perinatal hypoxia pups has been observed via reduction in cleaved caspase-3 activity [23]. However, whether or not G-CSF alleviates bacterial-induced apoptosis in the neonatal rat brain still requires further investigation.

Epigenetic modification at the *TNFA* gene locus that modulates the expression of TNF-α mRNA and protein expression results from a concerted and complex network of regulation such as DNA methylation, histone modification, and chromatin remodeling [24, 25]. The studies frequently analyzed monocytes and macrophages. However, there is no published experimental evidence showing whether histone modification in the *TNFA* gene locus also regulates TNF-α mRNA and protein expression in the brain of pups with LPS. Hence, in this study, we also investigated whether LPS enhance TNF-α expression via this epigenetic modification and G-CSF alleviated LPS-mediated histone modifications at the *TNFA* gene locus. Furthermore, in order to examine the performance of long-term cognitive functions in pups with neonatal bacterial infection being treated with G-CSF, we also used an eight-arm radial maze task to investigate the pups' cued reference and spatial working memory.

2. Materials and Methods

2.1. Experimental Animal Protocols. The Animal Care and Use Committee at Kaohsiung Medical University and E-DA Hospital (Kaohsiung, Taiwan) approved all experimental procedures. Sprague-Dawley (SD) rats were provided with a 12 hr light/dark cycle and housed in the animal care facility. The animals were divided into four experimental groups as follows: vehicle-control (control group), LPS-treated-alone group (LPS group), G-CSF- (30 μg/kg) alone group (G-CSF group), and LPS-treated plus G-CSF (30 μg/kg) group (LPS + G group), on postnatal day ten (P10) that were considered compatible with human neonates [26]. To determine whether a single inflammatory event during development can influence long-term cognitive functions in later life, male rats were injected intracerebrally. The scalp was shaved, and a burr hole was drilled 1 mm caudal to the bregma and 2.0 mm lateral to the midline. LPS at the desired dosage was injected via a Hamilton microsyringe into the ventricle over a 5 min period. Control groups received isovolumetric i.c.v. injection of saline. Mice were maintained at 36°C with LPS (*Escherichia coli*, serotype O26:B6; 1 mg/kg) or pyrogen-free saline. Immediately after LPS injection, additional groups of rats were also injected with G-CSF (30 μg/kg, single injection/day, subcutaneous injection) according to our previous study [22]. Brain tissue specimens of the target brain regions were collected on P17, and the memory functions and spatial learning were analyzed on P37–P58 employed as standard descriptions of adolescence [27].

2.2. Brain Tissue Slice Preparation. Bacterial meningitis may cause temporal lobe damage and epilepsy disorder [28, 29]. On P17, temporal lobe slices (400 μm) were collected and immediately placed into artificial cerebrospinal fluid (ACSF) in a humidified atmosphere of 95% O_2/5% CO_2 at 34.0 ± 0.5°C in an incubation chamber for an equilibrium period of at least one hour [30]. To obtain the target brain regions, the brain slices were incubated with ice-cold oxygenated ACSF and then cut into tissue blocks (0.1 × 0.5 cm) within 15 seconds of slicing the tissue. The brain tissues were then immediately frozen at −80°C until analysis, and all tissue slices were only ever thawed once.

2.3. Immunoblotting. After our customized treatments, the cells were lysed into cell lysis buffer (10 mM Tris (pH 7.4), 150 mM NaCl, 2 mM EDTA, 0.2% Triton X-100, 1 mM PMSF, and 1× protease inhibitor mixture). The protein concentration was then determined by using the BCA assay (Thermo Scientific, Rockford, IL, USA). Cell lysates were separated on SDS-PAGE and then transferred to nitrocellulose membranes. They were probed with an antibody against NF-κB (AbFrontier/LF-PA0062), pNF-κB (AbFrontier/LF-PA20342), TNF-α (SANTA CRUZ/SC-1351), and caspase-3 (Cell Signaling #9662). Our secondary antibodies were either rabbit anti-mouse IgG or goat anti-rabbit IgG (1 : 3000), depending on the primary antibody. Finally, the immunoreactive proteins were detected using the BioSpectrum 810 Imaging System (UVP).

2.4. Chromatin Immunoprecipitation Assay (ChIP). As in our previous study [31], 5×10^5 cells were treated for 10 min at room temperature with 1% formaldehyde, followed by sonication of DNAs and the immunoprecipitation of chromatin and then purification with the ChIP kit (ChIP kit number 17-295; Upstate Biotechnology, Lake Placid, NY, USA). Probes and primers were designed by analyzing the proximal promoter and intronic enhancer regions of the TNFA gene for the polymerase chain reaction (PCR) amplification of ChIP products. These regions included the following subregions relative to the transcription start site: TNF1 (T1; −2667 to −2686), TNF2 (T2; −2183 to −2202), TNF3 (T3; −1653 to −1672), TNF4 (T4; −174 to −496), and TNF5 (T5; −205 to −224). PCRs were performed on the ABI 7700 TaqMan thermocycler (Applied Biosystems).

2.5. Evaluation of Apoptosis. We performed double immunofluorescence analysis using laser-scanning confocal microscopy to analyze apoptosis in neuron cells in tissue. The staining protocol was described in a previous study [22] and briefly summarized in the following sentences. The brain samples were coronally cut at 30 μm and stained with anti-neuronal nuclei (NeuN) (clone A60, MAB377; Chemicon, Temecula, CA, USA) for neuron cell identification and with TUNEL (Sigma-Aldrich, 11684795910) for DNA break detection. TUNEL was performed according to the manufacturer's instruction. Secondary amplification was performed using a Cy3-conjugated anti-mouse antibody for NeuN staining and fluorescein-conjugated antibody for TUNEL staining. Negative controls for NeuN and TUNEL double labeling were obtained by omitting either the anti-NeuN antibody or the TdT enzyme in the TUNEL reaction. Images of epifluorescence were collected on a Leica (Nussloch, Germany) DMIRE2 microscope, and images of confocal fluorescence were collected using a Zeiss (Thornwood, NY, USA) LSM510 microscope.

2.6. Eight-Arm Radial Maze Task. Spatial memory tasks such as eight-arm radial maze and Morris water maze are tools used in evaluating temporal lobe lesions [32]. As in our previous study [33], an eight-arm radial maze was used to train rats on two memory tasks. In this test, two memory deficits can be recorded: (1) working memory error (WME): a rat goes to an arm with bait that it has already visited, and (2) reference memory error (RME): a rat visits an arm with no bait. If the forepaws of the rat crossed the midline of the arm, this was defined as having visited that arm. The rats were defined as having successfully completed the cued reference memory and spatial working memory tasks when there were no RMEs or WMEs for at least 2 days within a 3-day period.

2.7. Statistical Analysis. All data are presented as mean ± SEM. Statistical differences were determined by using one-way ANOVA followed by Bonferroni's t-test for post hoc multiple comparisons. A statistical significance level of $p < 0.05$ was applied to all tests.

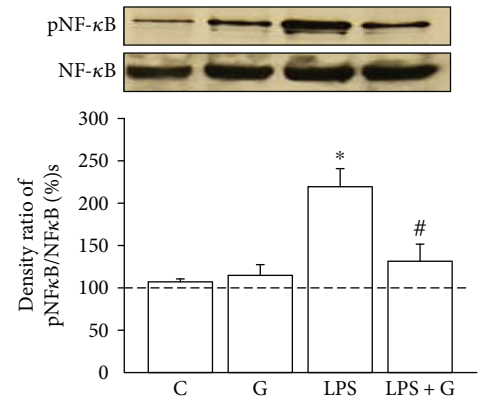

Figure 1: G-CSF alleviated the elevated pNF-κB due to LPS treatment. Western blot analysis was used to detect the phosphorylated NF-κB (pNF-κB) p65 levels in the brain cell. The experimental groups are indicated as follows: vehicle-control (C), LPS group (LPS), G-CSF group (G), and LPS + G group (LPS + G) ($n = 5$ animals for each experimental group). The results were expressed as relative level of pNF-κB to total NF-κB. In the LPS group, the ratio of pNF-κB to total NF-κB was significantly higher compared to that in the LPS + G group and control group. $^*p < 0.05$ compared with the control group. $^\#p < 0.05$ compared with the LPS group. Data are mean ± standard error of mean.

3. Results

3.1. G-CSF Alleviated the Enhancement of Phosphorylated NF-κB p65 in the Brain of Pups with LPS Treatment. Pups treated with LPS increased the expression of phosphorylated NF-κB p65 in the brain. There was a significant enhancement of phosphorylated NF-κB p65 (Figure 1) in the LPS group compared with the control group (LPS 219.4 ± 21.1% versus control 107 ± 3.2%, $p < 0.05$). There was also no significant difference in the LPS + G group compared to the control group. The results suggest that the changes of the rat brain experimentally exposed to LPS involved the NF-κB signaling pathway and that increased phosphorylated NF-κB expression could be alleviated by G-CSF therapy.

3.2. G-CSF Alleviated the Enhancement of TNF-α in the Brain of Neonatal Rats Treated with LPS. To demonstrate that LPS influenced the downstream signaling pathway of NF-κB, we examined the concentrations of TNF-α. The LPS group showed a significantly increased expression of TNF-α (Figure 2) compared with the control group (LPS 181.5± 9.2% versus control 103 ± 1.6%, $p < 0.05$). In the LPS + G group, TNF-α expression was significantly reduced compared with that in the LPS group. These findings reveal that G-CSF might be effective for alleviating the increase in TNF-α expression in the brain of pups experimentally exposed to LPS.

3.3. LPS-Mediated Histone Modifications at the TNFA Gene Locus. Epigenetic modifications regulate the expression of TNF-α in response to acute stimulations such as by LPS [24, 34]. A recent study analyzing macrophages and monocytes demonstrated that acetylated H3 and H4 mark active

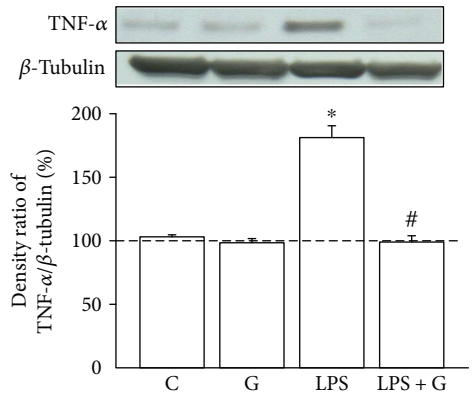

Figure 2: G-CSF alleviated the elevation of TNF-α expression levels. Effect of G-CSF on LPS-induced production of TNF-α. The experimental groups are indicated as follows: vehicle-control (C), LPS (LPS), G-CSF (G), and LPS + G (LPS + G) ($n = 5$ animals for each experimental group). The level of TNF-α expression was elevated in the LPS group compared with the control group. There were no significant differences between the LPS + G-CSF and control groups. $^{*}p < 0.05$ compared with the vehicle-control group. $^{\#}p < 0.05$ compared with the LPS group. β-Actin levels performed in parallel served as controls.

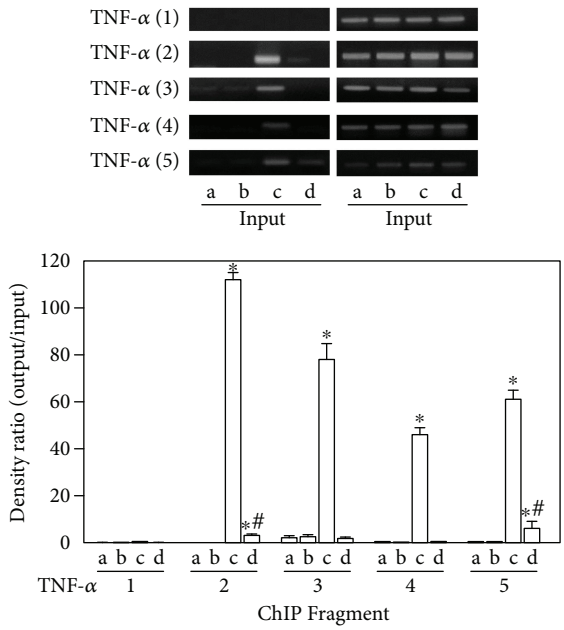

Figure 3: G-CSF therapy involved histone acetylation in the regulatory effect of LPS treatment on TNF-α expression. ChIP analyses of the relative levels of acetylated H3 at the *TNFA* gene locus included the following subregions relative to the transcription start site: TNF1 (T1; −2667 to −2686), TNF2 (T2; −2183 to −2202), TNF3 (T3; −1653 to −1672), TNF4 (T4; −174 to −496), and TNF5 (T5; −205 to −224). The groups (a–d) are as follows: (a) control, (b) G-CSF, (c) LPS, and (d) LPS + GCSF. The relative levels were normalized to the input DNAs and are shown as mean ± SD of the study subjects. The level of histone acetylation was significantly higher in the LPS group compared with the control group. $^{*}p < 0.05$ compared with the control group. $^{\#}p < 0.05$ compared with the LPS group.

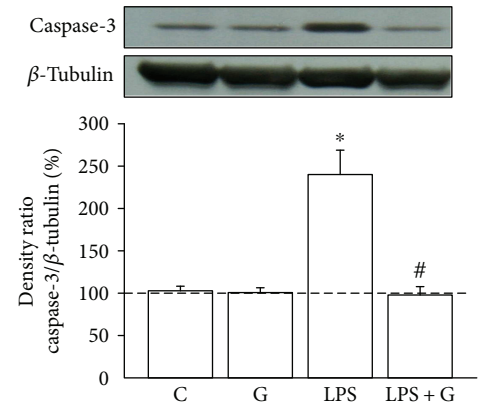

Figure 4: G-CSF alleviated the elevation of caspase-3 activity in pups treated with LPS. Effect of G-CSF on caspase-3 activity in the brain of pups experimentally exposed to LPS. The experimental groups are indicated as follows: vehicle-control (C), LPS (LPS), G-CSF (G), and LPS + G (LPS + G) ($n = 5$ animals for each experimental group). Caspase-3 activity was significantly elevated in the LPS group compared with the vehicle-control group. The caspse-3 activity also showed no significant differences between the LPS + G and control groups. $^{*}p < 0.05$ compared with the control group. $^{\#}p < 0.05$ compared with the LPS group. β-Actin levels performed in parallel served as controls.

transcription in the *TNFA* gene locus [24]. To examine whether the *TNFA* gene locus underwent histone modifications in neurons as the result of the LPS treatment and NF-κB activation, we performed ChIP analyses of the pups' brains treated with LPS, using PCR primers corresponding to five subregions (TNF1–5) in the TNFA promoter of the *TNFA* gene. The results showed that compared to the vehicle-control group, the neonatal rat brains treated with LPS significantly presented histone modifications at the *TNFA* gene locus. In Figure 2, upregulated TNF-α expression was noted in LPS-treated neurons. ChIP analyses revealed increased levels of trimethylated H3K4 at the promoter subregions, TNF2–5, of the *TNFA* gene in the neonatal rat brain of the LPS group (Figure 3). Further, a significant increase in trimethylated H3K4 at the TNF2–5 promoter subregions (Figure 3) was seen in the LPS + GSF group. This indicates that G-CSF can alleviate the brain damage of perinatal LPS exposure via epigenetic regulation in the *TNFA* gene promoter locus.

3.4. G-CSF Decreased Caspase-3 Activity Enhanced by LPS Treatment in the Brains of Neonatal Rats. Since we observed that G-CSF had anti-inflammatory effects and was regulated via epigenetic modification, we then investigated the antiapoptotic effect of G-CSF. As can be seen in Figure 4, caspase-3 activity in the LPS group was significantly higher than that in the control group (LPS 240.6 ± 28.1% versus control 103.4 ± 5.1%, $p < 0.05$). In the LPS + G group, caspase-3 activity was significantly lower compared with that in the LPS group, but no statistical significance was reached with respect to the control group. Therefore, G-CSF was found to have an antiapoptotic effect by decreasing the

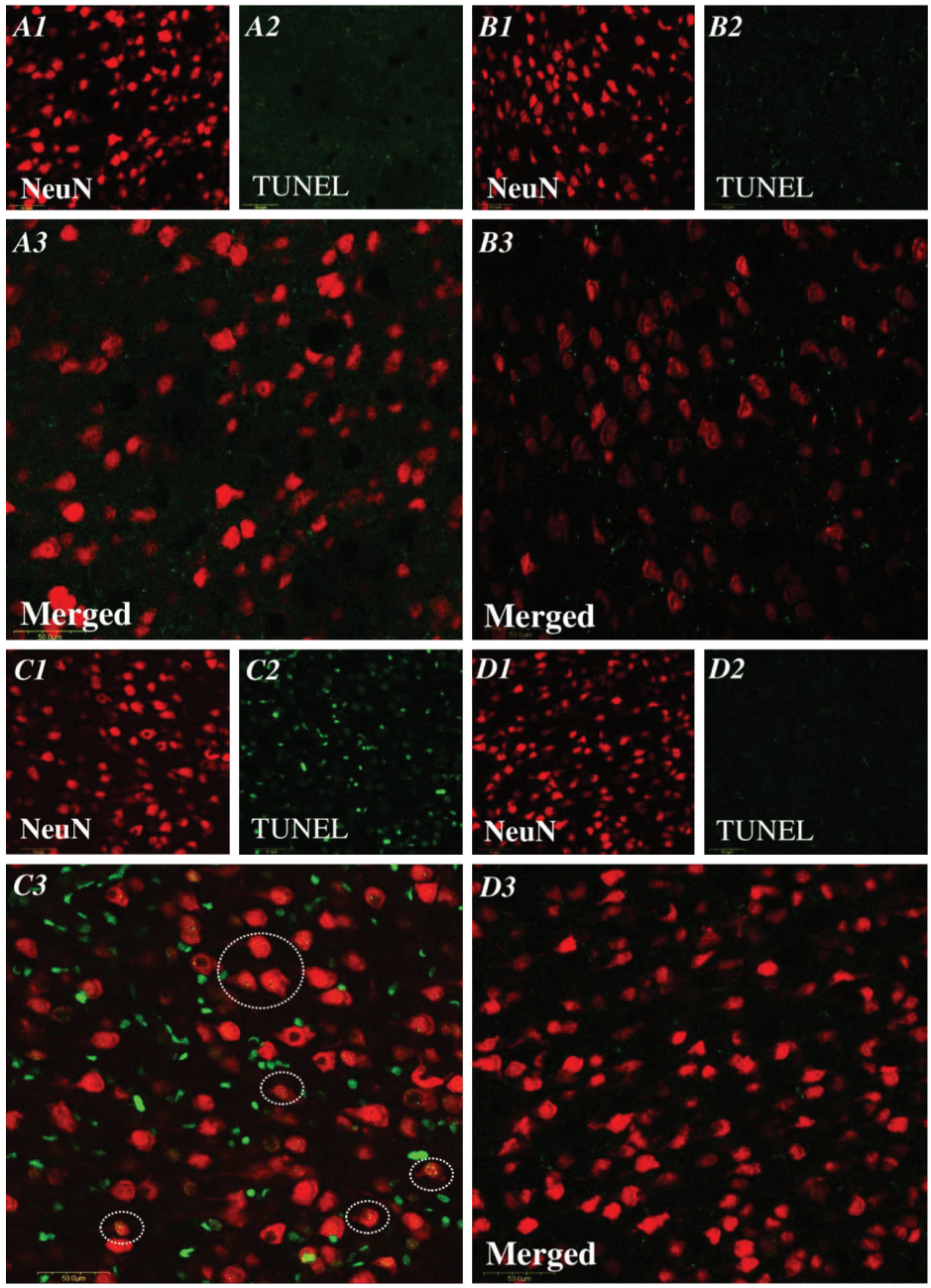

Figure 5: Effects of G-CSF on the increasing expression of neuronal apoptosis with LPS treatment. Colocalization of neuronal nucleus- (NeuN, red for neuron identification) and TUNEL- (green for apoptotic cells) positive cells, as assessed on P17, was identified by double immunofluorescence staining under laser-scanning confocal microscopy. The NeuN-positive cells (1), TUNEL-positive cells (2), and the combined pictures of the NeuN- and TUNEL-positive cells (3) are as follows: vehicle-control (A1–3), G-CSF (B1–3), LPS (C1–3), and LPS + G (D1–3) (30 mg/kg). The dotted circles reveal the representative neuronal apoptosis. Bar = 50 μm.

intensified caspase-3 activity in pups experimentally treated with LPS.

3.5. Evaluation of the Antiapoptotic Effect of G-CSF in Pup's Brain after Treatment with LPS. To confirm the decrease in caspase-3 activity, a confocal microscope was used to determine whether the G-CSF therapy alleviated the apoptosis in the brain of pups after LPS. We used neuronal marker NeuN (for mature neurons) and TUNEL to assess the level of apoptosis in the brain of pups. A declining trend in the coexpression of NeuN-positive cells with TUNEL-positive cells was revealed in the neonatal LPS group (Figure 5(c)) compared with the control rats (Figure 5(a)). In contrast, the increase in the number of TUNEL-positive cells colocalizing with NeuN-positive cells was observed in the LPS + G group (Figure 5(d)). In a quantitative analysis (Figure 6), the average number of cells exhibiting double staining with NeuN-positive and TUNEL-positive cells within the counted areas was significantly higher in the LPS group compared to the control group (LPS 45.1 ± 4.2 cells/μm^2 versus control

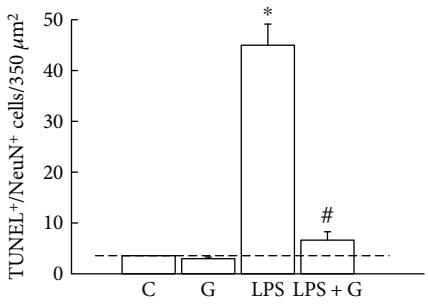

Figure 6: Quantified analysis of the effects of G-CSF on the increased expressions of neuronal apoptosis with LPS treatment. The experimental groups are indicated as follows: control (C), G-CSF (G), LPS (LPS), and LPS + G (LPS + G) (animals for each experimental group). Colocalization of neuronal nucleus- (NeuN-) positive and TUNEL-positive cells indicates apoptotic neuronal cells. $^{*}p < 0.05$ compared with the vehicle-control group. $^{\#}p < 0.05$ compared with the LPS group. Data are presented as mean ± standard error of the mean.

3.6 ± 0.1 cells/μm^2, 5 slides per animal, 5 animals, $p < 0.05$). In the LPS + G therapy, there was no significant difference with respect to the control group, but there was a significant decrease in the effect of apoptosis with respect to the LPS group. These results revealed that G-CSF therapy had a significant efficacy against the apoptosis caused by neonatal LPS treatment.

3.6. Using Eight-Arm Radial Maze Task to Evaluate Long-Term Cognitive Function. Figure 7 shows the long-term cognitive deficits in the working and cued reference memory tasks in the rats postneonatally treated with LPS after repeated daily training with the eight-arm maze task. Compared with the control group, the LPS group had more mean WMEs ($n = 10$ animals, $p < 0.05$, Figure 7(a)) and RMEs ($n = 10$ animals, $p < 0.05$, Figure 7(b)) in the first few days of life. In the LPS + G group, G-CSF therapy alleviated the decrease in mean RME and WME compared with that in the LPS-treated-alone group. Furthermore, the LPS group exhibited a significant increase in total mean RMEs and total mean WMEs compared with both the control and LPS + G groups. These results suggest that LPS exposure of the neonatal brain can lead to a decline in the ability of spatial memory formation and the insult can be alleviated after G-CSF therapy.

4. Discussion

In this study, our results show that the G-CSF therapy was useful in treating bacterial meningitis of neonates. Firstly, G-CSF alleviated the LPS-induced brain damage through the NF-κB pathway. Secondly, the effect of G-CSF therapy was via epigenetic regulation in the *TNFA* gene promoter locus by selective therapeutic action sites. Thirdly, G-CSF also diminished the increase in caspase-3 expression and apoptosis. Fourthly, working and cued reference memory impairments due to LPS exposure were alleviated by G-CSF therapy.

LPS, associated with gram-negative bacteria, was recognized by TLR4 to induce brain injury and increase the TNF-α expression via the NF-κB pathway [9]. To activate the NF-κB pathway, it depended on IκB kinase phosphorylation of the inhibitory molecules and phosphorylation of the P65 protein. Then, the phosphorylation of the P65 protein was translocated into the nucleus [35, 36]. This phosphorylated P65 protein has the ability to recruit histone acetyltransferases and lead to the production of proinflammatory factors, such as TNF-α. This study's findings are compatible with those of a previous study in that the LPS-exposed neonatal brain enhanced the expression of phosphorylated NF-κB p65 and TNF-α [35]. Several studies have established the possible mechanism explaining how LPS affects the production of TNF-α in adults. In this study, we provided evidence of this pathway in the neonatal rat brain.

Trimethylation of H3K4 played an important role in the initial recruitment of a methyltransferase complex (which includes a methyltransferase, mixed lineage leukemia (MLL), and WD repeat domain 5 (WDR5) protein scaffolds), which in turn mediates dimethylation to trimethylation conversion of histone H3 at K4 [37]. MLL1, one of the six members of the MLL family, has been reportedly associated with the P65 protein of the NF-κB family [38]. In the innate immune system, a previous study reported that the NF-κB regulated its downstream gene transcription (TNF-α) via MLL1 [38]. In the CNS, LPS-regulated TNF-α expression might also occur via NF-κB and its downstream epigenetic modulation. Although there are very few data about how LPS regulate TNF-α in the brain, LPS-regulated TNF-α via NF-κB in brain microglia has been shown in some brain disorders [39]. This study's findings can shed some further light on this issue. We showed that LPS affected TNF-α expression via NF-κB and its downstream reaction of variable patterns of histone modifications in neuron cells. Additionally, the neuroprotective effect of G-CSF not only alleviated the increase in NF-κB expression but also elevated the histone trimethylation of H3K4. Therefore, at last in part, the LPS and G-CSF both regulated the TNF-α expression at the epigenetic level. Furthermore, the significant enhancement of trimethylated H3K4 was found at the TNF2–5 promoter subregions but not at all the TNF promoter subregions after LPS exposure. Moreover, the G-CSF therapy cannot repair all the damages caused by LPS treatment.

Caspases are a group of cysteinyl-aspartate-specific proteases that have a marked influence on apoptotic cell death [40, 41]. Pups treated with LPS may induce proinflammatory cytokine release, such as TNF-α. The increased expression of TNF-α protein may result in the increase in caspase-3 cleavage and cause neuron apoptosis [42]. Also, caspase-3 is considered to be the effector caspase that is activated by caspase-8, caspase-9, and caspase-10. Since G-CSF has been reported to modulate LPS-induced apoptosis in microvascular endothelial cells via caspase-3 [43], we investigated caspase-3 activity to explore the protective effect of G-CSF in LPS-induced brain injury. Even though there have been many recent studies investigating the way to decrease the damage of neonatal meningitis, their results have been limited. Our results demonstrate that G-CSF decreased

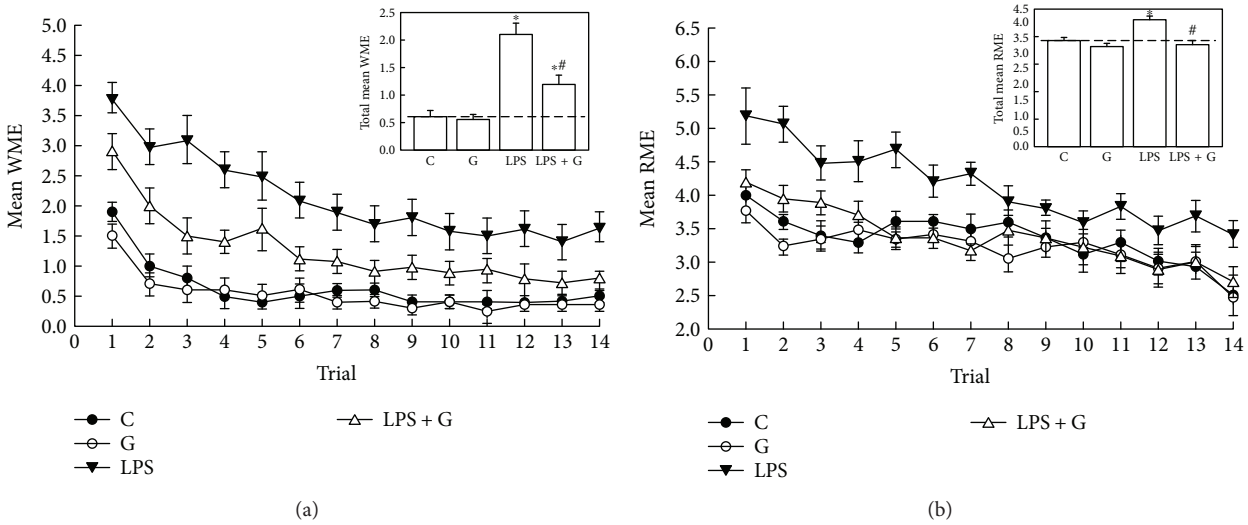

Figure 7: Impairment of the long-term performance of working and cued reference memory was found using an eight-arm radial maze task after LPS exposure. (a) One trial/day over 15 trials and average amount of working memory errors. The inset box reveals the average total mean working memory errors. (b) One trial/day over 15 trials and average amount of cued reference memory errors. The inset box reveals the average of total mean reference memory errors. Control group ($n = 10$ animals), G-CSF group ($n = 10$ animals), LPS group ($n = 10$ animals), and LPS + G group ($n = 10$ animals) are labeled as C, LPS, G, and LPS + G, respectively. Statistical analysis of the long-term performance of the working and cued reference memory revealed that the rats in the LPS group significantly differed from those in the vehicle-control and LPS + G groups. $^{*}p < 0.05$ compared with the control group. $^{\#}p < 0.05$ compared with the LPS group

caspase-3 activation and provided neuroprotective effects on fetal rat brain following experimental neonatal inflammation.

G-CSF has neuroprotective effects through the pathway of anti-inflammation, antiapoptosis, and neurogenesis in the CNS [44, 45]. Brain inflammation may cause blood-brain barrier injury and lead to leukocyte migration into injured tissue [44]. The anti-inflammatory effects of G-CSF happened though the pathway to reduce the level of cytokines, such as TNF-α and interlukin-1β, secreted by leukocytes, and to reduce T cell migration to the CNS [46]. G-CSF has also been noted to activate Bcl-2 and bcl-xl protein which reduces caspase-3 to prevent apoptosis through the JAK2/STAT3 pathway [21, 46]. This study provided evidence in a rat model that G-CSF can reduce the inflammatory response by reducing TNF-α via epigenetic regulation and can also have an antiapoptotic effect by reducing caspase-3 in neonatal meningitis.

In the CNS, neural stem cells, capable of self-renewal, are able to differentiate into neurons, oligodendrocytes, and astrocytes. When the brain suffers an injury or inflammatory accident, the permeability of the blood-brain barrier may change and then allow the G-CSF-induced neutrophil to pass [46]. This has been shown to stimulate the bone marrow to produce stem cells and induce their mobilization from the bone marrow to the brain, which will then induce neurogenesis in adult animals with ischemic or nonischemic disorder to improve functional outcomes [17, 18, 21, 23, 47–50]. Initially, G-CSF mobilizes hematopoietic progenitor cells from the bone marrow to peripheral blood, which then migrate to the site of neuronal damage through the CXC chemokine receptor 4 (CXCR4)/stromal cell-derived factor-1 (SDF-1) system [51]. Via the PIK/Akt pathway, G-CSF then enhances neurogenesis and neuroblast migration after stroke [46]. In addition, phosphorylated CREB$^{\text{Ser-133}}$ (pCREB$^{\text{Ser-133}}$), a DNA-binding transcription factor, plays an important role in the regulation of some immediate-early genes [52]. In an earlier study, we reported that G-CSF therapy alleviates the decrease in pCREB$^{\text{Ser-133}}$ and PSD-95 with NMDAR subunits within the CA1 region of the hippocampus after perinatal hypoxia and that G-CSF therapy provides beneficial effects for long-term cognitive deficits [53]. Given that LPS has been reported to modulate the NMDA receptor of glial cells with TNF-α [54], G-CSF might also work in treating brain damage from LPS exposure.

In recent years, our group has also focused on the neurogenesis effect of G-CSF on pups to investigate the therapy of perinatal hypoxia-ischemia brain injury [22]. G-CSF not only improved neurogenesis but also improved long-term cognitive function in the pups with experimentally induced perinatal hypoxia. However, whether the neuroprotective effects of G-CSF are also displayed in multiple brain regions after experimental LPS exposure remained unknown until the present study. Here, we have shown the efficacy of G-CSF therapy in the neonatal rat brain experimentally treated with LPS.

5. Conclusion

This study offers a new insight into how G-CSF therapy is able to recover the damage caused by LPS exposure through the decline of inflammation and apoptotic reaction and how G-CSF therapy can, at least in part, improve long-term functional outcomes (in terms of the improvement of impaired performance in spatial working and cued reference memory). And even more importantly, the effect of G-CSF was shown to occur through epigenetic regulation of the TNFA gene.

In addition, environment enrichment may provide a better outcome in LPS-exposed subjects, and early rehabilitation might be useful. This study suggests a new potential neuroprotective strategy that may be well tolerated with fewer side effects on the neonatal brain with bacterial meningitis. Although we are far from being able to apply this therapy in human neonates, our results provide an insight into neurological function defects in patients after neonatal bacterial infection.

Disclosure

The part of the preliminary data was presented as an abstract form in the 40th Session of the 18th Academic Symposium, Republic of China 2010.

Conflicts of Interest

The authors declare no conflict of interest.

Acknowledgments

This study was supported in part by grants from Yung-Ning Yang (EDAHP103028, EDAHP104032) and San-Nan Yang (NSC98-2320-B037-022-MY3, NCKUEDAH10304, and NCKUEDAH10411).

References

[1] M. Xu, Z. L. Sulkowski, P. Parekh et al., "Effects of perinatal lipopolysaccharide (LPS) exposure on the developing rat brain; modeling the effect of maternal infection on the developing human CNS," *Cerebellum*, vol. 12, no. 4, pp. 572–586, 2013.

[2] D. Harvey, D. E. Holt, and H. Bedford, "Bacterial meningitis in the newborn: a prospective study of mortality and morbidity," *Seminars in Perinatology*, vol. 23, no. 3, pp. 218–225, 1999.

[3] D. Grandgirard and S. L. Leib, "Strategies to prevent neuronal damage in paediatric bacterial meningitis," *Current Opinion in Pediatrics*, vol. 18, no. 2, pp. 112–118, 2006.

[4] H. E. Humphries, M. Triantafilou, B. L. Makepeace, J. E. Heckels, K. Triantafilou, and M. Christodoulides, "Activation of human meningeal cells is modulated by lipopolysaccharide (LPS) and non-LPS components of *Neisseria meningitidis* and is independent of Toll-like receptor (TLR)4 and TLR2 signalling," *Cellular Microbiology*, vol. 7, no. 3, pp. 415–430, 2005.

[5] E. B. Kopp and R. Medzhitov, "The Toll-receptor family and control of innate immunity," *Current Opinion in Immunology*, vol. 11, no. 1, pp. 13–18, 1999.

[6] G. Bonizzi and M. Karin, "The two NF-κB activation pathways and their role in innate and adaptive immunity," *Trends in Immunology*, vol. 25, no. 6, pp. 280–288, 2004.

[7] L. A. J. O'Neill and C. Kaltschmidt, "NF-κB: a crucial transcription factor for glial and neuronal cell function," *Trends in Neurosciences*, vol. 20, no. 6, pp. 252–258, 1997.

[8] V. Fridmacher, B. Kaltschmidt, B. Goudeau et al., "Forebrain-specific neuronal inhibition of nuclear factor-κB activity leads to loss of neuroprotection," *The Journal of Neuroscience*, vol. 23, no. 28, pp. 9403–9408, 2003.

[9] S. da Silveira Cruz-Machado, C. E. Carvalho-Sousa, E. K. Tamura et al., "TLR4 and CD14 receptors expressed in rat pineal gland trigger NFKB pathway," *Journal of Pineal Research*, vol. 49, no. 2, pp. 183–192, 2010.

[10] Y. Li, A. Ji, E. Weihe, and M. K. Schäfer, "Cell-specific expression and lipopolysaccharide-induced regulation of tumor necrosis factor α (TNFα) and TNF receptors in rat dorsal root ganglion," *The Journal of Neuroscience*, vol. 24, no. 43, pp. 9623–9631, 2004.

[11] B. Viviani, S. Bartesaghi, E. Corsini, C. L. Galli, and M. Marinovich, "Cytokines role in neurodegenerative events," *Toxicology Letters*, vol. 149, no. 1-3, pp. 85–89, 2004.

[12] B. Nimmervoll, R. White, J. W. Yang et al., "LPS-induced microglial secretion of TNFα increases activity-dependent neuronal apoptosis in the neonatal cerebral cortex," *Cerebral Cortex*, vol. 23, no. 7, pp. 1742–1755, 2013.

[13] K. Cui, H. Ashdown, G. N. Luheshi, and P. Boksa, "Effects of prenatal immune activation on hippocampal neurogenesis in the rat," *Schizophrenia Research*, vol. 113, no. 2-3, pp. 288–297, 2009.

[14] A. Sharangpani, A. Takanohashi, and M. J. Bell, "Caspase activation in fetal rat brain following experimental intrauterine inflammation," *Brain Research*, vol. 1200, pp. 138–145, 2008.

[15] J. E. Frampton, C. R. Lee, and D. Faulds, "Filgrastim - a review of its pharmacological properties and therapeutic efficacy in neutropenia," *Drugs*, vol. 48, no. 5, pp. 731–760, 1994.

[16] J. G. Kiang, M. Zhai, P. J. Liao, D. L. Bolduc, T. B. Elliott, and N. V. Gorbunov, "Pegylated G-CSF inhibits blood cell depletion, increases platelets, blocks splenomegaly, and improves survival after whole-body ionizing irradiation but not after irradiation combined with burn," *Oxidative Medicine and Cellular Longevity*, vol. 2014, Article ID 481392, 10 pages, 2014.

[17] N. Sheibani, E. F. Grabowski, D. A. Schoenfeld, and M. J. Whalen, "Effect of granulocyte colony-stimulating factor on functional and histoplathologic outcome after traumatic brain injury in mice," *Critical Care Medicine*, vol. 32, no. 11, pp. 2274–2278, 2004.

[18] W. C. Shyu, S. Z. Lin, H. I. Yang et al., "Functional recovery of stroke rats induced by granulocyte colony-stimulating factor-stimulated stem cells," *Circulation*, vol. 110, no. 13, pp. 1847–1854, 2004.

[19] J. Minnerup, J. Heidrich, J. Wellmann, A. Rogalewski, A. Schneider, and W. R. Schabitz, "Meta-analysis of the efficacy of granulocyte-colony stimulating factor in animal models of focal cerebral ischemia," *Stroke*, vol. 39, no. 6, pp. 1855–1861, 2008.

[20] Y. Ohki, B. Heissig, Y. Sato et al., "Granulocyte colony-stimulating factor promotes neovascularization by releasing vascular endothelial growth factor from neutrophils," *FASEB Journal*, vol. 19, no. 12, pp. 2005–2007, 2005.

[21] A. Schneider, C. Krüger, T. Steigleder et al., "The hematopoietic factor G-CSF is a neuronal ligand that counteracts programmed cell death and drives neurogenesis," *Journal of Clinical Investigation*, vol. 115, no. 8, pp. 2083–2098, 2005.

[22] Y. N. Yang, C. S. Lin, C. H. Yang, Y. H. Lai, P. L. Wu, and S. N. Yang, "Neurogenesis recovery induced by granulocyte-colony stimulating factor in neonatal rat brain after perinatal hypoxia," *Pediatrics and Neonatology*, vol. 54, no. 6, pp. 380–388, 2013.

[23] K. Yata, G. A. Matchett, T. Tsubokawa, J. Tang, K. Kanamaru, and J. H. Zhang, "Granulocyte-colony stimulating factor inhibits apoptotic neuron loss after neonatal hypoxia–ischemia in rats," *Brain Research*, vol. 1145, pp. 227–238, 2007.

[24] K. E. Sullivan, A. B. M. Reddy, K. Dietzmann et al., "Epigenetic regulation of tumor necrosis factor alpha," *Molecular and Cellular Biology*, vol. 27, no. 14, pp. 5147–5160, 2007.

[25] G. P. Dorneles, M. C. R. Boeira, L. L. Schipper et al., "Acute strenuous exercise induces an imbalance on histone H4 acetylation/histone deacetylase 2 and increases the proinflammatory profile of PBMC of obese individuals," *Oxidative Medicine and Cellular Longevity*, vol. 2017, Article ID 1530230, 12 pages, 2017.

[26] Y. Wang, P. T. Cheung, G. X. Shen et al., "Hypoxic-ischemic brain injury in the neonatal rat model: relationship between lesion size at early MR imaging and irreversible infarction," *AJNR American Journal of Neuroradiology*, vol. 27, no. 1, pp. 51–54, 2006.

[27] B. D. Semple, K. Blomgren, K. Gimlin, D. M. Ferriero, and L. J. Noble-Haeusslein, "Brain development in rodents and humans: identifying benchmarks of maturation and vulnerability to injury across species," *Progress in Neurobiology*, vol. 106-107, pp. 1–16, 2013.

[28] G. Ramantani and H. Holthausen, "Epilepsy after cerebral infection: review of the literature and the potential for surgery," *Epileptic Disorders*, vol. 19, no. 2, pp. 117–136, 2017.

[29] N. Cardenas-Rodriguez, E. Coballase-Urrutia, C. Pérez-Cruz et al., "Relevance of the glutathione system in temporal lobe epilepsy: evidence in human and experimental models," *Oxidative Medicine and Cellular Longevity*, vol. 2014, Article ID 759293, 12 pages, 2014.

[30] W. F. Chen, H. Chang, C. S. Wong, L. T. Huang, C. H. Yang, and S. N. Yang, "Impaired expression of postsynaptic density proteins in the hippocampal CA1 region of rats following perinatal hypoxia," *Experimental Neurology*, vol. 204, no. 1, pp. 400–410, 2007.

[31] C. H. Hung, S. N. Yang, P. L. Kuo et al., "Modulation of cytokine expression in human myeloid dendritic cells by environmental endocrine-disrupting chemicals involves epigenetic regulation," *Environmental Health Perspectives*, vol. 118, no. 1, pp. 67–72, 2010.

[32] V. D. Bohbot, R. Jech, E. Růzicka et al., "Rat spatial memory tasks adapted for humans: characterization in subjects with intact brain and subjects with selective medial temporal lobe thermal lesions," *Physiological Research*, vol. 51, Supplement 1, pp. S49–S65, 2002.

[33] C. S. Lin, P. L. Tao, Y. J. Jong et al., "Prenatal morphine alters the synaptic complex of postsynaptic density 95 with *N*-methyl-D-aspartate receptor subunit in hippocampal Ca1 subregion of rat offspring leading to long-term cognitive deficits," *Neuroscience*, vol. 158, no. 4, pp. 1326–1337, 2009.

[34] J. Y. Lee, N. A. Kim, A. Sanford, and K. E. Sullivan, "Histone acetylation and chromatin conformation are regulated separately at the TNF-α promoter in monocytes and macrophages," *Journal of Leukocyte Biology*, vol. 73, no. 6, pp. 862–871, 2003.

[35] P. Viatour, M. P. Merville, V. Bours, and A. Chariot, "Phosphorylation of NF-κB and IκB proteins: implications in cancer and inflammation," *Trends in Biochemical Sciences*, vol. 30, no. 1, pp. 43–52, 2005.

[36] Q. Liu, Y. Li, W. Jiang et al., "Inhibition of HSP90 promotes neural stem cell survival from oxidative stress through attenuating NF-κB/p65 activation," *Oxidative Medicine and Cellular Longevity*, vol. 2016, Article ID 3507290, 10 pages, 2016.

[37] Y. Dou, T. A. Milne, A. J. Ruthenburg et al., "Regulation of MLL1 H3K4 methyltransferase activity by its core components," *Nature Structural & Molecular Biology*, vol. 13, no. 8, pp. 713–719, 2006.

[38] X. Wang, K. Zhu, S. Li et al., "MLL1, a H3K4 methyltransferase, regulates the TNFα-stimulated activation of genes downstream of NF-κB," *Journal of Cell Science*, vol. 125, no. 17, pp. 4058–4066, 2012.

[39] T. A. Tran, A. D. Nguyen, J. Chang, M. S. Goldberg, J. K. Lee, and M. G. Tansey, "Lipopolysaccharide and tumor necrosis factor regulate parkin expression via nuclear factor-kappa B," *PLoS One*, vol. 6, no. 8, article e23660, 2011.

[40] G. M. Cohen, "Caspases: the executioners of apoptosis," *Biochemical Journal*, vol. 326, no. 1, pp. 1–16, 1997.

[41] E. S. Alnemri, D. J. Livingston, D. W. Nicholson et al., "Human ICE/CED-3 protease nomenclature," *Cell*, vol. 87, no. 2, pp. 171–171, 1996.

[42] Z. Cai, Y. Pang, S. Lin, and P. G. Rhodes, "Differential roles of tumor necrosis factor-α and interleukin-1 β in lipopolysaccharide-induced brain injury in the neonatal rat," *Brain Research*, vol. 975, no. 1-2, pp. 37–47, 2003.

[43] E. M. Schneider, I. Lorenz, X. Ma, and M. Weiss, "G-CSF modulates LPS-induced apoptosis and IL-8 in human microvascular endothelial cells: involvement of calcium signaling," *Annals of the New York Academy of Sciences*, vol. 1010, pp. 78–85, 2003.

[44] F. C. Barone and G. Z. Feuerstein, "Inflammatory mediators and stroke: new opportunities for novel therapeutics," *Journal of Cerebral Blood Flow & Metabolism*, vol. 19, no. 8, pp. 819–834, 1999.

[45] G. R. Montibeller, B. Schackmann, S. Urbschat, and J. M. K. Oertel, "Effect of granulocyte colony–stimulating factor on the cochlear nuclei after creation of a partial nerve lesion: an experimental study in rats," *Journal of Neurosurgery*, vol. 128, no. 1, pp. 296–303, 2017.

[46] I. Solaroglu, J. Cahill, V. Jadhav, and J. H. Zhang, "A novel neuroprotectant granulocyte-colony stimulating factor," *Stroke*, vol. 37, no. 4, pp. 1123–1128, 2006.

[47] S. O. Heard and M. P. Fink, "Counterregulatory control of the acute inflammatory response: granulocyte colony-stimulating factor has anti-inflammatory properties," *Critical Care Medicine*, vol. 27, no. 5, pp. 1019–1021, 1999.

[48] W. R. Schabitz, R. Kollmar, M. Schwaninger et al., "Neuroprotective effect of granulocyte colony-stimulating factor after focal cerebral ischemia," *Stroke*, vol. 34, no. 3, pp. 745–751, 2003.

[49] I. Solaroglu, V. Jadhav, and J. H. Zhang, "Neuroprotective effect of granulocyte-colony stimulating factor," *Frontiers in Bioscience*, vol. 12, no. 1, pp. 712–724, 2007.

[50] C. L. Gibson, N. C. Jones, M. J. W. Prior, P. M. W. Bath, and S. P. Murphy, "G-CSF suppresses edema formation and reduces interleukin-1β expression after cerebral ischemia in mice," *Journal of Neuropathology & Experimental Neurology*, vol. 64, no. 9, pp. 763–769, 2005.

[51] J. Imitola, K. Raddassi, K. I. Park et al., "Directed migration of neural stem cells to sites of CNS injury by the stromal cell-derived factor 1α/CXC chemokine receptor 4 pathway," *Proceedings of the National Academy of Sciences of the United States of America*, vol. 101, no. 52, pp. 18117–18122, 2004.

[52] P. E. Hughes, T. Alexi, M. Walton et al., "Activity and injury-dependent expression of inducible transcription factors,

growth factors and apoptosis-related genes within the central nervous system," *Progress in Neurobiology*, vol. 57, no. 4, pp. 421–450, 1999.

[53] W. F. Chen, J. H. Hsu, C. S. Lin et al., "Granulocyte-colony stimulating factor alleviates perinatal hypoxia-induced decreases in hippocampal synaptic efficacy and neurogenesis in the neonatal rat brain," *Pediatric Research*, vol. 70, no. 6, pp. 589–595, 2011.

[54] L. Weaver-Mikaere, A. J. Gunn, M. D. Mitchell, L. Bennet, and M. Fraser, "LPS and TNF alpha modulate AMPA/NMDA receptor subunit expression and induce PGE2 and glutamate release in preterm fetal ovine mixed glial cultures," *Journal of Neuroinflammation*, vol. 10, no. 1, 2013.

Hindawi
Oxidative Medicine and Cellular Longevity
Volume 2018, Article ID 9389784, 19 pages
https://doi.org/10.1155/2018/9389784

Research Article

Cardiac Autonomic Neuropathy as a Result of Mild Hypercaloric Challenge in Absence of Signs of Diabetes: Modulation by Antidiabetic Drugs

Ola Al-Assi,[1] Rana Ghali,[1] Ali Mroueh,[1] Abdullah Kaplan,[1] Nahed Mougharbil,[1] Ali H. Eid,[1] Fouad A. Zouein,[1] and Ahmed F. El-Yazbi[1,2]

[1]*Department of Pharmacology and Toxicology, Faculty of Medicine, The American University of Beirut, Beirut, Lebanon*
[2]*Department of Pharmacology and Toxicology, Faculty of Pharmacy, Alexandria University, Alexandria, Egypt*

Correspondence should be addressed to Fouad A. Zouein; fz15@aub.edu.lb and Ahmed F. El-Yazbi; ae88@aub.edu.lb

Received 2 October 2017; Revised 21 November 2017; Accepted 29 November 2017; Published 31 January 2018

Academic Editor: Mohamed A. Abdelmegeed

Cardiac autonomic neuropathy (CAN) is an early cardiovascular complication of diabetes occurring before metabolic derangement is evident. The cause of CAN remains elusive and cannot be directly linked to hyperglycemia. Recent clinical data report cardioprotective effects of some antidiabetic drugs independent of their hypoglycemic action. Here, we used a rat model receiving limited daily increase in calories from fat (HC diet) to assess whether mild metabolic challenge led to CAN in absence of interfering effects of hyperglycemia, glucose intolerance, or obesity. Rats receiving HC diet for 12 weeks showed reduction in baroreceptor sensitivity and heart rate variability despite lack of change in baseline hemodynamic and cardiovascular structural parameters. Impairment of cardiac autonomic control was accompanied with perivascular adipose inflammation observed as an increased inflammatory cytokine expression, together with increased cardiac oxidative stress, and signaling derangement characteristic of diabetic cardiomyopathy. Two-week treatment with metformin or pioglitazone rectified the autonomic derangement and corrected the molecular changes. Switching rats to normal chow but not to isocaloric amounts of HC for two weeks reversed CAN. As such, we conclude that adipose inflammation due to increased fat intake might underlie development of CAN and, hence, the beneficial effects of metformin and pioglitazone.

1. Introduction

Diabetes mellitus is a metabolic disorder characterized by hyperglycemia caused by reduced secretion or action of insulin or both [1]. Two main forms of diabetes exist, type 1 and type 2. Type 1 diabetes is an autoimmune disease characterized by the destruction of pancreatic β-cells with concomitant insulin deficiency and resistance. Type 2 diabetes encompasses insulin resistance and deficiency and accounts for 90–95% of diagnosed patients worldwide [1]. According to the 2014 World Health Organization (WHO) Global Report on Diabetes, the prevalence of diabetes is on the rise. About 422 million people have diabetes worldwide, and it is estimated that approximately 1.5 million died of a cause related to diabetes in 2012 [2]. The increased prevalence is thought to be triggered by changes in human behavior, lifestyle, and environment [3]. Rapid dietary changes towards high saturated fat, high sugar, refined, and low in fiber foods contributed to the increase in diabetes and cardiovascular diseases [3].

Cardiovascular complications are considered the major and primary cause of morbidity and mortality in diabetes, where eight out of ten diabetic patients die because of cardiovascular diseases [4]. While prediabetic patients are considered to be in an intermediate metabolic state that does not fulfill the diagnostic criteria of diabetes, studies found that they remain at an increased risk of cardiovascular disease [5, 6]. Indeed, a significant proportion of newly diagnosed diabetic patients had established microvascular complications at initial presentation [7] indicating that

pathological stages early in diabetes development constitute an important window for potential interventions to alleviate the detrimental sequelae of diabetes.

Recent studies detected early changes in cardiovascular autonomic control in diabetic patients before other signs of peripheral and autonomic neuropathies manifest [8, 9]. Cardiac autonomic neuropathy (CAN) represents a main cause of mortality in diabetic patients, where it is associated with a high risk of sudden death and cardiac arrhythmia [10]. The prevalence of diabetic CAN could reach up to 34% of type 2 diabetic patients [11]. Despite its documented negative impact on cardiovascular outcomes in type 2 diabetes patients [12], it remains as one of the least understood, recognized, and studied complications of diabetes [10]. While gross neuronal damage due to metabolic derangement could account for CAN in diabetic patients [10], the same cannot be considered for prediabetic patients [13]. Metabolic syndrome hallmarks, other than hyperglycemia, were implicated in the development of CAN in this patient cohort including obesity, triglyceride derangement, and insulin resistance [14].

Similar to other cardiovascular complications of diabetes, strong clinical data suggest that tight glycemic control can slow the progression and the development of autonomic dysfunction [15]. For the longest time, no data were available to describe a preferential positive outcome of using a particular therapeutic approach for glycemic control. Yet, recent clinical evidence from cardiovascular outcome trials [16, 17] suggests that treatment with a given molecule might provide protection against cardiovascular events in diabetic patients even when careful attempts are made to keep HbA1C% under close control. Of particular significance, favorable cardiovascular effects of antihyperglycemic drugs apart from their effect on glycemic control were observed in prediabetic patients treated by pioglitazone [18] and metformin [19] raising the question of whether these drugs could interfere with the early detrimental cardiovascular pathology prior to development of diabetes.

In this context, previous studies from our laboratory [20] showed that structural and functional vascular and hemodynamic alteration occurred prior to the development of hyperglycemia in a rat model of hypercaloric intake. The observed vascular dysfunction was reversed upon treatment with metformin or pioglitazone without changes in serum glucose level or advanced glycation end products. Significantly, multiple lines of evidence implicated increased caloric intake in the form of high-fat diets in increased central neuroinflammation prior to the development of signs of diabetes [21, 22]. Interestingly, not only are metformin and pioglitazone reported to have direct, glycemic-independent anti-inflammatory effects [23, 24], but also clinical evidence showed they possessed neuroprotective effects in patients with metabolic syndrome [25] and were effective in reducing CAN in diabetic patients [26]. As such, in the present study, we used a rat model of hypercaloric intake to examine whether CAN could develop as a consequence of mild metabolic challenge in the absence of hyperglycemia and peripheral markers of insulin resistance and cardiovascular involvement. We tested whether the determining factor was the overall caloric intake versus increased proportion of saturated fat in diet and if treatment with metformin and pioglitazone could potentially reverse the observed dysfunction.

2. Methods

2.1. Ethical Approval. All animal experiments were done according to an experimental protocol approved by the Institutional Animal Care and Use Committee in compliance with the Guide for Care and Use of Laboratory Animals of the Institute for Laboratory Animal Research of the National Academy of Sciences, USA.

2.2. Experimental Design. Male Sprague-Dawley rats (5-6 weeks of age; 150 g) were randomly divided into six groups (8 rats per group): (1) rats fed with normal chow diet (control, 3 Kcal/g), (2) rats fed with mild hypercaloric diet (HC, 4.035 Kcal/g) for 12 weeks, (3) rats fed with mild hypercaloric diet and treated with 100 mg/kg metformin at week 10 (Met), (4) rats fed with mild hypercaloric diet and treated with 2.5 mg/kg pioglitazone at week 10 (Pio), (5) rats fed with mild hypercaloric diet for 10 weeks, then switched to normal chow for the remaining 2 weeks (NC), (6) rats fed with mild hypercaloric diet ad libitum for 10 weeks, then switched to pair feeding with the same diet to match calorie intake of control rats on normal chow (HC-L). Normal chow diet (ENVIGO) was obtained from Teklad Rodent Diets (Madison, WI). This diet offers 3 Kcal/g distributed as follows: 32% from protein, 14% from fat (0.9% saturated fat by weight), and 54% from carbohydrates. The HC diet was prepared in house through the addition of food grade fructose (20% by weight, Santiveri foods, Spain) and hydrogenated vegetable oil (Mazola®, 15% by weight, BFSA). Major electrolytes and vitamins were supplemented to match the concentration in ENVIGO diet and as recommended by the American Institute of Nutrition [27]. The final composition of the HC diet by weight (calorie content) is 18.06% fat (38.68%, 5% saturated fat by weight), 15.8% protein (15.66%), and 46.13% carbohydrates (45.73%). Other than rats in group 6, all rats had free access to food and water for the full 12-week duration. Rats were kept in a temperature- and humidity-controlled room, in a 12-hour light/dark cycle. Body weight was measured weekly along with the anus-to-nose length (ANL), and calorie intake was calculated daily based on the amount of food consumed. At week 10, the treatment regimen was administered to different groups by daily oral gavage. The control groups received water gavage while drug treatment groups received freshly prepared aqueous suspensions of the antidiabetic agents.

2.3. Noninvasive Blood Pressure Measurement and Echocardiography. Rat blood pressure was measured noninvasively by tail cuff using CODA High Throughput Monitor (Kent Scientific, Torrington, CT) [28]. Measurement was performed at weeks 0, 4, 10, and 12. Any irregular or unacceptable recording noted as a false recording by the system was excluded. The parameters obtained are systolic (SBP), diastolic (DBP), mean arterial blood pressure (MAP), and

heart rate (HR). Echocardiography was performed in the parasternal long axis M-mode and B-mode to monitor heart function and visualize heart morphology using SonixTouch Q+ ultrasound (BK ultrasound, Peabody, MA) [29]. Measurements were performed at weeks 0, 4, 10, and 12. The parameters calculated were left ventricular diastole diameter (LVDd), left ventricular posterior wall diameter (LVPWd), left ventricle mass (LV mass), end diastolic volume (EDV), and ejection fraction (EF).

2.4. Random Blood Glucose Measurement and Oral Glucose Tolerance (OGT) Testing. Random glucose testing was performed at weeks 0, 4, 8, and 12. The lateral tail vein was pricked, and an enough quantity of blood was obtained. The measurement was done using Accu-Chek Performa glucometer (Roche Diagnostics, Basel, Switzerland). At the end of week 12, rats were fasted overnight. Rats were challenged using a 2 g/kg, 20% glucose solution administered by oral gavage [30]. They were gently restrained, and blood glucose was measured at 0, 15, 30, 60, and 120 minutes after glucose load. Blood was collected from a tail vein prick, and glucose was measured using Accu-Chek Performa glucometer.

2.5. Invasive Hemodynamic Recording in Anesthetized Rats. At the end of the treatment period, rats were instrumented for arterial pressure and heart rate recording as described previously [31]. Briefly, following anesthesia using 100 mg/kg phenobarbital (AUB-MC pharmacy), tracheostomy was performed and right carotid artery was isolated, cannulated, and connected to a Millar transducer to measure mean arterial pressure (MAP) and heart rate (HR). Data acquisition was performed by LabChart Pro 8 (AD Instruments Ltd., Dunedin, New Zealand). Afterwards, the left jugular vein was isolated, cannulated, and connected to a shunt for IV drug administration. The recording was allowed to stabilize for 30 minutes, and baseline invasive SBP, DBP, MAP, and HR were recorded.

Baroreceptor sensitivity (BRS) was assessed using the vasoactive method [32]. Increasing doses of phenylephrine (PE, 0.25, 0.5, 0.75, 1, and 2 μg) and sodium nitroprusside (SNP, 1, 2, 4, and 8 μg) were administered, and the changes in MAP and HR were recorded. Slope of the linear regression fit between ΔHR and ΔMAP at different PE and SNP doses was used as a measure of BRS. Heart rate variability (HRV) analysis was performed using the available software module as described previously [33]. Cardiac autonomic activity was assessed using two time domain and two frequency domain measures. Variables were estimated as a five-minute average through an area of a stable recording pattern. The standard deviation of beat-to-beat intervals (SDNN) and the root mean square of successive beat-to-beat differences in R-R interval durations (rMSSD) were assessed as measures of the overall autonomic balance and parasympathetic input to the heart, respectively [34–36]. Frequency domain analysis was performed using Fast Fourier Transform algorithms of R-R data series. Spectra were integrated into 2 specific frequency bands, low frequency (LF, 0.25–0.75 Hz) and high frequency (HF, 0.75–3 Hz) bands, corresponding to sympathetic and vagal outflows, respectively [36], and power spectral density was determined for these two bands.

2.6. Histopathology and Immunohistochemistry. At the end of the invasive hemodynamic recording, rats were decapitated. Brain was dissected, placed on ice, and the brainstem was isolated. The thoracic cavity was exposed, pericardiac and aortic perivascular adipose tissues were dissected, and the heart was flushed and isolated. Adipose tissue was flash frozen in liquid nitrogen and stored at −80°C. Brainstems were cut in half; one side fixed in formaldehyde while the other was stored at −80°C. Ventricles were horizontally cut into 3 sections (apex, midsection, and base). The midsection was placed in formaldehyde for further histological analysis. Other parts were flash frozen in liquid nitrogen and stored at −80°C. For histopathology and immunohistochemistry, ventricular midsections and fixed brainstems were embedded in paraffin, sectioned transversely, and placed on clean slides. Staining was performed simultaneously for accurate comparison. For demonstration of nucleus and cytoplasmic inclusions, hematoxylin and eosin stains were used, for the detection of cardiac fibrosis, Masson trichrome staining was performed, while for estimation of reactive oxygen species activity, dihydroethidium staining was performed on cryosectioned heart midsection and brainstem as described previously [37]. For detection of transforming growth factor-β (TGF-β), sections were incubated with the primary antibody (rabbit anti-TGFβ, 1 : 100, Abcam, Cambridge, UK) and detected using Novolink Polymer Detection Kit (Leica Biosystems, Buffalo Grove, IL) according to the manufacturer's protocol.

2.7. Western Blotting. Protein extraction and Western blotting were performed according to a method we previously developed and optimized [33, 38–40]. Briefly, the heart and brain tissue samples kept at −80°C were crushed under liquid nitrogen. 10 mg heart tissue and 40 mg brainstem tissue were transferred to 1 ml and 300 μl, respectively, of a protein extraction buffer containing 1% sodium dodecylsulfate (SDS), 0.9% NaCl, 80 mM Tris hydrochloride (pH 6.8), and 100 mM dithiothreitol. Tissue amounts used for protein extraction were optimized according to final protein concentration in preliminary experiments. Samples were heated at 95°C for 10 min, allowed to cool down and transferred to a rocking shaker and left overnight for protein extraction at 4°C. Aliquots with equal protein content from the extracts were then used for SDS-PAGE and blotted as described previously [38]. After transfer and fixation, nitrocellulose membranes were blocked with 5% skim milk (Bio-Rad, Hercules, CA, USA) in Tris-buffered saline containing 0.1% Tween 20 for two hours at room temperature. At this stage, membranes were cut at the appropriate molecular weights to allow for probing of multiple proteins within the same run. Membranes were incubated in a dilution of primary antibodies in 1% skim milk in 0.1% TBST (1 : 1000 for rabbit polyclonal anti-AMPKα, rabbit polyclonal P-AMPKα, and P-Erk1/2, Cell Signaling Technologies, Danvers, MA, and rabbit polyclonal anti-Erk1/2, Thermoscientific, Waltham,

MA, and 1 : 500 for rabbit polyclonal anti-interleukin (IL-1β), Abcam, Cambridge, UK) overnight at 4°C. After washing with 0.05% TBST (4 × 5 min), membranes were incubated in 1 : 10,000 biotin-conjugated goat anti-rabbit Ig for 1 h at room temperature followed by washing and incubation with 1 : 100,000 horse radish peroxidase-conjugated streptavidin for 30 minutes at room temperature. Blots of the brainstem samples were developed using the traditional two-step Western blotting using 1 : 5000 horse radish peroxidase-conjugated goat anti-rabbit secondary antibody in 0.1% TBST for one hour at room temperature. After washing 4 × 5 min with 0.05% TBST and 2 × 5 min with TBS, membranes were exposed to Clarity Western ECL substrate (BioRad, Hercules, CA) for 5 min following image detection using ChemiDoc imaging system (BioRad, Hercules, CA). Band optical density was measured using ImageJ software, and a ratio of arbitrary density units was obtained for the protein band of interest and the density of the band representing total protein for p-AMPK and p-Erk1/2 after stripping and reprobing, while IL-1β bands were normalized to actin as described previously [33, 38] to correct variabilities in loading and sample concentration.

2.8. Determination of IL-1β and Tumor Necrosis Factor (TNF-α) Expression in Perivascular Adipose Tissue by Quantitative Polymerase Chain Reaction (Q-PCR). Q-PCR was carried out as previously described [41]. Briefly, total RNA was extracted from adipose tissue using an RNeasy Mini kit with DNase treatment (Qiagen, Hilden, Germany) and first strand cDNA synthesized using the Sensiscript RT kit (Qiagen, Hilden, Germany) with oligo d(T) primer. Primer pairs to detect rat IL-1β and β-actin were designed and purchased from Sigma (St. Louis, MO). The primer sequences (5′–3′) were the following: IL-1β forward GCCTCAAGGGGAAGAA TCTATACC, reverse GGGAACTGTGCAGACTCAAACT; TNF-α forward ACCACGCTCTTCTGTCTACTG, reverse CTTGGTGGTTTGCTACGAC; β-actin forward GTCAGG TCATCACTATCGGCAAT and, reverse AGAGGTCTTTA CGGATGTCAACGT. Primer sets used had an efficiency of >90% that did not differ by >5% at the annealing temperature and produced a single peak with no evidence of additional amplicons or primer dimer formation during melt curve analysis. Q-PCR was performed with SYBR Green and a reaction with a hot start at 95°C for 5 min, followed by 40 cycles of 95°C for 15 s, 60°C for 1 min, and 72°C for 1 min. Threshold cycle was determined using a Bio-Rad iCycler (Hercules, CA) and vendor-supplied software, and transcript abundance was calculated by the $2^{-\Delta\Delta Ct}$ method using β-actin as the reference for normalization.

2.9. Chemicals. All chemicals were obtained from Sigma (St. Louis, MO) unless otherwise indicated. Pharmaceutical grade metformin HCl, phenylephrine, and pioglitazone were obtained as kind gifts from regional pharmaceutical manufacturers (Merck, Pharo Pharma, and Hikma Pharmaceuticals).

2.10. Statistical Analysis. Data were expressed as mean ± SEM. Comparisons between groups were done using one-way ANOVA followed by Dunnett post hoc test, as well as two-way ANOVA followed by Sidak's multiple comparisons test in comparing different time points or doses among groups using Graphpad Prism software. P value < 0.05 was considered statistically significant.

3. Results

3.1. Calorie Intake, Weight Variation, and Blood Glucose Levels. On a daily basis, HC-fed groups showed an increased energy intake of ~14 Kcal compared to rats on normal chow ($P < 0.05$ on most days, Figure 1(a)). Energy intake gradually increased for both groups and then plateaued three weeks into treatment. For the remainder of experimental period, the HC group consumed ~100 Kcal/24 hours, while the NC group intake continued at ~86 Kcal/24 hours.

After initial randomization, rats from all groups had approximately the same weight (172.7 g ± 4.94). Rats from different groups continued to gain weight similarly throughout the experiment (Figure 1(b)). BMI was calculated using ANL and showed no significant difference between different groups (data not shown). Weight change within each group in the last 2 weeks during the treatment was determined. Only rats receiving pioglitazone treatment showed significant increase in body weight when compared to control and HC rats (data not shown).

As for blood glucose levels, HC feeding did not induce any changes in random blood glucose levels through the first 10 weeks of treatment (Figure 1(c)). Treatment with metformin or pioglitazone produced no significant change in random blood glucose in week 12. By the end of week 12, no significant differences in OGT were found amongst the four treatment groups (Figure 1(d)).

3.2. Noninvasive Blood Pressure Measurement. Chronic feeding with HC did not induce detectable changes in blood pressure throughout the duration of the experiment. Figure 2 shows SBP (2a), DBP (2b), and MAP (2c) measured by tail cuff technique at different time points. Additionally, no significant differences were observed in HR recorded using the CODA monitor (2d). As well, rats receiving metformin or pioglitazone showed no significant difference in these parameters in the last two weeks.

3.3. Echocardiography. Echocardiography parameters calculated were left ventricular diastole diameter (LVDd), left ventricular posterior wall diameter (LVPWd), end diastolic volume (EDV), left ventricular mass (LV mass), and ejection fraction (EF). These parameters reflect the morphological (LVDd, LVPWd, and LV mass) and functional (EDV and EF) cardiac properties. Figure 3 depicts changes in these parameters normalized to body weight. No significant differences in echocardiography parameters were noticed among different treatment groups. However, these parameters showed an apparent rapid decrease in all groups in the early treatment phase. This is caused by the normalization of the parameters against the rat body weight, where the rate of increase in the parameters measured was much less than the rate of increase in body weight.

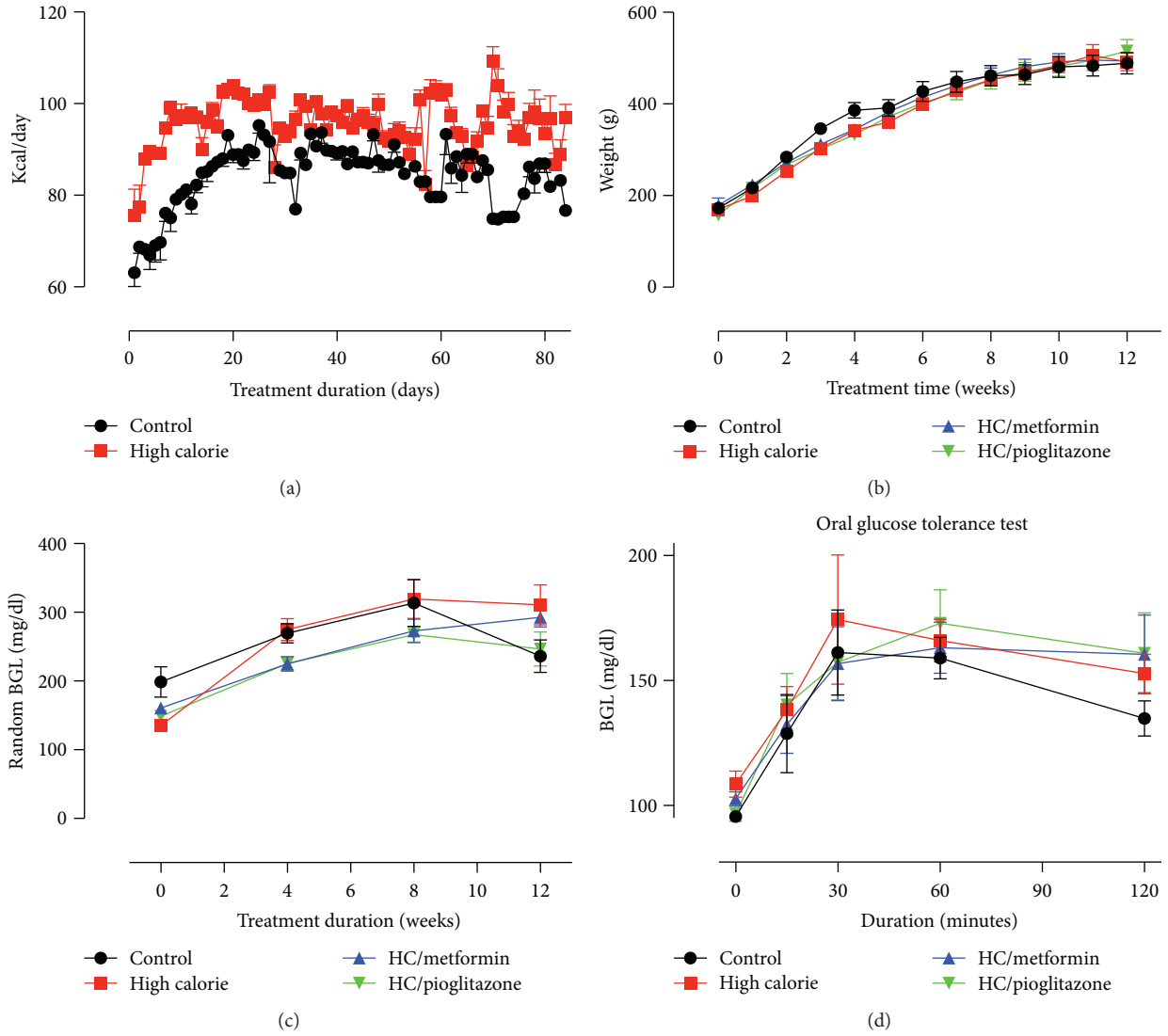

Figure 1: Daily calorie intake, body weight variation, and changes in blood glucose levels as a function of time in different treatment groups. (a) HC-fed rats (red) consumed higher calories on a daily basis compared to control rats on normal chow (black). Depicted data are mean ± SEM for eight control and 32 HC-fed rats. Daily calorie intake was significantly higher on most treatment days, $P < 0.05$ as estimated by two-way ANOVA. (b) No differences in weight gain were detected among the different treatment groups over twelve weeks of treatment. (c) No significant differences in random blood glucose levels were detected among the different treatment groups over twelve weeks of treatment. (d) At the end of the treatment period, different groups responded similarly to an oral glucose load. Data depicted in (b–d) represent mean ± SEM of values obtained from eight rats in each treatment groups.

3.4. Invasive Blood Pressure Measurement. At the conclusion of the 12-week treatment period, rats from different groups were instrumented for invasive hemodynamic recording. After 30 minutes of stabilization, a stable five-minute recording was used to calculate the invasive SBP, DBP, MAP, and HR. Similar to noninvasive measurements, no significant differences were detected in the baseline parameters of all treatment groups (data not shown).

3.5. Baroreceptor Sensitivity (BRS). After the equilibration period, a series of PE and SNP doses were administered and the resulting change in MAP (ΔMAP) and HR (ΔHR) was recorded. Figure 4 depicts representative tracings of the changes in MAP and HR in response to PE (4A) and SNP (4B). An exaggerated vasopressor response to PE was noted in the HC group (Figure 5(a)). A trend towards a reduction of the increased vasopressor response was evident for rats treated with metformin or pioglitazone that was statistically significant at 0.75 μg PE. No significant differences were detected in ΔHR in response to different PE doses among different treatment groups (Figure 5(b)). BRS was determined by the linear regression of ΔMAP versus ΔHR curves (Figure 5(c)). HC blunted BRS as seen in the reduced BRS line slope that was significantly lower than that of the control group. The recovery of BRS was significant in metformin- and pioglitazone-treated rats. Figure 5(d)

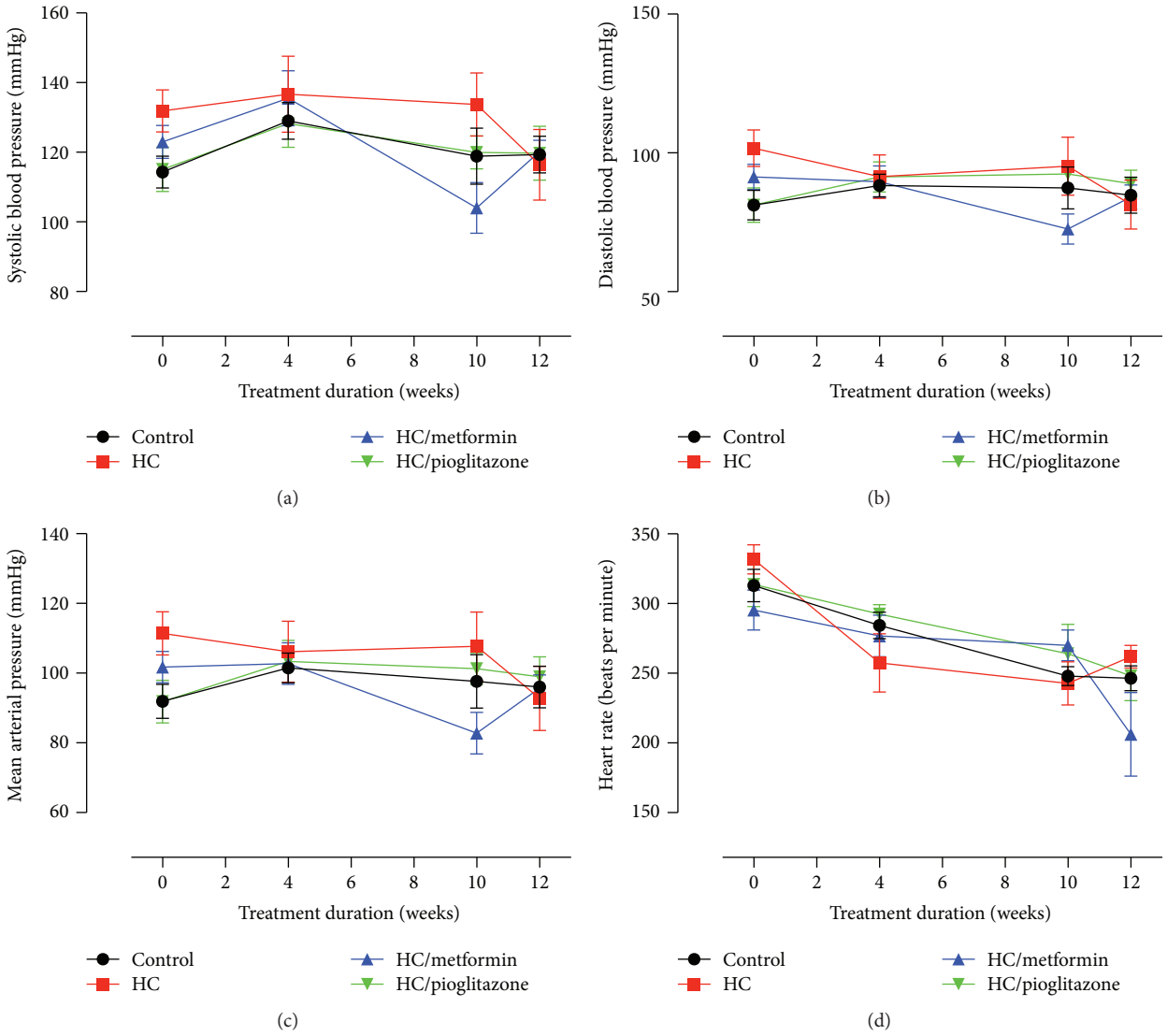

Figure 2: Noninvasive hemodynamic parameters of different treatment groups. No significant differences were detected among the different treatment groups in SBP (a), DBP (b), MAP (c), or HR (d) at baseline, 4, 10, and 12 weeks of treatment. Depicted data represent mean ± SEM of values obtained from eight rats in each treatment groups.

represents the statistical comparison of the regression line slopes. Neither ΔMAP nor ΔHR in response to SNP appeared to show significant differences among the different groups (data not shown). As well, there were no differences in BRS in response to SNP (Figure 5(e)) as can be inferred by the lack of statistical significance upon comparison of the slopes (Figure 5(f)).

3.6. Heart Rate Variability (HRV) Analysis. Following the equilibration period, a stable 15-minute recording of arterial pressure was analyzed for determination of time domain and frequency domain parameters. Figure 6(a) represents SDNN while Figure 6(b) represents rMSSD. Both time domain parameters were significantly reduced in HC rats. Groups treated with metformin or pioglitazone showed significant recovery in both parameters. HC group had an abolished power spectral density in LF and HF compared to the control group (Figures 6(c) and 6(d)). Treatment with both metformin and pioglitazone restored both powers to a level not different from that of the control group.

3.7. Microscopic, Oxidative Stress, and Signaling Protein Expression/Phosphorylation Changes in Ventricular Tissue. Figure 7(a) shows representative micrographs of ventricular midsection stained with H&E and trichrome, immunostained for TGF-β, in addition to cryosections exposed to DHE staining. In line with the lack of change in echocardiography parameters representing cardiac structure/function, H&E and trichrome staining showed normal myocyte arrangement and distribution without a noticeable increase in collagen deposition in sections from HC-fed rats compared to control rats. However, in agreement with the previous data from our laboratory [20], TGF-β staining was increased in HC-fed rats and decreased with metformin or

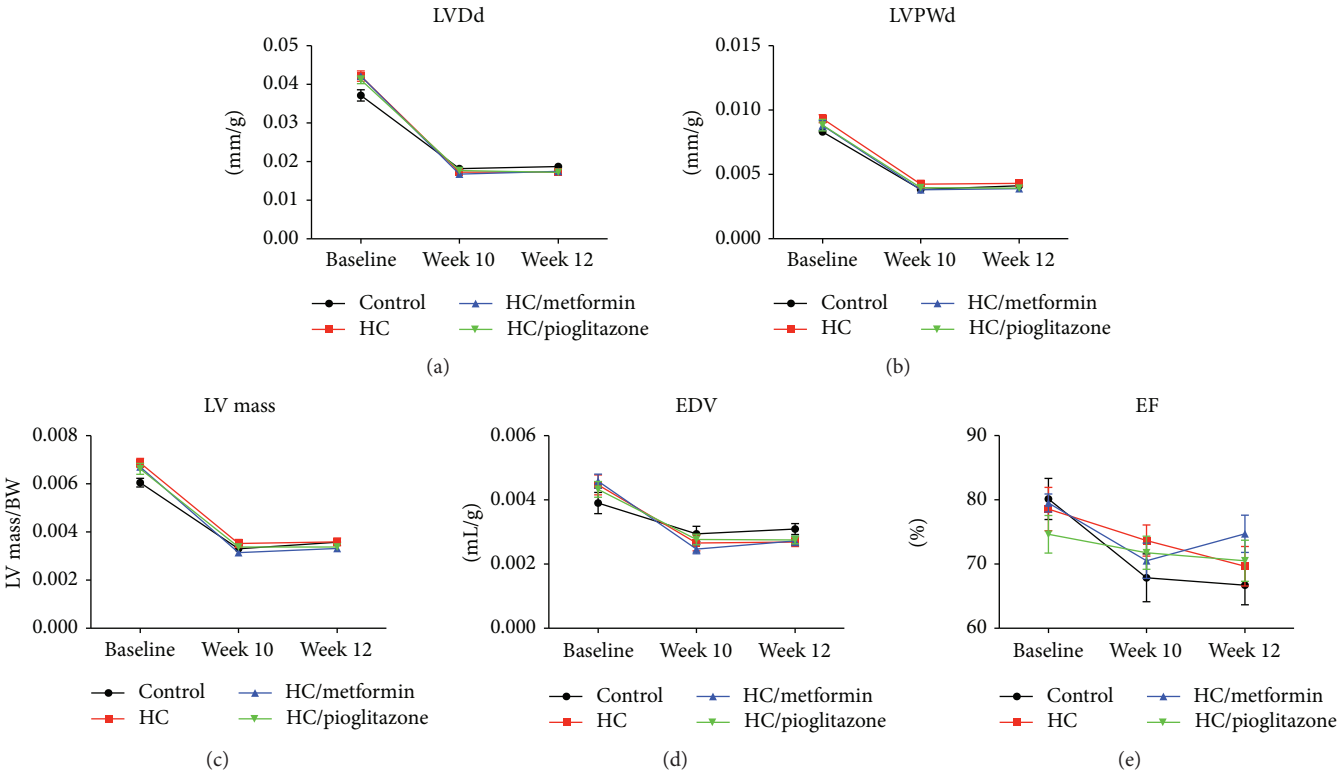

Figure 3: Echocardiographic parameters representing structural and functional aspects of the left ventricle. No significant differences were detected among the different treatment groups in LVDd (a), LVPWd (b), LV mass (c), EDV (d), or EF (e) at baseline, 10 and 12 weeks of treatment. Depicted data represent mean ± SEM of values obtained from eight rats in each treatment groups. All represented parameters are normalized to body weight (BW).

pioglitazone treatment. In addition, DHE staining showed an increased reactive oxygen species in tissue sections from HC-fed rats, which was reduced by treatment with metformin or pioglitazone.

On the other hand, multiple lines of evidence suggest that AMP-activated protein kinase (AMPK) phosphorylation is reduced in early stages of diabetic cardiomyopathy [42], whereas extracellular signal-regulated kinase (Erk1/2)/TGF-β signaling pathway is activated. AMPK and Erk1/2 phosphorylation levels were determined in ventricular tissue by Western blotting. Examination of ventricular protein extract showed reduced and increased phosphorylation of AMPK and Erk1/2, respectively, in tissues from HC rats (Figure 7(b)). These changes in protein phosphorylation were reversed following treatment with metformin or pioglitazone.

3.8. Changes in Oxidative Stress and Signaling Protein Expression/Phosphorylation in Brainstem. The effect of HC feeding and drug treatment on central neuronal sites in the brainstem controlling cardiac autonomic function was examined. The level of oxidative stress was assessed by DHE staining of cryosections from brainstem obtained from rats in different treatment groups. Compared to control rats, HC feeding increased reactive oxygen species in brainstem as can be seen in increased DHE staining intensity (Figure 8(a)). A trend towards a slight reduction in oxidative stress levels was observed in brainstem sections obtained from rats treated with metformin and pioglitazone; however, DHE staining remains noticeably higher than the control in these sections. Significantly, no changes were observed in TGF-β staining in brainstem sections from HC-fed rats compared to control (Figure 8(a)), neither were there changes in AMPK and Erk1/2 phosphorylation levels detected by Western blotting (Figure 8(b)).

3.9. The Effect of Drug Treatment on Adipose, Heart, and Brainstem Inflammatory Markers. Several lines of evidence implicated IL-1β in the pathogenesis of high-fat diet-induced inflammation together with increased expression in the adipose tissue in human obesity and insulin resistance [43]. As well, increased TNF-α mRNA levels were observed in adipose tissue from humans with early metabolic dysfunction [44] and rats fed a fat-rich diet [45]. As such, we examined the effect of HC feeding on IL-1β and TNF-α mRNA levels in perivascular and pericardiac adipose, together with IL-1β expression in the heart and brainstem. As shown in Figure 9, in line with the previous findings, HC feeding increased IL-1β and TNF-α expression levels in adipose tissue and in ventricular extracts. Significantly, similar to TGF-β expression and AMPK and Erk1/2 phosphorylation, no change in IL-1β expression was observed in brainstem tissue. Subsequent treatment with metformin or pioglitazone was associated with a reduction in IL-1β transcript and protein levels in adipose tissue and ventricular

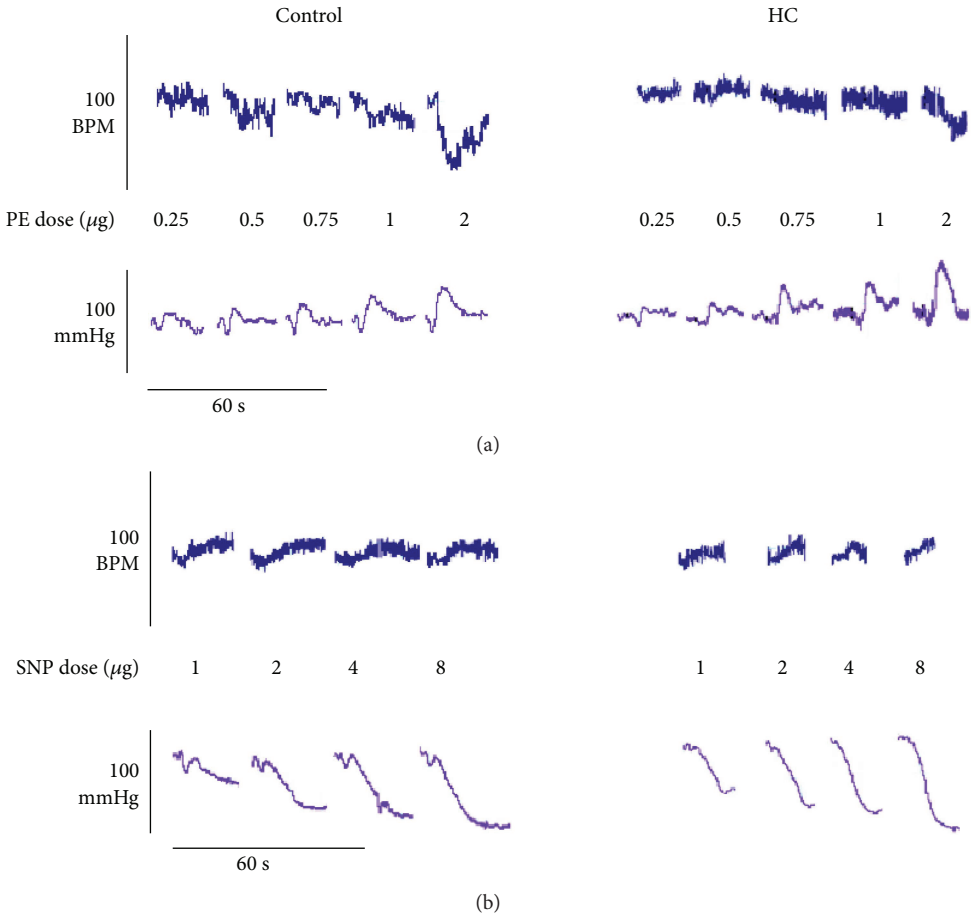

Figure 4: Representative tracings of the MAP and HR response of control (left) and HC-fed (right) rats to different doses of PE (a) and SNP (b). Vertical scale bars represent HR and MAP as indicated while horizontal scale bars represent time (60 s).

extracts, respectively, supporting a possible reduction of adipose inflammation in these treatment groups.

3.10. The Effect of Dietary Switching on the Observed Changes in Cardiac Autonomic Control. Previous literature implicated adipose inflammation and hypothalamic inflammatory signaling as consequences of high-fat feeding [46, 47], as opposed to increased calorie intake per se. In order to assess whether the observed deficit in cardiac autonomic control resulted from increased caloric intake versus an increased saturated fat proportion in diet, the effect of switching to normal chow (NC) or pair feeding with an isocaloric amount of our HC diet (HC-L) for the last two weeks on BRS and HRV was examined. Increased sensitivity to the vasopressor effect of PE persisted only in the HC-L group whereas a reduction similar to the effect obtained with metformin and pioglitazone treatments was seen in the NC group (Figure 10(a)). No significant changes were seen in HR (Figure 10(b)), and as such, BRS remained attenuated in HC-L but recovered in the NC group (Figures 10(c) and 10(d)). No differences were observed in the responses to SNP (data not shown). In parallel, deficits in time domain (Figures 10(e) and 10(f)) and frequency domain (Figures 10(g) and 10(h)) parameters of HRV persisted and recovered in the HC-L and NC groups, respectively.

4. Discussion

In the present study, we assessed whether cardiac structural and functional deterioration starts early in the course of metabolic alteration and examined the possibility of reversing these deleterious effects. To our knowledge, this is the first report of CAN occurring in the context of a metabolic challenge in the absence of detectable signs of obesity, hyperglycemia, or insulin resistance. As well, our present results highlight a potential involvement of adipose inflammation and a possible corrective role for metformin and pioglitazone that is not related to their blood glucose-lowering effect. In order to prove this association, hypercaloric intake in rats was used as a model of mild metabolic challenge. This model receives 38% of energy intake as fat, which is slightly higher than the American Diabetes Association daily total fat intake recommendations (20–35% energy as fat) [48] but within range of high-fat diet compositions (20–60% energy as fat) reported in the literature and used in validated rat models of obesity, insulin resistance, and diabetes [49]. While the increased dietary fat is the source of elevated calorie intake, a dietary composition containing fructose was chosen to simulate typical Western diets rich in refined sugars and saturated fat previously shown to be linked to cardiovascular pathologies in both rats and humans [50]. Fructose is

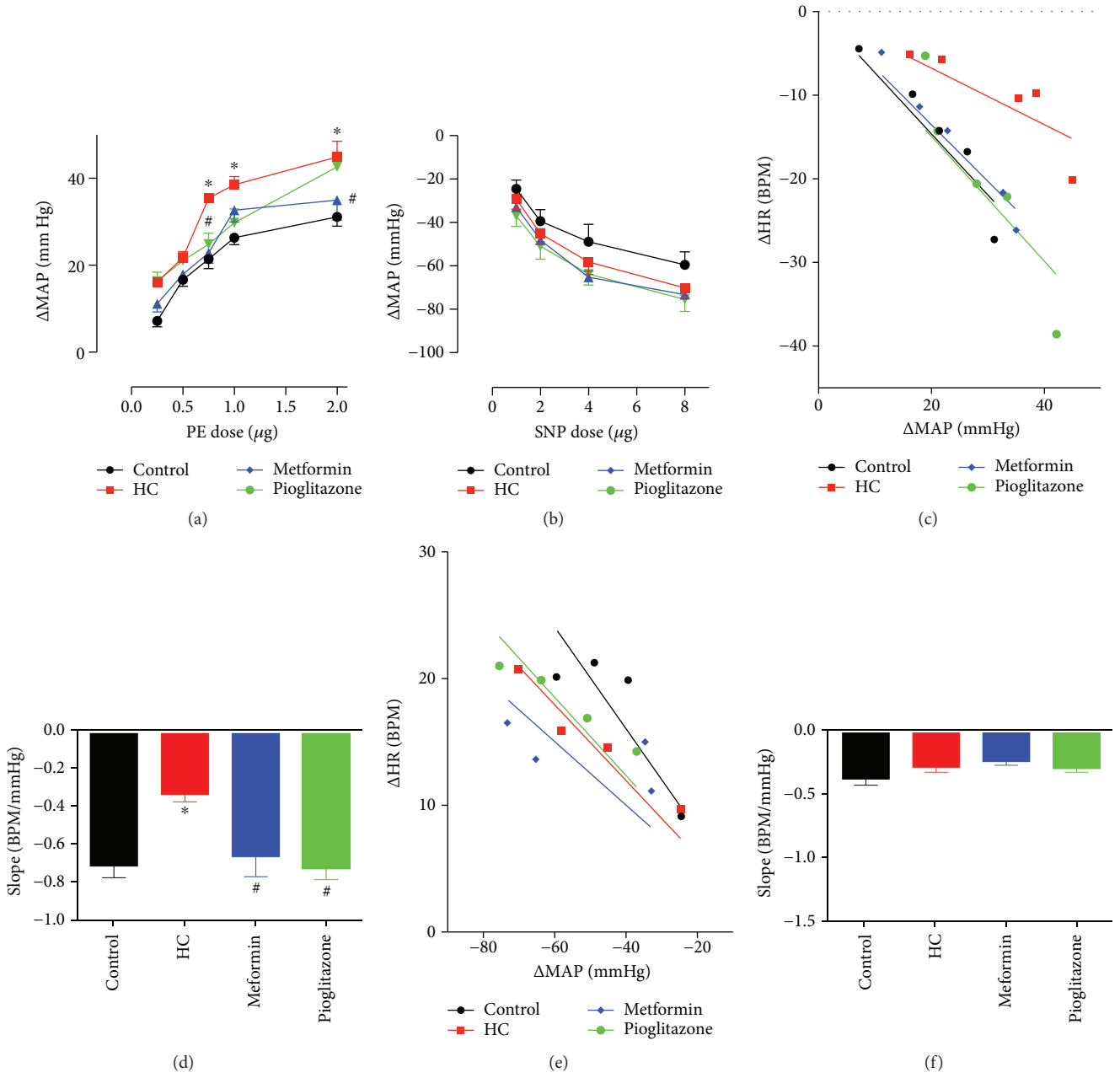

Figure 5: The effect of HC feeding and treatment with metformin or pioglitazone on BRS. (a) The pressor effect of different doses of PE in different treatment groups. ∗ and # denote $P < 0.05$ versus response at corresponding PE doses in control or HC-fed rats, respectively. Statistical significance was determined by two-way ANOVA followed by Sidak's post hoc test. (b) The reflex bradycardic response to different doses of PE in different treatment groups. (c) Best fit regression lines for the correlation between changes in MAP in response to increasing PE doses and reflex change in HR in different treatment groups. (d) Slope of the best fit regression line of the ΔMAP versus ΔHR relationship representing BRS in response to PE treatment. ∗ and # denote $P < 0.05$ versus slope in control or HC-fed rats, respectively. Statistical significance was determined by ANOVA followed by Dunnett post hoc test. (e) Best fit regression lines for the correlation between changes in MAP in response to increasing SNP doses and reflex change in HR in different treatment groups. (f) Slope of the best fit regression line of the ΔMAP versus ΔHR relationship representing BRS in response to SNP treatment. Depicted data represent mean ± SEM of values obtained from eight rats in each treatment groups.

particularly enriched in prepared foods, corn syrup additives, and carbonated beverages [51, 52]. Additionally, a recent comprehensive study [30] showed that, in contrast to high fat only, a combination of high-fat and high-fructose feeding on long term (8 months) led to the development of a more robust type 2 diabetes phenotype. Previous studies report that diets containing high fat alone and those with a combination of high fat/high fructose have similar detrimental effects on cardiovascular function in rats [30, 53–55]. In our previous studies [20], this diet was associated with the development of stable fasting hyperglycemia after 16 weeks of treatment and thus provided a

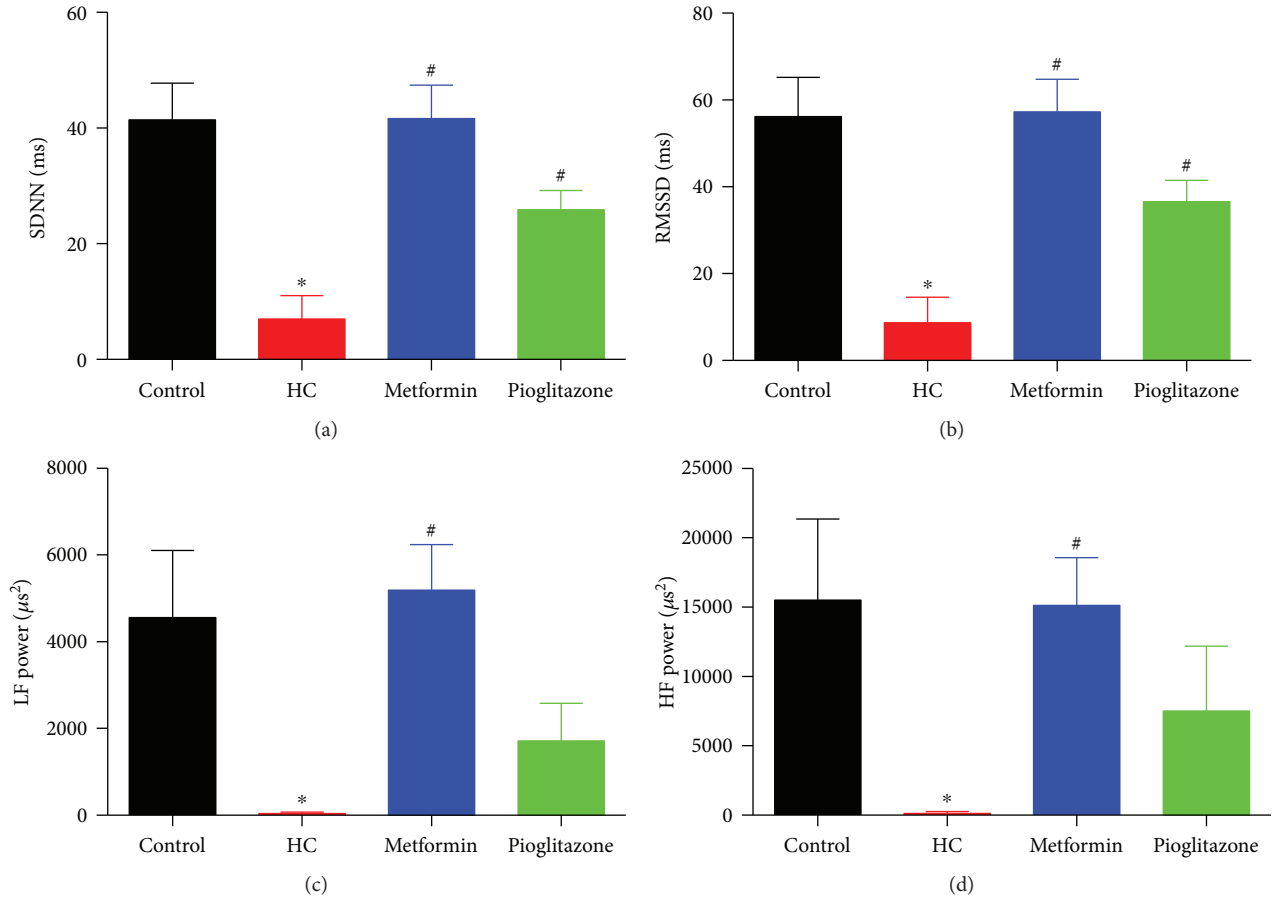

Figure 6: Changes in time domain and frequency domain HRV parameters in different treatment groups. (a), (b), (c), and (d) represent changes in SDNN, rMSSD, power spectral density of LF, and power spectral density of HF, respectively, among different treatment groups. $*$ and # denote $P < 0.05$ versus corresponding values in control or HC-fed rats, respectively. Statistical significance was determined by ANOVA followed by Dunnett post hoc test. Depicted data represent mean ± SEM of values obtained from eight rats in each treatment groups.

wider window for examination of potential molecular, structural, and functional changes occurring early in the course of metabolic challenge without interference from hyperglycemia or obesity.

No significant differences were noted among the control and HC groups in baseline BP and HR, random blood glucose levels, and OGT. Up to twelve weeks of treatment and prior to invasive examination and sacrifice, echocardiography revealed neither structural nor functional cardiac changes. Upon assessing cardiac autonomic control, multiple functional differences became apparent indicating a detrimental effect of high-calorie intake and a potential corrective effect of metformin, pioglitazone, and dietary interventions involving reduction of saturated fat intake. This detrimental effect was further corroborated by the observations of adverse molecular changes at the level of the myocardium (increased oxidative stress and TGF-β expression, decreased AMPK phosphorylation, and increased Erk1/2 phosphorylation), adipose tissue (increased inflammatory cytokine expression), and brainstem (increased oxidative stress).

Significantly, when compared to the control group, the HC group had an exaggerated vasopressor response to PE and blunted BRS and HRV. The increased response to PE is in line with the previous findings from our laboratory and from other groups showing an increased sensitivity to contractile agonists observed in isolated vessel preparations from rats receiving high-fat diet [20, 56, 57]. BRS alteration only in response to PE-driven changes in MAP implied that HC-fed rats had a reduction in vagal control but maintained integrity of sympathetic regulation. Alongside, reduction in SDNN signified a reduction in overall cardiac autonomic control and this was confirmed by the concomitant reduction in HF power (parasympathetic) and LF power (sympathetic). These results are in agreement with the previous findings in diabetic, prediabetic, and metabolic syndrome patients showing disrupted HRV parameters [58–61]. Of note, despite the lack of apparent functional or microscopic myocardial deficit, changes seen in TGF-β and IL-1β expression, oxidative stress, and AMPK and Erk1/2 phosphorylation imply an early molecular insult that might potentially lead to cardiac structural involvement over time. Indeed, reduced AMPK phosphorylation was observed in type 2 diabetic rat hearts and thought to contribute to cardiac metabolic remodeling and left ventricular dysfunction [42]. Moreover, the activation of TGF-β/Erk1/2 pathway was reported to contribute to increased fibrosis observed in the context of diabetic cardiomyopathy [42, 62]. As such, our treatment model represents the early cardiac molecular deterioration in

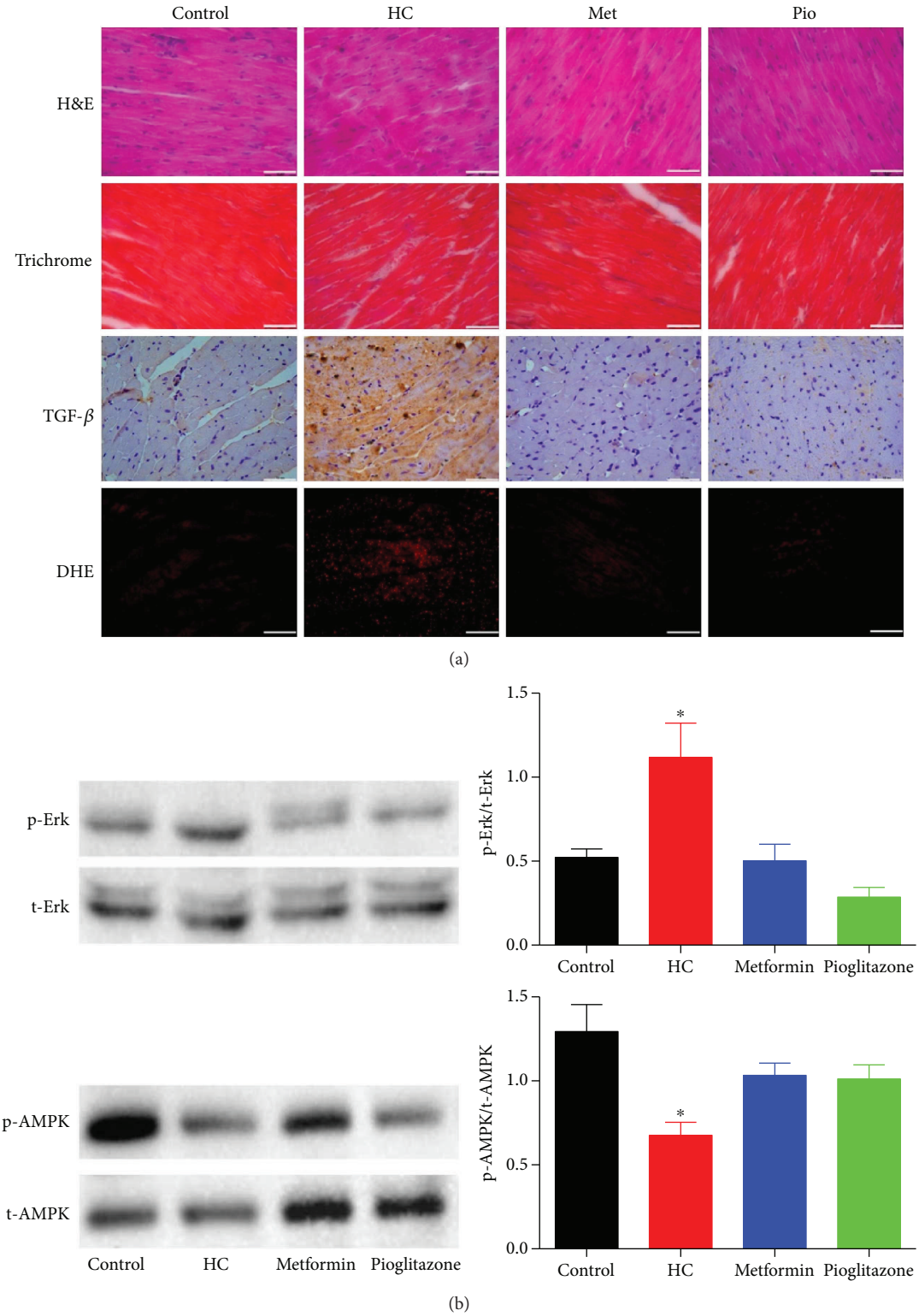

Figure 7: Cellular and molecular changes in ventricular tissue in response to HC feeding and the effect of treatment with metformin or pioglitazone. (a) Representative micrographs of histopathological staining, TGF-β immunostaining, and DHE staining of ventricular midsection. Data presented are serial sections obtained from the same tissue and are representative of tissues harvested from four rats in each group. Scale bars are 50 μm. (b) Changes in phosphorylation of Erk1/2 (above) and AMPK (below) in rat ventricles in response to HC feeding and treatment with metformin or pioglitazone. The depicted blots are representative of experiments performed on protein extracts from tissues harvested from four rats in each group. The bar graphs represent comparison of the normalized intensity of the phosphorylated protein bands. $*$ denotes $P < 0.05$ versus corresponding values in control rats. Statistical significance was determined by ANOVA followed by Dunnett post hoc test.

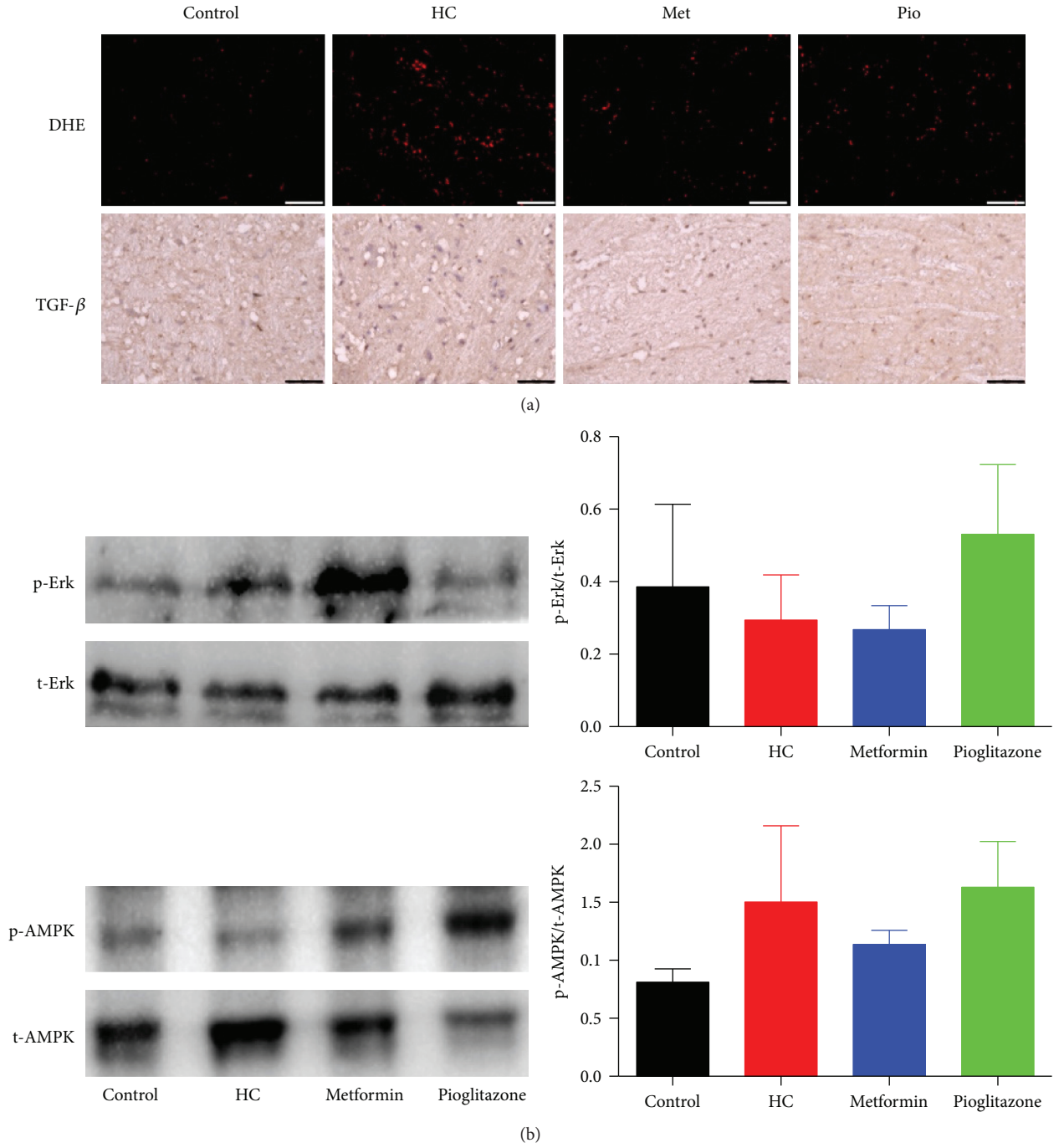

Figure 8: Cellular and molecular changes in brainstem in response to HC feeding and the effect of treatment with metformin or pioglitazone. (a) Representative micrographs of DHE and TGF-β immunostaining of brainstem sections. Data presented are serial sections obtained from the same tissue and are representative of tissues harvested from three rats in each group. Scale bars are 50 μm. (b) Changes in phosphorylation of Erk1/2 (above) and AMPK (below) in brainstem in response to HC feeding and treatment with metformin or pioglitazone. The depicted blots are representative of experiments performed on protein extracts from tissues harvested from three rats in each group. The bar graphs represent comparison of the normalized intensity of the phosphorylated protein bands.

the context of metabolic challenge preceding the development of diabetes.

From a central autonomic control perspective, recent work demonstrated that high-fat feeding was associated with increased oxidative stress in brain tissue that was linked to poor cognitive function [63]. In our model, we examined changes in the brainstem as the site for autonomic cardiovascular and vasomotor centers. CAN induced by HC feeding was associated with an increased oxidative stress. Indeed, a significant body of evidence links increased ROS production in brainstem to the autonomic dysregulation seen in cardiovascular disorders such as neurogenic hypertension

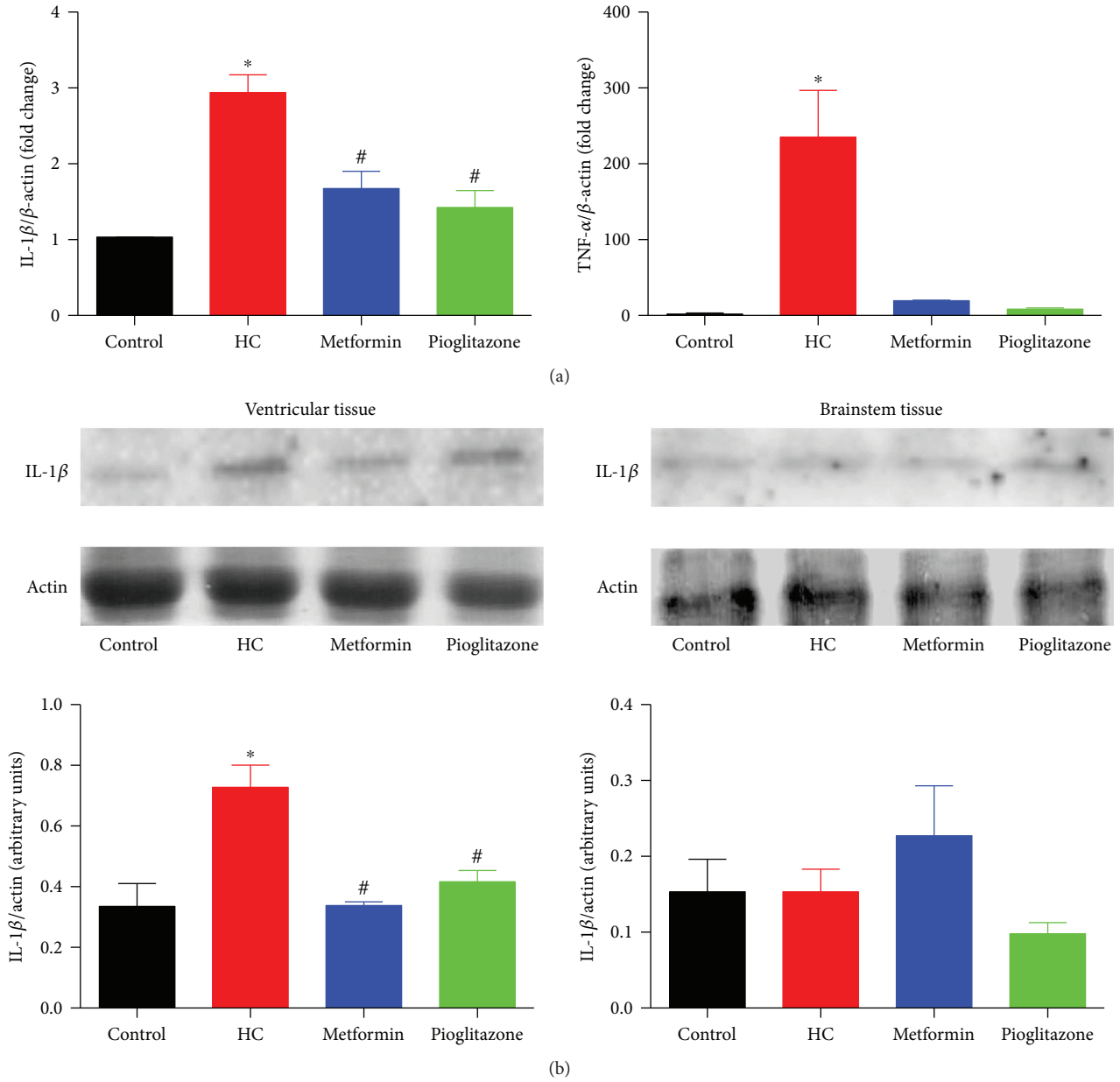

Figure 9: The effect of HC feeding and treatment with metformin or pioglitazone on inflammatory cytokine expression in perivascular adipose, ventricular, and brainstem tissues. (a) Changes in IL-1β (left) and TNF-α (right) mRNA levels in perivascular adipose tissue. Values were determined in triplicates of mRNA extracts from five different animals. (b) Representative Western blots showing changes in IL-1β expression levels in ventricular tissue (right) and brainstem tissue (left) in response to HC feeding and metformin or pioglitazone treatment. The depicted blots are representative of experiments performed on protein extracts from tissues harvested from three rats in each group. The bar graphs represent comparison of the normalized intensity of the protein bands. $*$ and # denote $P < 0.05$ versus corresponding values in control or HC-fed rats, respectively. Statistical significance was determined by ANOVA followed by Dunnett post hoc test. Depicted values represent mean ± SEM.

[64]. On the other hand, no changes were detected in either TGF-β staining, AMPK or Erk1/2 phosphorylation levels, or in IL-1β expression levels. This is consistent with a potentially reversible early insult that could possibly progress into more permanent neuronal apoptosis and damage [63].

As such, we proceeded to assess several possible approaches to reverse CAN in our model. A cardioprotective role for antidiabetic drugs beyond glucose lowering is being addressed with potential emphasis on their anti-inflammatory effects [65]. Metformin and pioglitazone were selected based on the previous studies showing their cardioprotective outcomes. In the Diabetes Prevention Program, metformin significantly reduced the myocardial infarction events in prediabetic patients and this effect persisted for a 10-year follow-up [19, 66]. Furthermore, the IRIS trial found that patients with insulin resistance receiving pioglitazone

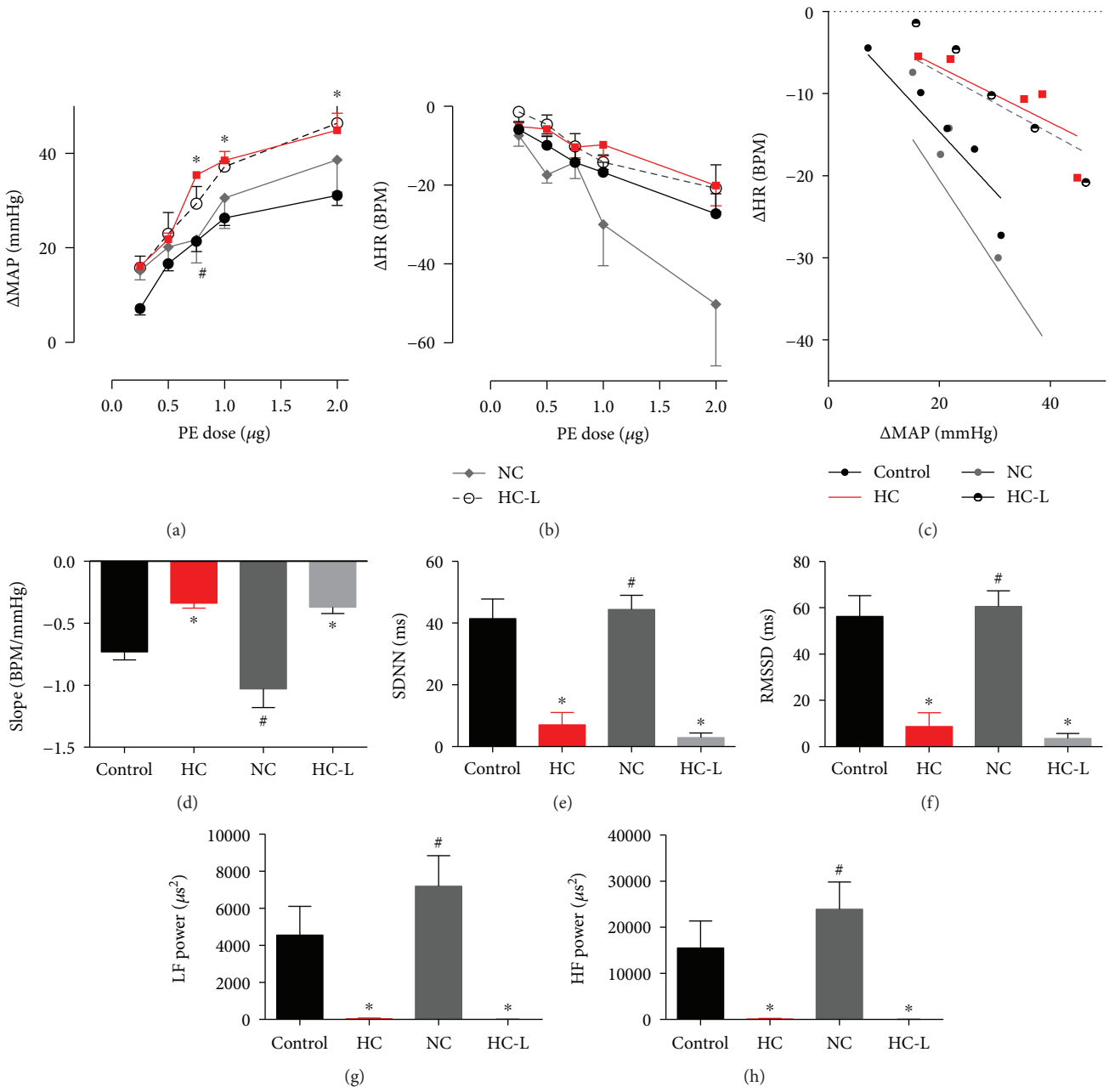

Figure 10: The effects of switching to normal chow (NC) versus isocaloric feeding with HC (HC-L) on BRS and HRV. (a) The pressor effect of different doses of PE. ∗ and # denote $P < 0.05$ versus response at corresponding PE doses in control or HC-fed rats, respectively. Statistical significance was determined by two-way ANOVA followed by Sidak's post hoc test. (b) The reflex bradycardic response to different doses of PE. (c) Best fit regression lines for the correlation between changes in MAP in response to increasing PE doses and reflex change in HR. (d) Slope of the best fit regression line of the ΔMAP versus ΔHR relationship representing BRS in response to PE treatment. (e) and (f) represent changes in time domain parameters of HRV, SDNN (e), and rMSSD (f). (g) and (h) represent changes in the power spectral density of LF (g) and HF (h). Data depicted represent mean ± SEM of values obtained from eight rats in control and HC groups and five rats in NC and HC-L groups. ∗ and # denote $P < 0.05$ versus slope in control or HC-fed rats, respectively. Statistical significance was determined by ANOVA followed by Dunnett post hoc test.

had a reduced risk of stroke or myocardial infarction [67]. Recent studies suggested that metformin has a direct anti-inflammatory action independent of improvement of metabolic parameters (hyperglycemia and insulin resistance) [23]. Through activating AMPK-dependent and AMPK-independent pathways, metformin inhibits multiple inflammatory cytokines that are believed to be responsible for the potential diabetes mellitus-independent cardioprotective [68] and neuroprotective anti-inflammatory activity [69]. Similarly, pioglitazone exerts an anti-inflammatory effect through binding to PPAR receptors leading to a reduced inflammatory cytokine production accounting for its cardioprotective and neuroprotective effects [70]. The presence of saturated fat in HC diet allows for the potential

association of adipose inflammatory pathways with the observed deleterious effects. Studies showed inflammatory changes in adipose tissue in response to high-fat feeding [45, 47, 71]. Indeed, in the present study, an increased expression of IL1-β and TNF-α was observed in adipose tissue of HC-fed rats consistent with prior research [43–45]. Significantly, pioglitazone [72] and metformin [73] were reported to reduce adipose inflammation. To this end, the effect of metformin and pioglitazone treatment in HC-fed rats was examined in this study. Both drugs were used in doses equivalent to the low end of those used in humans with the intent of having a minimal impact on blood glucose levels [24, 74]. The lack of an effect on blood glucose level was confirmed by regular random blood glucose measurement and OGT at the end of the treatment period.

As expected, no significance differences in noninvasive BP parameters and echocardiography were noted in metformin- or pioglitazone-treated rats. However, a trend towards a reduction of the increased vasopressor response to PE was evident for rats treated with metformin and pioglitazone. This is in agreement with findings from ex vivo experiments on isolated vessel preparations [20]. Both agents allowed recovery of BRS to values similar to those seen in control rats. In addition, time domain and frequency domain parameters recovered in rats treated by metformin or pioglitazone. Thus, the observed CAN recovery occurred independent of changes in blood glucose levels. Of note, the corrective effects observed in this study are mirrored by similar effects in diabetic patients. Studies investigating the effect of metformin on CAN in type 2 diabetic patients showed improved sympathovagal balance and HRV parameters [26, 75]. Similar results were also reported for pioglitazone [26, 76]. However, the recovery observed in the present study extends to the myocardial molecular derangement. Treatment with metformin or pioglitazone reversed the alterations in AMPK and Erk1/2 phosphorylation, together with TGF-β expression. As well, the observed increase in IL-1β and TNF-α adipose expression was attenuated by either treatment implying a positive impact on adipose inflammation. The putative anti-inflammatory effect extended to the reduction of the elevated cardiac IL-1β expression level observed in HC-fed rats.

Further evidence to support the potential association between adipose inflammation and CAN and to differentially assess the effect of high-calorie intake versus the nature of calorie source was obtained from the examination of two additional treatment groups. In the first group, the introduction of NC reduced the vasopressor response to PE and restored BRS. Whereas lowering the calorie intake while maintaining a high-saturated fat content of the chow elicited the same increased vasopressor response to PE seen in HC-fed rats and did not restore BRS. Time domain and frequency domain parameters were only restored by switching to normal chow (NC) and not lowering the calorie intake (HC-L). Consistent with these results, a previous study found that excess dietary fat, but not excess calories, increased inflammatory signals in hypothalamus which were attenuated by low-fat diet [46]. A potential link with CAN could be established considering the effect of adipose hormones on central neuronal activity. Among the adipokines, adiponectin and nesfatin have been found to exert metabolic and cardiovascular regulatory functions within the hypothalamic paraventricular nucleus [77]. Hence, it would be reasonable to assume that an alteration in the adipokine profile caused by adipose inflammation would have an impact on central neuronal function. In this regard, a neuroprotective mechanism for metformin or pioglitazone through normalizing the adipokine profile becomes plausible. While metformin is reported to penetrate blood-brain barrier [78], this ability remains highly questionable for pioglitazone [79]. Thus, in light of the absence of molecular changes consistent with signaling derangement and/or inflammation (apart from increased oxidative stress) in the brainstem compared to peripheral tissue, adipokine normalization becomes the more likely mechanism. Yet, this remains to be confirmed in future studies.

A potential limitation of the present study is the reduction of dietary protein intake due to displacement with the increased fat content. Gram for gram, the HC diet used in the present study offers 35% less protein than the normal chow. While major electrolytes were replaced, the displacement of dietary protein by refined constituents poses the added challenge of decreased intake of micronutrients including phosphorous [80, 81]. Dietary phosphorous is of particular relevance to the results of the present study given recent reports identifying its roles in regulating body weight [82], energy metabolism [83], postprandial lipemia [84], and glucose tolerance [85], implicating a potential effect on adipose tissue. Whether the results observed in this study are a direct consequence of increased dietary fat or an indirect response to micronutrient deficiency triggered by the refined diet remains to be established in future research.

In conclusion, the present study implicates the development of CAN and detrimental signaling changes in the myocardium as early consequences of mild metabolic challenge despite the normal gross cardiac structure/function and absence of signs of diabetes or impaired glucose tolerance. These early changes are likely the result of adipose inflammation and respond to interventions targeting this process. Our results highlight the importance of lifestyle changes involving reduction of the dietary content of saturated fat and provide novel insight regarding the implications of the anti-inflammatory action of metformin and pioglitazone. Future research would be required to elucidate a number of lingering questions. The potential effect of HC feeding and/or micronutrient deficiency on the adipokine profile needs to be systematically addressed. Whether an alteration in the relative abundance of different adipokines is related to the discrepant neuronal function and whether that ties into the early development of CAN remains to be determined. The question remains whether drugs like metformin and pioglitazone, and potentially statins, would exert a normalizing effect on the disrupted adipokine profile. On the other hand, without direct testing of blood-brain barrier penetration of metformin or pioglitazone, a direct neuronal effect cannot be ruled out. And finally, gender differences in the cardiac autonomic response to HC feeding requires

examination together with the potential detrimental effect on the offspring.

Disclosure

Preliminary results from this study were presented in a poster form at the American Heart Association Joint Scientific Sessions Meeting in San Francisco in September 2017.

Conflicts of Interest

The authors declare that they have no conflicts of interest.

Authors' Contributions

Ola Al-Assi, Rana Ghali, and Ali Mroueh contributed equally to this work.

Acknowledgments

This study was supported by funding Ahmed F. El-Yazbi through MPP Grant 320148 from the Faculty of Medicine at the American University of Beirut.

References

[1] American Diabetes Association, "Diagnosis and classification of diabetes mellitus," *Diabetes Care*, vol. 28, Supplement 1, pp. S37–S42, 2005.

[2] World Health Organization, *Global Report on Diabetes*, WHO Press, Geneva, Switzerland, 2014.

[3] H. V. Kuhnlein and O. Receveur, "Dietary change and traditional food systems of indigenous peoples," *Annual Review of Nutrition*, vol. 16, no. 1, pp. 417–442, 1996.

[4] S. M. Haffner, S. Lehto, T. Ronnemaa, K. Pyorala, and M. Laakso, "Mortality from coronary heart disease in subjects with type 2 diabetes and in nondiabetic subjects with and without prior myocardial infarction," *The New England Journal of Medicine*, vol. 339, no. 4, pp. 229–234, 1998.

[5] C. Giráldez-García, F. Javier Sangrós, A. Díaz-Redondo et al., "Cardiometabolic risk profiles in patients with impaired fasting glucose and/or hemoglobin A1c 5.7% to 6.4%: evidence for a gradient according to diagnostic criteria: the PREDAPS study," *Medicine*, vol. 94, no. 44, article e1935, 2015.

[6] Y. Huang, X. Cai, W. Mai, M. Li, and Y. Hu, "Association between prediabetes and risk of cardiovascular disease and all cause mortality: systematic review and meta-analysis," *BMJ*, vol. 355, article i5953, 2016.

[7] M. J. Fowler, "Microvascular and macrovascular complications of diabetes," *Clinical Diabetes*, vol. 26, no. 2, pp. 77–82, 2008.

[8] S. C. G. de Moura-Tonello, A. Porta, A. Marchi et al., "Cardiovascular variability analysis and baroreflex estimation in patients with type 2 diabetes in absence of any manifest neuropathy," *PLoS One*, vol. 11, no. 3, article e0148903, 2016.

[9] J. Svacinova, N. Honzikova, A. Krticka, I. Tonhajzerova, K. Javorka, and M. Javorka, "Diagnostic significance of a mild decrease of baroreflex sensitivity with respect to heart rate in type 1 diabetes mellitus," *Physiological Research*, vol. 62, no. 6, pp. 605–613, 2013.

[10] A. I. Vinik, T. Erbas, and C. M. Casellini, "Diabetic cardiac autonomic neuropathy, inflammation and cardiovascular disease," *Journal of Diabetes Investigation*, vol. 4, no. 1, pp. 4–18, 2013.

[11] D. Ziegler, K. Dannehl, H. Muhlen, M. Spuler, and F. A. Gries, "Prevalence of cardiovascular autonomic dysfunction assessed by spectral analysis, vector analysis, and standard tests of heart rate variation and blood pressure responses at various stages of diabetic neuropathy," *Diabetic Medicine*, vol. 9, no. 9, pp. 806–814, 1992.

[12] D. A. Chyun, F. J. T. Wackers, S. E. Inzucchi et al., "Autonomic dysfunction independently predicts poor cardiovascular outcomes in asymptomatic individuals with type 2 diabetes in the DIAD study," *SAGE Open Medicine*, vol. 3, 2015.

[13] A. Q. Green, S. Krishnan, F. M. Finucane, and G. Rayman, "Altered C-fiber function as an indicator of early peripheral neuropathy in individuals with impaired glucose tolerance," *Diabetes Care*, vol. 33, no. 1, pp. 174–176, 2010.

[14] R. Freeman, "Diabetic autonomic neuropathy," *Handbook of Clinical Neurology*, vol. 126, pp. 63–79, 2014.

[15] "The effect of intensive diabetes therapy on measures of autonomic nervous system function in the Diabetes Control and Complications Trial (DCCT)," *Diabetologia*, vol. 41, no. 4, pp. 416–423, 1998.

[16] S. P. Marso, G. H. Daniels, K. Brown-Frandsen et al., "Liraglutide and cardiovascular outcomes in type 2 diabetes," *The New England Journal of Medicine*, vol. 375, no. 4, pp. 311–322, 2016.

[17] B. Zinman, C. Wanner, J. M. Lachin et al., "Empagliflozin, cardiovascular outcomes, and mortality in type 2 diabetes," *The New England Journal of Medicine*, vol. 373, no. 22, pp. 2117–2128, 2015.

[18] W. N. Kernan, C. M. Viscoli, K. L. Furie et al., "Pioglitazone after ischemic stroke or transient ischemic attack," *The New England Journal of Medicine*, vol. 374, no. 14, pp. 1321–1331, 2016.

[19] Diabetes Prevention Program Research Group, "Long-term effects of lifestyle intervention or metformin on diabetes development and microvascular complications over 15-year follow-up: the diabetes prevention program outcomes study," *The Lancet Diabetes and Endocrinology*, vol. 3, pp. 866–875, 2015.

[20] A. El-Yazbi, M. El-Khatib, M. Fouda, F. Sleiman, E. Saad, H. Fouad et al., "High-calorie diet induces vascular and hemodynamic abnormalities in absence of change in blood glucose or insulin levels: modulation by oral anti-hyperglycemic drugs," *The FASEB Journal*, vol. 31, p. 1068.3, 2017.

[21] T. Maric, B. Woodside, and G. N. Luheshi, "The effects of dietary saturated fat on basal hypothalamic neuroinflammation in rats," *Brain, Behavior, and Immunity*, vol. 36, pp. 35–45, 2014.

[22] M. Milanski, G. Degasperi, A. Coope et al., "Saturated fatty acids produce an inflammatory response predominantly through the activation of TLR4 signaling in hypothalamus: implications for the pathogenesis of obesity," *The Journal of Neuroscience*, vol. 29, no. 2, pp. 359–370, 2009.

[23] Y. Saisho, "Metformin and inflammation: its potential beyond glucose-lowering effect," *Endocrine, Metabolic & Immune Disorders-Drug Targets*, vol. 15, no. 3, pp. 196–205, 2015.

[24] R. Nerla, D. Pitocco, F. Zaccardi et al., "Effect of pioglitazone on systemic inflammation is independent of metabolic control

and cardiac autonomic function in patients with type 2 diabetes," *Acta Diabetologica*, vol. 47, Supplement 1, pp. 117–122, 2010.

[25] L. Negrotto, M. F. Farez, and J. Correale, "Immunologic effects of metformin and pioglitazone treatment on metabolic syndrome and multiple sclerosis," *JAMA Neurology*, vol. 73, no. 5, pp. 520–528, 2016.

[26] O. O. Rowaiye, E. A. Jankowska, and B. Ponikowska, "Baroreceptor sensitivity and diabetes mellitus," *Cardiology Journal*, vol. 20, no. 5, pp. 453–463, 2013.

[27] P. G. Reeves, F. H. Nielsen, and G. C. Fahey Jr., "AIN-93 purified diets for laboratory rodents: final report of the American Institute of Nutrition ad hoc writing committee on the reformulation of the AIN-76A rodent diet," *The Journal of Nutrition*, vol. 123, no. 11, pp. 1939–1951, 1993.

[28] Y. Wang, S. E. Thatcher, and L. A. Cassis, "Measuring blood pressure using a noninvasive tail cuff method in mice," *Methods in Molecular Biology*, vol. 1614, pp. 69–73, 2017.

[29] G. Hanton, V. Eder, G. Rochefort, P. Bonnet, and J. M. Hyvelin, "Echocardiography, a non-invasive method for the assessment of cardiac function and morphology in preclinical drug toxicology and safety pharmacology," *Expert Opinion on Drug Metabolism & Toxicology*, vol. 4, no. 6, pp. 681–696, 2008.

[30] I. Lozano, R. Van der Werf, W. Bietiger et al., "High-fructose and high-fat diet-induced disorders in rats: impact on diabetes risk, hepatic and vascular complications," *Nutrition & Metabolism*, vol. 13, no. 1, 2016.

[31] R. Ghali-Ghoul, R. Tahseldar-Roumieh, and R. Sabra, "Effect of chronic administration of sildenafil on sodium retention and on the hemodynamic complications associated with liver cirrhosis in the rat," *European Journal of Pharmacology*, vol. 572, no. 1, pp. 49–56, 2007.

[32] H. M. El-Gowelli, K. S. Ibrahim, A. F. El-Yazbi, and M. M. El-Mas, "Role of NADPHox/Rho-kinase signaling in the cyclosporine-NSAIDs interactions on blood pressure and baroreflexes in female rats," *Life Sciences*, vol. 185, pp. 15–22, 2017.

[33] A. F. El-Yazbi, K. S. Ibrahim, H. M. El-Gowelli, N. M. El-Deeb, and M. M. El-Mas, "Modulation by NADPH oxidase of the chronic cardiovascular and autonomic interaction between cyclosporine and NSAIDs in female rats," *European Journal of Pharmacology*, vol. 806, pp. 96–104, 2017.

[34] A. G. Omar and M. M. El-Mas, "Time-domain evaluation of cyclosporine interaction with hemodynamic variability in rats," *Cardiovascular Drugs and Therapy*, vol. 18, no. 6, pp. 461–468, 2004.

[35] M. M. El-Mas and A. A. Abdel-Rahman, "Longitudinal studies on the effect of hypertension on circadian hemodynamic and autonomic rhythms in telemetered rats," *Life Sciences*, vol. 76, no. 8, pp. 901–915, 2005.

[36] P. K. Stein, M. S. Bosner, R. E. Kleiger, and B. M. Conger, "Heart rate variability: a measure of cardiac autonomic tone," *American Heart Journal*, vol. 127, no. 5, pp. 1376–1381, 1994.

[37] C. Tronel, G. Y. Rochefort, N. Arlicot, S. Bodard, S. Chalon, and D. Antier, "Oxidative stress is related to the deleterious effects of heme oxygenase-1 in an *in vivo* neuroinflammatory rat model," *Oxidative Medicine and Cellular Longevity*, vol. 2013, Article ID 264935, 10 pages, 2013.

[38] A. F. El-Yazbi, R. P. Johnson, E. J. Walsh, K. Takeya, M. P. Walsh, and W. C. Cole, "Pressure-dependent contribution of Rho kinase-mediated calcium sensitization in serotonin-evoked vasoconstriction of rat cerebral arteries," *The Journal of Physiology*, vol. 588, no. 10, pp. 1747–1762, 2010.

[39] A. F. El-Yazbi, K. S. Abd-Elrahman, and A. Moreno-Dominguez, "PKC-mediated cerebral vasoconstriction: role of myosin light chain phosphorylation versus actin cytoskeleton reorganization," *Biochemical Pharmacology*, vol. 95, no. 4, pp. 263–278, 2015.

[40] A. Moreno-Domínguez, A. F. El-Yazbi, H.-L. Zhu et al., "Cytoskeletal reorganization evoked by Rho-associated kinase- and protein kinase C-catalyzed phosphorylation of cofilin and heat shock protein 27, respectively, contributes to myogenic constriction of rat cerebral arteries," *Journal of Biological Chemistry*, vol. 289, no. 30, pp. 20939–20952, 2014.

[41] X. Z. Zhong, K. S. Abd-Elrahman, C. H. Liao et al., "Stromatoxin-sensitive, heteromultimeric Kv2.1/Kv9.3 channels contribute to myogenic control of cerebral arterial diameter," *The Journal of Physiology*, vol. 588, no. 22, pp. 4519–4537, 2010.

[42] X. Y. Liu, F. C. Liu, C. Y. Deng et al., "Left ventricular deformation associated with cardiomyocyte Ca^{2+} transients delay in early stage of low-dose of STZ and high-fat diet induced type 2 diabetic rats," *BMC Cardiovascular Disorders*, vol. 16, no. 1, p. 41, 2016.

[43] D. B. Ballak, R. Stienstra, C. J. Tack, C. A. Dinarello, and J. A. van Diepen, "IL-1 family members in the pathogenesis and treatment of metabolic disease: focus on adipose tissue inflammation and insulin resistance," *Cytokine*, vol. 75, no. 2, pp. 280–290, 2015.

[44] Y. E. Kang, J. M. Kim, K. H. Joung et al., "The roles of adipokines, proinflammatory cytokines, and adipose tissue macrophages in obesity-associated insulin resistance in modest obesity and early metabolic dysfunction," *PLoS One*, vol. 11, no. 4, article e0154003, 2016.

[45] L. Allen, L. Ramalingam, K. Menikdiwela et al., "Effects of delta-tocotrienol on obesity-related adipocyte hypertrophy, inflammation and hepatic steatosis in high-fat-fed mice," *The Journal of Nutritional Biochemistry*, vol. 48, pp. 128–137, 2017.

[46] K. A. Posey, D. J. Clegg, R. L. Printz et al., "Hypothalamic proinflammatory lipid accumulation, inflammation, and insulin resistance in rats fed a high-fat diet," *American Journal of Physiology - Endocrinology and Metabolism*, vol. 296, no. 5, pp. E1003–E1012, 2009.

[47] B. Sousa-Pinto, L. Gonçalves, A. R. Rodrigues et al., "Characterization of TGF-β expression and signaling profile in the adipose tissue of rats fed with high-fat and energy-restricted diets," *The Journal of Nutritional Biochemistry*, vol. 38, pp. 107–115, 2016.

[48] A. B. Evert, J. L. Boucher, M. Cypress et al., "Nutrition therapy recommendations for the management of adults with diabetes," *Diabetes Care*, vol. 36, no. 11, pp. 3821–3842, 2013.

[49] R. Buettner, J. Scholmerich, and L. C. Bollheimer, "High-fat diets: modeling the metabolic disorders of human obesity in rodents," *Obesity*, vol. 15, no. 4, pp. 798–808, 2007.

[50] P. Valensi, "Hypertension, single sugars and fatty acids," *Journal of Human Hypertension*, vol. 19, no. S3, pp. S5–S9, 2005.

[51] S. S. Elliott, N. L. Keim, J. S. Stern, K. Teff, and P. J. Havel, "Fructose, weight gain, and the insulin resistance syndrome," *The American Journal of Clinical Nutrition*, vol. 76, no. 5, pp. 911–922, 2002.

[52] W. C. Dornas, W. G. de Lima, M. L. Pedrosa, and M. E. Silva, "Health implications of high-fructose intake and current research," *Advances in Nutrition: An International Review Journal*, vol. 6, no. 6, pp. 729–737, 2015.

[53] H. Z. Toklu, J. Muller-Delp, Y. Sakaraya et al., "High dietary fructose does not exacerbate the detrimental consequences of high fat diet on basilar artery function," *Journal of Physiology and Pharmacology*, vol. 67, no. 2, pp. 205–216, 2016.

[54] H. A. Peredo, H. Lee, A. S. Donoso, V. Andrade, N. Sanchez Eluchans, and A. M. Puyo, "A high-fat plus fructose diet produces a vascular prostanoid alterations in the rat," *Autonomic & Autacoid Pharmacology*, vol. 34, no. 3-4, pp. 35–40, 2015.

[55] J.-P. Huang, M.-L. Cheng, C.-Y. Hung et al., "Docosapentaenoic acid and docosahexaenoic acid are positively associated with insulin sensitivity in rats fed high-fat and high-fructose diets," *Journal of Diabetes*, vol. 9, no. 10, pp. 936–946, 2017.

[56] J. I. Kim, "High fat diet confers vascular hyper-contractility against angiotensin II through upregulation of MLCK and CPI-17," *The Korean Journal of Physiology & Pharmacology*, vol. 21, no. 1, pp. 99–106, 2017.

[57] S. Ghatta and P. Ramarao, "Increased contractile responses to 5-hydroxytryptamine and angiotensin II in high fat diet fed rat thoracic aorta," *Lipids in Health and Disease*, vol. 3, no. 1, p. 19, 2004.

[58] H. Kudat, V. Akkaya, A. B. Sozen et al., "Heart rate variability in diabetes patients," *Journal of International Medical Research*, vol. 34, no. 3, pp. 291–296, 2006.

[59] E. B. Schroeder, L. E. Chambless, D. Liao et al., "Diabetes, glucose, insulin, and heart rate variability: The Atherosclerosis Risk in Communities (ARIC) study," *Diabetes Care*, vol. 28, no. 3, pp. 668–674, 2005.

[60] A. S. Balcıoğlu, S. Akıncı, D. Çiçek, A. Çoner, U. A. Bal, and İ. H. Müderrisoğlu, "Cardiac autonomic nervous dysfunction detected by both heart rate variability and heart rate turbulence in prediabetic patients with isolated impaired fasting glucose," *The Anatolian Journal of Cardiology*, vol. 16, no. 10, pp. 762–769, 2016.

[61] T. Koskinen, M. Kähönen, A. Jula et al., "Metabolic syndrome and short-term heart rate variability in young adults," *Diabetic Medicine*, vol. 26, no. 4, pp. 354–361, 2009.

[62] V. Soetikno, F. R. Sari, V. Sukumaran et al., "Curcumin prevents diabetic cardiomyopathy in streptozotocin-induced diabetic rats: possible involvement of PKC–MAPK signaling pathway," *European Journal of Pharmaceutical Sciences*, vol. 47, no. 3, pp. 604–614, 2012.

[63] P. Sa-nguanmoo, P. Tanajak, S. Kerdphoo et al., "SGLT2-inhibitor and DPP-4 inhibitor improve brain function via attenuating mitochondrial dysfunction, insulin resistance, inflammation, and apoptosis in HFD-induced obese rats," *Toxicology and Applied Pharmacology*, vol. 333, pp. 43–50, 2017.

[64] J. C. Cruz, A. F. L. Flôr, M. S. França-Silva, C. M. Balarini, and V. A. Braga, "Reactive oxygen species in the paraventricular nucleus of the hypothalamus alter sympathetic activity during metabolic syndrome," *Frontiers in Physiology*, vol. 6, p. 384, 2015.

[65] A. J. Scheen, N. Esser, and N. Paquot, "Antidiabetic agents: potential anti-inflammatory activity beyond glucose control," *Diabetes & Metabolism*, vol. 41, no. 3, pp. 183–194, 2015.

[66] P. King, I. Peacock, and R. Donnelly, "The UK prospective diabetes study (UKPDS): clinical and therapeutic implications for type 2 diabetes," *British Journal of Clinical Pharmacology*, vol. 48, no. 5, pp. 643–648, 1999.

[67] M. Lee, J. L. Saver, H. W. Liao, C. H. Lin, and B. Ovbiagele, "Pioglitazone for secondary stroke prevention: a systematic review and meta-analysis," *Stroke*, vol. 48, no. 2, pp. 388–393, 2017.

[68] A. R. Cameron, V. L. Morrison, D. Levin et al., "Anti-inflammatory effects of metformin irrespective of diabetes status," *Circulation Research*, vol. 119, no. 5, pp. 652–665, 2016.

[69] Q.-L. Mao-Ying, A. Kavelaars, K. Krukowski et al., "The anti-diabetic drug metformin protects against chemotherapy-induced peripheral neuropathy in a mouse model," *PLoS One*, vol. 9, no. 6, article e100701, 2014.

[70] R. Kapadia, J. H. Yi, and R. Vemuganti, "Mechanisms of anti-inflammatory and neuroprotective actions of PPAR-gamma agonists," *Frontiers in Bioscience*, vol. 13, no. 13, pp. 1813–1826, 2008.

[71] L. Dong, Y. Zhang, L. Yang, G. Liu, J. Ye, and H. Wang, "Effects of a high-fat diet on adipose tissue CD8+ T cells in young vs. adult mice," *Inflammation*, vol. 40, no. 6, pp. 1944–1958, 2017.

[72] M. Spencer, L. Yang, A. Adu et al., "Pioglitazone treatment reduces adipose tissue inflammation through reduction of mast cell and macrophage number and by improving vascularity," *PLoS One*, vol. 9, no. 7, article e102190, 2014.

[73] T. Qi, Y. Chen, H. Li et al., "A role for *PFKFB3*/iPFK2 in metformin suppression of adipocyte inflammatory responses," *Journal of Molecular Endocrinology*, vol. 59, no. 1, pp. 49–59, 2017.

[74] A. B. Nair and S. Jacob, "A simple practice guide for dose conversion between animals and human," *Journal of Basic and Clinical Pharmacy*, vol. 7, no. 2, pp. 27–31, 2016.

[75] D. Manzella, R. Grella, K. Esposito, D. Giugliano, M. Barbagallo, and G. Paolisso, "Blood pressure and cardiac autonomic nervous system in obese type 2 diabetic patients: effect of metformin administration," *American Journal of Hypertension*, vol. 17, no. 3, pp. 223–227, 2004.

[76] F. E. Gianiorio, M. Casu, V. Patrone, C. G. Egan, and G. Murialdo, "Effect of pioglitazone on cardiac sympathovagal modulation in patients with type 2 diabetes," *Acta Diabetologica*, vol. 48, no. 4, pp. 283–290, 2011.

[77] S. P. Loewen, A. R. Paterson, S. Y. Loh et al., "Sex-specific differences in cardiovascular and metabolic hormones with integrated signalling in the paraventricular nucleus of the hypothalamus," *Experimental Physiology*, vol. 102, no. 11, pp. 1373–1379, 2017.

[78] K. Labuzek, D. Suchy, B. Gabryel, A. Bielecka, S. Liber, and B. Okopien, "Quantification of metformin by the HPLC method in brain regions, cerebrospinal fluid and plasma of rats treated with lipopolysaccharide," *Pharmacological Reports*, vol. 62, no. 5, pp. 956–965, 2010.

[79] W. T. Festuccia, S. Oztezcan, M. Laplante et al., "Peroxisome proliferator-activated receptor-γ-mediated positive energy balance in the rat is associated with reduced sympathetic drive to adipose tissues and thyroid status," *Endocrinology*, vol. 149, no. 5, pp. 2121–2130, 2008.

[80] O. A. Obeid, "Low phosphorus status might contribute to the onset of obesity," *Obesity Reviews*, vol. 14, no. 8, pp. 659–664, 2013.

[81] S. A. Gibson, "Dietary sugars intake and micronutrient adequacy: a systematic review of the evidence," *Nutrition Research Reviews*, vol. 20, no. 2, pp. 121–131, 2007.

[82] J. J. Ayoub, M. J. A. Samra, S. A. Hlais, M. S. Bassil, and O. A. Obeid, "Effect of phosphorus supplementation on weight gain and waist circumference of overweight/obese adults: a randomized clinical trial," *Nutrition & Diabetes*, vol. 5, no. 12, article e189, 2015.

[83] M. Bassil and O. Obeid, "Phosphorus supplementation recovers the blunted diet-induced thermogenesis of overweight and obese adults: a pilot study," *Nutrients*, vol. 8, no. 12, 2016.

[84] J. Hazim, S. Hlais, H. Ghattas, D. Shatila, M. Bassil, and O. Obeid, "Phosphorus supplement alters postprandial lipemia of healthy male subjects: a pilot cross-over trial," *Lipids in Health and Disease*, vol. 13, no. 1, p. 109, 2014.

[85] M. Khattab, C. Abi-Rashed, H. Ghattas, S. Hlais, and O. Obeid, "Phosphorus ingestion improves oral glucose tolerance of healthy male subjects: a crossover experiment," *Nutrition Journal*, vol. 14, no. 1, p. 112, 2015.

Hindawi
Oxidative Medicine and Cellular Longevity
Volume 2018, Article ID 6717212, 10 pages
https://doi.org/10.1155/2018/6717212

Research Article

Hydrogen Sulfide Attenuates LPS-Induced Acute Kidney Injury by Inhibiting Inflammation and Oxidative Stress

Yuhong Chen,[1,2] Sheng Jin,[1] Xu Teng,[1] Zhenjie Hu,[2] Zhihong Zhang,[1] Xuan Qiu,[3] Danyang Tian,[1] and Yuming Wu[1,4,5]

[1]*Department of Physiology, Hebei Medical University, Hebei, China*
[2]*Intensive Care Unit, The Fourth Hospital of Hebei Medical University, Hebei, China*
[3]*Department of Endocrinology, The Third Hospital of Hebei Medical University, Hebei, China*
[4]*Hebei Collaborative Innovation Center for Cardio-Cerebrovascular Disease, Hebei, China*
[5]*Key Laboratory of Vascular Medicine of Hebei Province, Hebei, China*

Correspondence should be addressed to Yuming Wu; wuyum@yahoo.com

Received 27 August 2017; Revised 21 November 2017; Accepted 4 December 2017; Published 31 January 2018

Academic Editor: Mohamed A. Abdelmegeed

In order to investigate the protective mechanism of hydrogen sulfide (H_2S) in sepsis-associated acute kidney injury (SA-AKI), ten AKI patients and ten healthy controls were enrolled. In AKI patients, levels of creatinine (Cre), urea nitrogen (BUN), tumor necrosis factor-α (TNF-α) and interleukin-1β (IL-1β), and myeloperoxidase (MPO) activity as well as concentrations of malondialdehyde (MDA) and hydrogen peroxide (H_2O_2) were significantly increased compared with those of controls. However, plasma level of H_2S decreased and was linearly correlated with levels of Cre and BUN. After that, an AKI mouse model by intraperitoneal lipopolysaccharide (LPS) injection was constructed for *in vivo* study. In AKI mice, H_2S levels decreased with the decline of 3-MST activity and expression; similar changes were observed in other indicators mentioned above. However, the protein expressions of TLR4, NLRP3, and caspase-1 in mice kidney tissues were significantly increased 6 h after LPS injection. NaHS could improve renal function and kidney histopathological changes, attenuate LPS-induced inflammation and oxidative stress, and inhibit expressions of TLR4, NLRP3, and caspase-1. Our study demonstrated that endogenous H_2S is involved in the pathogenesis of SA-AKI, and exogenous H_2S exerts protective effects against LPS-induced AKI by inhibiting inflammation and oxidative stress via the TLR4/NLRP3 signaling pathway.

1. Introduction

AKI is a clinical syndrome caused by various factors and characterized by a rapid decline in renal function. Sepsis is the most common cause of AKI (40%–50%) in critically ill patients, and the mortality of SA-AKI is as high as 70% [1, 2]. The pathogenesis of SA-AKI is complicated, including inflammation, coagulation cascade activation, oxidative stress, microcirculatory disturbance, renal hypoperfusion, and renal venous congestion [3, 4]. Despite the growing understanding of the pathophysiological mechanisms of AKI, the development of pharmacological treatments for AKI shows little progress.

LPS is a normal component of cell wall of most Gram-negative bacteria, which can trigger cytokine synthesis, secretion, and a subsequent inflammatory process. Previous studies have demonstrated that LPS is one of the most important causes of sepsis and is involved in the pathogenesis of SA-AKI, which may lead to "cytokine storm," intensified oxidative stress, low blood pressure, renal hypoperfusion, and finally a gradual decline in renal function [5–7]. Toll-like receptors (TLRs) are the most important pattern-recognition receptors and play a key role in innate immunity. The major receptor for LPS is TLR4 [8, 9], which is activated after LPS binding, and induces downstream signaling cascades as well as expression of inflammatory

cytokines [10]. Nucleotide-binding domain and leucine-rich repeat protein-3 (NLRP3) inflammasome is one of the most important members of the Nod-like receptor (NLR) family, including NLRP3, the adaptor protein ASC, and a cysteine protease caspase-1. Abderrazak et al. [11] have found that NLRP3 inflammasome participated in the inflammatory process and may be critical for the development of sepsis and AKI. Activation of NLRP3 inflammasome could promote the maturation and release of proinflammatory cytokines IL-1β and IL-18. Another study found that NLRP3 expression induced by LPS was dose- and time-dependent, but it failed to induce NLRP3 expression in cells in the absence of TLR4 [12].

H_2S was considered to be toxic for a long time until endogenous H_2S was discovered in the rat brain [13]. H_2S is mainly synthesized from L-cysteine by two pyridoxal-5′-phosphate-(PLP-) dependent enzymes, namely, cystathionine β-synthase (CBS) and cystathionine γ-lyase (CSE), and one phosphate-independent enzyme, 3-mercaptopyruvate sulfurtransferase (3-MST) [14]. Recently, a new H_2S-synthesis pathway from D-cysteine by 3-MST along with D-amino acid oxidase (DAO) was discovered; moreover, D-cysteine was shown to be significantly superior to L-cysteine, particularly in the kidney and cerebellum [15]. Numerous studies have shown that H_2S might have a potential therapeutic effect on ischemia/reperfusion injury (IRI) in multiple organs and metabolic diseases by inhibiting inflammation and oxidative stress [16–21]. Huang et al. [16] have demonstrated that H_2S could protect against high glucose-induced inflammation and apoptosis by inhibiting the TLR4/NF-κB pathway and NLRP3 activation in H9c2 cardiomyocytes. Zhang et al. [19] suggested that treatment with H_2S could attenuate endotoxin-induced lung inflammation by inhibiting inducible nitric oxide synthase (iNOS) expression and nitric oxide (NO) production. Shibuya et al. [15] have reported that administration of D-cysteine could increase the H_2S level in kidney tissues and protect renal function from IRI. Ahmad et al. [20] and Han et al. [21] also demonstrated that exogenous H_2S accelerates kidney repair after IRI by inhibiting oxidative stress and inflammation. Although various effects of H_2S in disease have been discovered, the role of H_2S in the inflammatory process of sepsis has been a matter of debate for a long time. Whether H_2S protects renal function by regulating inflammation and oxidative stress in SA-AKI remains unclear.

The purpose of the trial was to examine the effect of H_2S on renal function during sepsis and the underlying mechanisms of H_2S in SA-AKI.

2. Materials and Methods

2.1. Patients and Blood Sample Collection. Ten patients with AKI (AKI group) were recruited from the ICU at the Fourth Hospital of Hebei Medical University in China from June 2016 to November 2016, and ten healthy donors (control group) were selected from the age-matched population. AKI is defined as an abrupt decrease in renal function (within 48 h) and diagnosed according to the definition of the Acute Dialysis Quality Initiative group [22]. All patients with AKI were infected with Gram-negative bacteria (covering 2 cases from *Acinetobacter baumannii*, 2 cases from *Pseudomonas aeruginosa*, 2 cases from *Klebsiella*, 3 cases from *Escherichia coli*, and 1 case from *Clostridium difficile*), and renal injury caused by renal and postrenal factors has been excluded. None of the patients had been treated with drugs that cause kidney damage before. The patients who are younger than 18 years old, pregnant, or with a history of chronic renal dysfunction were excluded. The general condition and medical history of all participants were recorded. Blood samples were prospectively obtained from each participant at admission; after centrifugation for 10 minutes at 4000 rpm, the supernatants were frozen at −80°C. Each patient provided written informed consent prior to the study. The protocol was approved by the Ethics Committee of the Fourth Hospital of Hebei Medical University (Shijiazhuang, China) and performed in accordance with all applicable laws, regulations, and guidelines in China (including good clinical practice guidelines), which are relating protection of human subjects as volunteers. The study complied with the published regulations of the Declaration of Helsinki.

2.2. Drugs and Chemicals. LPS and NaHS were obtained from Sigma (Sigma–Aldrich, USA). NaHS was prepared 30 minutes before use. Detection kits for TNF-α and IL-1β levels were purchased from Xinbosheng Bioengineering (Shenzhen, China). Detection kits for MDA, H_2O_2, and MPO activities were obtained from Jiancheng BioEngineering (Nanjing, China). Dihydroethidium (DHE) was obtained from Beyotime Biotechnology (Shanghai, China) and, before use, dissolved in dimethyl sulfoxide (DMSO) to the desired concentration. Bicinchoninic acid (BCA) reagent was purchased from Generay Biotechnology (Shanghai, China).

2.3. Animals and Treatments. Male wild-type C57BL/6 J mice (8–10 weeks) were purchased from Vital River Laboratories (Beijing, China), subsequently housed and bred in standard conditions (12 h light/dark cycle) under constant temperature (22°C ± 2°C) and humidity (60%), and given free access to food and water.

After two weeks, 24 mice were divided into three groups randomly ($n = 8$): control, LPS, and LPS + NaHS (50 μmol/L) groups. The LPS and LPS + NaHS groups were i.p. injected with LPS (5 mg/kg); in the control group, mice received an equal volume of saline (i.p.). Three hours after LPS treatment, the LPS + NaHS group received NaHS (50 μmol/kg, i.p.); the LPS group were injected with an equal volume of saline (i.p.). The blood and kidney tissues of mice were collected 6 h after LPS treatment. Blood samples were immediately spun for 10 minutes at 4000 rpm and frozen at −80°C. The left kidney tissues were fixed with paraformaldehyde (4%), and the right kidney tissues were frozen at −80°C. All animal studies were carried out under the Guide for the Care and Use of Laboratory Animals (1985, NIH) after a review by the Ethics Committee for Laboratory Animals Care and Use of Hebei Medical University.

2.4. Histological Analysis. The kidney tissues were fixed with paraformaldehyde (4%), after 48 hours, paraffin-embedded and sectioned into 4 μm thick, and then processed for

hematoxylin and eosin (H&E) staining and evaluated using a light microscope (Olympus BX40, Tokyo, Japan). Kidney histological changes were scored as the previous study described [23] and evaluated in a double-blind fashion. Kidney damage was estimated at 5 randomly selected fields in the outer medulla, and tubular injury was defined as cellular degeneration and vacuolization, reduction of brush border epithelium, tubular obstruction, and cast formation. According to the following criteria: 0 = normal; 1 = damage less than 25% of tubular area; 2 = damage between 25% and 50% of tubular area; 3 = damage between 50% and 75% of tubular area; and 4 = damage between 75% and 100% of tubular area.

2.5. Measurements of Cre and BUN Levels in Plasma. Plasma Cre and BUN levels in patients and mice were measured using an automatic biochemical analyzer (Cobas 6000, Roche, Switzerland).

2.6. Measurement of Inflammatory Cytokines in Plasma. The enzyme-linked immunosorbent assay (ELISA) kits were used to determine the plasma TNF-α and IL-1β levels in patients and mice.

2.7. Measurement of the MPO Activity and MDA and H_2O_2 Concentrations. The plasma of patients and kidney tissues of mice were collected as described above. MPO activity and MDA and H_2O_2 concentrations were measured with colorimetric detection kits.

2.8. Measurement of Reactive Oxygen Species (ROS) Level. ROS level in kidney tissues was measured by staining the fresh frozen sections with DHE. Fresh kidney tissues were mounted using Tissue-Tek O.C.T. Blocks were sectioned into 5 μm-thick slices, washed twice with prepared PBS, and incubated for 30 minutes with DHE (10 μmol/L). The resulting color reaction was immediately measured with a fluorescence microscopy (Leica, Germany).

2.9. Measurement of CSE and CBS and 3-MST Activities. CSE and CBS and 3-MST activities in kidney tissues were measured according to the previous study described [24]. Homogenates from kidney tissues were prepared in ice-cold PBS; after centrifugation at 4°C at 12,000 rpm for 20 minutes, the supernatants were separated for measurement and protein concentrations were quantified by BCA assay. The cofactor pyridoxal-5′-phosphate (2 mmol/L) and enzyme substrate L-cysteine (10 mmol/L) were incorporated to the supernatant; after incubation for 30 minutes, the mixture was used to detect CSE and CBS activity. The α-ketoglutarate (2 mmol/L) and L-cysteine (10 mmol/L) were incorporated to the supernatant; after incubation for 30 minutes, the mixture was used to detect 3-MST activity. The activities of these H_2S-generating enzymes were calculated by measuring H_2S concentrations in the reaction system and the amount of H_2S produced per microgram protein per hour.

2.10. Measurement of H_2S Levels. H_2S levels in the plasma and kidney tissues were detected according to previously described methods [25]. Homogenates from kidney tissues were prepared using cold Tris-HCl (100 mmol/L, pH 8.5); after centrifugation at 4°C at 12,000 rpm for 20 minutes, the supernatants were separated for measurement and protein concentrations were quantified by BCA assay. 30 μL supernatant or plasma, 80 μL monobromobimane (MBB, Sigma–Aldrich), and 10 μL ammonia (0.1%) were mixed, by shaking at room temperature for 1 h, and 10 μL formic acid (20%) was added to stop the reaction. Following a 10-minute centrifugation (15,000 rpm, 4°C), clear supernatants were frozen at −80°C for detection. H_2S levels were determined using a curve formed with sodium sulfide (0–40 μmol/L) standards. Plasma H_2S level was expressed as μmol/L, and the H_2S level in kidney tissues was expressed as μmol/g of protein.

2.11. Western Blot Analysis. Frozen right kidney specimens were dispersed mechanically in cold RIPA buffer. Proteins in the supernatants were extracted and quantified by BCA assay. After electrophoresis on 10% SDS-PAGE gels, the proteins were blotted to polyvinylidene fluoride (PVDF) membranes (Millipore-Upstate). After blocking in nonfat milk (5%) for 40minutes at room temperature, the membranes were incubated at 4°C for 12–18 hours with antibodies against CSE, CBS, 3-MST, TLR4, NLRP3, caspase-1, and β-actin (CSE and CBS were from Proteintech, USA; 3-MST and TLR4 were obtained from Abcam, USA; NLRP3 was obtained from Abnova, China; and β-actin was obtained from Irvine, USA). After washing three times with TBST, the membranes were incubated with secondary antibodies (Proteintech, USA) at room temperature for 2 h. Blots were detected with an enhanced chemiluminescence detection system (Sage Creation, Beijing, China). Band intensities were quantified using ImageJ software.

2.12. Statistical Analyses. All data analyses were performed using SPSS software version 21.0 (SPSS Inc., Chicago, IL, USA). Results were expressed as the mean ± S.E.M. For a comparison of more than two groups, a one-way analysis of variance (ANOVA), followed by the Student-Newman-Keuls test for multiple comparison, was applied. Comparisons between two groups were assessed by t-test. Statistical significance was defined as a p value of <0.05.

3. Results

3.1. H_2S Levels Correlated with Cre and BUN Levels in Patients with SA-AKI. The characteristics of the 10 healthy donors and 10 AKI patients are shown in Table 1. There were no statistically significant differences between the two groups when comparing general features. Compared with controls, plasma Cre (Figure 1(a)) and BUN (Figure 1(b)) levels were significantly higher in patients with SA-AKI, whereas H_2S levels were lower (Figure 1(c)). Furthermore, there was a significant inverse correlation between the levels of H_2S and Cre (Figure 1(d)) or BUN (Figure 1(e)). This indicated that H_2S level decreased during the pathological changes of SA-AKI.

3.2. Inflammatory Cytokine and Oxidative Stress Increased in Patients with SA-AKI. Plasma TNF-α and IL-1β levels increased in the AKI groups compared with those of the controls (Figures 1(f) and 1(g)). Furthermore, MPO activity

Table 1: Characteristics of control and SA-AKI patients.

	Control ($n = 10$)	AKI ($n = 10$)	p
Age, yrs, mean [SD]	65.3 [8.6]	70.7 [16.0]	NS
Gender, male (%)	5 (50)	6 (60)	NS
BMI, kg/m^2, mean [SD]	24.3 [1.8]	22.7 [2.2]	NS
Etiology of sepsis, by organ (n)	NA	Respiratory (4) Abdominal (3) Genitourinary (1) Intestines (2)	
Previous history of chronic kidney disease (yes/no)	0/10	0/10	NS
WBC, $\times 10^9$/L, mean [SD]	5.4 [1.4]	14.3 [3.1]	<0.001
CRP, mg/dL	5.9 [1.5]	41.2 [25.5]	0.002

BMI: body mass index; WBC: white blood cell; CRP: C-reactive protein; NS = not significant; NA = not applicable.

and plasma H_2O_2 and MDA concentrations of patients were measured. The results were shown in Figures 1(h)–1(j). MPO activity and H_2O_2 and MDA concentrations increased in the SA-AKI group compared with those in the control group.

3.3. H_2S Played a Role in LPS-Induced AKI. In LPS-induced AKI mice, H_2S levels in both the plasma and kidney tissues were significantly lower than those in the control groups (Figures 2(a) and 2(b)). H_2S was generated by CBS, CSE, and 3-MST enzymes; therefore, the activity and expression of these three enzymes were measured in the kidney samples. 3-MST activity significantly decreased in the kidney tissues of LPS-induced AKI mice compared with that in controls, but there were no differences in CBS and CSE activities (Figures 2(c) and 2(d)). The expression of 3-MST significantly decreased in LPS-induced AKI mice compared with that in controls, whereas there were no differences in CBS and CSE expression (Figures 2(e)–2(h)). However, treatment with NaHS (50 μmol/kg) significantly increased the LPS-induced reduction of H_2S levels in the plasma and kidney tissues (Figures 2(a) and 2(b)), which was accompanied by a decline in plasma Cre and BUN levels (Figures 2(i) and 2(g)). In addition, NaHS treatment significantly ameliorated renal pathological changes caused by LPS. (Figures 2(k) and 2(l)).

3.4. Exogenous H_2S Attenuated Inflammatory Cytokines and Oxidative Stress in Mice with LPS-Induced AKI. Consistent with the performance in SA-AKI patients, plasma TNF-α and IL-1β levels, MPO activity, the ROS levels, and H_2O_2 and MDA concentrations in the kidney tissues significantly increased in mice with LPS-induced AKI. However, exogenous H_2S could significantly attenuate these changes (Figures 3(a)–3(f)).

3.5. Exogenous H_2S Attenuated the Formation of NLRP3 in the Kidney Tissues of Mice with LPS-Induced AKI. The exogenous effects of H_2S on TLR4, NLRP3, and caspase-1 expressions were detected with Western blot analysis. The expressions of TLR4, NLRP3, and caspase-1 evidently increased in the LPS group compared with those of controls. However, exogenous H_2S significantly decreased the protein expressions of TLR4, NLRP3, and caspase-1 (Figure 4).

4. Discussion

Numerous studies have shown the protective effects of H_2S during diverse pathological processes [16–21]. Our study explored whether renal dysfunction during sepsis correlates with decreased H_2S levels and other possible mechanisms. After assessing the results of this study, we found that (1) LPS decreased the level of endogenous H_2S and reduced 3-MST activity and expression in the kidney and (2) exogenous supplement of NaHS ameliorated renal dysfunction by inhibiting inflammatory response and oxidative stress through TLR4/NLRP3 signaling pathways. These findings suggested that endogenous H_2S contributes to the pathogenesis of SA-AKI, whereas exogenous H_2S plays a protective role.

Sepsis is considered to be a systemic inflammatory response syndrome resulting from infection and often occurs in intensive care units. The related multiple organ dysfunction is a leading cause of death in critical patients. The kidney is the most vulnerable organ in sepsis, and mortality of SA-AKI may reach up to 70% [2]. The pathogenesis of SA-AKI is not completely understood. The three major changes that have been recognized in this disease process are inflammation, microcirculatory dysfunction, and cellular metabolic responses to sepsis [26]. LPS induces the release of inflammatory cytokines (especially TNF-α and IL-1β) through TLR4 signaling pathways and contributes to oxidative stress, which can activate tubular epithelial cells and result in functional damage to these cells, subsequently causing renal microcirculatory disturbance and hypoperfusion, which finally leads to SA-AKI [26–28]. The diagnosis of AKI mainly depends on clinical manifestations, urine volume, and blood biochemical markers. Cre and BUN are traditional and critical markers of renal function. MPO is a marker of neutrophil activity, while H_2O_2 and MDA are common markers of oxidative stress. In this study, we found that Cre and BUN levels, TNF-α and IL-1β levels, MPO activity, and H_2O_2 and MDA concentrations all significantly increased in the plasma of patients with SA-AKI. The mouse model of LPS-induced AKI was used to simulate the pathogenetic process of

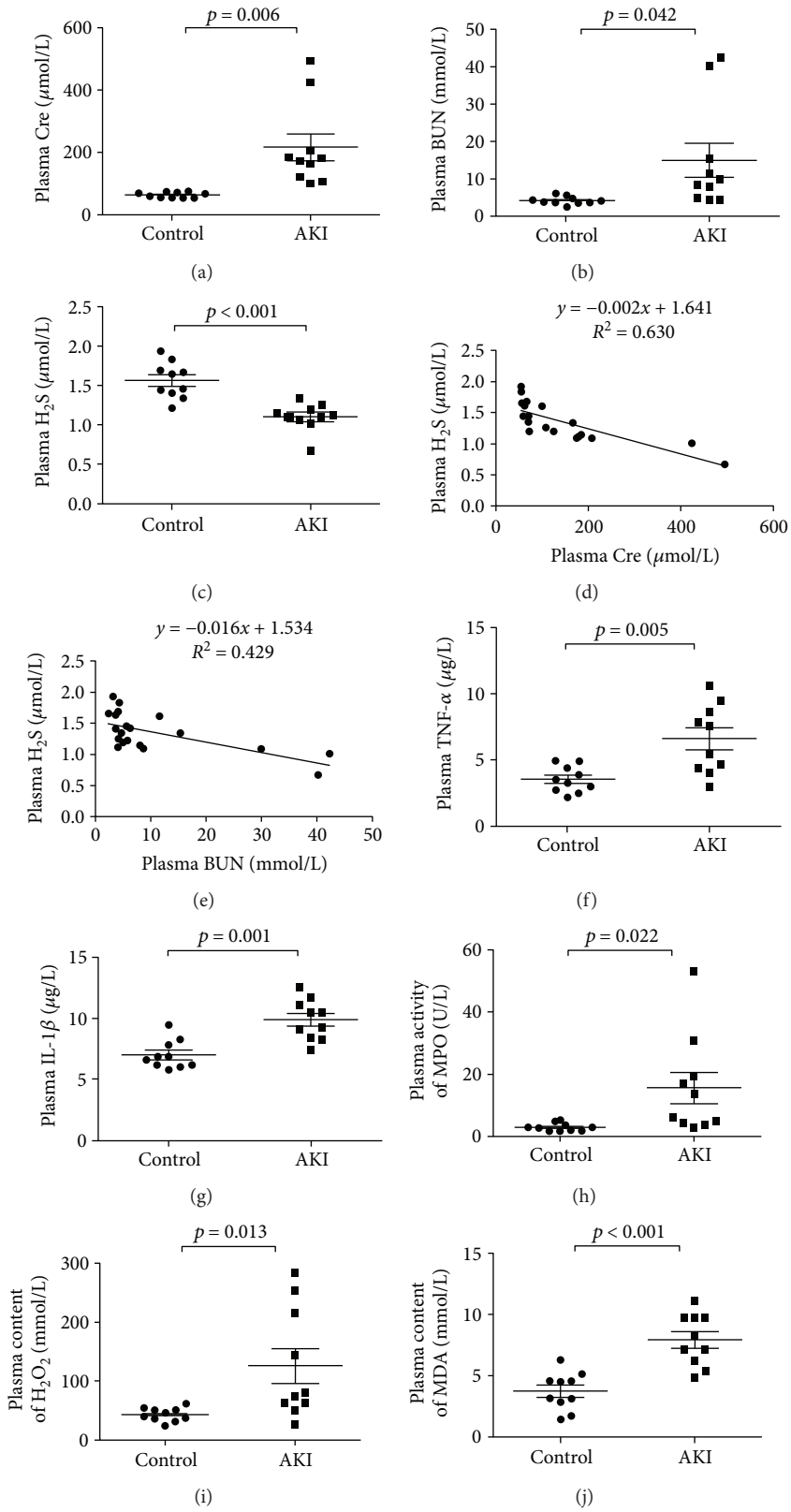

Figure 1: H_2S levels decreased in patients with SA-AKI. (a) Cre levels in the plasma of control and SA-AKI patients. (b) BUN levels in the plasma of control and SA-AKI patients. (c) H_2S levels in the plasma of control and SA-AKI patients. (d) Correlation between H_2S and Cre. (e) Correlation between H_2S and BUN. (f) TNF-α levels in the plasma of patients. (g) IL-1β levels in the plasma of patients. (h) The activities of MPO in the plasma of patients. (i) The concentrations of H_2O_2 in the plasma of patients. (j) The concentrations of MDA in the plasma of patients. Results are means ± SEM.

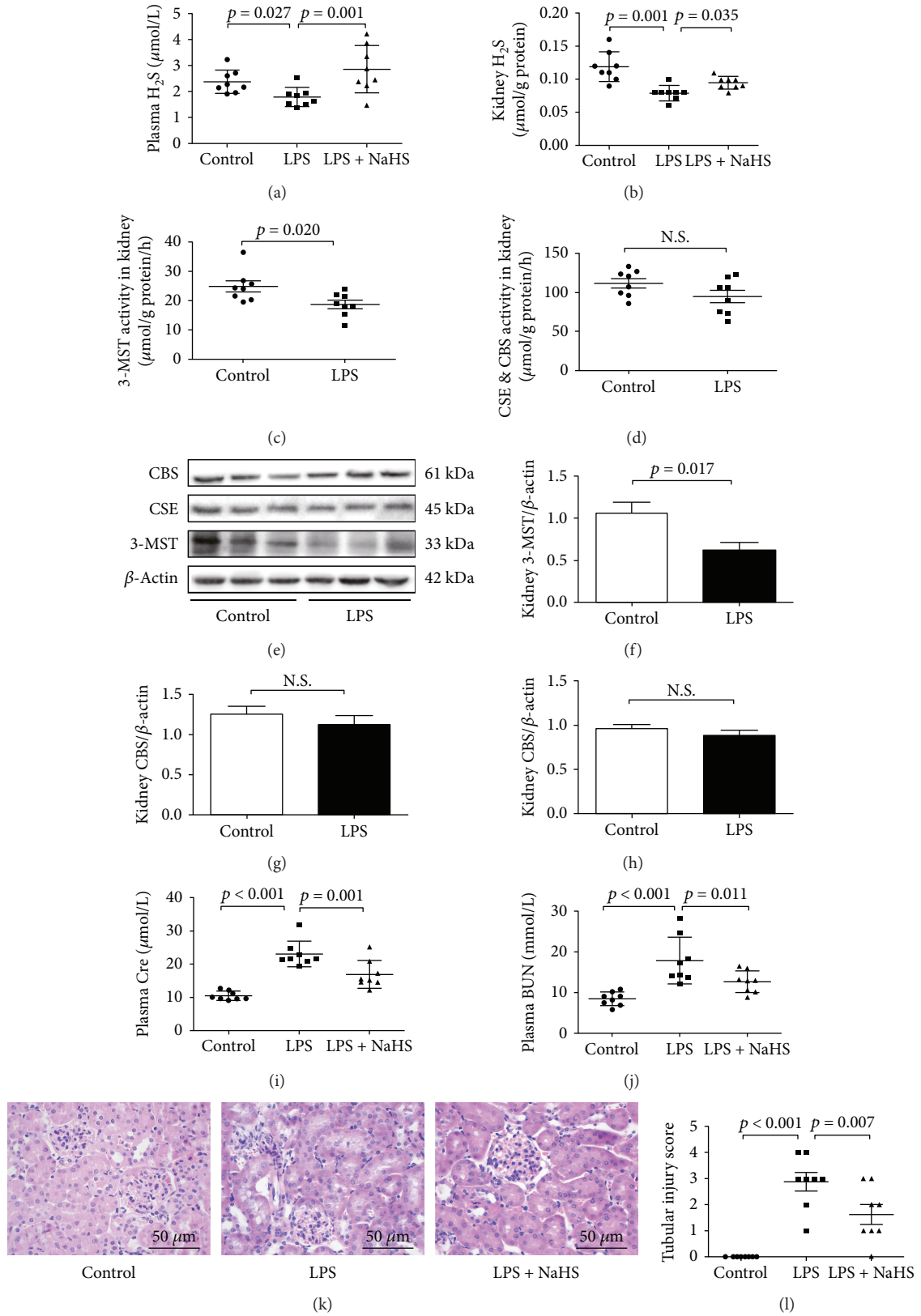

FIGURE 2: H_2S levels decreased in mice with LPS-induced AKI, exogenous H_2S could attenuate renal dysfunction. (a) H_2S levels in plasma. (b) H_2S levels in the kidney tissues. (c) 3-MST activity in the kidney tissues. (d) CBS&CSE activity in the kidney tissues. (e) Representative Western blots for 3-MST, CBS, and CSE expression in the kidney tissues. β-Actin was used as the internal control. (f–h) The quantitative analysis for 3-MST, CBS, and CSE expression in the kidney tissues. (i) Cre levels in plasma. (g) BUN levels in plasma. (k) Representative HE-stained right kidney sections (scale bar = 250 μm). (l) Kidney tubular injury score of three groups.

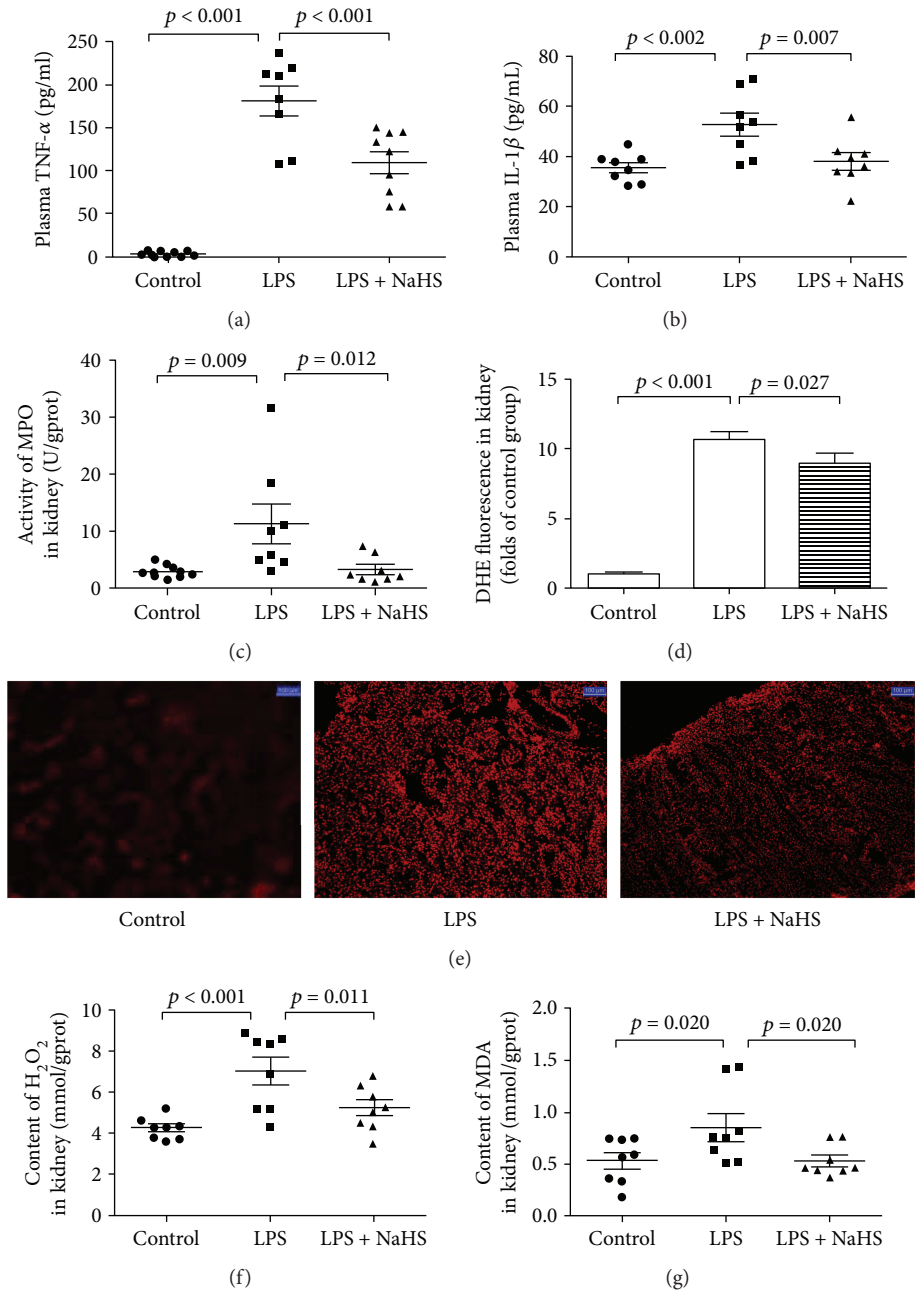

Figure 3: Exogenous H_2S attenuated inflammatory cytokine and oxidative stress in mice with LPS-induced AKI. (a) TNF-α levels in the plasma of mice. (b) IL-1β levels in the plasma of mice. (c) The activity of MPO in the kidney tissue of mice. (d) The ROS levels in the kidney tissue of mice. (e) DHE fluorescence in the kidney tissue of mice. (f) The concentrations of H_2O_2 in the kidney tissue of mice. (g) The concentrations of MDA in the kidney tissue of mice. Results are means ± SEM.

AKI, and similar changes were observed in the indicators mentioned above. These data were in agreement with the results of previous studies [6, 7, 10].

As was indicated in various studies, H_2S played an essential role in the renal system, in both physiological and pathological status, and H_2S levels were decreased in various kidney diseases [15, 20, 21]. To date, three enzymes and four pathways that are involved in the production of H_2S have been reported. Kimura's team [14, 29] has demonstrated the formation of H_2S from L-cysteine by CBS, CSE, and 3-MST coupled with cysteine aminotransferase (CAT); in addition, 3-MST along with DAO can produce H_2S from D-cysteine. Furthermore, they found that the three enzymes are abundant in the kidney, but CBS and CSE are localized in the cytoplasm, whereas 3-MST is mainly found in the mitochondria, and the pathway of H_2S production from D-cysteine by 3-MST/DAO only exists in the kidney and brain. To explain the effect of endogenous H_2S in the course of SA-AKI, we measured the levels of H_2S both in patients and mice with SA-AKI; similar to that demonstrated previously [15, 20], H_2S levels significantly decreased and were inversely related to the renal function. To explore the reasons for the decline

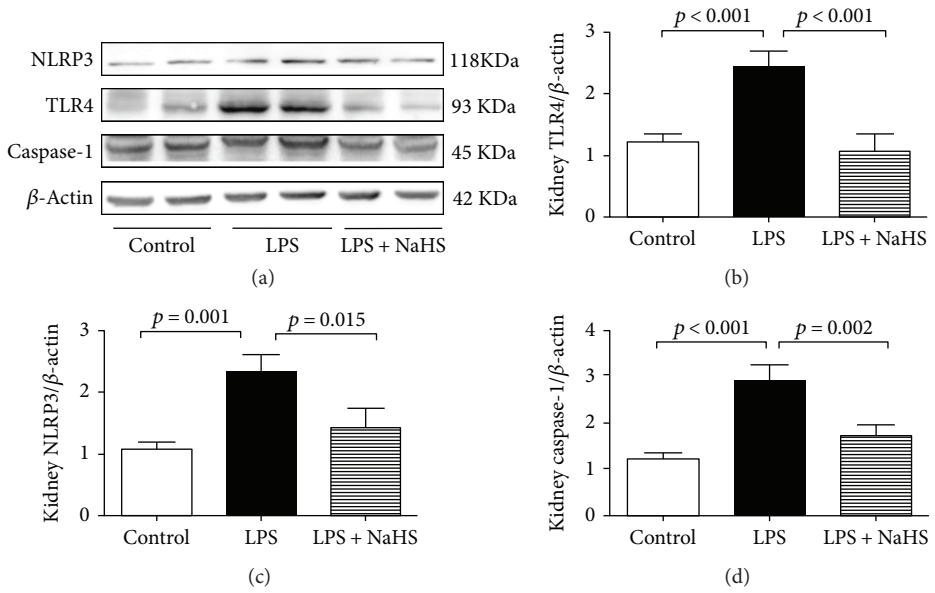

Figure 4: Exogenous H_2S attenuated the formation of inflammasome in mice with LPS-induced AKI. (a) Representative Western blots for TLR4, NLRP3, and caspase-1 expression in the kidney tissues. β-Actin was used as the internal control. (b–d) The quantitative analysis for TLR4, NLRP3, and caspase-1 protein expression in the kidney tissues.

in H_2S levels, we measured the activity of the three enzymes and their expression in the kidney tissues of mice and found that the activity and expression of both CBS and CSE in the kidney did not significantly change after LPS stimulation, but the 3-MST activity significantly decreased; moreover, 3-MST expression was downregulated, which may have contributed to the decrease of H_2S. Although experimental studies [20, 21] indicated that protein expressions of CBS and CSE are decreased in kidney dysfunction caused by IRI models, the pathogenesis of SA-AKI is not exactly the same as that of ischemia reperfusion. From Kimura's report [29], we have also found that kidney D-cysteine can produce 60 times more H_2S compared with L-cysteine, and D-cysteine is more efficient in protecting renal function. Therefore, we inferred that LPS may affect the H_2S production mainly through the D-cysteine/DAO/3-MST pathway, although the mechanisms are still unclear and need further study.

On the basis of the above findings, we evaluated the potential therapeutic utility of exogenous H_2S on SA-AKI. NaHS, an H_2S donor, was extensively used in various animal models of renal IRI and proven to ameliorate kidney damage [21, 30]. Based on previous studies and preexperimental results, we administered NaHS (50 μmol/kg) 3 h after LPS injection. NaHS had been demonstrated to increase H_2S levels in both plasma and kidney tissues of LPS-induced AKI mice and H_2S levels close to the normal range. Renal function and histological changes were also improved after NaHS administration, shown by a reduction of Cre and BUN levels in plasma as well as kidney injury score. These results were similar to those of Chen et al. [31], who found that the plasma H_2S level is lower in rabbit with SA-AKI derived from the urinary tract, and treatment of NaHS could improve the H_2S level, renal function, and pathological changes.

Inflammatory response is a cornerstone in the pathogenesis of SA-AKI. As one of the most important pattern-recognition proteins, TLR4 acts as a major receptor for LPS. Cunningham et al. [8] found that LPS binds to TLR4 in the kidney and induces the release of proinflammatory cytokines, especially TNF-α and IL-1β, which play an essential role during AKI. Fu et al. [32] demonstrated that inhibition of TLR4 could alleviate LPS-induced kidney injury. Meanwhile, Luo et al. [33] have demonstrated that NLRP3 is another important inflammatory regulator in sepsis-induced organ injury. NLRP3 could activate caspase-1, and subsequently, the cleavage and secretion of proinflammatory cytokines (IL-1β and IL-18) are promoted. Alfonso-Loeches et al. [34] showed the crosstalk between TLR4 and NLRP3 and found that activation of NLRP3 and secretion of inflammatory cytokines mostly disappeared in chronic alcohol-fed TLR4 knockout mice, which suggested that NLRP3 activation depends on TLR4 function. Over the years, various studies have shown the key role of H_2S as a mediator of inflammation in various clinical settings. Shibuya et al. [15] demonstrated that H_2S suppressed high glucose-induced cardiomyocyte inflammation by inhibiting the TLR4/NF-κB pathway and NLRP3 activation. Moreover, Tan et al. [35] also identified the protective effect of endogenous H_2S on renal IRI by suppressing inflammatory response through the inhibition of the TLR pathway. Zhang et al. [19] demonstrated that H_2S could attenuate LPS-induced acute lung injury by reducing oxidative stress and inhibiting inflammation. Similar findings have been reported by Li et al. [36], who tested the role of H_2S in mice with acute lung injury and found that exogenous H_2S reduced lung permeability by suppressing oxidative stress and inflammation. Chen et al. [31] revealed that by inhibiting NF-κB, H_2S was able to decrease the plasma level of TNF-α and increase IL-10 level. To

investigate the anti-inflammatory mechanism of H_2S, we observed the effects of H_2S on TLR4/NLRP3 signaling pathway and found that LPS could increase TLR4, NLRP3, and caspase-1 expression in kidney tissues, accompanied by plasma elevation of downstream inflammatory factors (TNF-α and IL-1β) and oxidative stress markers (MPO, H_2O_2, and MDA). In addition, our results showed that treatment with NaHS at 50 μmol/kg could protect renal function by suppressing the release of inflammatory cytokines and oxidative stress, as well as TLR4, NLRP3, and caspase-1 expression.

5. Conclusion

In conclusion, our study suggested that endogenous H_2S is involved in the pathogenesis of SA-AKI, and exogenous H_2S exerts protective effects by inhibiting inflammation and oxidative stress via the TLR4/NLRP3 signaling pathway. These findings will shed light on the role of H_2S as a therapeutic agent for renal diseases.

Conflicts of Interest

The authors declare that there are no conflicts of interests regarding the publication of this paper.

Authors' Contributions

Yuhong Chen and Sheng Jin contributed equally to this work.

Acknowledgments

This study was supported by the National Natural Science Foundation of China (Grant nos. 31171098, 30400513, and 31671185), the Natural Science Foundation of Hebei Province of China (H2017206269), the Specialized Research Fund for the Doctoral Program of Higher Education of China (no. 20121323110008), the Hebei Province for Innovation Talents Support Plan (Grant LJRC017), and the Office of Education Foundation of Hebei Province of China (QN2016144).

References

[1] E. A. Hoste, S. M. Bagshaw, R. Bellomo et al., "Epidemiology of acute kidney injury in critically ill patients: the multinational AKI-EPI study," *Intensive Care Medicine*, vol. 41, no. 8, pp. 1411–1423, 2015.

[2] S. Uchino, J. A. Kellum, R. Bellomo et al., "Acute renal failure in critically ill patients: a multinational, multicenter study," *JAMA*, vol. 294, no. 7, pp. 813–818, 2005.

[3] H.-P. Shum, W.-W. Yan, and T. M. Chan, "Recent knowledge on the pathophysiology of septic acute kidney injury: a narrative review," *Journal of Critical Care*, vol. 31, no. 1, pp. 82–89, 2016.

[4] R. Bellomo, J. A. Kellum, C. Ronco et al., "Acute kidney injury in sepsis," *Intensive Care Medicine*, vol. 43, no. 6, pp. 816–828, 2017.

[5] D. H. Kim, Y. JJ, A. S. Lee et al., "COMP-angiopoietin-1 decreases lipopolysaccharide-induced acute kidney injury," *Kidney International*, vol. 76, no. 11, pp. 1180–1191, 2009.

[6] A. Zarjou and A. Agarwal, "Sepsis and acute kidney injury," *Journal of the American Society of Nephrology*, vol. 22, no. 6, pp. 999–1006, 2011.

[7] H. Wang and S. Ma, "The cytokine storm and factors determining the sequence and severity of organ dysfunction in multiple organ dysfunction syndrome," *The American Journal of Emergency Medicine*, vol. 26, no. 6, pp. 711–715, 2008.

[8] P. N. Cunningham, Y. Wang, R. Guo, G. He, and R. J. Quigg, "Role of Toll-like receptor 4 in endotoxin-induced acute renal failure," *The Journal of Immunology*, vol. 172, no. 4, pp. 2629–2635, 2004.

[9] K. Takeda and S. Akira, "Toll-like receptors in innate immunity," *International Immunology*, vol. 17, no. 1, pp. 1–14, 2005.

[10] E. B. Byun, N. Y. Sung, J. N. Park, M. S. Yang, S. H. Park, and E. H. Byun, "Gamma-irradiated resveratrol negatively regulates LPS-induced MAPK and NF-κB signaling through TLR4 in macrophages," *International Immunopharmacology*, vol. 25, no. 2, pp. 249–259, 2015.

[11] A. Abderrazak, T. Syrovets, D. Couchie et al., "NLRP3 inflammasome: from a danger signal sensor to a regulatory node of oxidative stress and inflammatory diseases," *Redox Biology*, vol. 4, pp. 296–307, 2015.

[12] F. G. Bauernfeind, G. Horvath, A. Stutz et al., "Cutting edge: NF-κB activating pattern recognition and cytokine receptors license NLRP3 inflammasome activation by regulating NLRP3 expression," *The Journal of Immunology*, vol. 183, no. 2, pp. 787–791, 2009.

[13] M. W. Warenycia, L. R. Goodwin, C. G. Benishin et al., "Acute hydrogen sulfide poisoning: demonstration of selective uptake of sulfide by the brainstem by measurement of brain sulfide levels," *Biochemical Pharmacology*, vol. 38, pp. 973–981, 1989.

[14] H. Kimura, "Hydrogen sulfide: its production, release and functions," *Amino Acids*, vol. 41, no. 1, pp. 113–121, 2011.

[15] N. Shibuya, S. Koike, M. Tanaka, M. Ishigami-Yuasa, Y. Kimura, and Y. Ogasawara, "A novel pathway for the production of hydrogen sulfide from D-cysteine in mammalian cells," *Nature Communications*, vol. 4, p. 1366, 2013.

[16] Z. Huang, X. Zhuang, C. Xie et al., "Exogenous hydrogen sulfide attenuates high glucose-induced cardiotoxicity by inhibiting NLRP3 inflammasome activation by suppressing TLR4/NF-κB pathway in H9C2 cells," *Cellular Physiology and Biochemistry*, vol. 40, no. 6, pp. 1578–1590, 2016.

[17] D. Avanzato, A. Merlino, S. Porrera, R. Wang, L. Munaron, and D. Mancardi, "Role of calcium channels in the protective effect of hydrogen sulfide in rat cardiomyoblasts," *Cellular Physiology and Biochemistry*, vol. 33, no. 4, pp. 1205–1214, 2014.

[18] Q. Yu, Z. Lu, L. Tao et al., "ROS-dependent neuroprotective effects of NaHS in ischemia brain injury involves the PARP/AIF pathway," *Cellular Physiology and Biochemistry*, vol. 36, no. 4, pp. 1539–1551, 2015.

[19] H. X. Zhang, S. J. Liu, X. L. Tang et al., "H_2S attenuates LPS-induced acute lung injury by reducing oxidative/nitrative stress and inflammation," *Cellular Physiology and Biochemistry*, vol. 40, no. 6, pp. 1603–1612, 2016.

[20] A. Ahmad, G. Olah, B. Szczesny, M. E. Wood, M. Whiteman, and C. Szabo, "AP39, a mitochondrially targeted hydrogen sulfide donor, exerts protective effects in renal epithelial cells subjected to oxidative stress *in vitro* and in acute renal injury *in vivo*," *Shock*, vol. 45, no. 1, pp. 88–97, 2015.

[21] S. J. Han, J. I. Kim, J. W. Park, and K. M. Park, "Hydrogen sulfide accelerates the recovery of kidney tubules after renal ischemia/reperfusion injury," *Nephrology Dialysis Transplantation*, vol. 30, pp. 1497–1506, 2015.

[22] KDIGO AKI Work Group, "KDIGO clinical practice guideline for acute kidney injury," *Kidney International Supplements*, vol. 2, pp. 1–138, 2012.

[23] A. Leelahavanichkul, H. Yasuda, K. Doi et al., "Methyl-2-acetamidoacrylate, an ethyl pyruvate analog, decreases sepsis-induced acute kidney injury in mice," *American Journal of Physiology - Renal Physiology*, vol. 295, no. 6, pp. F1825–F1835, 2008.

[24] B. B. Tao, S. Y. Liu, C. C. Zhang et al., "VEGFR2 functions as an H_2S-targeting receptor protein kinase with its novel Cys1045–Cys1024 disulfide bond serving as a specific molecular switch for hydrogen sulfide actions in vascular endothelial cells," *Antioxidants & Redox Signaling*, vol. 19, no. 5, pp. 448–464, 2013.

[25] S. Jin, S. X. Pu, C. L. Hou et al., "Cardiac H_2S generation is reduced in ageing diabetic mice," *Oxidative Medicine and Cellular Longevity*, vol. 2015, Article ID 758358, 14 pages, 2015.

[26] H. Gomez and J. A. Kellum, "Sepsis-induced acute kidney injury," *Current Opinion in Critical Care*, vol. 22, no. 6, pp. 546–553, 2016.

[27] K. A. Seely, J. H. Holthoff, and S. T. Burns, "Hemodynamic changes in the kidney in a pediatric rat model of sepsis-induced acute kidney injury," *American Journal of Physiology - Renal Physiology*, vol. 301, no. 1, pp. F209–F217, 2011.

[28] D. N. Grigoryev, M. Liu, H. T. Hassoun, C. Cheadle, K. C. Barnes, and H. Rabb, "The local and systemic inflammatory transcriptome after acute kidney injury," *Journal of the American Society of Nephrology*, vol. 19, no. 3, pp. 547–558, 2008.

[29] H. Kimura, "Physiological role of hydrogen sulfide and polysulfide in the central nervous system," *Neurochemistry International*, vol. 63, no. 5, pp. 492–497, 2013.

[30] F. Azizi, B. Seifi, M. Kadkhodaee, and P. Ahghari, "Administration of hydrogen sulfide protects ischemia reperfusion-induced acute kidney injury by reducing the oxidative stress," *Irish Journal of Medical Science*, vol. 185, no. 3, pp. 649–654, 2015.

[31] X. Chen, W. Xu, Y. Wang et al., "Hydrogen sulfide reduces kidney injury due to urinary-derived sepsis by inhibiting NF-κB expression, decreasing TNF-α levels and increasing IL-10 levels," *Experimental and Therapeutic Medicine*, vol. 8, no. 2, pp. 464–470, 2014.

[32] H. Fu, Z. Hu, X. Di, Q. Zhang, R. Zhou, and H. Du, "Tenuigenin exhibits protective effects against LPS-induced acute kidney injury via inhibiting TLR4/NF-κB signaling pathway," *European Journal of Pharmacology*, vol. 791, pp. 229–234, 2016.

[33] Y. P. Luo, L. Jiang, K. Kang et al., "Hemin inhibits NLRP3 inflammasome activation in sepsis-induced acute lung injury, involving heme oxygenase-1," *International Immunopharmacology*, vol. 20, no. 1, pp. 24–32, 2014.

[34] S. Alfonso-Loeches, J. Urena-Peralta, M. J. Morillo-Bargues, J. Morillo-Bargues, U. Gómez-Pinedo, and C. Guerri, "Ethanol-induced TLR4/NLRP3 neuroinflammatory response in microglial cells promotes leukocyte infiltration across the BBB," *Neurochemical Research*, vol. 41, no. 1-2, pp. 193–209, 2015.

[35] Z. Tan, Y. Shi, Y. Yan, W. Liu, G. Li, and R. Li, "Impact of endogenous hydrogen sulfide on toll-like receptor pathway in renal ischemia/reperfusion injury in rats," *Renal Failure*, vol. 37, no. 4, pp. 727–733, 2015.

[36] H. D. Li, Z. R. Zhang, Q. X. Zhang, Z. C. Qin, D. M. He, and J. S. Chen, "Treatment with exogenous hydrogen sulfide attenuates hyperoxia-induced acute lung injury in mice," *European Journal of Applied Physiology*, vol. 113, no. 6, pp. 1555–1563, 2013.

Hindawi
Oxidative Medicine and Cellular Longevity
Volume 2017, Article ID 8024857, 18 pages
https://doi.org/10.1155/2017/8024857

Research Article

Exercise Combined with *Rhodiola sacra* Supplementation Improves Exercise Capacity and Ameliorates Exhaustive Exercise-Induced Muscle Damage through Enhancement of Mitochondrial Quality Control

Yaoshan Dun, Suixin Liu, Wenliang Zhang, Murong Xie, and Ling Qiu

Cardiac Rehabilitation Center, Department of Rehabilitation, Xiangya Hospital of Central South University, Changsha 410008, China

Correspondence should be addressed to Suixin Liu; heartsuixin@126.com

Received 22 June 2017; Accepted 1 October 2017; Published 22 November 2017

Academic Editor: Aditya Sen

Mounting evidence has firmly established that increased exercise capacity (EC) is associated with considerable improvements in the survival of patients with cardiovascular disease (CVD) and that antistress capacity is a prognostic predictor of adverse cardiovascular events in patients with CVD. Previous studies have indicated that aerobic exercise (AE) and supplementation with *Rhodiola sacra* (RS), a natural plant pharmaceutical, improve EC and enable resistance to stress; however, the underlying mechanism remains unclear. This study explored the ability of AE and RS, alone or combined, to improve EC and ameliorate exhaustive exercise- (EE-) induced stress and elucidate the mechanism involved. We found that AE and RS significantly increased EC in mice and ameliorated EE-induced stress damage in skeletal and cardiac muscles (SCM); furthermore, a synergistic effect was detected for the first time. To our knowledge, the present work is the first to report that AE and RS activate mitophagy, mitochondrial dynamics, and biogenesis in SCM, both in the resting state and after EE. These data indicate that AE and RS synergistically improve EC in mice and protect SCM from EE-induced stress by enhancing mitochondrial quality control, including the activation of mitophagy, mitochondrial dynamics, and biogenesis, both at rest and after EE.

1. Introduction

Cardiovascular disease (CVD) is the leading cause of disease death worldwide [1]. It has been firmly established that low level of exercise capacity (EC) is associated with cardiovascular disease mortality and all-cause mortality in patients with CVD [2]. A growing body of epidemiological and clinical evidence demonstrates that EC is a potentially stronger predictor of mortality than established risk factors such as smoking, hypertension, high cholesterol, and type 2 diabetes mellitus [3, 4]. Moreover, numerous recent studies have shown that each 1 MET increment (MET, a multiple of the resting metabolic rate approximating 3.5 $ml \cdot kg^{-1} \cdot min^{-1}$) in EC is associated with considerable (10%–25%) improvement in survival [5]. A recent scientific statement from the American Heart Association recommended the use of EC as a clinical vital sign [5]. In addition, antistress capacity is currently used as prognostic predictors of major adverse cardiovascular events, including cardiac and all-cause death, nonfatal myocardial infarction, and coronary revascularization, PTCA/CABG, in patients with CVD [6–8]. Kaplan-Meier survival estimates showed a significantly worse outcome in patients presenting with elevated oxidative stress levels [8]. Improved antistress capacity was found to reduce the area of skeletal muscle damage after ischemia or hypoxia [9] as well as the incidence of malignant ventricular arrhythmia after a previous myocardial infarction [10]. Therefore, the development of strategies to improve EC and the capacity to resist acute stress-induced damage are of great clinical significance. This study examined the ability of both nondrug intervention-based and pharmaceutical supplementation to enhance EC and the capacity to resist acute stress-

induced damage, with a focus on aerobic exercise (AE) and supplementation with *Rhodiola sacra* (RS), a traditional natural plant pharmaceutical.

EC reflects the integrated ability to transport oxygen from the atmosphere to the mitochondria to perform physical work. It therefore quantifies the mitochondrial function of an individual and is dependent on a linked chain of processes that include pulmonary ventilation and diffusion [11], right and left ventricular functions [12], and the ability of skeletal and cardiac muscle (SCM) cells to receive and use the oxygen and nutrients delivered by the blood [13]. In addition, mitochondria are multifunctional organelles whose quality is closely related to antistress capacity [14]. Thus, the mitochondrial quality in SCM is the prime factor influencing EC and the degree of acute stress-induced damage in an individual. However, few studies have been performed on the relationship between the mitochondrial quality in SCM and EC and the ability to resist acute stress-induced muscle damage. Mitochondrial quality control (MQC) functions on molecular, organellar, and largely intraorganellar levels. On the organellar level, there is an interplay among mitophagy, mitochondrial dynamics, and biogenesis [15].

On the one hand, mitochondrial fission, a component of mitochondrial dynamics, combined with mitophagy promotes the isolation and elimination of damaged mitochondrial components [15]; this process is vital for the maintenance of cell homeostasis. As oxidative stress increases and damaged mitochondria accumulate, fission, mediated by dynamin-related protein-1 (DRP1) [16], isolates damaged components for elimination. Mitochondrial depolarization induced by damage allows for the transposition of BCL2/adenovirus E1B 19 kDa protein-interacting protein 3 (BNIP3) to the mitochondrial membrane as a target of the autophagosome [17]. p62 also plays a role in targeting cargo to the autophagosome and is subsequently degraded during autophagy and mitophagy [18]. Assembly of the phagosome involves the conjugation of microtubule-associated protein 1 light chain 3 (LC3) with phosphatidylethanolamine to form LC3-II. On the other hand, mitochondrial fusion, another component of mitochondrial dynamics, combined with mitochondrial biogenesis produces new mitochondria. Mitochondria biogenesis is regulated by the AMP-activated protein kinase (AMPK)/peroxisome proliferator-activated receptor-γ coactivator 1α (PGC-1α) signaling pathway [19] through its activation of nuclear respiratory factor (NRF)-1, NRF-2, transcription factor A mitochondrial (TFAM), and transcription factor B mitochondrial (TFBM) [20].

AE is widely recognized as an effective approach to increase EC. However, further studies are required to determine the underlying mechanism. Several recent studies have suggested that AE ameliorates age-associated deterioration in mitochondrial biogenesis in rats [21], activates skeletal muscle autophagy [22], and triggers the AMPK/PGC-1α signaling pathway [23], which is pivotal for the regulation of mitochondrial biogenesis [24]. In addition, numerous lines of evidence indicate that regular exercise provides cardioprotection [25] and reduces chemical substance-induced oxidative stress and proteolysis in skeletal muscle [26]. However, few studies have been performed on the effect of AE on protecting SCM with a focus on MQC.

The combination of nondrug intervention (exercise)-based and pharmaceutical supplementation is commonly used in clinical practice. Natural plant pharmaceuticals have fewer side effects and higher acceptability than synthesized chemical drugs. RS, a traditional natural plant pharmaceutical, is widely distributed at high altitudes in the Arctic and mountainous regions throughout Europe and Asia [27]. For the last century, this plant has been well known for its physiological benefits such as fatigue elimination and prevention of high-altitude sickness [28]. Mounting evidence demonstrates that RS enhances exercise performance [28] and prolongs lifespan in *Drosophila melanogaster* [29] and silkworms [30] and ameliorates the oxidative stress induced by EE in rats [31]. Two recent studies have demonstrated that RS activates autophagy in bladder cancer cells [32]; further, this plant has been shown to promote mitochondrial biogenesis and reduce apoptosis induced by hydrogen peroxide in endothelial cells [33]. However, only a few studies have been performed to investigate the effects of RS supplementation on EE-induced muscle damage; further, none of these studies has addressed the effects of RS supplementation on enhancing MQC in SCM.

In this study, we explored the effects of AE and RS supplementation, alone and combined, on EC in mice and on protection against EE-induced SCM stress and then investigated their respective mechanisms with a focus on MQC, including mitophagy, mitochondrial dynamics, and biogenesis.

2. Materials and Methods

2.1. Ethics Statement. All animal protocols were approved by the Hunan Provincial People's Hospital Animal Care and Use Committee under the guidelines of the Chinese Academy of Sciences (approval ID: SYXK 2015-0013).

2.2. Rhodiola sacra (RS). Highly pure extract from the root of RS was provided by Tibet Rhodiola Pharmaceutical Holding Company. HPLC-MS analysis revealed that the main effective contents are salidroside ($C_{14}H_{20}O_7$, 2.62%) and flavone ($C_{27}H_{30}O_{16}$, 3.27%). The preparation and inspection of the extract complied with The Chinese Pharmacopoeia 2015 (inspection report number C1051612067). To prepare a solution of the extract, extract powder was mixed with distilled water (50 mg/ml). The dosage was based on the weight of each mouse, at a liquid/weight ratio of 0.1 ml/10 g. The mice were administered with the extract by gavage every morning between 9 a.m. and 10 a.m. for five consecutive weeks.

2.3. Animal and Study Design. Male C57BL/6J mice (8 weeks old) were purchased from Hunan SJA Laboratory Animal Co. Ltd. (Changsha, Hunan, China), certification number SCXK 2011-0003. The mice were housed in temperature-controlled ($22 \pm 2^{\circ}$C) quarters with a 12 : 12 h light-dark cycle with free access to water and food. The mice were allowed to adapt to the conditions and fed for 1 week before the experiment. The mice were then divided into the control

(Con, $n = 10$), placebo (P, $n = 10$), aerobic exercise (AE, $n = 10$), *Rhodiola sacra* (RS, $n = 10$), and exercise combined with *Rhodiola sacra* (AE + RS, $n = 10$) groups. The mice in the P group were administered with normal saline at a dose of 0.1 ml/10 g weight, those in the RS group were given *Rhodiola sacra* solution as described previously, and those in the exercise group performed an AE training program (see below for details). After the 5-week experimental period, each group was randomly and equally divided into normal ($n = 5$) and exhaustive exercise (EE, $n = 5$) subgroups, and the mice in the EE subgroups completed an EE protocol (see below for details) prior to sacrificing, after about 12 h. All mice were anesthetized via an intraperitoneal injection of 5% chloral hydrate (0.1 ml/10 g weight) and then sacrificed after taking a blood sample by removing the eyeball.

2.4. Animal Aerobic Exercise Training Protocol. Mice in the AE and AE + RS groups underwent a moderate intensity swim training protocol, as described previously [31], with modifications. The mice were placed in a Morris water maze pool (type number XR-XM101-R, 60 cm high, 120 cm in diameter) with a water depth of 30 cm maintained at 30 ± 2°C. The mice initially swam freely for 10 min on the first day; swimming time was then gradually increased to 60 min/day by adding 10 min each day. Then, the swim training consisted of 4 weekly sessions of 60 min of forced swimming with the mice tethered to a stick with string, 5 d/week. After the sessions, the mice were dried gently with towels and a blower and returned to their cages. To avoid circadian variations in physical activity, the swimming exercise sessions were performed between 9 a.m. and 2 p.m., when the mice have been previously confirmed to exhibit minimal variations in aerobic capacity [34].

2.5. Exhaustive Exercise (EE) Protocol. A previously described EE protocol was used with some modifications [35]. The mice in the EE subgroups ($n = 25$, 5 per group) performed a forced weight-loaded swimming session. The load (5% of their body weight) was composed of a lead sheath (0.8 mm thick, 0.5 cm wide) attached to the tail root of the mouse, which was then gently placed in the water. The conditions and equipment used in the test were consistent with those used in the AE training protocol. The mice were then made to swim until exhaustion, as defined as the failure to rise to the surface of the water to breathe within a 7-second period. All mice underwent a preadaptation period 2 days before the formal protocol.

2.6. Assessment of Exercise Capacity. The mice in the EE subgroups ($n = 25$, 5 per group) performed the EE protocol, and the duration of forced weight-loaded swimming until exhaustion was recorded as a measure of EC.

2.7. Measurement of the Function of Mitochondria. To determine whether AE and RS, alone and combined, enhance the function of mitochondria in mouse SCM, we analyzed the expression of citrate synthase (CS). CS, the first and rate-limiting enzyme of the tricarboxylic acid cycle, plays a key role in regulating energy production during mitochondrial respiration [36].

2.8. Measurement of Exhaustive Exercise-Induced Skeletal and Cardiac Muscle Damage. To determine the degree of muscle damage, serum samples from mice in the EE subgroup were assayed for creatine kinase (CK) using an assay kit (A032, Nanjing Jiancheng Bioengineering Institute, China), as CK is a marker of damage in CK-rich tissues such as SCM [37]. In addition, to further confirm the evidence of EE-induced muscle damage and assess the degree of muscle damage, the morphology of muscle fibers and mitochondria was observed using transmission electron microscopy (Tecnai G2 Spirit, FEI, USA).

2.9. Assessment of the Level of Mitochondrial Oxidative Stress in Skeletal and Cardiac Muscles. The xanthine oxidase method was used to determine the activity of manganese superoxide dismutase (MnSOD) in skeletal (gastrocnemius) and cardiac (left ventricle) muscles, according to the manufacturer's instructions (A001-2, Nanjing Jiancheng Bioengineering Institute, China). The thiobarbituric acid (TBA) method was applied to detect the mitochondrial content of malondialdehyde (MDA) in skeletal (gastrocnemius) and cardiac (left ventricle) muscles, according to the manufacturer's instructions (A003-2, Nanjing Jiancheng Bioengineering Institute, China).

2.10. Isolation of Mitochondria from Skeletal and Cardiac Muscles. The mitochondria from skeletal (quadriceps femoris) and cardiac (left ventricle) muscles of the mice were isolated using differential centrifugation according to established protocols (G006, Nanjing Jiancheng Bioengineering Institute, China).

2.11. Assessment of Autophagy and Mitophagy. Autophagy and mitophagy in skeletal (quadriceps femoris) and cardiac (left ventricle) muscles were analyzed by Western blotting of tissue extracts with antibodies against LC3 (microtubule-associated protein 1 light chain 3), p62 (SQSTM1, sequestosome), and BNIP3 (BCL2/adenovirus E1B 19 kDa protein-interacting protein 3). TEM was used to further confirm evidence of autophagy.

2.12. Assessment of Mitochondrial Dynamics. Mitochondrial dynamics in skeletal (quadriceps femoris) and cardiac (left ventricle) muscles was analyzed by Western blotting of tissue extracts with antibodies against DRP1 and MFN1.

2.13. Assessment of Mitochondrial Biogenesis. The activation of the AMPK/PGC-1α signaling pathway in skeletal (quadriceps femoris) and cardiac (left ventricle) muscles was analyzed by Western blotting and RT-qPCR.

2.14. Protein Assay. For protein content analysis, skeletal (quadriceps femoris) and cardiac (left ventricle) muscle samples were homogenized and analyzed by Western blotting. The following antibodies were used: BNIP3 (ab109362, rabbit, 1 : 1000), p-AMPK (ab131357, rabbit, 1 : 500) from Abcam (USA); PGC-1α (sc-13067, rabbit, 1 : 200) from Santa Cruz (USA); CS (16131-1-AP, rabbit, 1 : 1000), LC 3 I/II (14600-1-AP, rabbit, 1 : 500), AMPK (10929-2-AP, rabbit, 1 : 500), DRP1 (12957-1-AP, rabbit, 1 : 500), MFN1

Table 1: Sequence of primers used for RT-qPCR assays.

Genes	Primer sequences	
	Forward primer (5′→3′)	Reverse primer (5′→3′)
AMPK	CGGGGTCATTCTCTATGCTT	TTTAAACCACTCGTGTTCCCT
PGC-1α	ATGCCTGCCCAGTACCTGA	CGCAGCTCACAAAATACTGTCC
GAPDH	GCGACTTCAACAGCAACTCCC	CACCCTGTTGCTGTAGCCGTA

(13798-1-AP, rabbit, 1 : 500), and p62 (18420-1-AP, rabbit, 1 : 1000) from Proteintech (USA); and GAPDH (AP0063, rabbit, 1 : 5000) from Bioworld (USA). Membranes were analyzed and quantified using the Quantity One Imaging System (BIO-RAS, USA). Protein expression was normalized to that of GAPDH.

2.15. Gene Expression. Total RNA was extracted from skeletal (quadriceps femoris) and cardiac (left ventricle) muscles (TRIzol, Invitrogen, CA, USA). AMPK and PGC-1α mRNA levels were quantified by real-time reverse transcription PCR (RT-qPCR) analysis and normalized to those of GAPDH. Primer sequences are listed in Table 1.

2.16. Statistical Analyses. Data are presented as mean ± SD. A single-factor analysis of variance (ANOVA) was used to analyze the results of the EE test, as well as serum CK, protein, and gene expression levels. Statistical analyses were conducted using SPSS statistical software 21.0 (IBM, USA). A significance level of 0.05 was used for all analyses.

3. Results

3.1. Effects of Aerobic Exercise and Rhodiola sacra, Alone and Combined, on Mice Exercise Capacity and the Underlying Mechanism

3.1.1. AE and RS, Alone and Combined, Increase Mice Exercise Capacity. The duration of forced weight-loaded swimming until exhaustion was recorded as a measure of EC, as described previously. A significantly increased duration of swimming was observed in the AE group compared with that in the Con group (30.60 ± 24.22 versus 15.25 ± 7.18 min, $P < 0.01$, $n = 5$). Similarly, the duration of swimming was twenty times longer following in mice administered RS compared with those that received the placebo (312.60 ± 51.61 versus 15.00 ± 4.97 min, $P < 0.01$). The combination of AE and RS further significantly increased the duration of swimming compared with AE or RS alone ($n = 5$ mice, $P < 0.01$) (Figure 1).

3.1.2. AE and RS, Alone and Combined, Enhance the Function of Mitochondria in Skeletal and Cardiac Muscles. To determine whether AE and RS, alone and combined, enhance the function of mitochondria in mouse SCM, we analyzed the expression of CS. Both AE and RS supplementation significantly increased the level of CS in SCM ($P < 0.05$). The combination of AE and RS supplementation further increased the expression of CS in SCM ($P < 0.05$) (Figure 2).

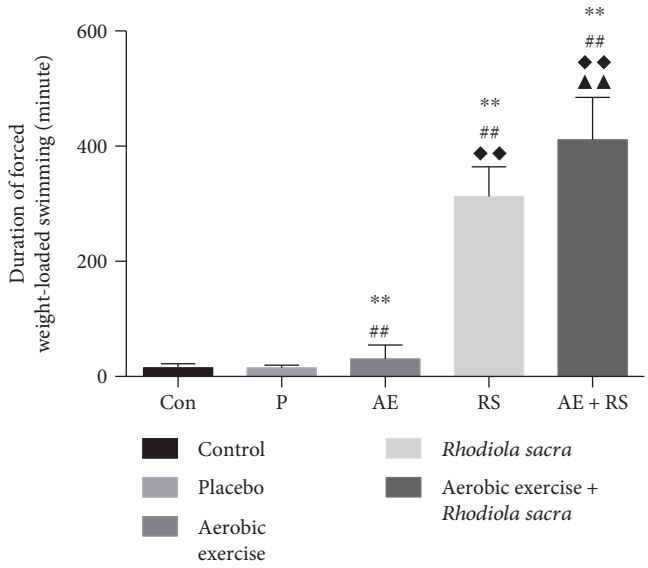

Figure 1: Effects of aerobic exercise and *Rhodiola sacra* supplementation, alone and combined, on the duration of forced weight-loaded swimming in mice; Con, control; P, placebo; AE, aerobic exercise; RS, *Rhodiola sacra*; AE + RS, aerobic exercise combined with *Rhodiola sacra*; $^{**}P < 0.01$ versus Con; $^{\#\#}P < 0.01$ versus P; $^{\blacklozenge\blacklozenge}P < 0.01$ versus AE; $^{\blacktriangle\blacktriangle}P < 0.01$ versus RS. $n = 5$ mice. All data are expressed as mean ± SD.

3.1.3. AE and RS, Alone and Combined, Activate Autophagy and Mitophagy in Skeletal and Cardiac Muscles. To determine whether AE and RS, alone and combined, activate autophagy and mitophagy in mouse SCM, we analyzed the ratio of LC3-II/LC3-I and the expression of p62, which are markers of autophagic activity [33], and the expression of BNIP3, a mitophagy biomarker, by Western blotting [38]. Autophagosomes were detected by TEM. Both AE training and RS supplementation significantly increased the number of autophagosomes, ratio of LC3-II/LC3-I, and level of BNIP3 and decreased the level of p62 compared with that in the Con and P groups ($P < 0.05$). Similarly, the combination of AE and RS further increased the number of autophagosomes, ratio of LC3-II/LC3-I, and level of BNIP3 and decreased the level of p62 in mouse SCM compared with that in the AE or RS groups ($P < 0.05$) (Figure 3).

3.1.4. AE Activates Mitochondrial Dynamics in Skeletal and Cardiac Muscles. DRP1 and MFN1 are, respectively, associated with mitochondrial fission and fusion. Therefore, to determine whether AE and RS, alone and combined,

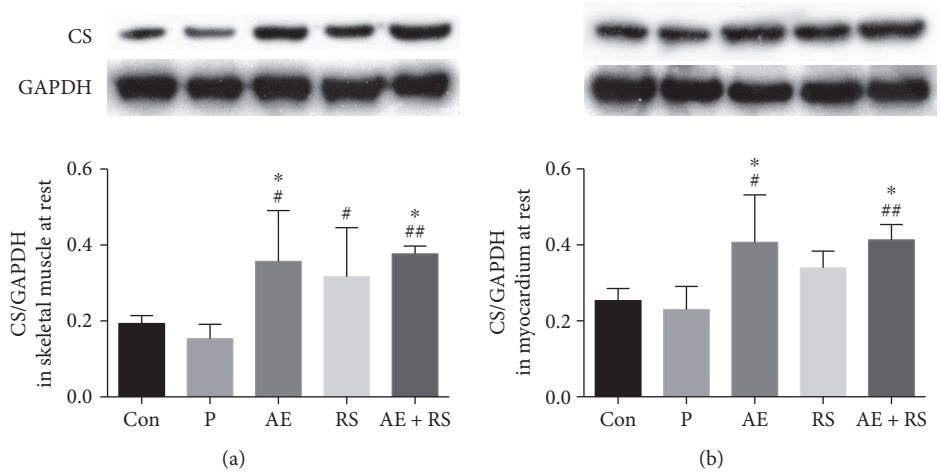

Figure 2: Effects of aerobic exercise and *Rhodiola sacra* supplementation, alone and combined, on the expression of citrate synthase (CS) in mouse skeletal (a) and cardiac muscles (b). $^{*}P < 0.05$ versus Con; $^{\#}P < 0.05$, $^{\#\#}P < 0.01$ versus P.

stimulate mitochondrial dynamics in SCM, we evaluated the expression levels of these proteins by Western blotting. AE significantly increased the levels of both DRP1 and MFN1 in mouse SCM ($P < 0.01$). However, RS supplementation did not increase the levels of DRP1 and MFN1 in the muscles of mice in the resting state (Figure 4).

3.1.5. The AMPK/PGC-1α Signaling Pathway Is a Pivotal Regulator of Mitochondrial Biogenesis. Therefore, to analyze the effects of AE and RS, alone and combined, on mitochondrial biogenesis in mouse SCM, we analyzed this pathway by Western blotting and RT-qPCR analysis. AE significantly activated the AMPK/PGC-1α signaling pathway in SCM, while RS significantly activated this pathway in skeletal muscle. A synergistic effect was detected both in SCM (Figure 5).

3.2. Effects of AE and RS, Alone and Combined, on Exhaustive Exercise-Induced Skeletal and Cardiac Muscle Damage and the Underlying Mechanism

3.2.1. AE and RS, Alone and Combined, Ameliorate EE-Induced Skeletal and Cardiac Muscle Damage. To demonstrate that EE causes SCM damage and investigate the protective effects of AE and RS, alone and combined, we assessed the ultrastructure of SCM by TEM and determined the activity of serum creatine kinase (CK) using a colorimetric method. SCM from mice subject to EE exhibited characteristics of fiber necrosis, mitochondrion edema, and mitochondrial cristae dissolution and degradation; in addition, serum CK activity in mice exhausted from exercise was 2.8 times higher than that in normal ($n = 5$ mice, $P < 0.01$). Both AE and RS ameliorated SCM damage caused by EE; serum CK activities in mice pretreated with AE or RS were lower than those in the Con and P groups ($P < 0.05$). Moreover, synergistic effects of AE and RS on the amelioration of EE-induced muscle damage were detected. Serum CK activity in mice receiving combined pretreatment with AE and RS supplementation was, respectively, 11% and 24% lower than that in mice pretreated with AE or RS alone (Figure 6).

3.2.2. AE and RS, Alone and Combined, Reduced the Level of Mitochondrial Oxidative Stress in Skeletal and Cardiac Muscles of Mice after EE. To determine whether AE and RS supplementation, alone and combined, improved mitochondrial oxidative stress in SCM, we measured manganese superoxide dismutase (MnSOD) activity in SCM and malonaldehyde (MDA) content in mitochondria. Mice pretreated with AE or RS exhibited a 19% to 30% higher MnSOD activity and a 21% to 27% lower MDA content than those in the Con and P groups in skeletal muscle ($P < 0.05$); Mice pretreated with AE or RS exhibited a 31% to 39% higher MnSOD activity and a 21% to 38% lower MDA content than those in the Con and P groups in myocardium ($P < 0.05$). The combination of AE and RS showed a synergistic effect ($P < 0.05$) (Figure 7).

3.2.3. AE and RS, Alone and Combined, Activate Autophagy and Mitophagy in Mouse Skeletal and Cardiac Muscles after EE. AE significantly increased the number of autophagosomes, ratio of LC3-II/LC3-I, and level of BNIP3 and reduced the level of p62 in SCM of mice exhausted from exercise ($P < 0.05$). RS had the same effect in skeletal muscle ($P < 0.05$). AE and RS were found to have synergistic effects via increasing the ratio of LC3-II/LC3-I and BNIP3 levels and decreasing the p62 level in SCM of mice after EE ($P < 0.05$) (Figures 6(b), 6(c), and 8).

3.2.4. AE and RS, Alone and Combined, Activate Mitochondrial Dynamics in Skeletal Muscle of Mice after Exhaustive Exercise. Both AE and RS significantly increased the levels of DRP1 and MFN1 ($P < 0.05$) in skeletal muscle of mice exhausted from exercise ($P < 0.05$); the two factors were found to have a synergistic effect (Figure 9).

3.2.5. AE and RS, Alone and Combined, Activate Mitochondrial Biogenesis in Skeletal Muscle of Mice after Exhaustive Exercise. Both AE and RS activated the AMPK/PGC-1α signaling pathway in skeletal muscle of mice exhausted from exercise ($P < 0.05$); a synergistic effect was detected ($P < 0.05$) (Figure 10).

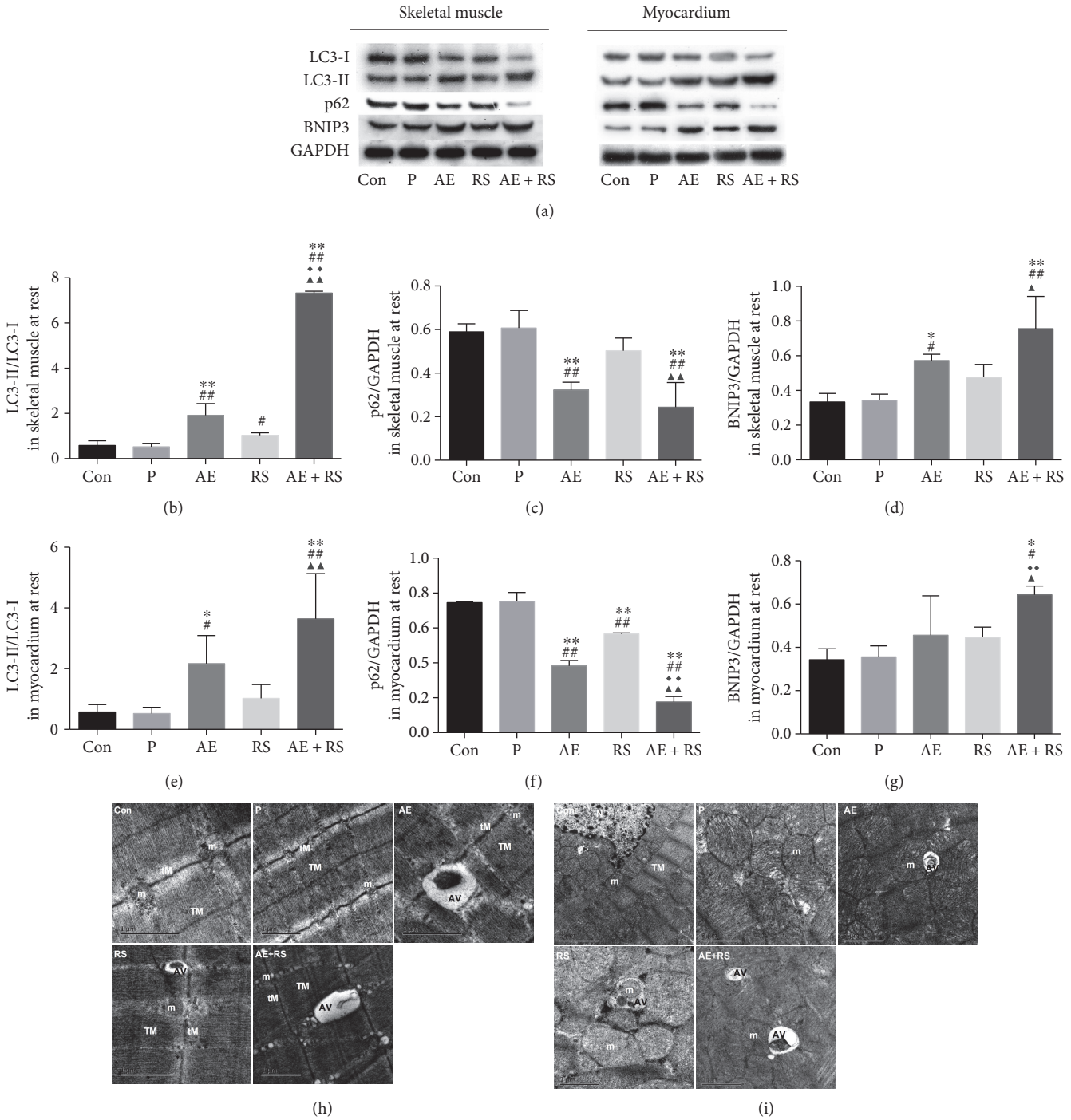

Figure 3: Effects of aerobic exercise and *Rhodiola sacra* supplementation, alone and combined, on the ratio of LC3-II/LC3-I (b), level of p62 (c), and level of BNIP3 (d) in mouse skeletal muscle and the ratio of LC3-II/LC3-I (e), level of p62 (f), and level of BNIP3 (g) in mouse myocardium; bands from the Western blotting analysis (a). Transmission electron micrographs of mouse skeletal (h) and cardiac (i) muscles: TEM image; AV: autophagic vacuole, m: mitochondria, tM: thin myofilament, TM: thick myofilament, *N. nucleus*. Scale bar = 1 or 2 μm. $^{*}P < 0.05$, $^{**}P < 0.01$ versus Con; $^{\#}P < 0.05$, $^{\#\#}P < 0.01$ versus P; $^{\blacklozenge\blacklozenge}P < 0.01$ versus AE; $^{\blacktriangle}P < 0.05$, $^{\blacktriangle\blacktriangle}P < 0.01$ versus RS.

4. Discussion

In this study, we showed that AE and RS supplementation increased EC in mice and ameliorated SCM damage induced by EE, and a synergistic effect was detected. The corresponding mechanism is involved in the enhancement of MQC in mouse SCM, including the activation of mitophagy, mitochondrial dynamics, and biogenesis.

4.1. AE and RS, Alone and Combined, Improved Exercise Capacity in Mice through the Enhancement of Mitochondrial Quality Control in SCM. In the first part of this study, we

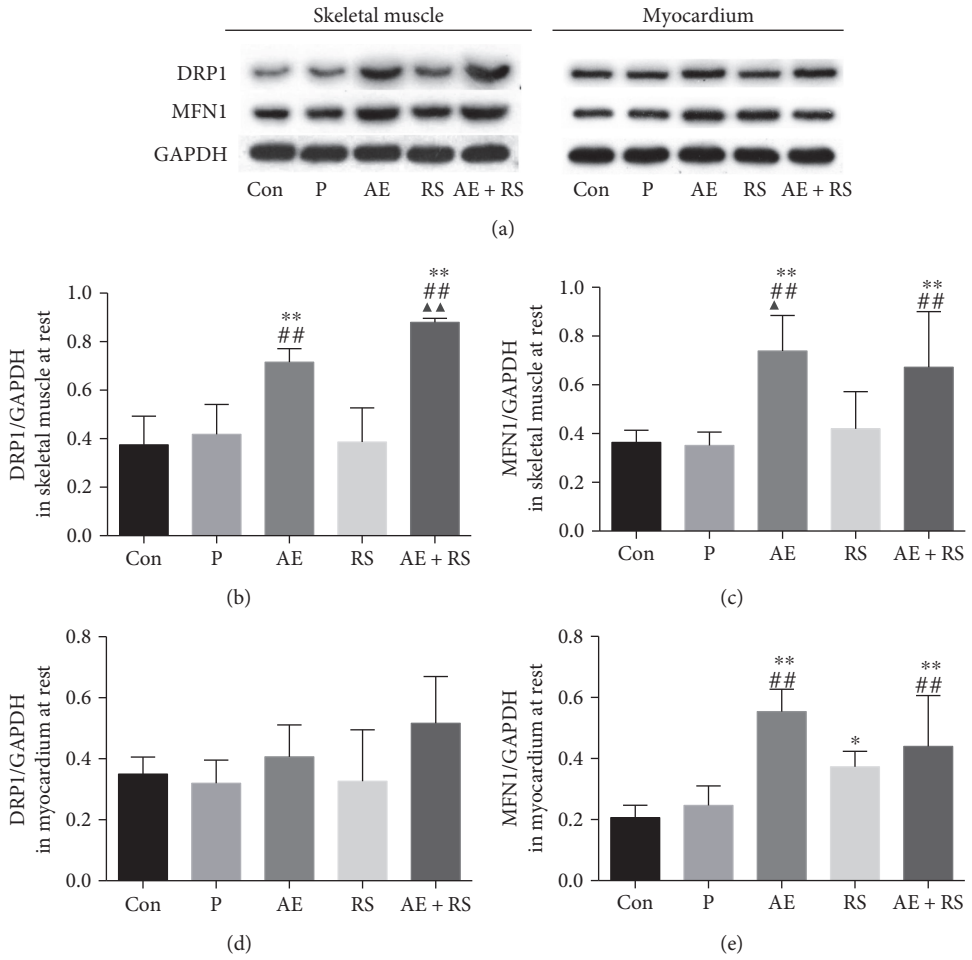

Figure 4: Effects of aerobic exercise and *Rhodiola sacra* supplementation, alone and combined, on the levels of dynamin-related protein 1 (b) and mitochondrial fusion 1 (c) in mouse skeletal muscle and DRP (d) 1 and MFN1 (e) in mouse myocardium; bands from the Western blotting analysis (a). $^{*}P < 0.05$, $^{**}P < 0.01$ versus Con; $^{\#\#}P < 0.01$ versus P; $^{\blacktriangle}P < 0.05$, $^{\blacktriangle\blacktriangle}P < 0.01$ versus RS.

investigated the effects of AE and RS, alone and combined, on EC in mice and the underlying mechanism with a focus on MQC. EC is a potentially stronger predictor of mortality than established risk factors such as smoking, hypertension, high cholesterol, and type 2 diabetes mellitus [3, 4], and it has been recommended for use as a clinical vital sign by the American Heart Association [5]. We found that both AE and RS significantly increased the duration of forced weight-loaded swimming of mice, which is a measure of EC [35]. These results are in accordance with those of previous studies [39, 40]. Moreover, we report, for the first time, that AE combined with RS supplementation synergistically induce a significant increase in EC in mice.

Mitochondria play a vital role in enhancing EC through the regulation of substrate metabolism and energy production, as well as their influence on skeletal muscle size and function [41]. On the organellar level, MQC is a network of interactions between mitophagy, mitochondrial dynamics, and biogenesis [15]. This dynamic process allows the mitochondria to share components, such as mitochondrial DNA, and to eliminate damaged components through mitophagy. Mitochondrial biogenesis and mitophagy contribute to the homeostasis of mitochondria within cells [41]. Any defect in mitophagy, mitochondrial dynamics, or biogenesis will lead to mitochondrial dysfunction, resulting in low EC [42]. In this study, we found that AE significantly increases the expression of CS and activates mitophagy, mitochondrial dynamics, and biogenesis in skeletal muscle. Further, AE was found to induce myocardial autophagy and mitochondrial biogenesis in the myocardium. These results indicate that AE enhances the function of mitochondria and MQC of SCM.

RS is a member of the *Rhodiola* family that is grown in Tibet in China [27]; this natural plant pharmaceutical is well known for its physiological benefits such as elimination of fatigue [43], enhancement of EC [28], and prolongation of lifespan [29, 30]. Several recent studies have demonstrated that RS activates autophagy [44] and mitochondrial biogenesis in endothelial cells [33] and the myocardium in rats [45]. Here, we report for the first time that RS enhances the function of mitochondria in SCM and activates autophagy and mitochondrial biogenesis in mouse skeletal muscle. Notably, RS was found to be as effective as AE in improving EC; however, RS alone was not as effective as AE in activating autophagy. This is likely because the mechanism by which RS improves EC is not limited to activation of autophagy; for

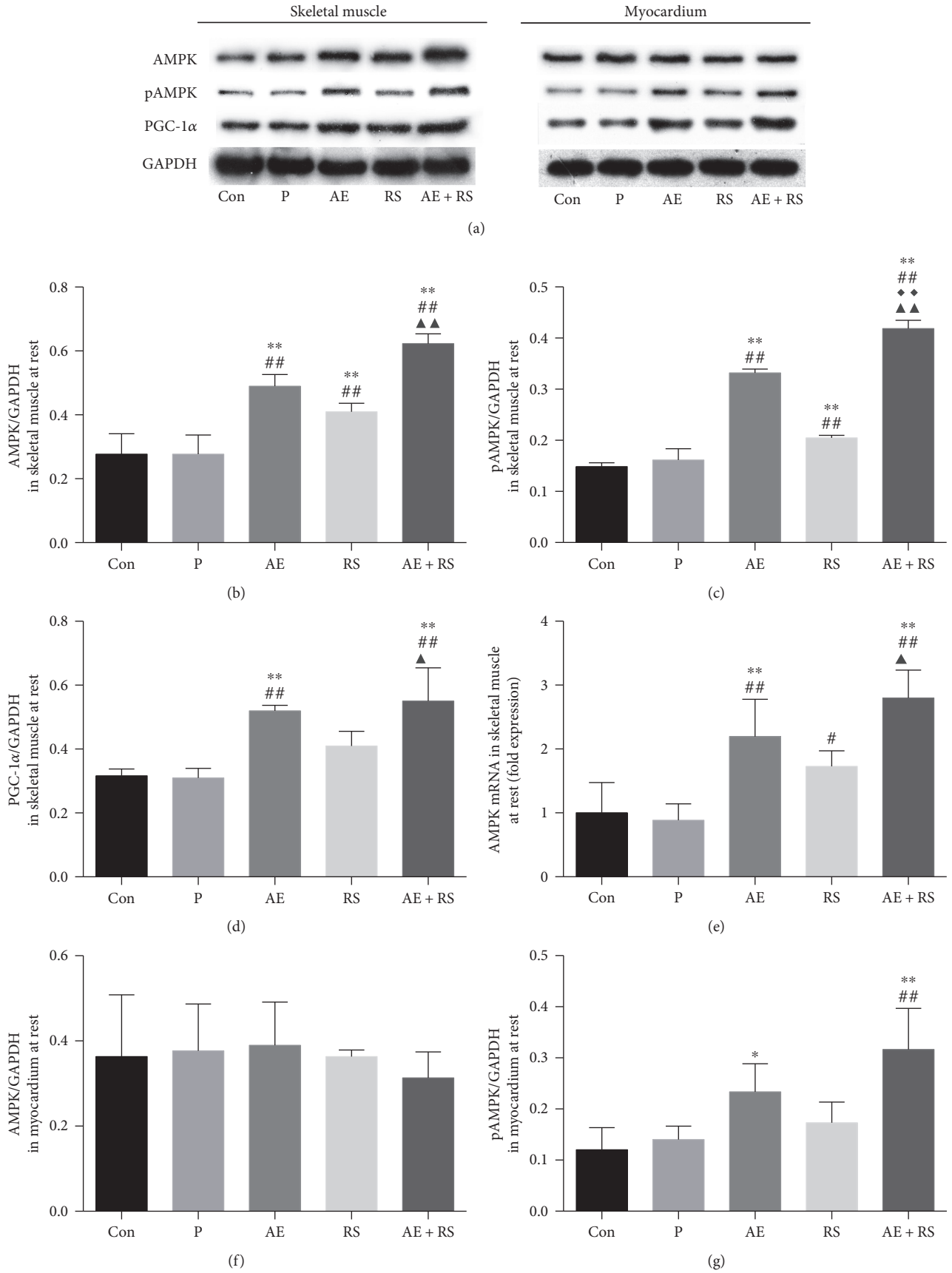

Figure 5: Continued.

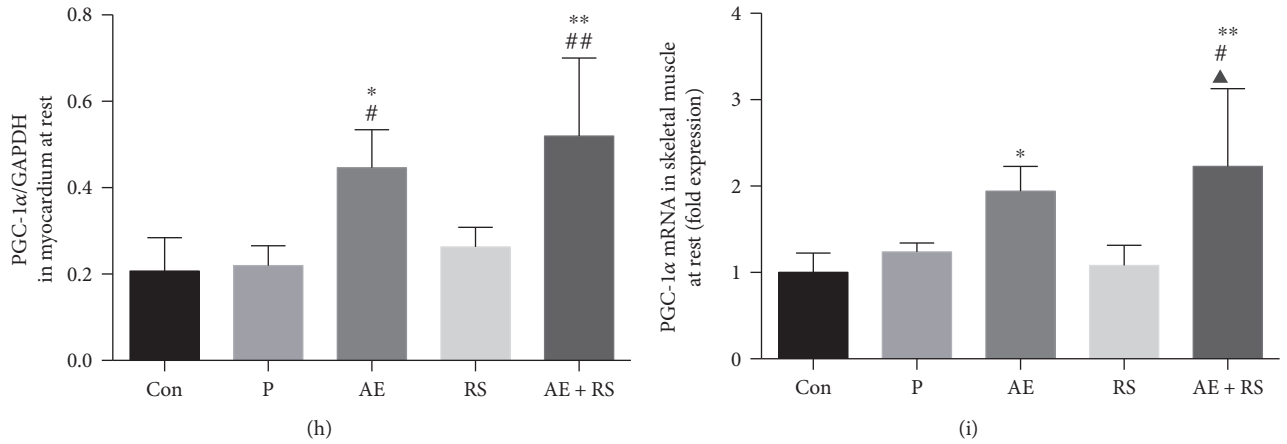

Figure 5: Effects of aerobic exercise, with and without *Rhodiola sacra* supplementation, on the levels of AMPK (b), pAMPK (c), PGC-1α (d), AMPK mRNA (e), and PGC-1α mRNA (i) in mouse skeletal muscle and AMPK (f), pAMPK (g), and PGC-1α (h) in mouse myocardium; bands from the Western blotting analysis (a). $^{*}P < 0.05$, $^{**}P < 0.01$ versus Con; $^{\#}P < 0.05$, $^{\#\#}P < 0.01$ versus P; $^{\blacklozenge\blacklozenge}P < 0.01$ versus AE; $^{\blacktriangle}P < 0.05$, $^{\blacktriangle\blacktriangle}P < 0.01$ versus RS.

example, RS also increases hepatic glycogen synthesis [46]. In contrast to previously reported findings [45], the present study indicated that RS did not significantly increase mitochondrial biogenesis in myocardium. This difference may be attributed to the animal model used: it is possible that the effects of RS on mitochondrial biogenesis are more obvious in damaged myocardium [45] than in normal myocardium. This hypothesis is in accordance with that of a previous study [27] in which *Rhodiola* was categorized as an adaptogen owing to its ability to increase resistance to a variety of chemical, biological, and physical stressors. Our results also provide additional evidence for the adaptogen characteristic of RS in strengthening mitochondrial biogenesis in myocardium in mice subject to AE, which is a type of physical stressor. However, the mechanism underlying the adaptogen characteristic of RS requires further investigation. These results suggest that RS enhances the function of mitochondria and the MQC in SCM, especially following stress.

In addition, for the first time, we showed that AE and RS have a synergistic effect on improving EC and mitochondrial function in SCM. Mice treated with a combination of AE and RS exhibited the longest duration of forced weight-loaded swimming; this was 13.7 times that of the AE group and 1.3 times that of the RS group. Furthermore, the former exhibited greater muscle strength than the AE- or RS-alone groups. Our results indicate that at least two vital factors contribute to this synergistic effect: first, the combination of AE and RS further activates mitophagy in skeletal muscle, which promotes the elimination of dysfunctional or unnecessary mitochondria and supports skeletal muscle plasticity in response to AE. Second, the combination further activates autophagy and mitochondrial biogenesis in the myocardium, which contributes to improving myocardial energy metabolism. These findings suggest that AE and RS have a synergistic effect on improving MQC in SCM. However, the mechanism by which the synergistic effect of AE and RS increases EC is not limited to the improvement of MQC in SCM, as the increase in EC was significantly higher than that during mitophagy, mitochondrial dynamics, and biogenesis in SCM. This study focused on the MQC in the SCM; our next study will aim to analyze the mechanisms by which the synergistic effect of AE and RS increases EC.

4.2. AE and RS, Alone and Combined, Ameliorate Exhaustive Exercise-Induced Skeletal and Cardiac Muscle Damage through the Enhancement of Mitochondrial Quality Control. In the second part of this study, we investigated the protective effect of AE and RS, alone and combined, on EE-induced SCM damage and examined the corresponding mechanism, with a focus on MQC. We found that the level of serum CK, an indicator of muscle damage, significantly increased in mice exhausted by exercise. Morphological analysis using TEM showed that mice exhausted by exercise exhibited fiber necrosis, mitochondrion edema, and mitochondrial cristae dissolution and degradation in SCM. These results indicate that EE, a fatal stressor, caused SCM damage; this finding is in accordance with those of previous studies [45, 47].

EE-induced SCM damage is associated with oxidative stress, which leads to damage to the mitochondrial membrane [48]. Damaged mitochondrial membranes promote the opening of the permeability transition pores, resulting in mitochondrial swelling and the release of apoptosis-inducing factor into the cytosol. Once released, these factors initiate apoptotic signaling and contribute to muscle damage [20]. Mitophagy combined with mitochondrial fission, a process of mitochondrial dynamics, promotes the isolation and elimination of damaged components of mitochondria [15], which is a vital process for the maintenance of cell homeostasis. In addition, mitochondria are produced by mitochondrial biogenesis, which is regulated by PGC-1α. These organelles undergo cycles of fusion, mediated by mitofusin (MFN) 1, to form elongated mitochondrial networks [20, 49]. The activation of these three processes and their balance are vital in protecting against EE-induced muscle damage caused by mitochondrial oxidative stress. The uncoupling of mitophagy and mitochondrial biogenesis during ageing contributes to the overproliferation of damaged mitochondria and decrease in cellular function [50].

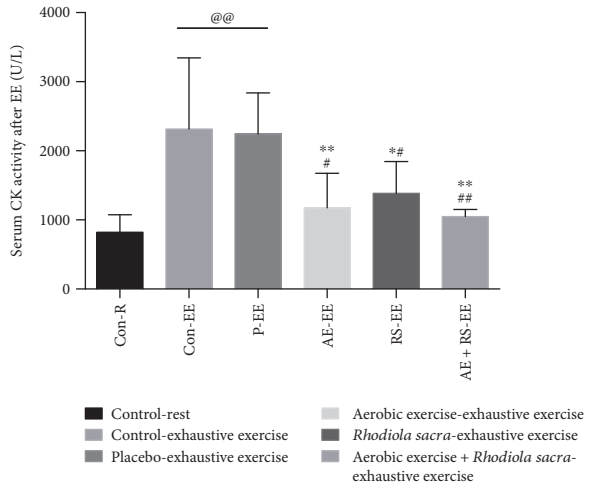

(a)

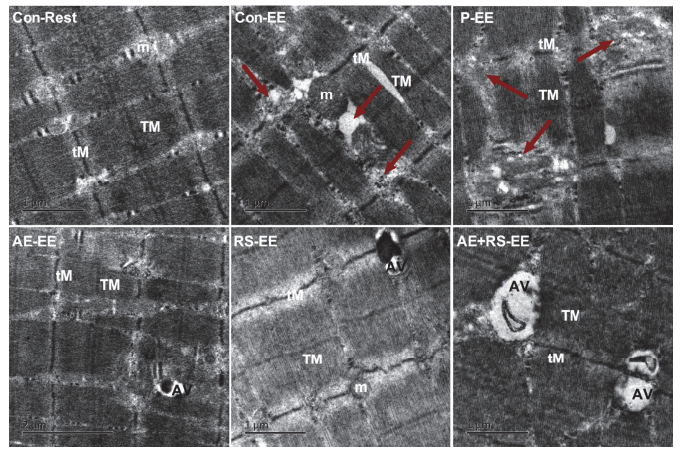

(b)

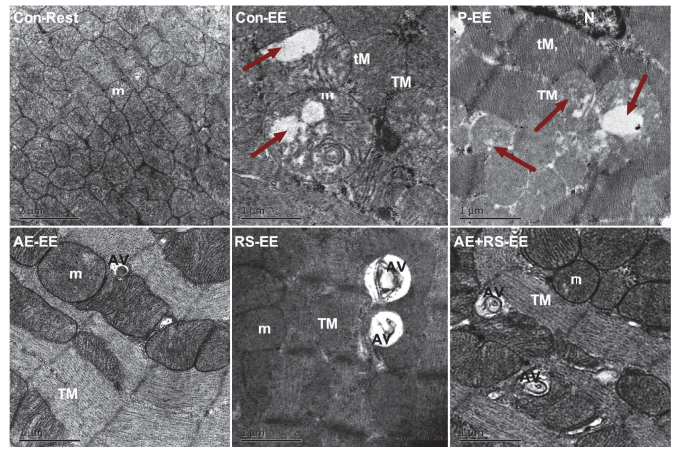

(c)

Figure 6: Effects of aerobic exercise and *Rhodiola sacra* supplementation, alone and combined, on skeletal and cardiac muscle damage caused by exhaustive exercise-induced stress; serum creatine kinase activity (a) and transmission electron micrograph of skeletal (b) and cardiac (c) muscles in mice exhausted from exercise; R: rest; EE: exhaustive exercise; Con-Rest: control-rest; Con-EE: control-exhaustive exercise; P-EE: placebo-exhaustive exercise; AE-EE: aerobic exercise-exhaustive exercise; RS-EE: *Rhodiola sacra*-exhaustive exercise; AE + RS-EE: aerobic exercise combined with *Rhodiola sacra*-exhaustive exercise. TEM image shows damaged myofiber or mitochondria (red arrow); AV: autophagic vacuole; m: mitochondria; tM: thin myofilament; TM: thick myofilament; scale bar = 1 or 2 μm; $^{@@}P < 0.01$ versus Con-N, $^{*}P < 0.05$, $^{**}P < 0.01$ versus Con-EE, $^{\#}P < 0.05$, $^{\#\#}P < 0.01$ versus P-EE; $n = 5$ mice.

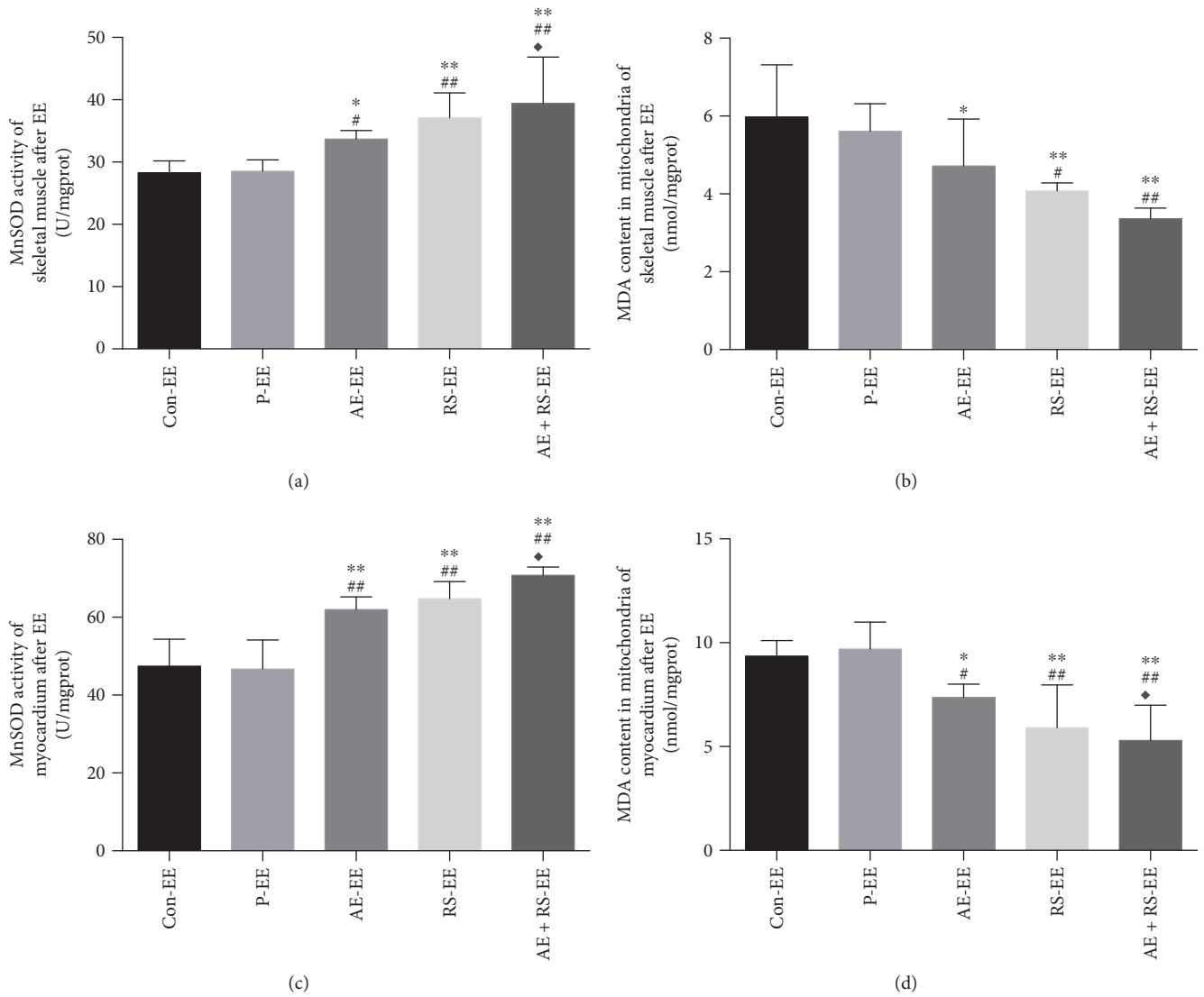

Figure 7: Effects of aerobic exercise and *Rhodiola sacra supplementation*, alone and combined, on MnSOD activity (a) in skeletal muscle and MDA content in mitochondria (b) in skeletal muscle and on MnSOD activity (c) in myocardium and MDA content in mitochondria (c) in myocardium of mice exhausted from exercise. $^{*}P < 0.05$, $^{**}P < 0.01$ versus Con-EE; $^{\#}P < 0.05$, $^{\#\#}P < 0.01$ versus P-EE; $^{\blacklozenge}P < 0.05$ versus AE-EE.

Recent studies have suggested that mitochondria are a target for exercise-induced cardioprotection [51]. Similarly, Vainshtein et al. proposed that exercise increases mitochondrial turnover and that this is partly coordinated by PGC-1α [42]. In order to address the question of whether AE ameliorates EE-induced muscle damage, reduces the level of oxidative stress in SCM, and enhances myocardial protection in mice exhausted from exercise, we analyzed the ultrastructure of SCM and measured CK levels and MnSOD activity in SCM and the MDA content in the mitochondria of SCM of mice exhausted from exercise. We found that AE significantly ameliorated SCM damage induced by EE, improved muscle mitochondrial oxidative stress, and enhanced myocardial protection in these mice. Furthermore, AE significantly activated autophagy and mitophagy in SCM and promoted mitochondrial dynamics and biogenesis in the skeletal muscle of mice exhausted from exercise. These results suggest that the enhancement of MQC is involved in the protective effects of AE on EE-induced SCM damage caused by mitochondrial oxidative stress.

RS is a medicinal plant with demonstrated adaptogenic properties [27]. Several recent studies showed that RS root extract improved stress tolerance in silkworm (*Bombyx mori*) [30], protected C2C12 myotubes against peroxide-induced oxidative stress through the modulation of the molecular chaperone HSP70 [52], and maintained cell membrane permeability by resisting oxidative stress caused by cold, hypoxia, and restraint [53]. Moreover, Abidov et al. concluded that *Rhodiola* enhances mitochondrial function [54]. Liu et al. proposed that *Rhodiola* induces autophagy [32]. In this study, we showed that RS significantly ameliorated SCM damage and improved SCM mitochondrial oxidative stress both induced by EE. Moreover, we report for the first time that RS significantly activated autophagy and mitophagy in

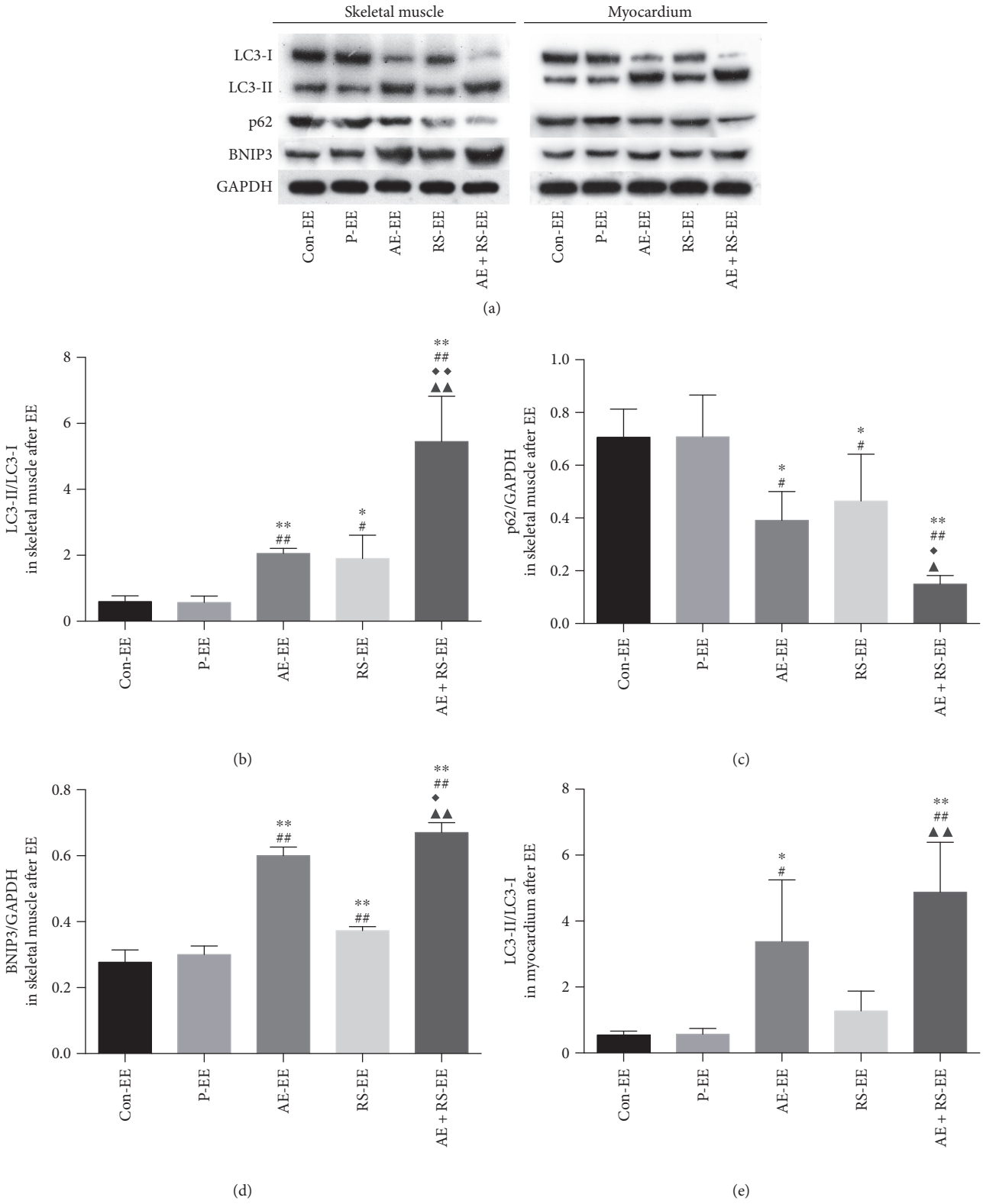

Figure 8: Continued.

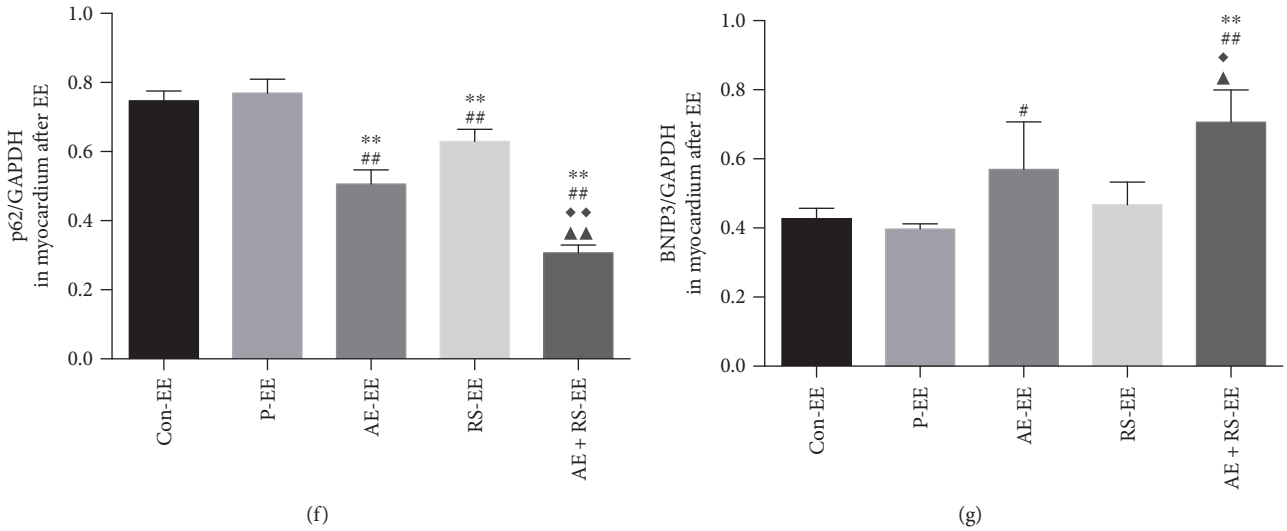

Figure 8: Effects of aerobic exercise and *Rhodiola sacra* supplementation, alone and combined, on the ratio of LC3-II/LC3-I (b), level of p62 (c), and level of BNIP3 (d) in skeletal muscle and on the ratio of LC3-II/LC3-I (e), level of p62 (f), and level of BNIP3 (g) in myocardium of mice exhausted from exercise; bands from the Western blotting analysis (a); $^{*}P < 0.05$, $^{**}P < 0.01$ versus Con-EE, $^{\#}P < 0.05$, $^{\#\#}P < 0.01$ versus P-EE. $^{\blacklozenge}P < 0.05$, $^{\blacklozenge\blacklozenge}P < 0.01$ versus AE-EE. $^{\blacktriangle}P < 0.05$, $^{\blacktriangle\blacktriangle}P < 0.01$ versus RS-EE.

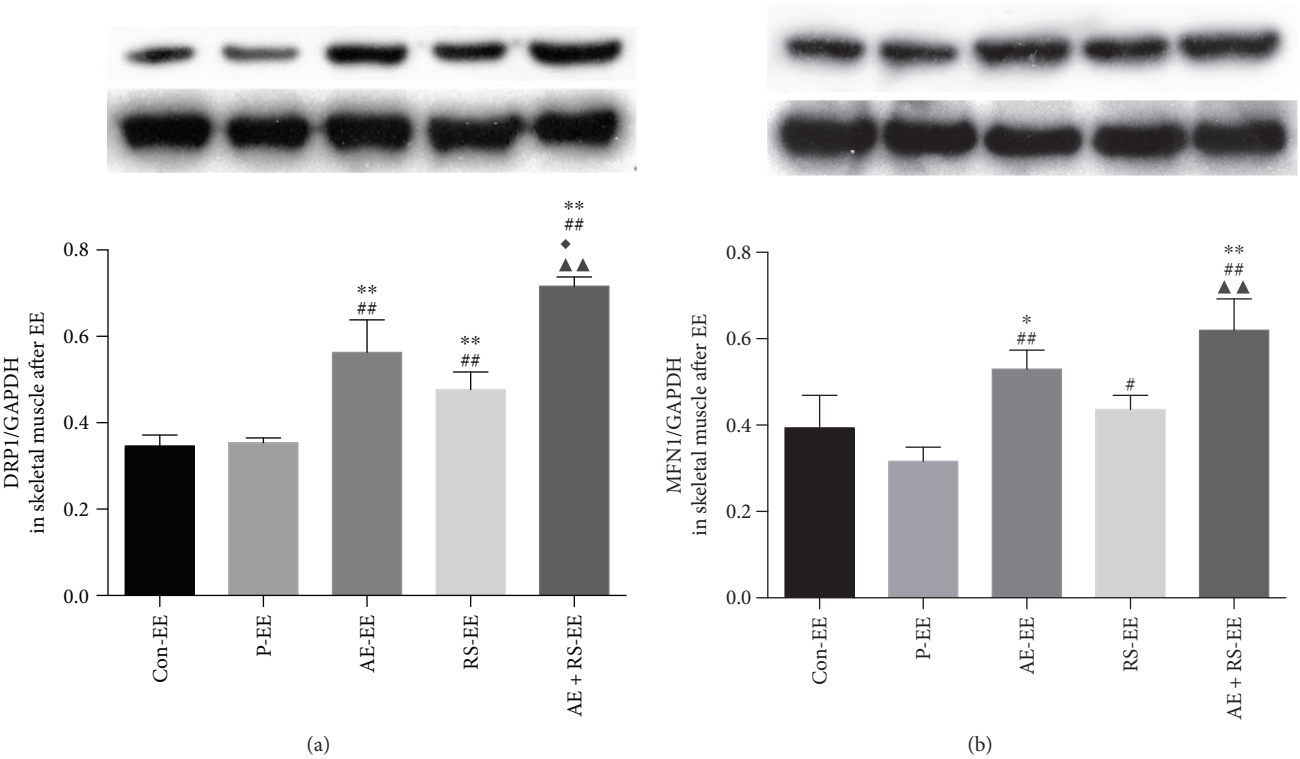

Figure 9: Effects of aerobic exercise and *Rhodiola sacra* supplementation, alone and combined, on the levels of DRP1 (a) and MFN1 (b) in the skeletal muscle of mice exhausted from exercise. $^{*}P < 0.05$, $^{**}P < 0.01$ versus Con-EE; $^{\#}P < 0.05$, $^{\#\#}P < 0.01$ versus P-EE; $^{\blacklozenge}P < 0.05$ versus AE-EE; $^{\blacktriangle\blacktriangle}P < 0.01$ versus RS-EE.

SCM and promoted mitochondrial dynamics and biogenesis in skeletal muscle of mice exhausted from exercise. RS was shown to be as effective as AE in ameliorating EE-induced muscle damage; however, RS alone was not as effective as AE in activating autophagy. This is likely because the mechanism by which RS reduces EE-induced muscle damage is not limited to the activation of autophagy, but also include other mechanisms; for example, RS increases the expression of muscle-protective factors [52]. These results indicate that the enhancement of MQC is involved in the protective effects of RS on EE-induced SCM damage caused by mitochondrial oxidative stress.

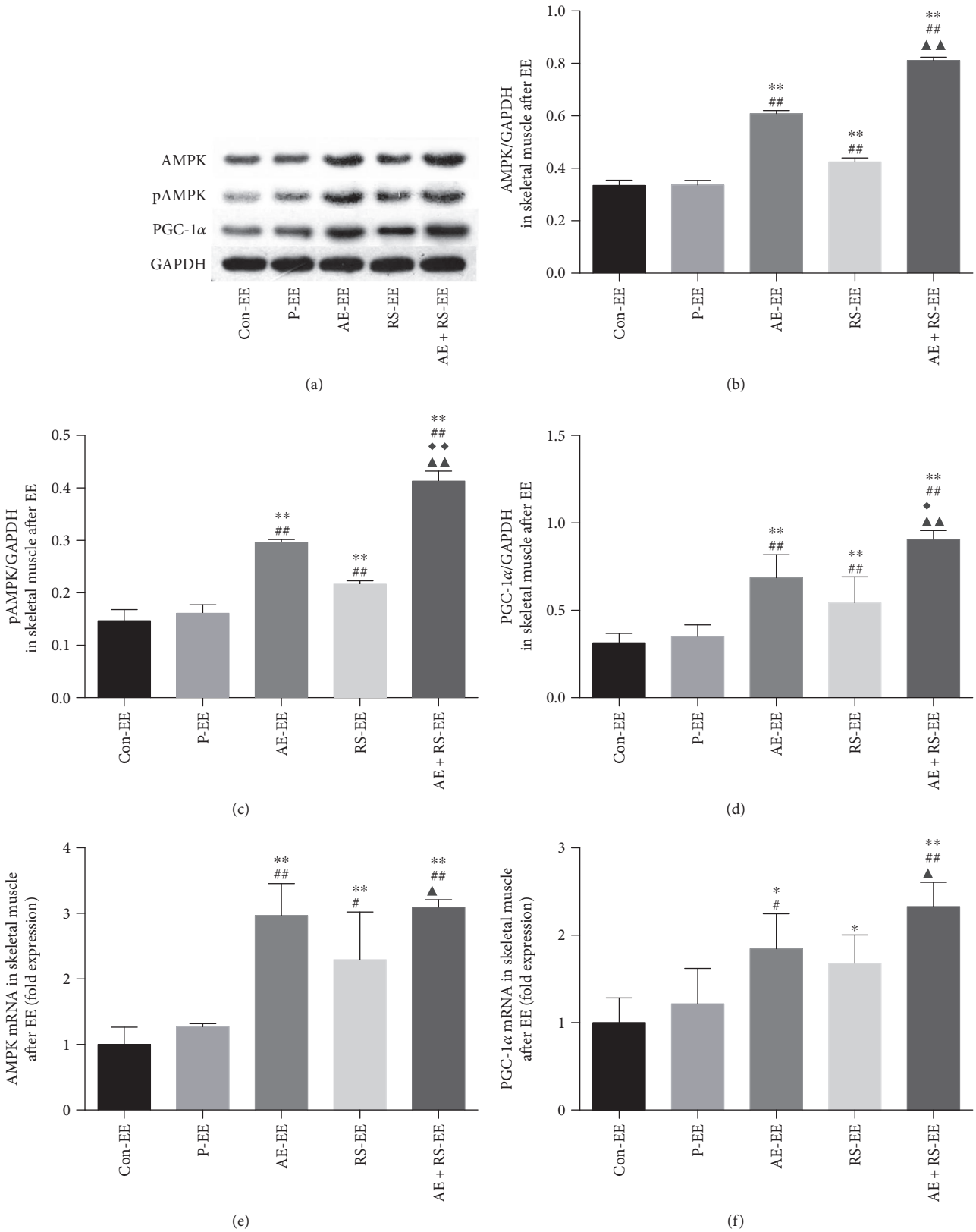

Figure 10: Effects of aerobic exercise and *Rhodiola sacra* supplementation, alone and combined, on the levels of AMPK (b), pAMPK (c), PGC-1α (d), AMPK mRNA (e), and PGC-1α mRNA (f) in skeletal muscle of mice exhausted from exercise; bands from the Western blotting analysis (a). $^{*}P < 0.05$, $^{**}P < 0.01$ versus Con-EE; $^{\#}P < 0.05$, $^{\#\#}P < 0.01$ versus P-EE; $^{\blacklozenge}P < 0.05$, $^{\blacklozenge\blacklozenge}P < 0.01$ versus AE-EE; $^{\blacktriangle}P < 0.05$, $^{\blacktriangle\blacktriangle}P < 0.01$ versus RS-EE.

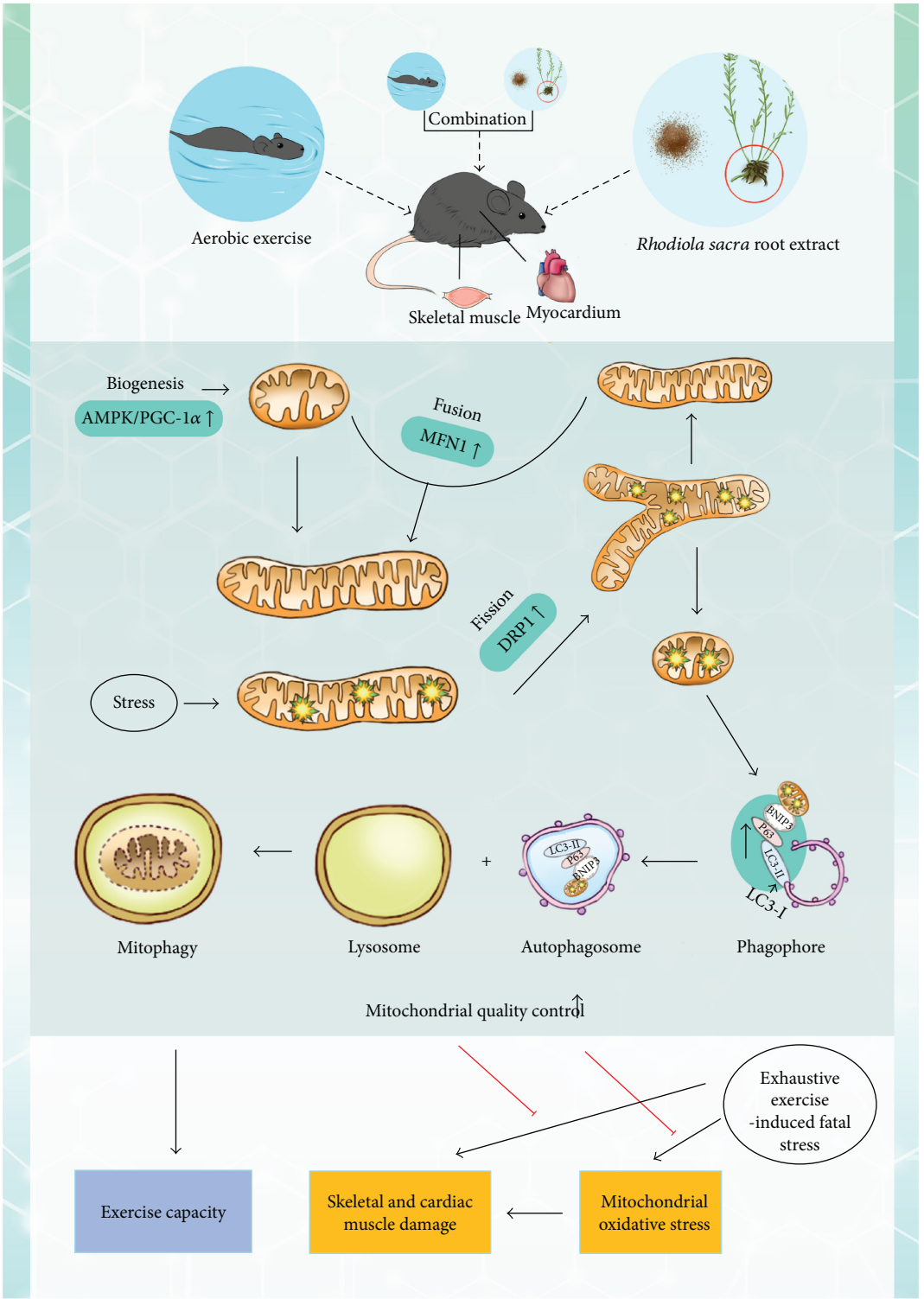

Figure 11: Schematic diagram of the putative mechanism by which aerobic exercise and *Rhodiola sacra*, alone and combined, improve exercise capacity and ameliorate muscle damage induced by exhaustive exercise in mice: Aerobic exercise and *Rhodiola sacra*, alone and combined, enhanced mitochondrial quality control, including mitophagy, mitochondrial dynamics, and biogenesis, in SCM of mice. These effects contribute to the enhancement of mitochondrial function and exercise capacity and protection against SCM damage caused by excessive mitochondrial oxidative stress resulting from EE.

In addition, for the first time, we showed that AE combined with RS had synergistic protective effects on ameliorating EE-induced SCM damage. Mice treated with the combination of AE and RS exhibited 11% and 24% lower activity levels of serum CK and less damage than those treated with AE or RS alone. Our data indicate that at least two vital factors contribute to this synergistic protective effect. First, AE combined with RS activates autophagy and mitophagy, mitochondrial dynamics, and biogenesis in skeletal muscle. Second, the combination further activates autophagy and mitophagy in myocardium. These findings suggest that the synergistic effect of AE and RS in ameliorating SCM damage caused by EE is related to the enhancement of MQC. However, the mechanism involved is not limited to improve MQC in SCM. This study focused on MQC in SCM; analyses of the mechanism of the synergistic protective effect of AE and RS will be performed in our next study.

It should be noted that this study did not use an inhibitor or agonist to verify the results; we aim to overcome this limitation in our next study.

5. Conclusion

In this study, we showed that AE and RS significantly increase EC in mice and ameliorate EE-induced SCM damage caused by mitochondrial oxidative stress; further, it was demonstrated, for the first time, that RS supplementation and AE exert synergistic effects. Moreover, the present study is the first to show that AE and RS enhance MQC, both in the resting state and after EE, through the activation of mitophagy, mitochondrial dynamics, and biogenesis in skeletal or cardiac muscles (Figure 11). AE combined with RS supplementation thus provides a novel strategy to reduce the risks of all-cause mortality and adverse cardiovascular events in patients with CVD.

Conflicts of Interest

The authors declare that there is no conflict of interest regarding the publication of this article.

Acknowledgments

This work was supported by grants from the Natural Science Foundation of China (Grant no. 81672262), the Hunan Province Natural Science Foundation of China (Grant no. 2013SK5076), and the National Development and Reform Commission Foundation of China (Grant no. [2012]1521).

References

[1] R. Lozano, M. Naghavi, K. Foreman et al., "Global and regional mortality from 235 causes of death for 20 age groups in 1990 and 2010: a systematic analysis for the Global Burden of Disease Study 2010," *The Lancet*, vol. 380, no. 9859, pp. 2095–2128, 2012.

[2] R. Korpelainen, J. Lämsä, K. M. Kaikkonen et al., "Exercise capacity and mortality – a follow-up study of 3033 subjects referred to clinical exercise testing," *Annals of Medicine*, vol. 48, no. 5, pp. 359–366, 2016.

[3] D. L. Swift, C. J. Lavie, N. M. Johannsen et al., "Physical activity, cardiorespiratory fitness, and exercise training in primary and secondary coronary prevention," *Circulation Journal*, vol. 77, no. 2, pp. 281–292, 2013.

[4] J. Myers, P. McAuley, C. J. Lavie, J. P. Despres, R. Arena, and P. Kokkinos, "Physical activity and cardiorespiratory fitness as major markers of cardiovascular risk: their independent and interwoven importance to health status," *Progress in Cardiovascular Diseases*, vol. 57, no. 4, pp. 306–314, 2015.

[5] R. Ross, S. N. Blair, R. Arena et al., "Importance of assessing cardiorespiratory fitness in clinical practice: a case for fitness as a clinical vital sign: a scientific statement from the American Heart Association," *Circulation*, vol. 134, no. 24, pp. e653–e699, 2016.

[6] J. Du, D. Zhang, Y. Yin et al., "The personality and psychological stress predict major adverse cardiovascular events in patients with coronary heart disease after percutaneous coronary intervention for five years," *Medicine*, vol. 95, no. 15, article e3364, 2016.

[7] A. Dominguez-Rodriguez, S. Rodríguez, P. Abreu-Gonzalez, P. Avanzas, and R. A. Juarez-Prera, "Black carbon exposure, oxidative stress markers and major adverse cardiovascular events in patients with acute coronary syndromes," *International Journal of Cardiology*, vol. 188, pp. 47–49, 2015.

[8] C. Vassalle, S. Bianchi, D. Battaglia, P. Landi, F. Bianchi, and C. Carpeggiani, "Elevated levels of oxidative stress as a prognostic predictor of major adverse cardiovascular events in patients with coronary artery disease," *Journal of Atherosclerosis and Thrombosis*, vol. 19, no. 8, pp. 712–717, 2012.

[9] P. D. Addison, P. C. Neligan, H. Ashrafpour et al., "Noninvasive remote ischemic preconditioning for global protection of skeletal muscle against infarction," *American Journal of Physiology - Heart and Circulatory Physiology*, vol. 285, no. 4, pp. H1435–H1443, 2003.

[10] M. R. Schmidt, M. Smerup, I. E. Konstantinov et al., "Intermittent peripheral tissue ischemia during coronary ischemia reduces myocardial infarction through a K_{ATP}-dependent mechanism: first demonstration of remote ischemic perconditioning," *American Journal of Physiology - Heart and Circulatory Physiology*, vol. 292, no. 4, pp. H1883–H1890, 2007.

[11] R. Malhotra, B. P. Dhakal, A. S. Eisman et al., "Pulmonary vascular distensibility predicts pulmonary hypertension severity, exercise capacity, and survival in heart failure," *Circulation: Heart Failure*, vol. 9, no. 6, 2016.

[12] J. I. Blomster, S. Svedlund, H. U. Westergren, and L. M. Gan, "Coronary flow reserve as a link between exercise capacity, cardiac systolic and diastolic function," *International Journal of Cardiology*, vol. 217, pp. 161–166, 2016.

[13] H. Van Remoortel, E. De Buck, V. Compernolle, L. Deldicque, and P. Vandekerckhove, "The effect of a standard whole blood donation on oxygen uptake and exercise capacity: a systematic review and meta-analysis," *Transfusion*, vol. 57, no. 2, pp. 451–462, 2017.

[14] Y. T. Wu, S. B. Wu, and Y. H. Wei, "Roles of sirtuins in the regulation of antioxidant defense and bioenergetic function of mitochondria under oxidative stress," *Free Radical Research*, vol. 48, no. 9, pp. 1070–1084, 2014.

[15] M. T. Figge, H. D. Osiewacz, and A. S. Reichert, "Quality control of mitochondria during aging: is there a good and a bad side of mitochondrial dynamics?," *BioEssays*, vol. 35, no. 4, pp. 314–322, 2013.

[16] D. H. Cho, T. Nakamura, J. Fang et al., "S-nitrosylation of Drp1 mediates β-amyloid-related mitochondrial fission and neuronal injury," *Science*, vol. 324, no. 5923, pp. 102–105, 2009.

[17] Y. Zhu, S. Massen, M. Terenzio et al., "Modulation of serines 17 and 24 in the LC3-interacting region of Bnip3 determines pro-survival mitophagy versus apoptosis," *Journal of Biological Chemistry*, vol. 288, no. 2, pp. 1099–1113, 2013.

[18] S. Pankiv, T. H. Clausen, T. Lamark et al., "p62/SQSTM1 binds directly to Atg8/LC3 to facilitate degradation of ubiquitinated protein aggregates by autophagy," *Journal of Biological Chemistry*, vol. 282, no. 33, pp. 24131–24145, 2007.

[19] S. Jäger, C. Handschin, J. St-Pierre, and B. M. Spiegelman, "AMP-activated protein kinase (AMPK) action in skeletal muscle via direct phosphorylation of PGC-1α," *Proceedings of the National Academy of Sciences of the United States of America*, vol. 104, no. 29, pp. 12017–12022, 2007.

[20] H. N. Carter, C. C. Chen, and D. A. Hood, "Mitochondria, muscle health, and exercise with advancing age," *Physiology*, vol. 30, no. 3, pp. 208–223, 2015.

[21] E. Koltai, N. Hart, A. W. Taylor et al., "Age-associated declines in mitochondrial biogenesis and protein quality control factors are minimized by exercise training," *American Journal of Physiology - Regulatory, Integrative and Comparative Physiology*, vol. 303, no. 2, pp. R127–R134, 2012.

[22] E. Ferraro, A. M. Giammarioli, S. Chiandotto, I. Spoletini, and G. Rosano, "Exercise-induced skeletal muscle remodeling and metabolic adaptation: redox signaling and role of autophagy," *Antioxidants & Redox Signaling*, vol. 21, no. 1, pp. 154–176, 2014.

[23] C. W. Taylor, S. A. Ingham, J. E. Hunt, N. R. Martin, J. S. Pringle, and R. A. Ferguson, "Exercise duration-matched interval and continuous sprint cycling induce similar increases in AMPK phosphorylation, PGC-1α and VEGF mRNA expression in trained individuals," *European Journal of Applied Physiology*, vol. 116, no. 8, pp. 1445–1454, 2016.

[24] L. Li, L. Xiao, Y. Hou et al., "Sestrin2 silencing exacerbates cerebral ischemia/reperfusion injury by decreasing mitochondrial biogenesis through the AMPK/PGC-1α pathway in rats," *Scientific Reports*, vol. 6, article 30272, 2016.

[25] E. Marongiu and A. Crisafulli, "Cardioprotection acquired through exercise: the role of ischemic preconditioning," *Current Cardiology Reviews*, vol. 10, no. 4, pp. 336–348, 2014.

[26] A. J. Smuder, A. N. Kavazis, K. Min, and S. K. Powers, "Exercise protects against doxorubicin-induced oxidative stress and proteolysis in skeletal muscle," *Journal of Applied Physiology*, vol. 110, no. 4, pp. 935–942, 2011.

[27] G. S. Kelly, "*Rhodiola rosea*: a possible plant adaptogen," *Alternative Medicine Review*, vol. 6, no. 3, pp. 293–302, 2001.

[28] A. Parisi, E. Tranchita, G. Duranti et al., "Effects of chronic *Rhodiola rosea* supplementation on sport performance and antioxidant capacity in trained male: preliminary results," *Journal of Sports Medicine and Physical Fitness*, vol. 50, no. 1, pp. 57–63, 2010.

[29] M. Jafari, J. S. Felgner, I. I. Bussel et al., "*Rhodiola*: a promising anti-aging Chinese herb," *Rejuvenation Research*, vol. 10, no. 4, pp. 587–602, 2007.

[30] C. Chen, J. Song, M. Chen et al., "*Rhodiola rosea* extends lifespan and improves stress tolerance in silkworm, *Bombyx mori*," *Biogerontology*, vol. 17, no. 2, pp. 373–381, 2016.

[31] S. C. Huang, F. T. Lee, T. Y. Kuo, J. H. Yang, and C. T. Chien, "Attenuation of long-term *Rhodiola rosea* supplementation on exhaustive swimming-evoked oxidative stress in the rat," *The Chinese Journal of Physiology*, vol. 52, no. 5, pp. 316–324, 2009.

[32] Z. Liu, X. Li, A. R. Simoneau, M. Jafari, and X. Zi, "*Rhodiola rosea* extracts and salidroside decrease the growth of bladder cancer cell lines via inhibition of the mTOR pathway and induction of autophagy," *Molecular Carcinogenesis*, vol. 51, no. 3, pp. 257–267, 2012.

[33] S. Xing, X. Yang, W. Li et al., "Salidroside stimulates mitochondrial biogenesis and protects against H_2O_2-induced endothelial dysfunction," *Oxidative Medicine and Cellular Longevity*, vol. 2014, Article ID 904834, 13 pages, 2014.

[34] K. Matsumoto, K. Ishihara, K. Tanaka, K. Inoue, and T. Fushiki, "An adjustable-current swimming pool for the evaluation of endurance capacity of mice," *Journal of Applied Physiology*, vol. 81, no. 4, pp. 1843–1849, 1996.

[35] T. S. Yeh, H. L. Chuang, W. C. Huang, Y. M. Chen, C. C. Huang, and M. C. Hsu, "*Astragalus membranaceus* improves exercise performance and ameliorates exercise-induced fatigue in trained mice," *Molecules*, vol. 19, no. 3, pp. 2793–2807, 2014.

[36] T. L. Cheng, C. C. Liao, W. H. Tsai et al., "Identification and characterization of the mitochondrial targeting sequence and mechanism in human citrate synthase," *Journal of Cellular Biochemistry*, vol. 107, no. 5, pp. 1002–1015, 2009.

[37] S. J. Moat, T. Korpimäki, P. Furu et al., "Characterization of a blood spot creatine kinase skeletal muscle isoform immunoassay for high-throughput newborn screening of Duchenne muscular dystrophy," *Clinical Chemistry*, vol. 63, no. 4, pp. 908–914, 2017.

[38] T. Zhang, L. Xue, L. Li et al., "BNIP3 protein suppresses PINK1 kinase proteolytic cleavage to promote mitophagy," *Journal of Biological Chemistry*, vol. 291, no. 41, pp. 21616–21629, 2016.

[39] N. A. Sobol, K. Hoffmann, K. S. Frederiksen et al., "Effect of aerobic exercise on physical performance in patients with Alzheimer's disease," *Alzheimer's & Dementia*, vol. 12, no. 12, pp. 1207–1215, 2016.

[40] E. E. Noreen, J. G. Buckley, S. L. Lewis, J. Brandauer, and K. J. Stuempfle, "The effects of an acute dose of *Rhodiola rosea* on endurance exercise performance," *Journal of Strength and Conditioning Research*, vol. 27, no. 3, pp. 839–847, 2013.

[41] A. P. Russell, V. C. Foletta, R. J. Snow, and G. D. Wadley, "Skeletal muscle mitochondria: a major player in exercise, health and disease," *Biochimica et Biophysica Acta (BBA) - General Subjects*, vol. 1840, no. 4, pp. 1276–1284, 2014.

[42] A. Vainshtein, L. D. Tryon, M. Pauly, and D. A. Hood, "Role of PGC-1α during acute exercise-induced autophagy and mitophagy in skeletal muscle," *American Journal of Physiology - Cell Physiology*, vol. 308, no. 9, pp. C710–C719, 2015.

[43] V. D. Petkov, D. Yonkov, A. Mosharoff et al., "Effects of alcohol aqueous extract from *Rhodiola rosea L.* roots on learning and memory," *Acta Physiologica et Pharmacologica Bulgarica*, vol. 12, no. 1, pp. 3–16, 1986.

[44] X. T. Zheng, Z. H. Wu, Y. Wei et al., "Induction of autophagy by salidroside through the AMPK-mTOR pathway protects vascular endothelial cells from oxidative stress-induced apoptosis," *Molecular and Cellular Biochemistry*, vol. 425, no. 1-2, pp. 125–138, 2017.

[45] Z. Ping, L. F. Zhang, Y. J. Cui et al., "The protective effects of salidroside from exhaustive exercise-induced heart injury by enhancing the *PGC-1α–NRF1/NRF2* pathway and mitochondrial respiratory function in rats," *Oxidative Medicine and Cellular Longevity*, vol. 2015, Article ID 876825, 9 pages, 2015.

[46] K. T. Lin, S. W. Hsu, F. Y. Lai, T. C. Chang, L. S. Shi, and S. Y. Lee, "*Rhodiola crenulata* extract regulates hepatic glycogen and lipid metabolism via activation of the AMPK pathway," *BMC Complementary and Alternative Medicine*, vol. 16, no. 1, p. 127, 2016.

[47] H. Li, W. Miao, J. Ma et al., "Acute exercise-induced mitochondrial stress triggers an inflammatory response in the myocardium via NLRP3 inflammasome activation with mitophagy," *Oxidative Medicine and Cellular Longevity*, vol. 2016, Article ID 1987149, 11 pages, 2016.

[48] L. M. Popovic, N. R. Mitic, I. Radic et al., "The effect of exhaustive exercise on oxidative stress generation and antioxidant defense in guinea pigs," *Advances in Clinical and Experimental Medicine*, vol. 21, no. 3, pp. 313–320, 2012.

[49] M. A. Kluge, J. L. Fetterman, and J. A. Vita, "Mitochondria and endothelial function," *Circulation Research*, vol. 112, no. 8, pp. 1171–1188, 2013.

[50] K. Palikaras, E. Lionaki, and N. Tavernarakis, "Coordination of mitophagy and mitochondrial biogenesis during ageing in *C. elegans*," *Nature*, vol. 521, no. 7553, pp. 525–528, 2015.

[51] A. Ascensão, J. Lumini-Oliveira, P. J. Oliveira, and J. Magalhães, "Mitochondria as a target for exercise-induced cardioprotection," *Current Drug Targets*, vol. 12, no. 6, pp. 860–871, 2011.

[52] A. Hernández-Santana, V. Pérez-López, J. M. Zubeldia, and M. Jiménez-del-Rio, "A *Rhodiola rosea* root extract protects skeletal muscle cells against chemically induced oxidative stress by modulating heat shock protein 70 (HSP70) expression," *Phytotherapy Research*, vol. 28, no. 4, pp. 623–628, 2014.

[53] V. Gupta, S. S. Lahiri, S. Sultana, R. K. Tulsawani, and R. Kumar, "Anti-oxidative effect of *Rhodiola imbricata* root extract in rats during cold, hypoxia and restraint (C–H–R) exposure and post-stress recovery," *Food and Chemical Toxicology*, vol. 48, no. 4, pp. 1019–1025, 2010.

[54] M. Abidov, F. Crendal, S. Grachev, R. Seifulla, and T. Ziegenfuss, "Effect of extracts from *Rhodiola rosea* and *Rhodiola crenulata (Crassulaceae)* roots on ATP content in mitochondria of skeletal muscles," *Bulletin of Experimental Biology and Medicine*, vol. 136, no. 6, pp. 585–587, 2003.

Hindawi
Oxidative Medicine and Cellular Longevity
Volume 2017, Article ID 6109061, 14 pages
https://doi.org/10.1155/2017/6109061

Research Article

Immediate Early Response Gene X-1 (IEX-1) Mediates Ischemic Preconditioning-Induced Cardioprotection in Rats

Ming-Jiang Xu,[1,2] Yan Cai,[1] Aijuan Qu,[3] John Y.-J. Shyy,[4] Wenjing Li,[1] and Xian Wang[1]

[1]*Department of Physiology and Pathophysiology, School of Basic Medical Science, Peking University Health Science Center, Key Laboratory of Molecular Cardiovascular Science, Ministry of Education, Beijing, China*
[2]*Basic Medical School, Wuhan University, Wuhan, China*
[3]*Department of Physiology and Pathophysiology, School of Basic Medical Science, Capital Medical University, Key Laboratory of Remodeling-Related Cardiovascular Diseases, Ministry of Education, Beijing, China*
[4]*Department of Medicine, University of California, San Diego, San Diego, CA 92093, USA*

Correspondence should be addressed to Ming-Jiang Xu; mingjiangxu@gmail.com and Xian Wang; xwang@bjmu.edu.cn

Received 13 June 2017; Accepted 24 August 2017; Published 29 October 2017

Academic Editor: Aditya Sen

Reversible myocardial ischemia/reperfusion (I/R) or ischemic preconditioning (IPC) is associated with an immediate genomic response; IPC-induced immediate early genes are associated with reduced infarct size. Because the immediate early response gene X-1 (IEX-1) plays a central role in cell apoptosis, we examine whether IEX-1 exerts protective effects against I/R injury. We found that the IEX-1 mRNA level was increased in the IPC-imposed rat heart. However, it was downregulated in the I/R rat heart, which was prevented by in situ IPC. When IEX-1 was knocked down, the protective effects imposed by IPC were lessened. Local gene delivery of Ad-IEX-1 to the left ventricle greatly diminished cardiac infarct size and improved systolic functions of I/R hearts in rats. In contrast, knocking down IEX-1 expression exacerbates myocardial infarction. Overexpression of IEX-1 in neonatal rat cardiomyocytes significantly reduced hypoxia-reoxygenation-induced intracellular and mitochondrial ROS accumulation and cell apoptosis. Furthermore, IPC-induced phosphorylation and particle translocation of PKCε were impaired by knocking down IEX-1 in vivo, and overexpressing IEX-1 showed similar cardioprotection imposed by IPC. Our results demonstrate that IPC increases IEX-1 expression, which may promote phosphorylation and particle translocation of PKCε and thus reduce intracellular ROS accumulation. These beneficial effects reduce cardiomyocyte apoptosis and necrosis to alleviate cardiac infarction.

1. Introduction

Timely reperfusion after myocardial ischemia is the definitive strategy to salvage myocardium at risk of lethal injury. However, abrupt restoration of blood flow to the ischemic myocardium carries the potential of introducing additional cardiomyocyte injury and death [1, 2]. Such reperfusion injury (RI) involves opening of the mitochondrial permeability transition pore (MPTP) under the conditions of calcium overload and oxidative stress that accompany reperfusion. Protection from MPTP opening and hence RI can be mediated by ischemic preconditioning (IPC) where the prolonged ischemic period is preceded by one or more brief cycles of ischemia and reperfusion [3, 4].

There is a plethora of data implicating many different signaling pathways in preconditioning, and the relevant role of each remains hotly debated. And of them, there is extensive evidence that protein kinase C (PKC) plays a central role in preconditioning [5]. There remains some controversy over which of the many PKC isoforms may be involved in IPC. Nevertheless, there is a large body of evidence to implicate PKCε and as important players in IPC [5]. The proposed mechanism of PKCε-mediated cardioprotection is that generation of mitochondrial ROS during IPC may lead to

activation of PKCδ. This increases adenosine generation and release leading to activation of phospholipase C. Generation of diacylglycerol and inositol-triphosphate results in calcium release and activation of PKCε [5]. However, there is rare study about whether PKC activation is regulated by immediate early genes.

IPC, that is, cyclic episodes of short durations of ischemia and reperfusion (I/R), potentiates redox signaling to convert the death signals into survival ones to protect the ischemic heart [6]. A previous study has shown that IPC induces the expression of proto-oncogenes or immediate early genes such as c-Fos, c-Myc, c-Jun, and Egr-1 in isolated rat hearts, which was associated with improved ventricular function and reduced infarct size [7–9], but the underlying mechanism involving in immediate early genes protecting an ischemia heart remains elusive.

Immediate early response gene X-1 (IEX-1), also known as p22/PRG1 in rat or the mouse homologue gly96, is a novel stress-induced immediate early gene. It can be rapidly upregulated in various cell types by irradiation, viral infection, inflammatory cytokines, chemical carcinogens, growth factors, and hormones under the control of transcription factors such as NF-κB/rel, p53, Sp1, c-Myc, and AP-1 (reviewed by Wu) [10]. Like other immediate early genes, IEX-1 plays a pivotal role in cell survival under stress conditions [11–16]. Decreased IEX-1 expression is proved to associate with enhanced apoptosis in a titin-deficient mouse model of dilated cardiomyopathy [17]. Furthermore, IEX-1 has the ability of regulating several protein kinase activities, such as ERK and Akt, through interacting with protein phosphatase 2A (PP2A) [18, 19].

In the present study, we examine whether IEX-1 exerts protective effects against I/R injury imposed on rat neonatal and adult hearts. We found that IEX-1 expression was downregulated in the ischemic rat heart, but was rescued by IPC. The restored IEX-1 expression not only decreased the I/R-induced apoptosis and necrosis but also alleviates cardiac infarction. The putative mechanisms include increased activation of PKC and attenuated I/R-induced ROS accumulation.

2. Materials and Methods

2.1. Adenoviral Vector Construction. Replication-deficient adenoviral vectors containing human IEX-1 cDNA (Ad-IEX-1) or GFP (Ad-GFP) under the control of the cytomegalovirus (CMV) promoter were constructed and prepared according to the manufacturer's instruction (BD Biosciences, San Jose, CA). Adenoviral vectors carrying bacterial β-galactosidase (Ad-β-Gal) were kindly provided by Prof. H. Cheng (Peking University, China).

2.2. Rat Model of Myocardial Ischemia and IPC. All animals received humane care in compliance with the Institutional Authority for Laboratory Animal Care of Peking University Health Science Center. The Sprague-Dawley (SD) rat heart ischemia and IPC surgical procedures were described previously [20]. Briefly, after thoracotomy, rats underwent 30 min of myocardial ischemia, then 3 or 24 h of reperfusion. For IPC treatment, before lethal I/R, rats underwent three cycles of short I/R (4 min/4 min). Local gene delivery was performed with protocols previously described [21]. Four days before ischemia, 5×10^9 plaque-forming unit (pfu) adenovirus in 250 μl of virus solution was injected intramyocardially into the left ventricular muscular wall.

2.3. In Vivo Small Interfering RNA Repression. We injected siRNA/transfection agent solution into the left ventricle muscle wall to achieve sufficient siRNA concentrations for IEX-1 repression within cardiac tissues. Rats were anesthetized by intraperitoneal injection of sodium pentobarbital (60 mg/kg). After thoracotomy, siRNA (20 μg siRNA/kg body weight) together with transfection agent solution (jet-PEI, PolyPlus transfection) was intramyocardially injected in 5 predetermined regions in the left anterior descending (LAD) area. A total of 250 μl of siRNA/transfection agent solution was delivered. Injections were performed by a single investigator in a blinded fashion. Stealth siRNA targeting rat IEX-1 (sense: cca aca uug cca aga gga ucc ucu u; antisense: aag agg auc cuc uug gca aug uug g) and control siRNA (Cat number: 12935300) were synthesized by Invitrogen (Invitrogen, CA). Two days after injection, cardiac tissue around the injected area was excised, and IEX-1 levels were determined by real-time PCR and Western blot.

2.4. Neonatal Rat Ventricular Cardiomyocyte Culture. Neonatal rat ventricular cardiomyocytes were isolated from 1- to 2-day-old Sprague-Dawley rats [22]. Experiments were performed at day 3 in culture. For hypoxia/ reoxygenation (H/R), cells were cultured in hypoxia buffer (in mmol/l NaCl 118, $NaHCO_3$ 24, KCl 16, KH_2PO_4 1, $CaCl_2$ 2.5, $MgCl_2$ 1.2, Na^+ EDTA 0.5, and Na^+ lactate 20, pH 6.2) and underwent $<1\%$ $O_2 + 5\%$ CO_2 + argon treatment for 4 h, then were transferred to 5% CO_2 + 95% air for reoxygenation. And 10 min hypoxia followed with 10 min reoxygenation was considered as one cycle of preconditioning.

2.5. Real-Time PCR and Western Blot Analysis and Immunostaining. For details of real-time PCR, Western blot analysis, and immunostaining, see the online-only Data Supplement available online at https://doi.org/10.1155/2017/6109061.

2.6. Measurement of ROS Accumulation. The accumulation of intracellular ROS and mitochondrial ROS was detected with luminol-derived chemiluminescence, DCFH-DA, and MitoTracker® Red CM-H2XRos (for details, see the online-only Data Supplement).

2.7. Statistical Analysis. All values are expressed as mean ± SEM. Comparisons between more than 2 groups were analyzed by one-way ANOVA followed by Tukey-Kramer post hoc testing. A $P < 0.05$ was considered statistically significant.

The authors had full access to the data and take responsibility for its integrity. All authors have read and agree to the manuscript as written.

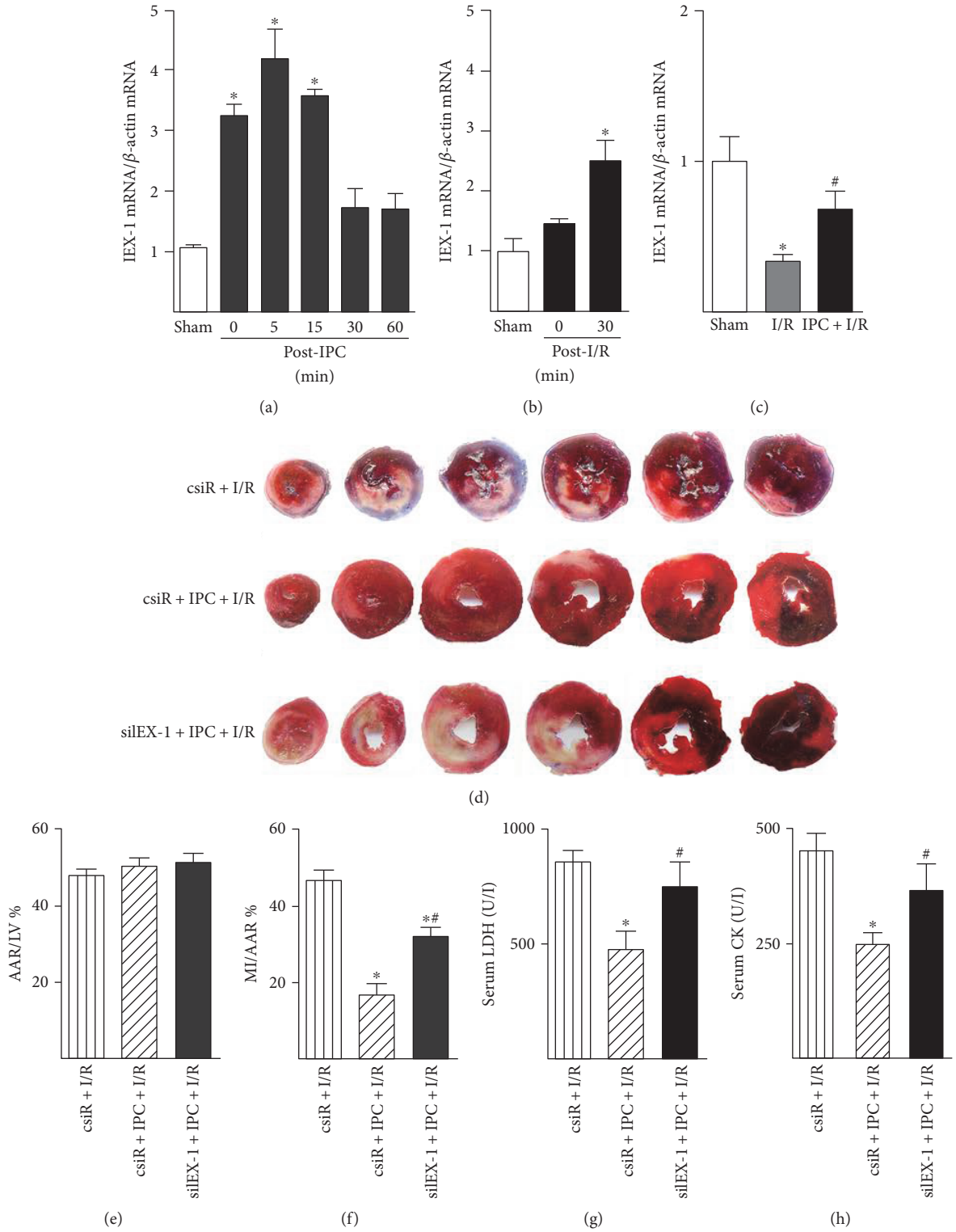

Figure 1: IEX-1-mediated IPC-induced cardioprotection. (a) IEX-1 mRNA level in rat hearts post-IPC was detected by quantitative real-time PCR ($n = 5$~6). (b) IEX-1 mRNA level in rat hearts postischemia (30 min) or I/R (30 min/30 min). (c) IEX-1 mRNA level in rat hearts subjected to sham operation (Sham), I/R (30 min/3 h), or IPC prior I/R ($n = 6$~10). (d). 5 μg scrambled siRNA (csiR) or siRNA targeting IEX-1 (siIEX-1) with transfection reagent in 250 μl of saline was directly injected intramyocardially into the left ventricular muscular wall. 2 days after the injection, rats underwent I/R (30 min/24 h) or IPC prior I/R ($n = 6$~7), then hearts were excised and sliced for infarction analysis by Evans blue and triphenyltetrazolium chloride (TTC) attaining; (e) percentage of the area at risk (AAR) to the left ventricle (LV) and (f) infarct area (MI) to AAR were determined by computer-assisted planimetry. (g) Serum lactate dehydrogenase (LDH) and (h) creatine kinase (CK) activity were measured at the end of 24-hour reperfusion. $n = 7$~10, $^{*}P < 0.05$ versus csiR + I/R, $^{\#}P < 0.05$ versus csiR + IPC + I/R.

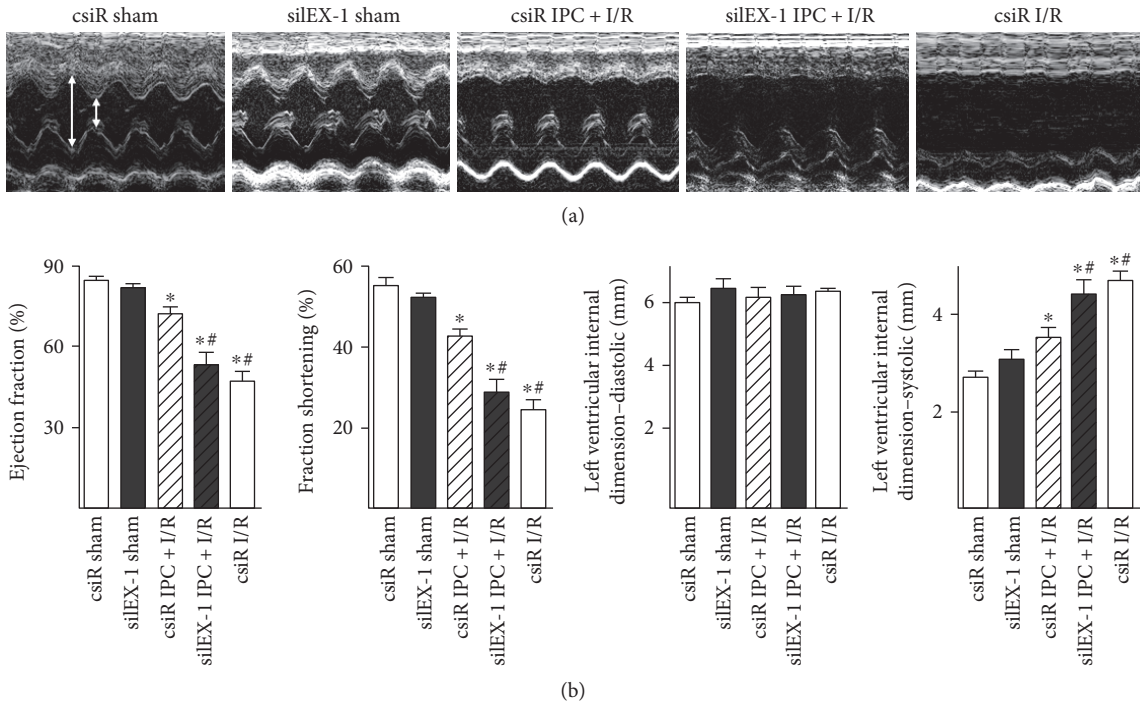

Figure 2: Echocardiography-assessed cardiac function. (a) Echocardiographic images showing systolic and diastolic dimensions (arrows) measured by M-mode in the parasternal short axis view at the level of the papillary muscles. (b) Summarized mean echo data of ejection fraction, fractional shortening, diastolic internal dimension, and systolic internal dimension. $n = 9$~14, $^{*}P < 0.05$ versus csiR sham, $^{\#}P < 0.05$ versus csiR IPC + I/R.

3. Results

3.1. IEX-1-Mediated IPC-Induced Cardioprotection. We used a model of in situ IPC of intermittent coronary occlusion to examine first the expression of IEX-1 in the rat heart. As shown in Figure 1(a), the IEX-1 mRNA level was increased rapidly in the IPC-imposed heart, peaked at 5 min, and declined thereafter, which remained higher than the basal level at 1 h (Figure 1(a)). Lethal ischemia (30 min) itself does not promote IEX-1 expression, although the IEX-1 mRNA level increased at early reperfusion (30 min) (Figure 1(b)); it decreased at 3 h reperfusion (Figure 1(c)), and the level of IEX-1 mRNA was higher in hearts that underwent IPC prior to I/R than that in hearts receiving I/R only (Figure 1(c)). The IEX-1 protein level decreased at 3 h reperfusion which was rescued by IPC prior to I/R (Supplemental Figure 1A and B).

Because IPC could induce IEX-1 expression, we then investigated whether the increased level of IEX-1 is involved in IPC-mediated cardiac protection. Small interfering RNA targeting rat IEX-1 (siIEX-1) was used to knock down IEX-1 expression in hearts. As shown in Figures 1(d), 1(e), and 1(f), in situ IPC protected the heart, revealed by decreased infarct size, in the scrambled siRNA (csiR) group, but not in the siIEX-1 group. These were parallel, confirmed by decreased release of lactate dehydrogenase (LDH) and creatine kinase (CK) to serum in the csiR group, but not in the siIEX-1 group (Figures 1(g) and 1(h)).

IEX-1 knockdown impaired the protective effects of IPC, which was further confirmed by echocardiography analysis. As shown in Figures 2(a) and 2(b), impaired systolic function post-I/R was observed in the I/R group, assessed by ejection fraction (EF), fraction shortening (FS), and systolic left ventricular internal dimension (LVID-s), while IPC-imposed rats showed improved systolic function post-I/R in the csiR group. Of note, depraved systolic function was observed in the rats treated with siIEX-1 prior to IPC, which was similar to that in I/R alone rats.

3.2. IEX-1 Overexpression Attenuates Myocardial Infarction. To investigate a functional contribution of IEX-1 to postischemic cardioprotection, we developed an adenoviral vector expressing human IEX-1 (Ad-IEX-1). In the experimental group, Ad-IEX-1 was directly injected into the left ventricle wall, whereas control groups received Ad-GFP or saline. Four days post the injection, rat hearts were excised. The overexpression of IEX-1 in the cardiac muscle was confirmed by Western blot (Figure 3(a)) and immunostaining (Supplemental Figure 2A). As shown in Figures 3(b), 3(c), and 3(d), IEX-1 overexpression caused significant cardioprotection. A significant decrease in infarct size of the hearts was found in these animals, when compared with that of hearts receiving saline or Ad-GFP. In addition, these rats exhibited lower levels of serum LDH and CK (Figures 3(e) and 3(f)). As well, the accident rate of cell apoptosis in the area at risk, assessed by TUNEL staining, was significantly reduced in IEX-1 overexpressed rats (Figure 3(g)).

To examine the functional consequences resulting from Ad-IEX-1 gene delivery, we measured cardiac systolic

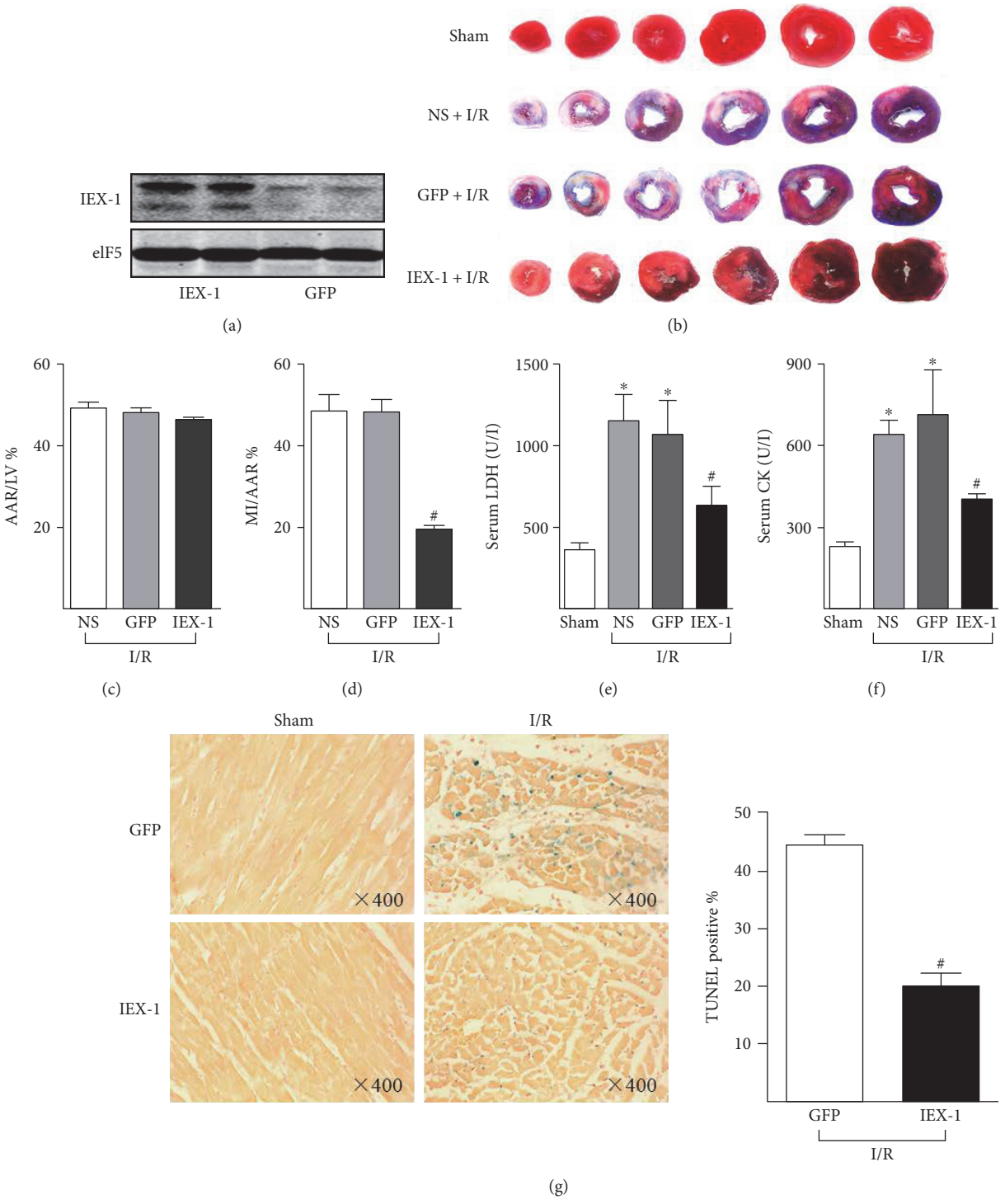

FIGURE 3: IEX-1 overexpression attenuates myocardial infarction. Rats were injected with saline (NS) ($n = 7$), Ad-GFP ($n = 11$), or Ad-IEX-1 ($n = 8$) for 4 days, then underwent I/R (30 min/24 h). (a) Western blot analysis confirmed overexpression of IEX-1 in the left ventricle after four days of local adenovirus delivery. (b) Representative images of the infarct heart stained by Evans blue and TTC. (c) Ratios of AAR to LV and (d) MI to AAR were shown. (e) Serum LDH and (f) CK activity were measured at the end of 24-hour reperfusion. (g) After subjected to I/R, hearts were excised for slicing, then TUNEL staining was performed for assessing cardiac cell apoptosis post-I/R. $^{*}P < 0.05$ versus Sham, $^{\#}P < 0.05$ versus GFP.

function by echocardiography and measurement of cardiac hemodynamics parameters. Of note, impaired systolic functions post-I/R, assessed by EF, FS, and LVID-s, were observed in the GFP group, while Ad-IEX-1 delivery rats showed improved post-I/R systolic functions (Figures 4(a) and 4(b)). Similarly, catheter-mediated measurement of

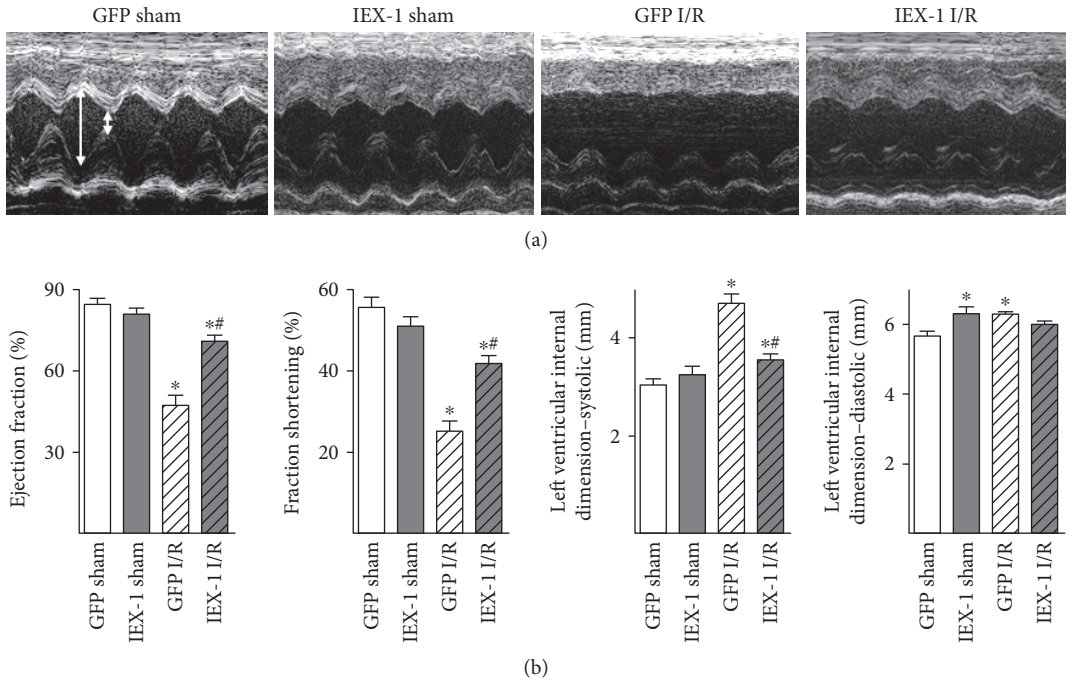

Figure 4: IEX-1 overexpression improved cardiac function post-I/R assessed by echocardiography. (a) Echocardiographic images showing systolic and diastolic dimensions (arrows) measured by M-mode in the parasternal short axis view at the level of the papillary muscles. (b) Echo data of ejection fraction, fractional shortening, systolic internal dimension, and diastolic internal dimension. $n = 7$~9, $^{*}P < 0.05$ versus GFP sham, $^{\#}P < 0.05$ versus GFP I/R.

cardiac hemodynamics parameters showed that mean arterial pressure, left ventricular systolic pressure, maximal rates of pressure increase and decrease were significantly impaired post-I/R, whereas these parameters were improved in Ad-IEX-1 delivery rats (Supplemental Table 1).

3.3. SiRNA Knocking Down IEX-1 Exacerbates Myocardial Infarction. In the reciprocal approach, we used siRNA to repress the cardiac expression of IEX-1 in vivo. An amount of 5 μg of IEX-1 siRNA (siIEX-1) together with transfection reagent was directly injected into the rat left ventricular wall. The IEX-1 mRNA level was reduced at 48 h postinjection (Figure 5(a)), and the corresponding reduction of protein was confirmed by Western blot (Figure 5(b)) and immunostaining (Supplemental Figure 2B). Responding to I/R (30 min/24 h), rats with siIEX-1 injection showed significantly increased infarct size expressed as the percentage of the left ventricle area (~7%), when compared with animals with control siRNA (Figures 5(c) and 5(d)). Similarly, plasma LDH and CK activity were increased in rats receiving siIEX-1 (Figure 5(e) and 5(f)).

3.4. IEX-1 Inhibits H/R-Induced ROS Accumulation. Because ROS accumulation at the end of ischemia and during reperfusion exacerbates cardiomyocyte injury [23, 24] and PKCε diminishing these ROS levels is a critical step in preconditioning [3], thus, we tested the role of IEX-1 in H/R-induced ROS accumulation. Neonatal rat cardiomyocytes were infected with 10 MOI of adenovirus and subjected to hypoxia for 4 h, then submitted to chemiluminescence or fluorescence analysis for intracellular ROS accumulation. Intracellular ROS was significantly reduced in cells overexpressing IEX-1 (~74% reduction in chemiluminescence, Figure 6(a), and ~69% reduction in DCF fluorescence, Figure 6(b)).

During H/R, mitochondrion seems to be the main source of ROS in cardiomyocytes [25]. After 4 h hypoxia, cardiomyocytes were incubated with MitoTracker Red CM-H2XRos to probe the mitochondrial ROS (Supplemental Figure 3). Confocal microscopy revealed that neonatal rat cardiomyocytes undergoing H/R displayed a 5.5-fold increase in fluorescence intensity, which was significantly reduced in cells receiving Ad-IEX-1 (Figure 6(c)), indicating that IEX-1 is able to decrease mitochondrial ROS accumulation.

3.5. IEX-1 Reduces H/R-Induced Cardiomyocyte Injury. The increased ROS is a primary stimulus for the mitochondrial death pathway. Then, we used an in vitro H/R model to study the effects of IEX-1 on H/R-induced cardiomyocyte death. Neonatal cardiomyocytes were infected with Ad-GFP or Ad-IEX-1 at 5, 10, or 20 MOI. After H/R insult, Ad-IEX-1-infected cells showed less morphological changes than those infected with Ad-GFP (Supplemental Figure 4A). Overexpression of IEX-1, but not GFP, greatly reduced LDH release in conditioned media (Supplemental Figure 4B). As well, caspase-3 cleavage, an indication of apoptosis, reduced in cells overexpressing IEX-1 (Figure 7(a)). After H/R, caspase-3 cleavage increased as reoxygenation time was prolonged in both Ad-GFP- and Ad-IEX-1-infected cells. However, the cleaved caspase-3 was less in cells overexpressing IEX-1 at all time points (Figure 7(b)). Concurrently, caspase-3/7 activity attenuated in cells infected with Ad-IEX-1,

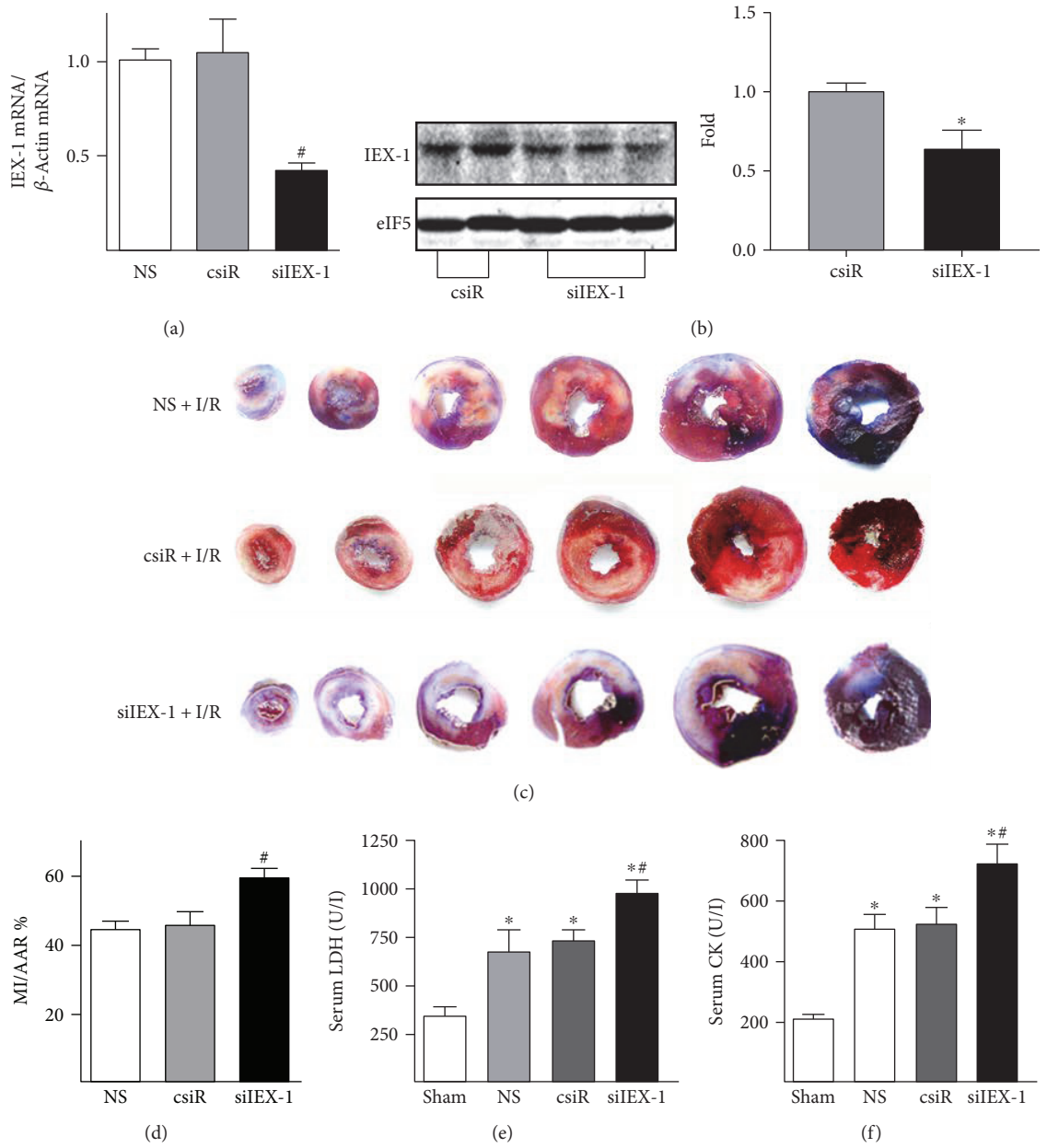

FIGURE 5: siRNA repression of IEX-1 exacerbates myocardial infarction. 5 μg csiR or siIEX-1 with transfection reagent in 250 μl of saline (NS) was directly injected intramyocardially into the left ventricular muscular wall. 2 days after, (a) IEX-1 mRNA levels and (b) protein levels were determined. (c) 2 days after siRNA injection, rats underwent I/R (30 min/24 h). Representative images of heart infarction assessed by Evans blue and TTC staining were shown. (d) Infarct sizes are expressed as ratio of MI to AAR. (e) Serum LDH and (f) CK activity were measured at the end of 24 h reperfusion. $n = 5$ in each group. $^{*}P < 0.05$ versus sham, $^{\#}P < 0.05$ versus NS or csiR.

compared with those with Ad-GFP (Figure 7(c)). Under H/R, the percentage of TUNEL-positive (apoptotic) cells was also reduced by IEX-1 (Figure 8(d)). Moreover, there was a decrease in mitochondrial cytochrome c leakage to cytoplasm in IEX-1 overexpressed cells (Figures 7(e) and 7(f)). Together, these data indicate that IEX-1 overexpression imposes protective effects on neonatal rat cardiomyocytes under H/R.

3.6. IEX-1 Promotes PKCε Phosphorylation and Mitochondrial Translocation. Then, we found clear particle translocation of PKCε in cardiac cells subjected to IPC prior to I/R, which was also observed similarly in the IEX-1 overexpressed heart; in contrast to these, particle translocation of PKCε was significantly inhibited when siIEX-1 was administered to knock down heart IEX-1 (Figure 8(a)). Then, we further detected phosphor-PKCε in hearts after IPC + I/R; of note, the increased level of phosphor-PKCε by IPC was abolished by IEX-1 knocking down (Figure 8(b)).

Multiple studies have demonstrated that activation of protein kinase Cε (PKCε) is critical for the protective phenotype of IPC against myocardial I/R injury [5]. Thus, we

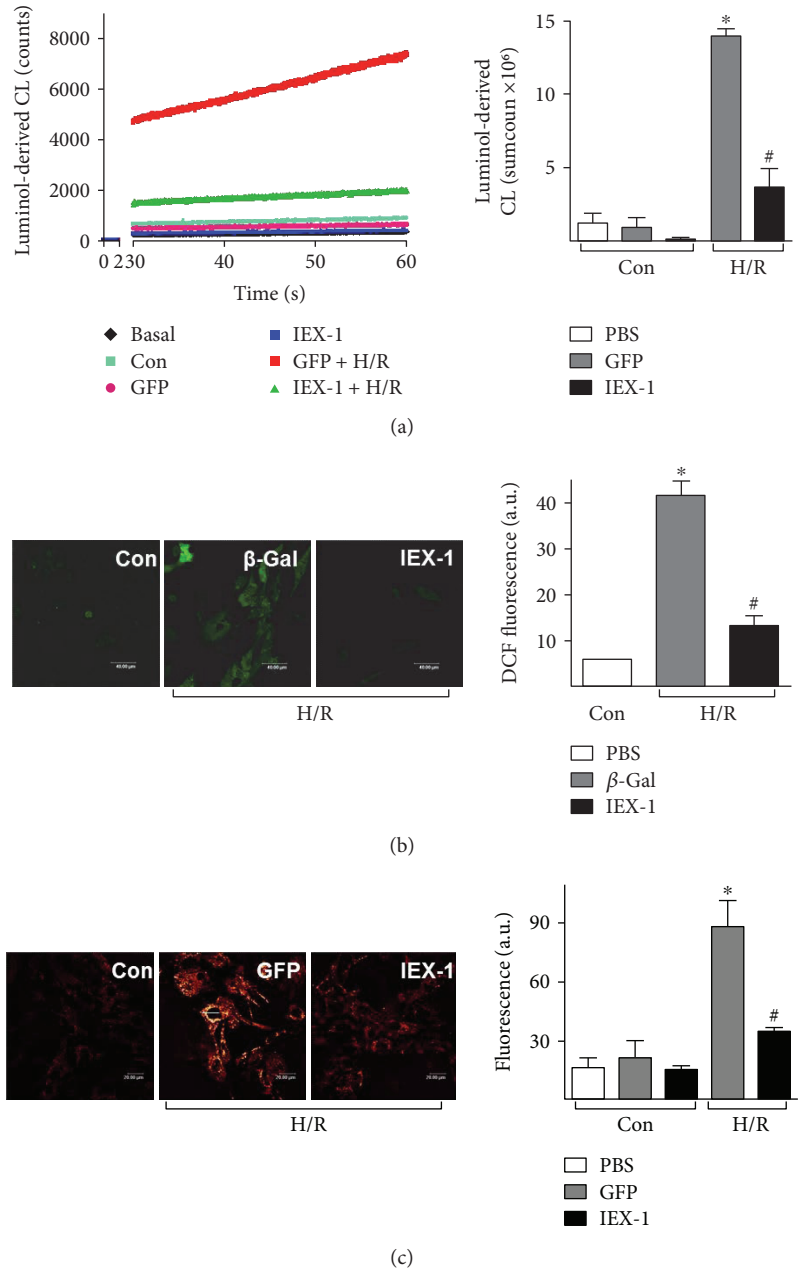

Figure 6: IEX-1 overexpression inhibits H/R-induced ROS accumulation. Neonatal rat cardiomyocytes were infected with adenovirus at 10 MOI for 36 h, then underwent H/R (4 h/30 min). (a) ROS levels measured by luminol chemiluminescence (left). The column data are the sum counts of the 30-minute measurement period (right). (b) Intracellular ROS were detected by DCFH-DA (scale bar = 40 μm), and (c) mitochondrial ROS were detected by MitoTracker Red CM-H2XRos probe with confocal microscopy (scale bar = 20 μm). $^{*}P < 0.05$ versus Ctrl, $^{\#}P < 0.05$ versus GFP or β-Gal.

confirmed these results in cultured cardiomyocytes. First, in vitro IPC, termed hypoxia preconditioning (HPC), induced by short-term hypoxia and reoxygenation similarly increased IEX-1 expression at both the mRNA level (Figure 8(c, d)) and the protein level (Supplemental Figure 5A and B). Thereafter, we overexpressed IEX-1 in cultured cardiomyocytes, and phosphor-PKCε was increased in cells receiving Ad-IEX-1 at both normal culture and post-H/R (Figure 8(e)). Furthermore, Western blot showed that IEX-1 overexpression increased the PKCε protein level in the mitochondrial fraction (Figure 8(f)). And PKCε inhibitor abolished the protective effect of IEX-1 on H/R-induced caspase-3 activation (Figure 8(g)).

4. Discussion

This study shows that IEX-1 is pivotal in IPC-induced cardioprotection against I/R-induced injury. We found that IPC, commonly used in coronary intervention and coronary artery bypass grafting [26, 27], could increase IEX-1

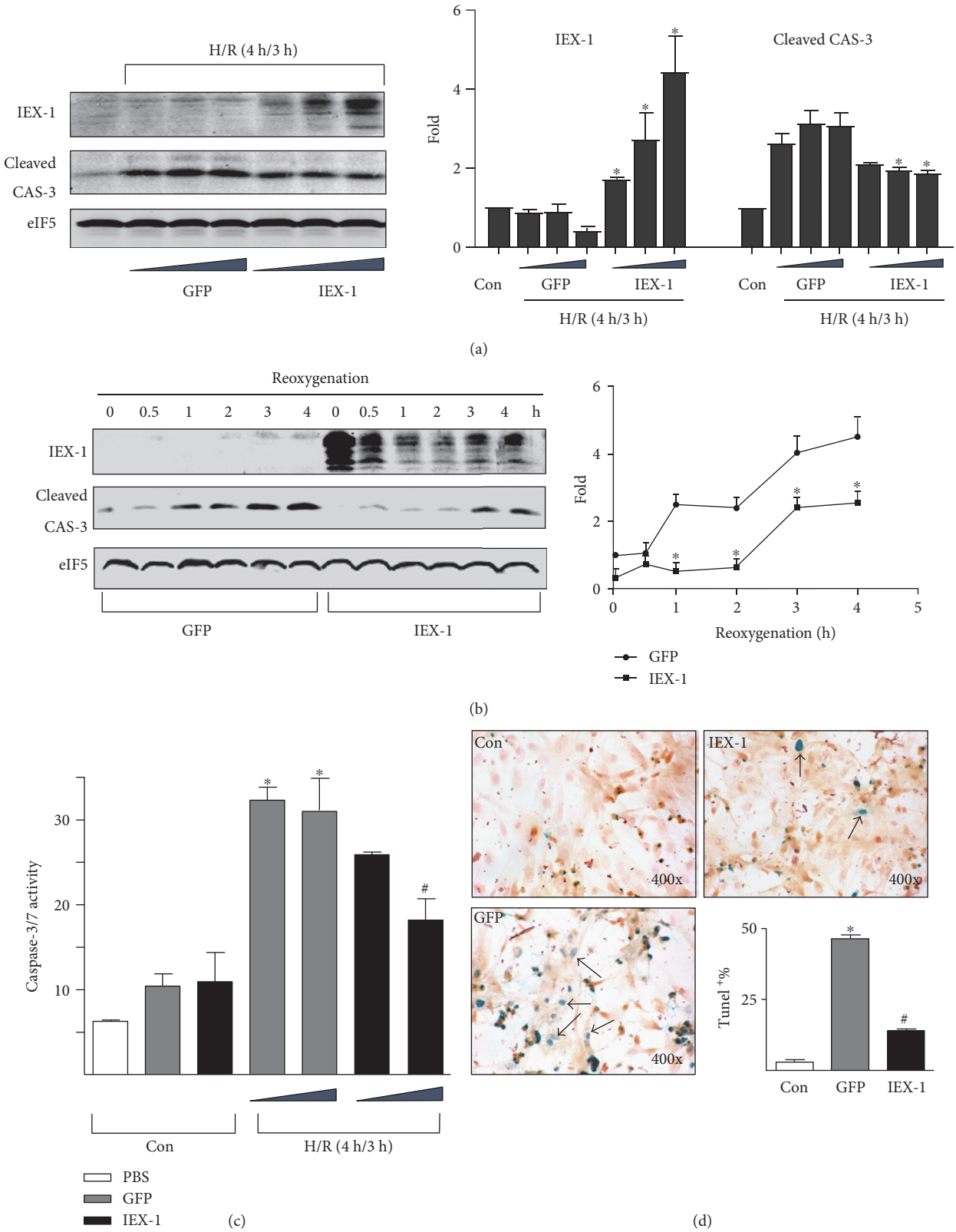

Figure 7: Continued.

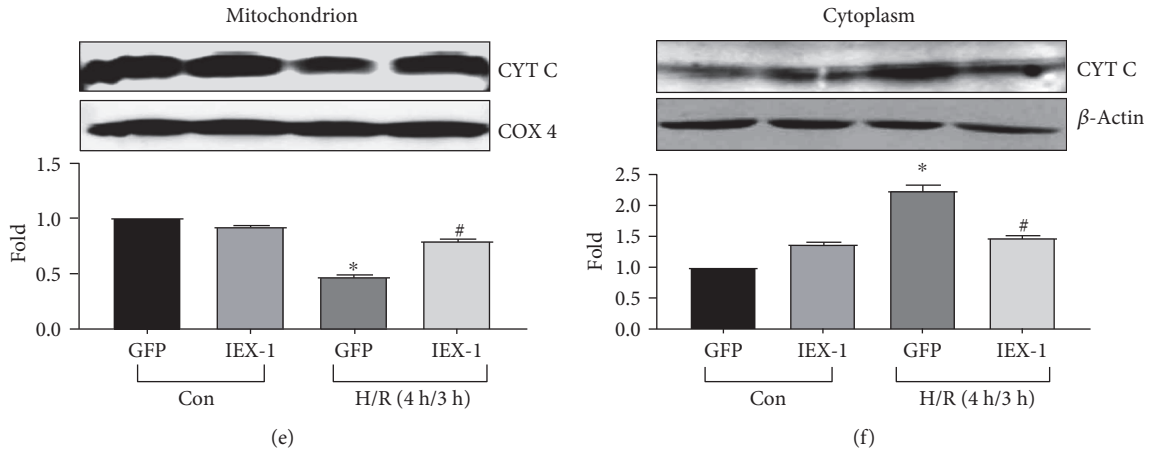

Figure 7: IEX-1 overexpression attenuated H/R-induced cardiomyocyte injury. (a) Cardiomyocytes were infected with Ad-GFP or Ad-IEX-1 (5, 10, and 20 MOI), then underwent H/R. Results are from one representative experiment of three. (b) Cardiomyocytes were infected with 10 MOI adenoviruses, then underwent hypoxia (4 h) and reoxygenation for the indicated time. (c) Cardiomyocytes together with the medium were collected after H/R, total caspase-3/7 activity was detected. Triangle represents adenovirus infection of 5 and 10 MOI. (d) Cardiomyocytes underwent H/R, and TUNEL staining was performed to assess cell apoptosis. Arrows show TUNEL-positive cells, and the ratio of TUNEL-positive cells was calculated. Results are from one representative experiment of four. (e) Mitochondrial and (f) cytoplasmic fractions were isolated from cardiomyocytes, and proteins were probed with an anti-cytochrome c antibody. eIF5, COX4, or β-actin expression was a control for protein loading. Each column represents results from at least 3 independent experiments. $^{*}P < 0.05$ versus control (Con or corresponding time points), $^{\#}P < 0.05$ versus the corresponding GFP group.

expression in ischemic hearts in vivo. When IEX-1 expression was inhibited by siRNA, the protective effects imposed by IPC were lessened. Using gain-of-function approaches, we demonstrated that hearts with exogenously expressed IEX-1 enhanced their tolerance to I/R. In the complementary experiments, siRNA knocking down the endogenous IEX-1 exacerbated the cardiac injury. The molecular basis underlying such a protective effect involves, but not limits to, the promotion of PKCε phosphorylation and attenuation of H/R-induced ROS accumulation and cell death.

Reversible myocardial I/R during human cardiac surgery or mouse IPC is associated with an immediate genomic response [28, 29]. IPC induces the expression of proto-oncogenes or immediate early genes such as *c-Fos*, *c-Myc*, *c-Jun*, and *Egr-1* in isolated rat hearts, which is associated with improved ventricular function and reduced infarct size [7–9]. Our results show that *Iex-1* mRNA was rapidly induced by IPC, suggesting that increased IEX-1 expression would contribute to the protective effects of IPC. The thesis was supported by the fact that siRNA knocking down the endogenous IEX-1 exacerbated the cardiac injury and abolished the protective effects induced by IPC, while overexpressing IEX-1 exhibited similar protective effects to IPC. The antiapoptotic effect of IEX-1 on the cardiomyocyte is in line with several previous studies. IEX-1-transgenic mice showed reduced T-cell apoptosis triggered by FAS ligation or T-cell receptor/CD3 complex [30]. IEX-1 overexpression considerably decreased the p73β-mediated and staurosporin-induced CHO cell death [12, 16]. However, IEX-1 has also been shown to increase the rate of apoptosis in CHO cells, HaCaT keratinocytes [15], Hela cells [13], or HEK293 cells [14]. The distinct role of IEX-1 in terms of pro- or antiapoptosis may thus depend on cell types, expression level, and kinds of stimulus. Through transcription factors such as NF-κB/REL complexes, p53, SP1, C-MYC, and AP-1, IEX-1 can be induced in a wide variety of cell types by irradiation, viral infection, inflammatory cytokines, chemical carcinogens, growth factors, and hormones (reviewed in 16), and C-MYC, NF-κB, and AP-1 are IPC responsive [31]; these transcriptional factors are likely to be involved in the immediate induction of IEX-1 by IPC.

Ample evidence implicates that mitochondrion-originated ROS, NADH-dependent microsomes, and NOS are very likely to constitute in the initial injury in cardiomyocytes at the end of ischemia and during reperfusion [25, 32–35]. ROS that resulted from stress can cause lipid peroxidation, protein oxidization, and DNA strand breaks, which affect normal cardiac functions. Although ROS is generated during hypoxia [36], a robust burst of ROS occurs after reoxygenation [37]. In the heart, mitochondria are probably the principal source of ROS after reoxygenation and/or reperfusion [25]. The increased ROS in turn is a primary stimulus for MPTP opening, leading to an impaired mitochondrial membrane [38, 39]. Indeed, opening MPTP, releasing cytochrome c from mitochondria, and activating caspase cascade may be a series of events that induce irreversible injury during reperfusion [39–41]. IEX-1 overexpression reduced ROS accumulation, evidenced by decreased luminal-derived chemiluminescence, DCF fluorescence, and Red CM-H2XRos fluorescence, and limited cytochrome c leakage from mitochondria to cytoplasm. Thus, IEX-1 may be involved in maintaining mitochondrial membrane integrity and preventing the mitochondrial death pathway through inhibiting mitochondrial ROS production.

Mitochondria mediate diverse cellular functions including energy generation and ROS production and contribute

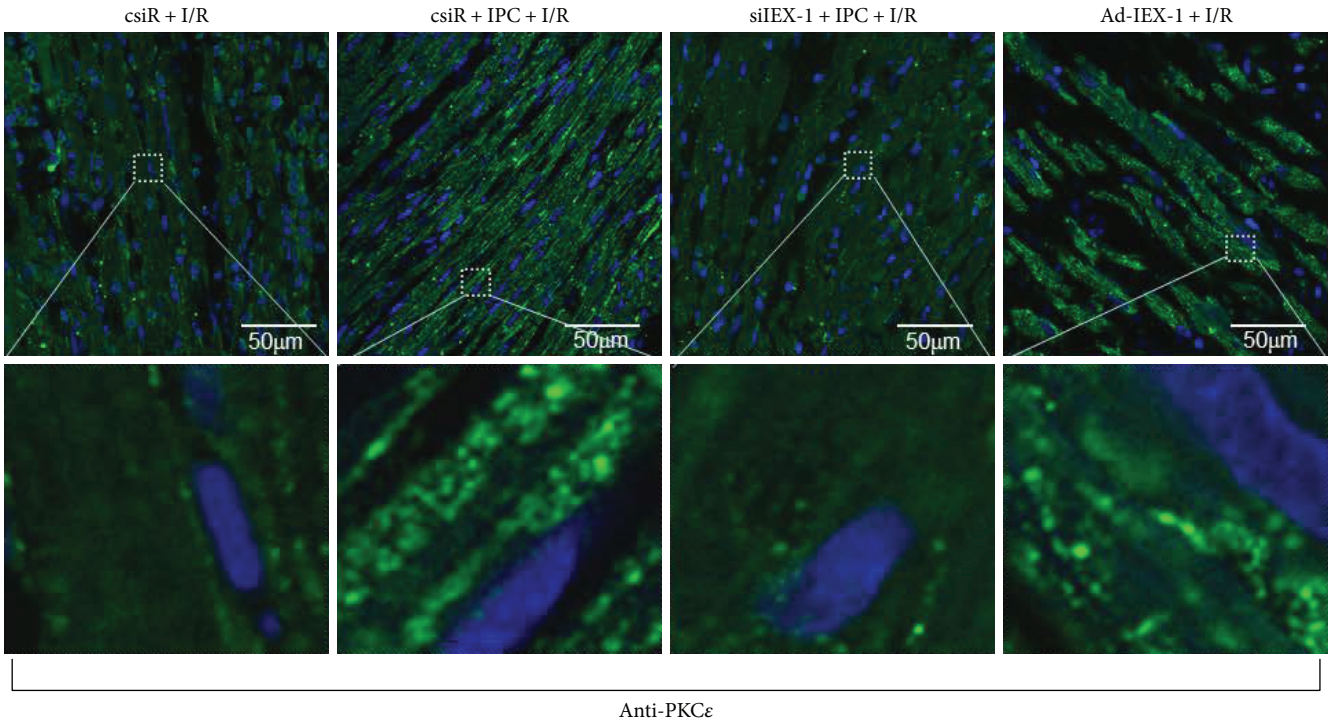

(a)

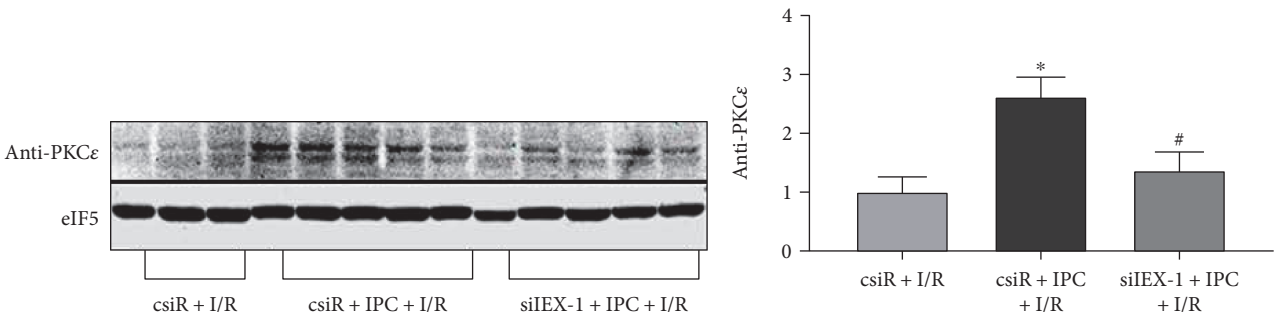

(b)

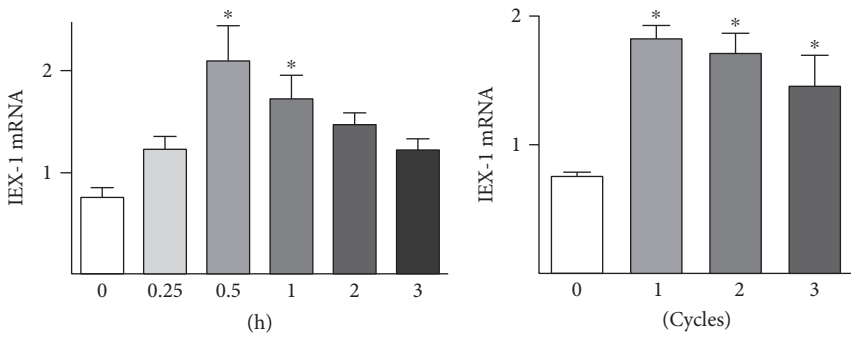

(c) (d)

Figure 8: Continued.

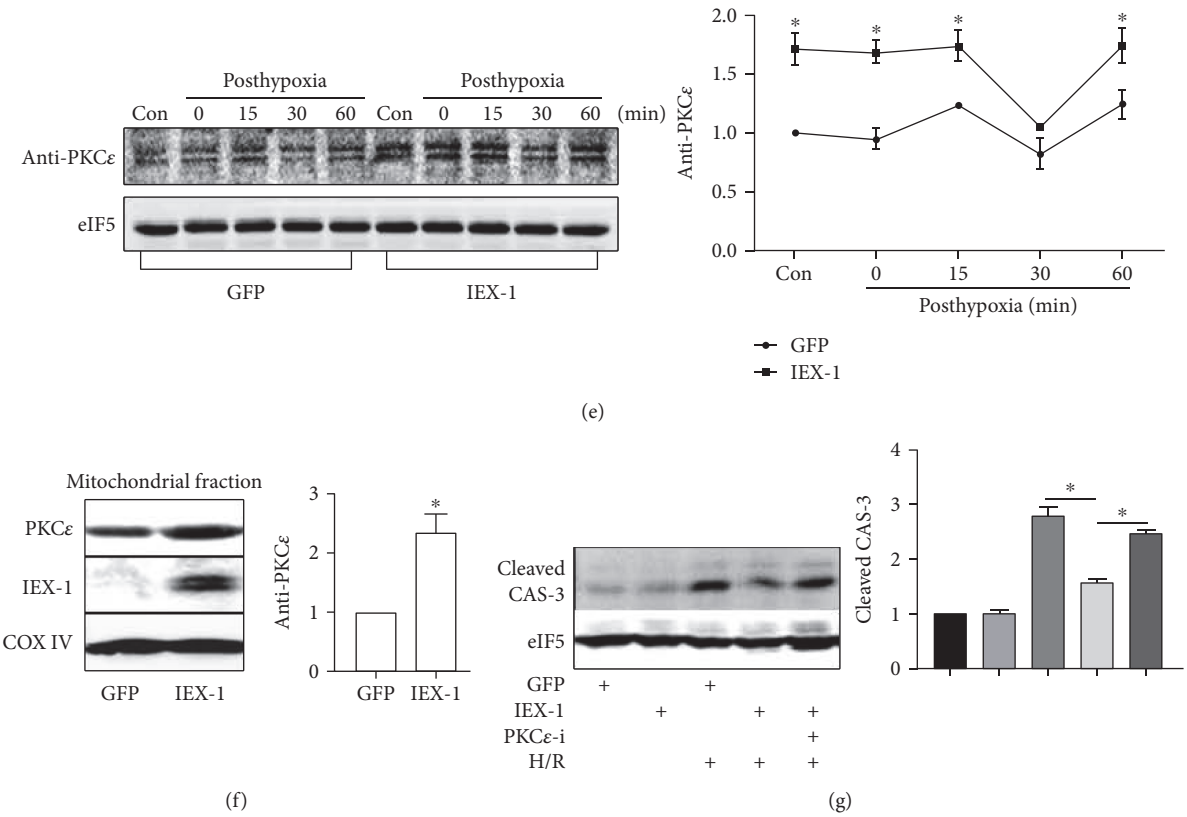

Figure 8: IEX-1 promotes PKCε phosphorylation. (a) Rat hearts were locally delivered with siRNA or Ad-IEX-1, then underwent I/R (30 min/24 h) or IPC prior to I/R as indicated. Particle location of PKCε was identified by immunofluorescence assay with confocal microscopy; (b) the same heart samples were homogenated for Western blot analysis of phosphor-PKCε. (c) Time course of IEX-1 mRNA expression in neonatal rat cardiomyocytes after hypoxia preconditioning (HPC, 1 cycle of short H/R, 10 min each). (d) Effect of increasing HPC cycles on IEX-1 mRNA expression. (e) Neonatal rat cardiomyocytes were infected with adenovirus at 10 MOI for 36 h, then underwent hypoxia (4 h) and reoxygenation for the indicated time. Phosphor-PKCε were detected. (f) Cardiomyocytes were overexpressed with GFP or IEX-1. Mitochondrial particles were isolated and lysed for Western blot. (g) Cardiomyocytes were overexpressed with GFP or IEX-1 or treated with PKCε inhibitor (PKCεV1–2, 20 μM) and then subjected to H/R. $^{*}P < 0.05$ versus the csiR or 0 group or corresponding time points, $^{\#}P < 0.05$ versus csiR + IPC + I/R.

to signal transduction. Mitochondria are also key regulators of cell viability and play a central role in necrotic and apoptotic cell death pathways induced by cardiac I/R injury. PKCε plays a critical role in cardioprotective signaling pathways that protect the heart from I/R [42]. Emerging evidence suggests that the cardioprotective target of PKCε resides at the mitochondria, including mitoK$_{ATP}$ (mitochondrial ATP-sensitive K^{+} channel) [43], components of the MPTP [44], and components of the electron transport chain [45], and phosphorylation and mitochondrial translocation of PKCε are required for cardioprotection [46]. It has been reported that cytoplasm location, including mitochondrial location, of IEX-1 is critical for its antiapoptotic and antioxidant effects [12]. In the present study, we found that IEX-1 and PKCε colocalized in mitochondrion; IEX-1 expression is necessary for IPC-induced phosphorylation of PKCε both in vivo and in vitro and promotes mitochondrial translocation of PKCε. Because activating PKCε is critical for IPC-induced cardioprotection against I/R, promoting PKCε activation may be the main mechanism for IEX-1-mediating IPC-induced cardioprotection, as PKCε inhibitor blocked the protective effect of IEX-1. However, the mechanisms for IEX-1-promoting PKCε phosphorylation and mitochondrial translocation remain to be elucidated. Of note, the interaction of IEX-1 with PP2A is the central role for IEX-1-modulating ERK and AKT activity [18, 19], which may also be the mechanism for IEX-1-promoting PKCε activity. On the other side, the potential effects of IEX-1 on ERK and AKT activity may also contribute to the cardioprotection, as the AKT-ERK-NO pathway is another important mechanism for IPC-induced cardioprotection [47].

In summary, we demonstrate that IEX-1 is critical in preventing oxidative stress-induced cardiac injury and mediates IPC-induced cardioprotection in rats. In addition to this newly found antioxidative effect, IEX-1 also exhibits inhibitory effects on hypertension, neointima formation, and cardiac hypertrophy [48–50]. Thereby, IEX-1 would be a cardioprotective gene. The identification of an early response gene involved in I/R-induced heart insult may reveal a new therapeutic strategy to explore targets for ischemic heart diseases.

Conflicts of Interest

The authors declare that they have no conflicts of interest.

Acknowledgments

The authors thank Professors Youyi Zhang and Heping Cheng from Peking University for their advice. This study was supported by the Major National Basic Research Program of China (no. 2006CB503802), the National Natural Science Foundation of China (no. 30821001, no. 30500198 to Wenjing Li, and no. 81470557 to Ming-Jiang Xu) and a "111" grant of the Ministry of Education awarded to Xian Wang, and the National Heart, Lung, and Blood Institute (HL77448, HL88940 to John Y.-J. Shyy).

References

[1] E. Braunwald and R. A. Kloner, "Myocardial reperfusion: a double-edged sword?," *The Journal of Clinical Investigation*, vol. 76, no. 5, pp. 1713–1719, 1985.

[2] J. Vinten-Johansen, "Reperfusion injury: idle curiosity or therapeutic vector?," *Journal of Thrombosis and Thrombolysis*, vol. 4, no. 1, pp. 59–61, 1997.

[3] A. P. Halestrap, S. J. Clarke, and I. Khaliulin, "The role of mitochondria in protection of the heart by preconditioning," *Biochimica et Biophysica Acta (BBA) - Bioenergetics*, vol. 1767, no. 8, pp. 1007–1031, 2007.

[4] A. Skyschally, R. Schulz, and G. Heusch, "Pathophysiology of myocardial infarction: protection by ischemic pre- and post-conditioning," *Herz*, vol. 33, no. 2, pp. 88–100, 2008.

[5] K. Inagaki, E. Churchill, and D. Mochly-Rosen, "Epsilon protein kinase C as a potential therapeutic target for the ischemic heart," *Cardiovascular Research*, vol. 70, no. 2, pp. 222–230, 2006.

[6] D. K. Das and N. Maulik, "Preconditioning potentiates redox signaling and converts death signal into survival signal," *Archives of Biochemistry and Biophysics*, vol. 420, no. 2, pp. 305–311, 2003.

[7] H. Aebert, T. Cornelius, T. Ehr et al., "Expression of immediate early genes after cardioplegic arrest and reperfusion," *The Annals of Thoracic Surgery*, vol. 63, no. 6, pp. 1669–1675, 1997.

[8] D. K. Das, R. M. Engelman, and Y. Kimura, "Molecular adaptation of cellular defences following preconditioning of the heart by repeated ischaemia," *Cardiovascular Research*, vol. 27, no. 4, pp. 578–584, 1993.

[9] R. Zimmermann, J. Andres, T. Brand et al., "Cardiac gene expression after brief coronary occlusion," *Zeitschrift für Kardiologie*, vol. 84, Supplement 4, pp. 159–165, 1995.

[10] M. X. Wu, "Roles of the stress-induced gene IEX-1 in regulation of cell death and oncogenesis," *Apoptosis*, vol. 8, no. 1, pp. 11–18, 2003.

[11] J. Garcia, Y. Ye, V. Arranz, C. Letourneux, G. Pezeron, and F. Porteu, "IEX-1: a new ERK substrate involved in both ERK survival activity and ERK activation," *The EMBO Journal*, vol. 21, no. 19, pp. 5151–5163, 2002.

[12] L. Shen, J. Guo, C. Santos-Berrios, and M. X. Wu, "Distinct domains for anti- and pro-apoptotic activities of IEX-1," *The Journal of Biological Chemistry*, vol. 281, no. 22, pp. 15304–15311, 2006.

[13] A. Arlt, O. Grobe, A. Sieke et al., "Expression of the NF-κB target gene IEX-1 (p22/PRG1) does not prevent cell death but instead triggers apoptosis in Hela cells," *Oncogene*, vol. 20, no. 1, pp. 69–76, 2001.

[14] O. Grobe, A. Arlt, H. Ungefroren et al., "Functional disruption of IEX-1 expression by concatemeric hammerhead ribozymes alters growth properties of 293 cells," *FEBS Letters*, vol. 494, no. 3, pp. 196–200, 2001.

[15] D. Schilling, M. R. Pittelkow, and R. Kumar, "IEX-1, an immediate early gene, increases the rate of apoptosis in keratinocytes," *Oncogene*, vol. 20, no. 55, pp. 7992–7997, 2001.

[16] S. Gonzalez, M. M. Perez-Perez, E. Hernando, M. Serrano, and C. Cordon-Cardo, "p73β-Mediated apoptosis requires $p57^{kip2}$ induction and IEX-1 inhibition," *Cancer Research*, vol. 65, no. 6, pp. 2186–2192, 2005.

[17] Q. Zhou, J. K. Hahn, B. Neupane et al., "Dysregulated IER3 expression is associated with enhanced apoptosis in titin-based dilated cardiomyopathy," *International Journal of Molecular Sciences*, vol. 18, no. 4, 2017.

[18] C. Letourneux, G. Rocher, and F. Porteu, "B56-containing PP2A dephosphorylate ERK and their activity is controlled by the early gene IEX-1 and ERK," *The EMBO Journal*, vol. 25, no. 4, pp. 727–738, 2006.

[19] G. Rocher, C. Letourneux, P. Lenormand, and F. Porteu, "Inhibition of B56-containing protein phosphatase 2As by the early response gene IEX-1 leads to control of Akt activity," *The Journal of Biological Chemistry*, vol. 282, no. 8, pp. 5468–5477, 2007.

[20] Y. H. Zhu, T. M. Ma, and X. Wang, "Gene transfer of heat-shock protein 20 protects against ischemia/reperfusion injury in rat hearts," *Acta Pharmacologica Sinica*, vol. 26, no. 10, pp. 1193–1200, 2005.

[21] V. Jayasankar, Y. J. Woo, L. T. Bish et al., "Inhibition of matrix metalloproteinase activity by TIMP-1 gene transfer effectively treats ischemic cardiomyopathy," *Circulation*, vol. 110, no. 11, Supplement 1, pp. II180–II186, 2004.

[22] R. D. Rakhit, M. H. Mojet, M. S. Marber, and M. R. Duchen, "Mitochondria as targets for nitric oxide-induced protection during simulated ischemia and reoxygenation in isolated neonatal cardiomyocytes," *Circulation*, vol. 103, no. 21, pp. 2617–2623, 2001.

[23] H. P. Grill, J. L. Zweier, P. Kuppusamy, M. L. Weisfeldt, and J. T. Flaherty, "Direct measurement of myocardial free radical generation in an in vivo model: effects of postischemic reperfusion and treatment with human recombinant superoxide dismutase," *Journal of the American College of Cardiology*, vol. 20, no. 7, pp. 1604–1611, 1992.

[24] D. J. Hearse, "Reperfusion-induced injury: a possible role for oxidant stress and its manipulation," *Cardiovascular Drugs and Therapy*, vol. 5, Supplement 2, pp. 225–235, 1991.

[25] G. Ambrosio, J. L. Zweier, C. Duilio et al.et al., "Evidence that mitochondrial respiration is a source of potentially toxic oxygen free radicals in intact rabbit hearts subjected to ischemia and reflow," *The Journal of Biological Chemistry*, vol. 268, no. 25, pp. 18532–18541, 1993.

[26] D. P. Jenkins, W. B. Pugsley, A. M. Alkhulaifi, M. Kemp, J. Hooper, and D. M. Yellon, "Ischaemic preconditioning reduces troponin T release in patients undergoing coronary artery bypass surgery," *Heart*, vol. 77, no. 4, pp. 314–318, 1997.

[27] M. S. Marber, D. S. Latchman, J. M. Walker, and D. M. Yellon, "Cardiac stress protein elevation 24 hours after brief ischemia or heat stress is associated with resistance to myocardial infarction," *Circulation*, vol. 88, no. 3, pp. 1264–1272, 1993.

[28] S. Arab, I. E. Konstantinov, C. Boscarino et al., "Early gene expression profiles during intraoperative myocardial ischemia-reperfusion in cardiac surgery," *The Journal of Thoracic and Cardiovascular Surgery*, vol. 134, no. 1, pp. 74–81, 2007, 81 e1-2.

[29] I. E. Konstantinov, S. Arab, J. Li et al., "The remote ischemic preconditioning stimulus modifies gene expression in mouse myocardium," *The Journal of Thoracic and Cardiovascular Surgery*, vol. 130, no. 5, pp. 1326–1332, 2005.

[30] Y. Zhang, S. F. Schlossman, R. A. Edwards, C. N. Ou, J. Gu, and M. X. Wu, "Impaired apoptosis, extended duration of immune responses, and a lupus-like autoimmune disease in IEX-1-transgenic mice," *Proceedings of the National Academy of Sciences of the United States of America*, vol. 99, no. 2, pp. 878–883, 2002.

[31] G. Jancso, J. Lantos, B. Borsiczky, Z. Szanto, and E. Roth, "Dynamism of NF-κB and AP-1 activation in the signal transduction of ischaemic myocardial preconditioning," *European Surgical Research*, vol. 36, no. 3, pp. 129–135, 2004.

[32] R. Ferrari, C. Ceconi, S. Curello, O. Alfieri, and O. Visioli, "Myocardial damage during ischaemia and reperfusion," *European Heart Journal*, vol. 14, Supplement G, pp. 25–30, 1993.

[33] H. K. Mohazzab, P. M. Kaminski, and M. S. Wolin, "Lactate and PO_2 modulate superoxide anion production in bovine cardiac myocytes: potential role of NADH oxidase," *Circulation*, vol. 96, no. 2, pp. 614–620, 1997.

[34] Y. Xia, V. L. Dawson, T. M. Dawson, S. H. Snyder, and J. L. Zweier, "Nitric oxide synthase generates superoxide and nitric oxide in arginine-depleted cells leading to peroxynitrite-mediated cellular injury," *Proceedings of the National Academy of Sciences of the United States of America*, vol. 93, no. 13, pp. 6770–6774, 1996.

[35] G. Heusch, K. Boengler, and R. Schulz, "Cardioprotection: nitric oxide, protein kinases, and mitochondria," *Circulation*, vol. 118, no. 19, pp. 1915–1919, 2008.

[36] L. B. Becker, T. L. vanden Hoek, Z. H. Shao, C. Q. Li, and P. T. Schumacker, "Generation of superoxide in cardiomyocytes during ischemia before reperfusion," *The American Journal of Physiology*, vol. 277, no. 6, Part 2, pp. H2240–H2246, 1999.

[37] L. G. Kevin, A. K. Camara, M. L. Riess, E. Novalija, and D. F. Stowe, "Ischemic preconditioning alters real-time measure of O_2 radicals in intact hearts with ischemia and reperfusion," *American Journal of Physiology-Heart and Circulatory Physiology*, vol. 284, no. 2, pp. H566–H574, 2003.

[38] A. P. Halestrap, S. J. Clarke, and S. A. Javadov, "Mitochondrial permeability transition pore opening during myocardial reperfusion—a target for cardioprotection," *Cardiovascular Research*, vol. 61, no. 3, pp. 372–385, 2004.

[39] D. J. Hausenloy, H. L. Maddock, G. F. Baxter, and D. M. Yellon, "Inhibiting mitochondrial permeability transition pore opening: a new paradigm for myocardial preconditioning?," *Cardiovascular Research*, vol. 55, no. 3, pp. 534–543, 2002.

[40] M. Juhaszova, D. B. Zorov, S. H. Kim et al., "Glycogen synthase kinase-3β mediates convergence of protection signaling to inhibit the mitochondrial permeability transition pore," *The Journal of Clinical Investigation*, vol. 113, no. 11, pp. 1535–1549, 2004.

[41] J. N. Weiss, P. Korge, H. M. Honda, and P. Ping, "Role of the mitochondrial permeability transition in myocardial disease," *Circulation Research*, vol. 93, no. 4, pp. 292–301, 2003.

[42] G. R. Budas and D. Mochly-Rosen, "Mitochondrial protein kinase Cε (PKCε): emerging role in cardiac protection from ischaemic damage," *Biochemical Society Transactions*, vol. 35, Part 5, pp. 1052–1054, 2007.

[43] M. Jaburek, A. D. Costa, J. R. Burton, C. L. Costa, and K. D. Garlid, "Mitochondrial PKCε and mitochondrial ATP-sensitive K^+ channel copurify and coreconstitute to form a functioning signaling module in proteoliposomes," *Circulation Research*, vol. 99, no. 8, pp. 878–883, 2006.

[44] C. P. Baines, C. X. Song, Y. T. Zheng et al., "Protein kinase Cε interacts with and inhibits the permeability transition pore in cardiac mitochondria," *Circulation Research*, vol. 92, no. 8, pp. 873–880, 2003.

[45] M. Ogbi and J. A. Johnson, "Protein kinase Cε interacts with cytochrome c oxidase subunit IV and enhances cytochrome c oxidase activity in neonatal cardiac myocyte preconditioning," *The Biochemical Journal*, vol. 393, Part 1, pp. 191–199, 2006.

[46] Y. Ohnuma, T. Miura, T. Miki et al., "Opening of mitochondrial K_{ATP} channel occurs downstream of PKC-ε activation in the mechanism of preconditioning," *American Journal of Physiology-Heart and Circulatory Physiology*, vol. 283, no. 1, pp. H440–H447, 2002.

[47] M. V. Cohen and J. M. Downey, "Signalling pathways and mechanisms of protection in pre- and postconditioning: historical perspective and lessons for the future," *British Journal of Pharmacology*, vol. 172, no. 8, pp. 1913–1932, 2015.

[48] G. W. De Keulenaer, Y. Wang, Y. Feng et al., "Identification of IEX-1 as a biomechanically controlled nuclear factor-κB target gene that inhibits cardiomyocyte hypertrophy," *Circulation Research*, vol. 90, no. 6, pp. 690–696, 2002.

[49] P. C. Schulze, G. W. de Keulenaer, K. A. Kassik et al., "Biomechanically induced gene iex-1 inhibits vascular smooth muscle cell proliferation and neointima formation," *Circulation Research*, vol. 93, no. 12, pp. 1210–1217, 2003.

[50] S. L. Sommer, T. J. Berndt, E. Frank et al., "Elevated blood pressure and cardiac hypertrophy after ablation of the gly96/IEX-1 gene," *Journal of Applied Physiology*, vol. 100, no. 2, pp. 707–716, 2006.

Hindawi
Oxidative Medicine and Cellular Longevity
Volume 2017, Article ID 1401790, 9 pages
https://doi.org/10.1155/2017/1401790

Research Article

Baicalin Attenuates Subarachnoid Hemorrhagic Brain Injury by Modulating Blood-Brain Barrier Disruption, Inflammation, and Oxidative Damage in Mice

Xianqing Shi, Yongjian Fu, SongSong Zhang, Hao Ding, and Jin Chen

Intensive Care Unit, Guizhou Province People's Hospital, Guiyang, Guizhou Province 550002, China

Correspondence should be addressed to Xianqing Shi; shixianqing@126.com

Received 31 May 2017; Revised 23 June 2017; Accepted 3 July 2017; Published 24 August 2017

Academic Editor: Aditya Sen

In subarachnoid hemorrhagic brain injury, the early crucial events are edema formation due to inflammatory responses and blood-brain barrier disruption. Baicalin, a flavone glycoside, has antineuroinflammatory and antioxidant properties. We examined the effect of baicalin in subarachnoid hemorrhagic brain injury. Subarachnoid hemorrhage was induced through filament perforation and either baicalin or vehicle was administered 30 min prior to surgery. Brain tissues were collected 24 hours after surgery after evaluation of neurological scores. Brain tissues were processed for water content, real-time PCR, and immunoblot analyses. Baicalin improved neurological score and brain water content. Decreased levels of tight junction proteins (occludin, claudin-5, ZO-1, and collagen IV) required for blood-brain barrier function were restored to normal level by baicalin. Real-time PCR data demonstrated that baicalin attenuated increased proinflammatory cytokine (IL-1β, IL-6, and CXCL-3) production in subarachnoid hemorrhage mice. In addition to that, baicalin attenuated microglial cell secretion of IL-1β and IL-6 induced by lipopolysaccharide (100 ng/ml) dose dependently. Finally, baicalin attenuated induction of NOS-2 and NOX-2 in SAH mice at the mRNA and protein level. Thus, we demonstrated that baicalin inhibited microglial cell activation and reduced inflammation, oxidative damage, and brain edema.

1. Introduction

The outcome of hospital admission due to aneurysmal subarachnoid hemorrhage (SAH) is very poor [1]. The major reason for mortality is poor clinical grade during admission, age, aneurysm rebleeding, and vasospasm-associated cerebral infarction [2]. Most studies on SAH were addressed on vasospasm due to the fact that it can significantly hinder blood flow, which correlates with ischemic brain as well as infarction [3]. Prevention of such mortality and development of new therapies depend on understanding the molecular events after SAH. SAH-associated brain injury is a complex process involving inflammation, brain edema, microglial cell activation, oxidative damage, and blood-brain barrier disruption [4]. Each molecular event is crucial and thus can regulate the outcome of the brain injury.

The animal model for SAH is well established, and numerous studies are reported in mice [5]. Recently, few plant-derived natural active ingredients mediated protection in brain injury after SAH has been reported [6–8]. Traditional Chinese medicines have been used for the treatment of various types of diseases for over thousands of years. One of the active ingredients in traditional Chinese medicine, baicalin, is widely used for inflammatory diseases including brain inflammation [9–11]. Pharmacokinetics studies show that baicalin is quickly absorbed and has longer stability in the plasma for over 12 hours [12, 13], thus emerging as a multitherapeutic agent [14].

In this study, we demonstrated baicalin attenuated brain injury after SAH in multistep mechanisms including microglial cell activation, inflammation, modulation of blood-brain barrier function, and oxidative damage.

2. Method

2.1. Animal Ethical Approval. This study received permission from the Animal Care and Research Committee of Guizhou Province People's Hospital. Adult male C57BL/6 mice (25–30 g) were provided by the animal center of Guizhou Medical University (approval number SCXK (Guizhou) 2002-0001, Guiyang, China).

2.2. Animal Surgery Model. We performed the SAH model in mice as described earlier [15]. We observed 31% mortality consistent with published method [15]. Baicalin was administered 15 minutes after surgical procedure at a dose of 100 mg/kg intraperitoneally (i.p.). Sham-operated mice administered with either vehicle (described as control throughout the study) or baicalin at a dose of 100 mg/kg intraperitoneally (i.p.) underwent the same procedure but were not subjected to perforation.

2.3. SAH Grade Assessment. SAH grade by bleeding scale in filament perforation subarachnoid hemorrhage was performed according to a previously described 18-point-score method [16]. In brief, the basal cistern was divided into 6 segments and the subarachnoid blood clots are assessed in each of these segments to allot a score from 0 to 3.

2.4. Neurologic Score. Neurologic score was determined as described previously [17]. This is an 18-point Garcia scale and a 4-point balance beam test with slight modification. Six tests, namely, spontaneous activity, spontaneous movement of four limbs, forepaw stretching, climbing, proprioception, response to whisker stimulation (score 3–18), and adding balance beam test (score 0–4). All experiments were performed by two blinded researchers.

2.5. Tissue Collection and Brain Water Content (Brain Edema). The animals were sacrificed under deep anesthesia (5% isoflurane), and brains were sectioned as brain stem, left and right hemisphere, and cerebellum. The tissues were weighed under wet condition followed by reweighing after drying at 105°C for 24 hours. The percentage of water content was calculated as $([\text{wet weight} - \text{dry weight}] / \text{wet weight}) \times 100\%$ as described earlier [18].

2.6. Quantitative Real-Time PCR. Total RNA was extracted from whole brain tissue (left and right hemisphere) according to the manufacturer's protocol (Qiagen RNeasy Mini Kit, Qiagen, Hilden, Germany). Total RNA was reverse transcribed into cDNA by Qiagen Reverse Transcription Kit (Qiagen, Hilden, Germany). Real-time PCR was carried out using 7500 Real-Time PCR system (Applied Biosystems) with 200 pM PCR primers. Each sample was analyzed using SYBR green (Applied Biosystems) as fluorescent detector and actin as endogenous control. All primers were obtained from RT qPCR Primer assay kits (SAB Bioscience). The data were analyzed and expressed as fold using comparative Ct method.

2.7. Immunoblot. Proteins from perforation side tissue samples were isolated by lysing in RIPA buffer with protease inhibitor cocktail (Roche). The proteins were quantified with bicinchoninic acid protein assay kit (Beyotime Biotech, China). Equal amount of proteins were loaded onto gradient PAGE, transferred into nitrocellulose membrane. After blocking with 10% nonfat milk in PBS-Tween20, membranes were incubated with antibodies IBA1, GAPDH, p65, histone H3, NOS2, and NOX2 (Abcam China, Shanghai, China). After repeated washing, the membrane was incubated with corresponding secondary antibodies (Beyotime, Shanghai, China) followed by chemiluminescence detection.

2.8. Microglia Cell Isolation and Cell Culture. Microglial cells from heathy adult mouse were isolated as described before [19]. Cells were plated onto cell culture flasks in Dulbecco's modified Eagle's medium/Ham's F-12 (DMEM/F12, Life Technologies) with 10% fetal bovine serum (FBS, Life Technologies). Lipopolysaccharide at 100 ng/ml was added for 24 hours, and culture supernatant were quantified for IL1β and IL6 cytokine using Quantikine ELISA kit (R&D System, USA). The cell pellet was processed with N-PER nuclear extraction kit for Western blot experiments.

2.9. Statistics. All values are expressed as the mean standard derivation. One-way analysis of variance followed by Tukey's multiple comparisons test was used for comparisons between two groups, and c2 tests were used for behavior score analyses. A minimum p value < 0.05 was considered statistically significant.

3. Results

3.1. Baicalin Improved Neurological Score and Brain Edema in SAH Mice. Neurological score was determined 24 hours after SAH surgery. There was no significant difference in SAH grade between SAH with vehicle or baicalin treatment group (Figure 1(a)). However, neurological scores were significantly lower in SAH groups compared to control or baicalin-treated sham-operated mice. Baicalin-treated mice improved in neurological score compared to vehicle-treated SAH mice, and it was statistically significant ($p = 0.004$) (Figure 1(b)). Brain edema as determined by brain water content was examined. As reported previously, SAH significantly increased water content in both left and right hemispheres. Baicalin treatment reduced brain water content in both hemispheres in a statistically significant manner ($p = 0.025$ for the left and $p = 0.043$ for the right) (Figure 1(c)).

3.2. Baicalin Attenuated Increased Blood-Brain Barrier (BBB) Permeability and Tight Junction Protein Degradation in SAH Mice. Blood-brain barrier (BBB) function is critical as SAH increases its permeability [20]. We used Evans blue extravasation assays to determine BBB permeability. SAH induced permeability. Baicalin treatment restored BBB function to normal level (Figure 2(a)). The effect was significant in the right hemisphere ($p < 0.05$), whereas a similar trend was observed in the left hemisphere. Tight junction transmembrane proteins such as occludin and claudin along with ZO-1 proteins have a crucial role in maintaining blood brain barrier function [21]. These proteins were degraded in SAH and thus contribute to permeability increase. We observed a decrease in protein level of occludin, claudin-5,

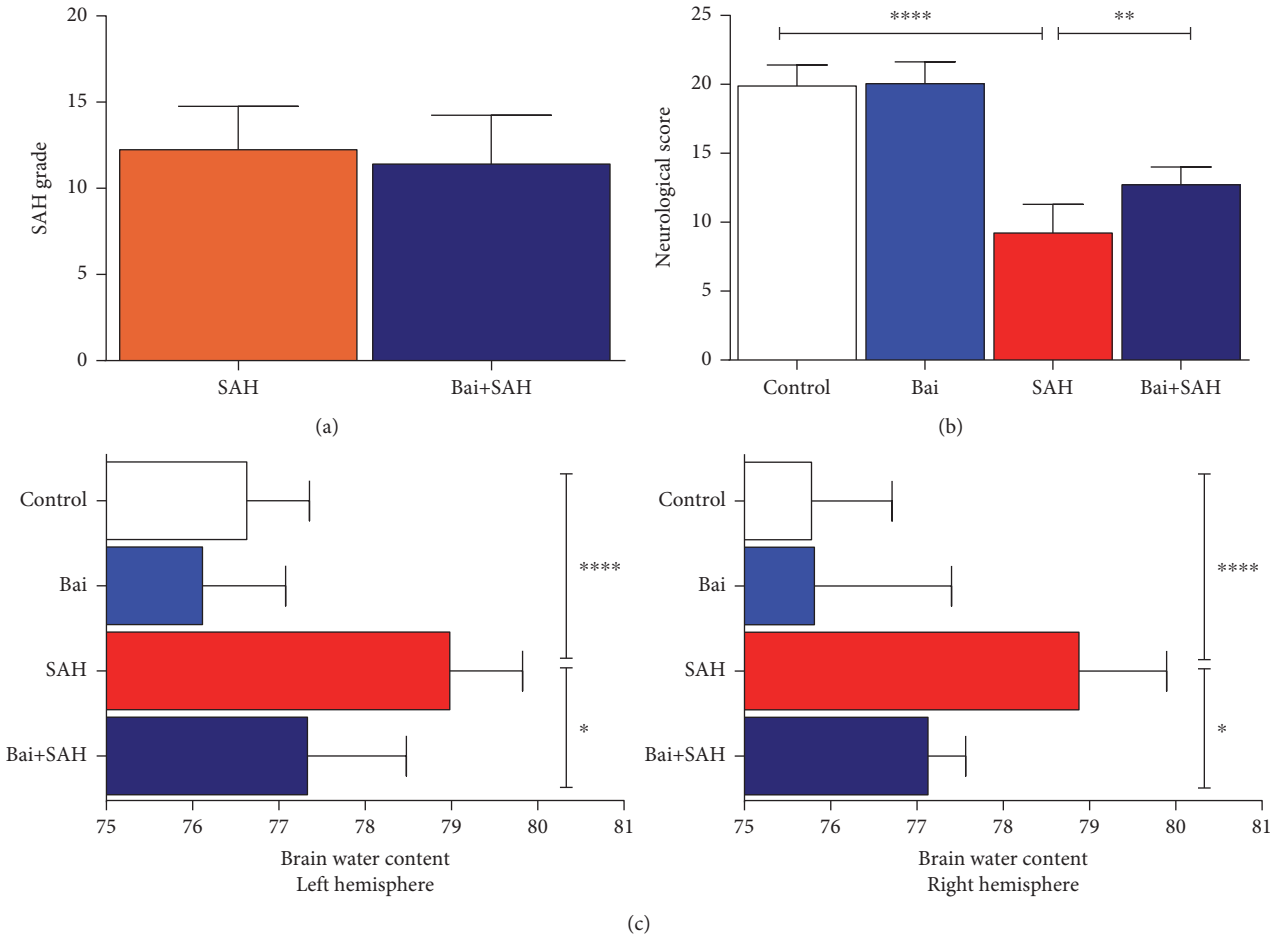

Figure 1: Neurological score and brain edema 24 hours after SAH. (a) SAH grading scores in SAH with either vehicle or baicalin posttreatment groups. (b) Neurological score for each group 24 hours after SAH. Values are mean ± standard deviation. $N = 6$ in each group, $****$ represents $p < 0.0001$, and $**$ represents $p < 0.005$. (c) Effect of baicalin on brain water content in the left and right hemispheres 24 hours after SAH. $N = 6$ in each group, $****$ represents $p < 0.0001$, and $*$ represents $p < 0.05$.

ZO-1, and collagen IV by SAH. Baicalin treatment restored the protein levels close to normal (Figure 2(b)).

3.3. Baicalin Attenuated Production of Inflammatory Cytokines and Inflammation in SAH Mice. Release of cytokines particularly IL-1β has a critical role in early brain injury of SAH mice [20]. We determined three cytokines, IL-1β, IL-10, and CXCL-3, by real-time PCR in total brain samples. All three cytokines were increased 24 hours after SAH. Baicalin treatment attenuated significantly IL-1β, IL-10, and CXCL-3 cytokine mRNA levels (Figure 3). To address further, we also examined the amount of inflammation using microglial cell marker IBA-1 by real-time PCR (Figure 4(a)) and immunoblotting (Figure 4(b)). Both data were consistent with an earlier finding that the increase of glial cell population (inflammatory response) occurred after SAH brain injury. Baicalin attenuated inflammatory response significantly.

3.4. Baicalin Attenuated Glial Cell Activation In Vitro. We investigated primary microglial cells for activation by LPS and protection by baicalin. Primary microglial cells were stimulated with LPS (100 ng/ml). Pretreatment with baicalin dose dependently inhibited secretion of proinflammatory cytokines IL-1β and IL-6 (Figure 5(a)). LPS induced nuclear localization of p65 NFκB in primary microglial cells and was attenuated by baicalin in a dose-dependent manner (Figure 5(b)).

3.5. Baicalin Attenuated Induction of NOS-2 and NOX-2 in SAH Mice. Glial cell activation is associated with NOS-2 (iNOS) and NOX-2 induction [22–24] in brain injury. These two enzymes in glial cell lead to oxidative damage in the brain [25]. In SAH mice, both NOS-2 and NOX-2 were induced and baicalin attenuated induction of both enzymes in a statistically significant level as evidenced by real-time PCR (Figure 6(a)). The mRNA data were further confirmed by immunoblot analyses (Figure 6(b)).

4. Discussions

Our evaluation on the effect of baicalin on SAH in mice demonstrated that baicalin reduced proinflammatory cytokine production and oxidative damage-causing sources. SAH is a subtype of stroke where the mortality is very high and the

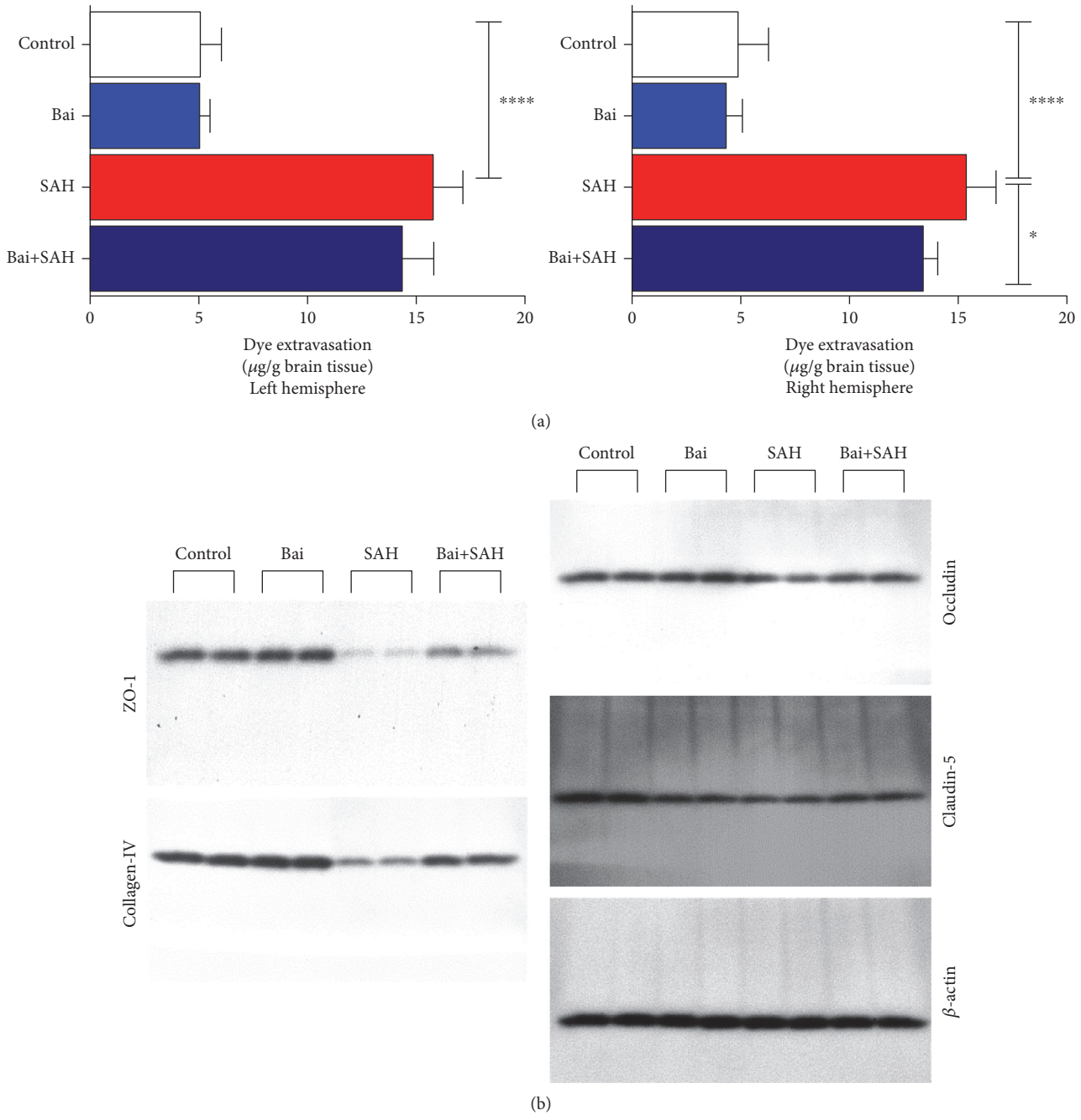

Figure 2: Effect of baicalin on BBB permeability and tight junction proteins in SAH mice. (a) Evans blue dye extravasation was observed in each set after SAH. The result demonstrated that BBB permeability was increased and attenuated by baicalin. Values are mean ± standard deviation. $N = 6$ in each group, $****$ represents $p < 0.0001$, and $*$ represents $p < 0.05$. (b) Western blot analyses of occludin, claudin-5, ZO-1, and collagen IV.

survivors also have difficultly in the long term. The first 72 hours is a critical time for all SAH patients. Most clinical cases are caused by rupture of intracranial aneurysms located in the brain arteries [26]. It is technically difficult to produce aneurysms to study in animal models, but a previously published method of filament perforation model for SAH in mice demonstrates in a standardized and reproducible manner [15]. We demonstrated by SAH grading that the data was reproducible among all samples. However, the posttreatment of baicalin did significantly affect neurological scores. It is recently reported that baicalin administration reduces infract volume in mouse cerebral ischemia model [27]. Thus, the effect of baicalin in brain injury is beneficial.

An increase in BBB permeability after SAH has been reported in patients and animal models [28]. The difference in BBB disruption of the intraparenchymal vessels after SAH may have possible pathophysiologic implications in relation to brain edema and microcirculatory disturbances

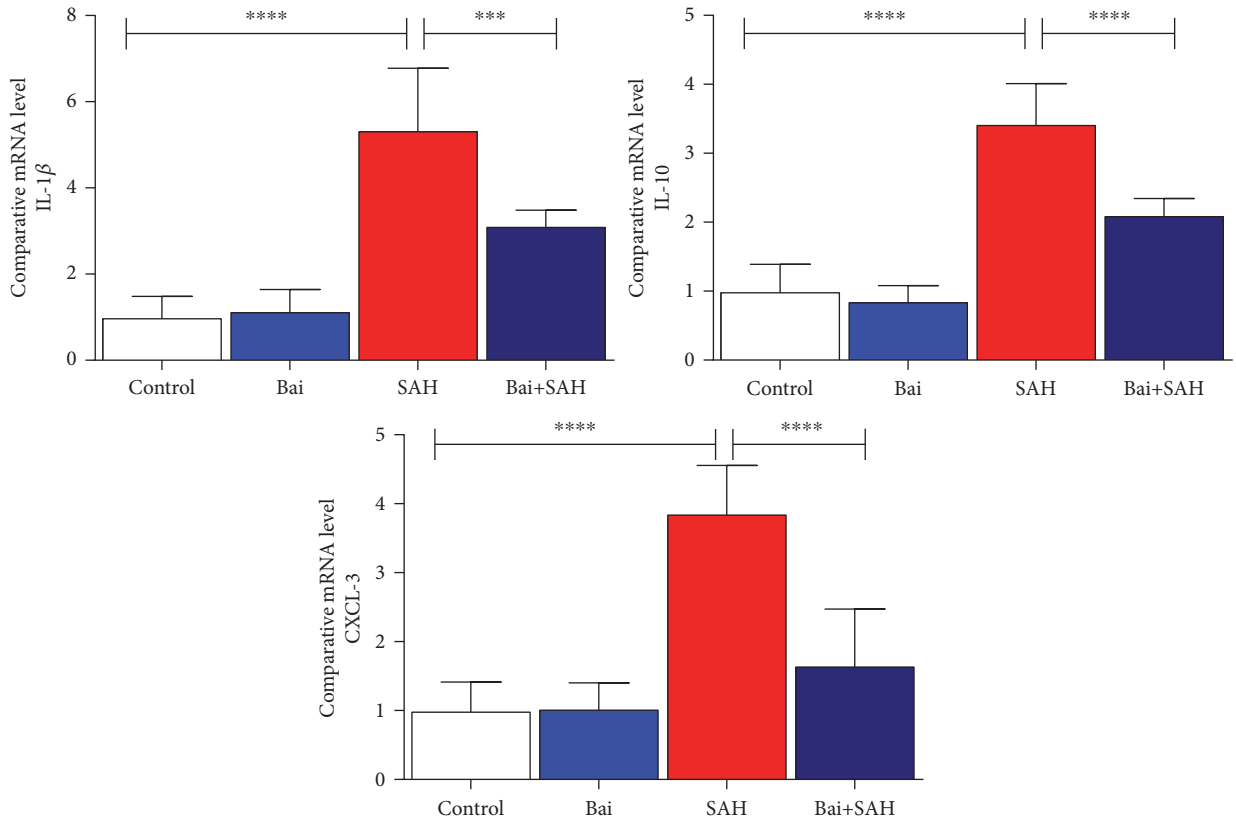

FIGURE 3: Effect of baicalin on proinflammatory cytokine mRNA expression in SAH mice. Real-time PCR analyses of IL-1β, IL-6, and CXCL-3. Values are mean ± standard deviation. $N = 6$ in each group, **** represents $p < 0.0001$, and *** represents $p < 0.0005$.

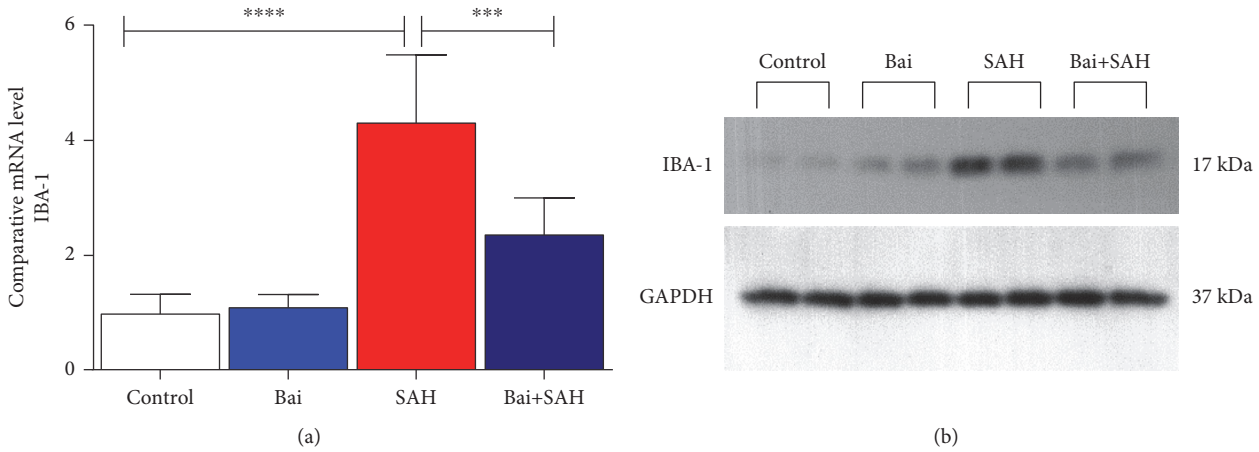

FIGURE 4: Effect of baicalin on glial cell activation marker IBA-1 expression in SAH mice. (a) Real-time PCR analyses of IBA-1. Values are mean ± standard deviation. $N = 6$ in each group, **** represents $p < 0.0001$, *** represents $p < 0.0005$. (b) Immunoblot analyses of IBA-1 along with loading control GAPDH.

occurring during the early clinical course of patients suffering with SAH [29]. Our data demonstrated that baicalin restored SAH-mediated BBB function significantly in the right hemisphere, and a similar trend was observed in the left hemisphere. This effect might be due to the fact that baicalin also modulated glial cell activation and their population difference in the two hemispheres.

Inflammation plays a critical role in brain injury after SAH [30]. The early release of inflammatory cytokines is also associated with brain edema [31]. In our study, we observed that baicalin attenuated proinflammatory cytokine production and also associated brain edema (Figure 7). Glial cells in microglia modulate microcirculatory blood flow and synaptic plasticity [32]. After release of proinflammatory

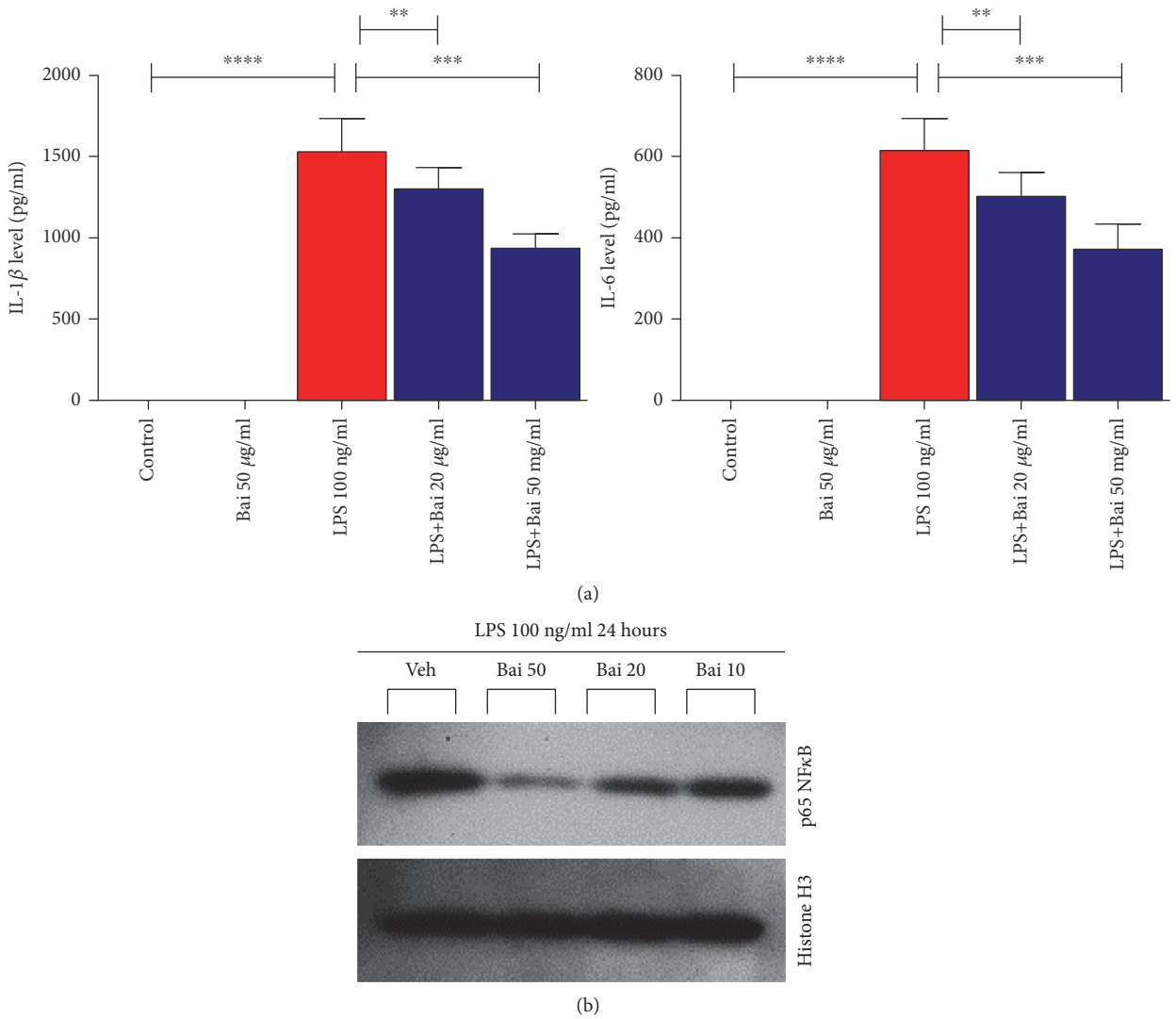

Figure 5: Effect of baicalin on glial cell activation in vitro. (a) Baicalin dose dependently inhibited the secretion of proinflammatory cytokines IL-1β and IL-6, which were determined by ELISA. $N = 6$ in each group, $****$ represents $p < 0.0001$, and $***$ represents $p < 0.0005$. (b) Immunoblot analyses of p65 from nuclear fraction along with loading control histone H3. $**$ represents $p < 0.005$.

cytokines in microglia, glial cell activation occurs. After activation, those cells quickly change to phagocytose any unwanted particles and secrete more proinflammatory cytokines to facilitate an immune response [33]. We have demonstrated that baicalin can modulate microglial cell activation *in vitro* (Figure 7). This is a critical step to contain brain injury and oxidative damage as severe immune response leads to edema and more oxidative damage-associated neuronal cell death. Baicalin is effective in many other inflammatory disorders [34–36].

NF-κB is crucial for glial cell function and regulates many genes, which encode important protein players involved in immune function and inflammation [37]. NF-κB plays a critical role in the early stage of SAH [38]. We also observed a similar pattern in our model, and baicalin attenuated the process. Experimental data suggest that a cascade of physiological events occur very early after the initial insult associated with SAH, causing a long-term cognitive deficit [39]. Our data demonstrate that the beneficial effect of baicalin at early injury can have a therapeutic benefit in the long term, and further experiments are required to assess that.

NOS-2 and NOX-2 are implicated in oxidative damage of subarachnoid hemorrhagic brain injury [40–42]. We observed baicalin attenuated induction of both enzymes. NOS-2 is a major generator of nitric oxide, which leads to deadly peroxynitrite radicals [43, 44]. Oxidative damage is responsible for a poor prognosis of SAH patients. NOX-2, which generates superoxide radical, has been present in perihematomal neurons and astrocytes of SAH animals [45]. Thus, our study indicated that baicalin-mediated reduction of both enzymes in SAH attenuated oxidative damage and cell death (Figure 7).

Traditional herbal medicine is considered to be the bench mark for multitarget therapy with promising future [46].

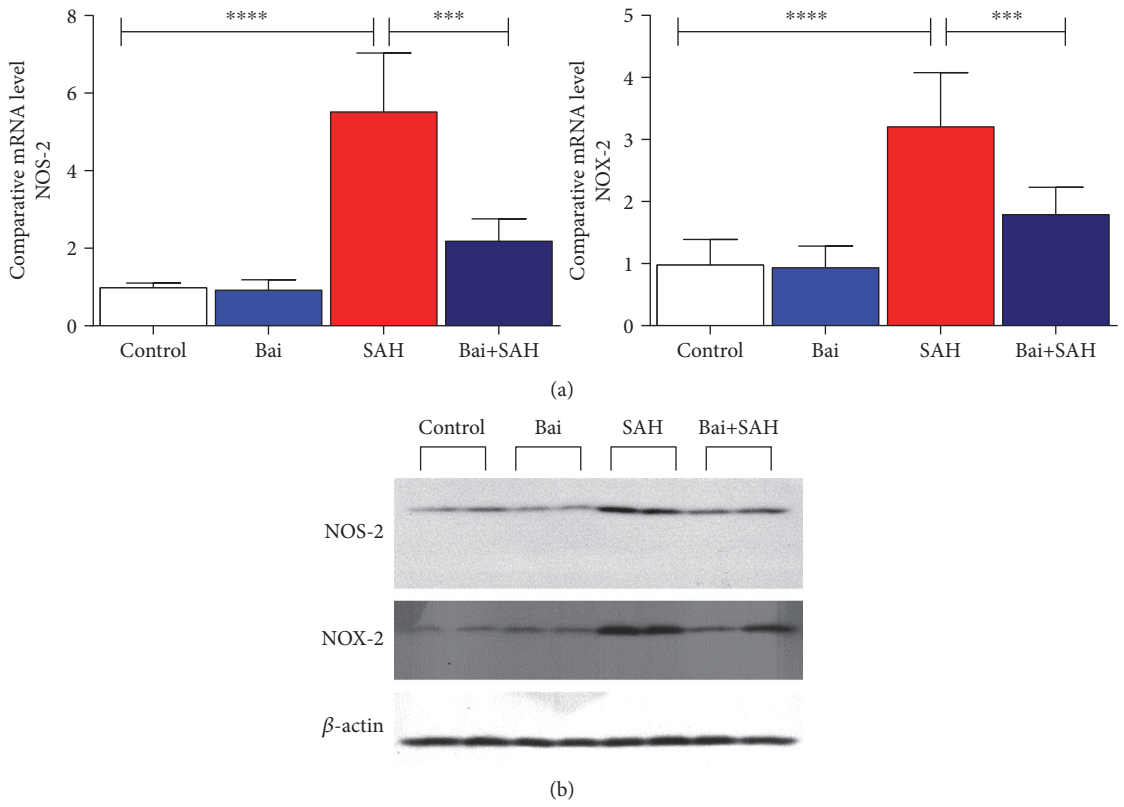

Figure 6: Effect of baicalin on NOS-2 and NOX-2 mRNA expression in SAH mice. (a) Real-time PCR analyses were performed on two oxidative stress-generating enzymes NOS-2 and NOX-2. Values are mean ± standard deviation. $N = 6$ in each group, $****$ represents $p < 0.0001$, and $***$ represents $p < 0.0005$. (b) Immunoblot analyses of NOS-2 and NOX-2 from total brain lysates with loading control beta-actin.

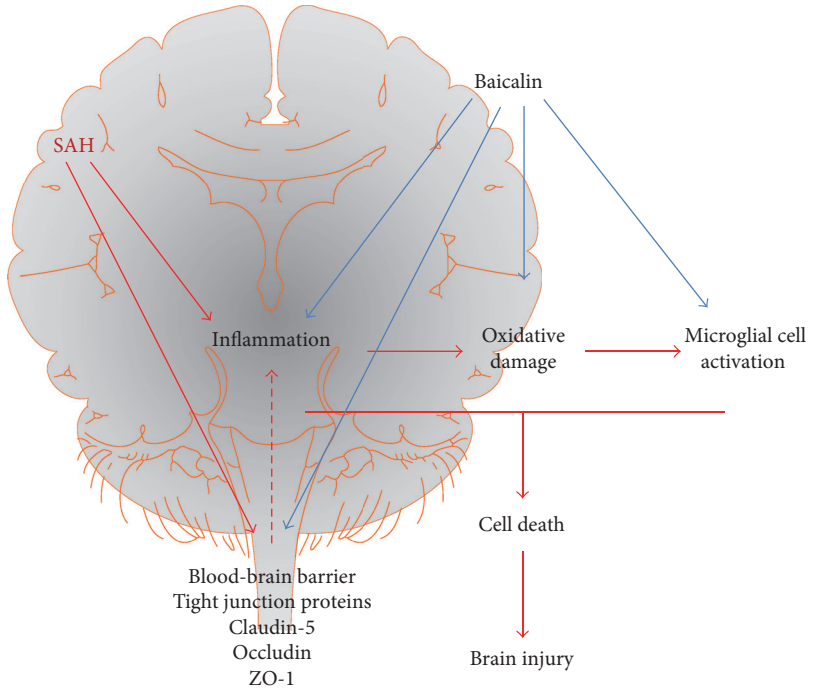

Figure 7: Schematic diagram of baicalin-mediated protection in SAH mice. SAH injury in brain leads to three physiological responses, namely, inflammation, microglial cell activation, and oxidative damage, which lead to cellular injury and cell death. Baicalin modulates all three physiological processes and thus attenuated SAH-mediated brain injury. Baicalin also restores blood-brain barrier function impaired by SAH, where degradation of tight junction proteins was modulated.

Baicalin, which is also part of many traditional Chinese medicines, has been demonstrated to have a potential role in many tissue injury animal models including liver, kidney, heart, pancreatitis, and brain [34, 47]. Baicalin is studied for robust pharmacokinetics and is a potential candidate for drug development [14].

5. Conclusion

We provided first preclinical evidence that baicalin protected against subarachnoid hemorrhagic brain injury. The process of attenuation was mediated through modulation of inflammation, brain water content, improving tight junction proteins, microglial cell activation, and oxidative damage. Additionally, we demonstrated that baicalin inhibited lipopolysaccharide-induced activation of primary microglial cells. However, a future study for detailed mechanism including M1/M2 polarization of microglial cells by baicalin may lead to potential new therapeutic development.

Disclosure

The funders had no role in the study design, data collection and analysis, decision to publish, or preparation of the manuscript.

Conflicts of Interest

The authors have nothing to report in this study.

Authors' Contributions

Jin Chen and Hao Ding are responsible for the evaluation and interpretation of the study. Yongjian Fu and SongSong Zhang gave technical support.

Acknowledgments

The authors thank all the staff at the laboratory. This study was supported by a grant from the Department of Science and Technology of Guizhou Province (Grant no. 2016[1095]).

References

[1] H. Lantigua, S. Ortega-Gutierrez, J. M. Schmidt et al., "Subarachnoid hemorrhage: who dies, and why?," *Critical Care*, vol. 19, p. 309, 2015.

[2] E. C. Haley Jr., N. F. Kassell, and J. C. Torner, "The International Cooperative Study on the timing of aneurysm surgery. The North American experience," *Stroke*, vol. 23, pp. 205–214, 1992.

[3] C. P. Nolan and R. L. Macdonald, "Can angiographic vasospasm be used as a surrogate marker in evaluating therapeutic interventions for cerebral vasospasm?," *Neurosurgical Focus*, vol. 21, article E1, 2006.

[4] S. Chen, H. Feng, P. Sherchan et al., "Controversies and evolving new mechanisms in subarachnoid hemorrhage," *Progress in Neurobiology*, vol. 115, pp. 64–91, 2014.

[5] H. Jeon, J. Ai, M. Sabri et al., "Neurological and neurobehavioral assessment of experimental subarachnoid hemorrhage," *BMC Neuroscience*, vol. 10, p. 103, 2009.

[6] X. Lan, X. Han, Q. Li et al., "Pinocembrin protects hemorrhagic brain primarily by inhibiting toll-like receptor 4 and reducing M1 phenotype microglia," *Brain, Behavior, and Immunity*, vol. 61, pp. 326–339, 2017.

[7] X. Lan, W. Wang, Q. Li, and J. Wang, "The natural flavonoid pinocembrin: molecular targets and potential therapeutic applications," *Molecular Neurobiology*, vol. 53, pp. 1794–1801, 2016.

[8] J. Yuan, W. Liu, H. Zhu et al., "Curcumin attenuates blood-brain barrier disruption after subarachnoid hemorrhage in mice," *The Journal of Surgical Research*, vol. 207, pp. 85–91, 2017.

[9] C. P. Chang, W. T. Huang, B. C. Cheng, C. C. Hsu, and M. T. Lin, "The flavonoid baicalin protects against cerebrovascular dysfunction and brain inflammation in experimental heatstroke," *Neuropharmacology*, vol. 52, pp. 1024–1033, 2007.

[10] K. L. Huang, C. S. Chen, C. W. Hsu et al., "Therapeutic effects of baicalin on lipopolysaccharide-induced acute lung injury in rats," *The American Journal of Chinese Medicine*, vol. 36, pp. 301–311, 2008.

[11] J. Y. Wan, X. Gong, L. Zhang, H. Z. Li, Y. F. Zhou, and Q. X. Zhou, "Protective effect of baicalin against lipopolysaccharide/D-galactosamine-induced liver injury in mice by up-regulation of heme oxygenase-1," *European Journal of Pharmacology*, vol. 587, pp. 302–308, 2008.

[12] M. F. Zeng, L. M. Pan, H. X. Zhu, Q. C. Zhang, and L. W. Guo, "Comparative pharmacokinetics of baicalin in plasma after oral administration of Huang-Lian-Jie-Du-Tang or pure baicalin in MCAO and sham-operated rats," *Fitoterapia*, vol. 81, pp. 490–496, 2010.

[13] P. L. Tsai and T. H. Tsai, "Pharmacokinetics of baicalin in rats and its interactions with cyclosporin A, quinidine and SKF-525A: a microdialysis study," *Planta Medica*, vol. 70, pp. 1069–1074, 2004.

[14] N. R. Srinivas, "Baicalin, an emerging multi-therapeutic agent: pharmacodynamics, pharmacokinetics, and considerations from drug development perspectives," *Xenobiotica*, vol. 40, pp. 357–367, 2010.

[15] K. Schuller, D. Buhler, and N. Plesnila, "A murine model of subarachnoid hemorrhage," *Journal of Visualized Experiments*, vol. 21, no. 81, article e50845, 2013.

[16] T. Sugawara, R. Ayer, V. Jadhav, and J. H. Zhang, "A new grading system evaluating bleeding scale in filament perforation subarachnoid hemorrhage rat model," *Journal of Neuroscience Methods*, vol. 167, pp. 327–334, 2008.

[17] P. Kraft, T. Schwarz, E. Gob et al., "The phosphodiesterase-4 inhibitor rolipram protects from ischemic stroke in mice by reducing blood-brain-barrier damage, inflammation and thrombosis," *Experimental Neurology*, vol. 247, pp. 80–90, 2013.

[18] G. Xi, Y. Hua, R. R. Bhasin, S. R. Ennis, R. F. Keep, and J. T. Hoff, "Mechanisms of edema formation after intracerebral hemorrhage: effects of extravasated red blood cells on blood flow and blood-brain barrier integrity," *Stroke*, vol. 32, pp. 2932–2938, 2001.

[19] J. K. Lee and M. G. Tansey, "Microglia isolation from adult mouse brain," *Methods in Molecular Biology*, vol. 1041, pp. 17–23, 2013.

[20] T. Sozen, R. Tsuchiyama, Y. Hasegawa et al., "Role of interleukin-1beta in early brain injury after subarachnoid hemorrhage in mice," *Stroke*, vol. 40, pp. 2519–2525, 2009.

[21] B. V. Zlokovic, "The blood-brain barrier in health and chronic neurodegenerative disorders," *Neuron*, vol. 57, pp. 178–201, 2008.

[22] J. S. Won, Y. B. Im, L. Key, I. Singh, and A. K. Singh, "The involvement of glucose metabolism in the regulation of inducible nitric oxide synthase gene expression in glial cells: possible role of glucose-6-phosphate dehydrogenase and CCAAT/enhancing binding protein," *The Journal of Neuroscience*, vol. 23, pp. 7470–7478, 2003.

[23] Y. Kifle, J. Monnier, S. E. Chesrown, M. K. Raizada, and H. S. Nick, "Regulation of the manganese superoxide dismutase and inducible nitric oxide synthase gene in rat neuronal and glial cells," *Journal of Neurochemistry*, vol. 66, pp. 2128–2135, 1996.

[24] K. Dohi, H. Ohtaki, T. Nakamachi et al., "Gp91phox (NOX2) in classically activated microglia exacerbates traumatic brain injury," *Journal of Neuroinflammation*, vol. 7, p. 41, 2010.

[25] O. M. Ogundele, A. O. Omoaghe, D. C. Ajonijebu et al., "Glia activation and its role in oxidative stress," *Metabolic Brain Disease*, vol. 29, pp. 483–493, 2014.

[26] J. van Gijn, R. S. Kerr, and G. J. Rinkel, "Subarachnoid haemorrhage," *Lancet*, vol. 369, pp. 306–318, 2007.

[27] Q. Liu, J. Liu, P. Wang et al., "Poly-dimensional network comparative analysis reveals the pure pharmacological mechanism of baicalin in the targeted network of mouse cerebral ischemia," *Brain Research*, vol. 1666, pp. 70–79, 2017.

[28] A. Germano, D. d'Avella, C. Imperatore, G. Caruso, and F. Tomasello, "Time-course of blood-brain barrier permeability changes after experimental subarachnoid haemorrhage," *Acta Neurochirurgica*, vol. 142, pp. 575–580, 2000, discussion 580-571.

[29] H. Johshita, N. F. Kassell, and T. Sasaki, "Blood-brain barrier disturbance following subarachnoid hemorrhage in rabbits," *Stroke*, vol. 21, pp. 1051–1058, 1990.

[30] V. Z. Zheng and G. K. Wong, "Neuroinflammation responses after subarachnoid hemorrhage: a review," *Journal of Clinical Neuroscience*, vol. 42, 2017.

[31] N. Schallner, R. Pandit, R. LeBlanc 3rd et al., "Microglia regulate blood clearance in subarachnoid hemorrhage by heme oxygenase-1," *The Journal of Clinical Investigation*, vol. 125, pp. 2609–2625, 2015.

[32] B. J. van Dijk, M. D. Vergouwen, M. M. Kelfkens, G. J. Rinkel, and E. M. Hol, "Glial cell response after aneurysmal subarachnoid hemorrhage - functional consequences and clinical implications," *Biochimica et Biophysica Acta (BBA) - Molecular Basis of Disease*, vol. 2016, pp. 492–505, 1862.

[33] H. Kettenmann, U. K. Hanisch, M. Noda, and A. Verkhratsky, "Physiology of microglia," *Physiological Reviews*, vol. 91, pp. 461–553, 2011.

[34] B. Dinda, S. Dinda, S. DasSharma, R. Banik, A. Chakraborty, and M. Dinda, "Therapeutic potentials of baicalin and its aglycone, baicalein against inflammatory disorders," *European Journal of Medicinal Chemistry*, vol. 131, pp. 68–80, 2017.

[35] A. Bitto, F. Squadrito, N. Irrera et al., "Flavocoxid, a nutraceutical approach to blunt inflammatory conditions," *Mediators of Inflammation*, vol. 2014, Article ID 790851, 8 pages, 2014.

[36] C. Li, G. Lin, and Z. Zuo, "Pharmacological effects and pharmacokinetics properties of Radix Scutellariae and its bioactive flavones," *Biopharmaceutics & Drug Disposition*, vol. 32, pp. 427–445, 2011.

[37] L. A. O'Neill and C. Kaltschmidt, "NF-kappa B: a crucial transcription factor for glial and neuronal cell function," *Trends in Neurosciences*, vol. 20, pp. 252–258, 1997.

[38] R. P. Ostrowski, A. R. Colohan, and J. H. Zhang, "Molecular mechanisms of early brain injury after subarachnoid hemorrhage," *Neurological Research*, vol. 28, pp. 399–414, 2006.

[39] J. Cahill, J. W. Calvert, and J. H. Zhang, "Mechanisms of early brain injury after subarachnoid hemorrhage," *Journal of Cerebral Blood Flow and Metabolism*, vol. 26, pp. 1341–1353, 2006.

[40] L. Zhang, J. Wu, X. Duan et al., "NADPH oxidase: a potential target for treatment of stroke," *Oxidative Medicine and Cellular Longevity*, vol. 2016, Article ID 5026984, 9 pages, 2016.

[41] D. Hanggi and H. J. Steiger, "Nitric oxide in subarachnoid haemorrhage and its therapeutics implications," *Acta Neurochirurgica*, vol. 148, pp. 605–613, 2006.

[42] D. Ding, R. M. Starke, A. S. Dumont et al., "Therapeutic implications of estrogen for cerebral vasospasm and delayed cerebral ischemia induced by aneurysmal subarachnoid hemorrhage," *BioMed Research International*, vol. 2014, Article ID 727428, 9 pages, 2014.

[43] S. Iqbal, E. G. Hayman, C. Hong et al., "Inducible nitric oxide synthase (NOS-2) in subarachnoid hemorrhage: regulatory mechanisms and therapeutic implications," *Brain Circulation*, vol. 2, pp. 8–19, 2016.

[44] T. Sayama, S. Suzuki, and M. Fukui, "Role of inducible nitric oxide synthase in the cerebral vasospasm after subarachnoid hemorrhage in rats," *Neurological Research*, vol. 21, pp. 293–298, 1999.

[45] L. Zhang, Z. Li, D. Feng et al., "Involvement of Nox2 and Nox4 NADPH oxidases in early brain injury after subarachnoid hemorrhage," *Free Radical Research*, vol. 51, pp. 316–328, 2017.

[46] L. Gao, J. Hao, Y. Y. Niu et al., "Network pharmacology dissection of multiscale mechanisms of herbal medicines in stage IV gastric adenocarcinoma treatment," *Medicine (Baltimore)*, vol. 95, article e4389, 2016.

[47] H. Xiang, Q. Zhang, B. Qi et al., "Chinese herbal medicines attenuate acute pancreatitis: pharmacological activities and mechanisms," *Frontiers in Pharmacology*, vol. 8, p. 216, 2017.

Hindawi
Oxidative Medicine and Cellular Longevity
Volume 2017, Article ID 3140680, 10 pages
https://doi.org/10.1155/2017/3140680

Research Article

Ameliorative Effect of Daidzein on Cisplatin-Induced Nephrotoxicity in Mice via Modulation of Inflammation, Oxidative Stress, and Cell Death

Hongzhou Meng,[1] Guanghou Fu,[1] Jie Shen,[1] Kezhen Shen,[2] Zhijie Xu,[1] Yiming Wang,[1] Baiye Jin,[1] and Hao Pan[1]

[1]*Department of Urology, the First Affiliated Hospital, College of Medicine, Zhejiang University, Hangzhou, Zhejiang, China*
[2]*Key Laboratory of Combined Multi-Organ Transplantation, Ministry of Public Health, the First Affiliated Hospital, College of Medicine, Zhejiang University, Hangzhou, Zhejiang, China*

Correspondence should be addressed to Hao Pan; panhao1977@163.com

Received 28 April 2017; Revised 14 June 2017; Accepted 20 June 2017; Published 2 August 2017

Academic Editor: Aditya Sen

Oxidative stress and inflammation are part and parcel of cisplatin-induced nephrotoxicity. The purpose of this work is to study the role of soy isoflavone constituent, daidzein, in cisplatin-induced renal damage. Cisplatin-induced nephrotoxicity was evident by the histological damage in proximal tubular cells and by the increase in serum neutrophil gelatinase-associated lipocalin (NGAL), blood urea nitrogen (BUN), creatinine, and urinary kidney injury molecule-1 (KIM-1). Cisplatin-induced cell death was shown by TUNEL staining and caspase-3/7 activity. Daidzin treatment reduced all kidney injury markers (NGAL, BUN, creatinine, and KIM-1) and attenuated cell death (apoptotic markers). In cisplatin-induced kidney injury, renal oxidative/nitrative stress was manifested by the increase in lipid peroxidation and protein nitration. Cisplatin induced the reactive oxygen species-generating enzyme NOX-2 and impaired antioxidant defense enzyme activities such as glutathione peroxidase (GPX) and superoxide dismutase (SOD) activities. Cisplatin-induced oxidative/nitrative stress was attenuated by daidzein treatment. Cisplatin induced CD11b-positive macrophages in kidneys and daidzein attenuated CD11b-positive cells. Daidzein attenuated cisplatin-induced inflammatory cytokines tumor necrosis factor α (TNFα), interleukin 10 (IL-10), interleukin 18 (IL-18), and monocyte chemoattractant protein-1 (MCP-1). Daidzein attenuated cell death *in vitro*. Our data suggested that daidzein attenuated cisplatin-induced kidney injury through the downregulation of oxidative/nitrative stress, immune cells, inflammatory cytokines, and apoptotic cell death, thus improving kidney regeneration.

1. Introduction

Cisplatin is a commonly used anticancer drug for the treatment of solid tumors. The mechanism of cancer cell killing is through its DNA-binding properties by forming adducts and stopping replication of cancer cells. One of the major side effects of cisplatin is nephrotoxicity and is mediated by preferential absorption of cisplatin in proximal tubules through a specific transporter [1]. Hydration has been used to alleviate this issue with some success. However, the dose-dependent nephrotoxicity is thus a limiting factor during cisplatin chemotherapy. The mechanism of cisplatin-mediated nephrotoxicity is mediated by apoptotic cell death induced by oxidative stress and inflammation.

Cisplatin is mainly excreted by kidneys, and high concentration of cisplatin accumulated there due to the basolateral organic cation system [2]. Cisplatin also accumulates in mitochondria and modulates its bioenergetics [3]. However, substantial literatures indicate that oxidative stress plays a critical role in renal damage [4]. Cell death associated

with oxidative stress leads to inflammatory response and is highly relevant to the pathogenesis of cisplatin-induced nephrotoxicity [5].

Various natural bioactive compounds, which have antioxidant and anti-inflammatory properties, exhibit renoprotective activity in an animal model of cisplatin nephrotoxicity. Daidzein is found in soybeans and is a constituent of Chinese traditional medicine Nao Mai Tong formula. Daidzein is an isoflavone and has antioxidant, anti-inflammatory, and phytoestrogenic properties. Daidzein demonstrates anti-inflammatory effects on endotoxin-induced RAW 264.7 macrophages [6]. In a clinical trial, both soy and purified daidzein improved renal function [7]. Daidzein also inhibits STAT-1 and NF-κB activations in an activated macrophage [8]. Daidzein has cardioprotective and antiarthritogenic effects on rheumatoid arthritis. A clinical trial (ClinicalTrials.gov NCT02075112) is currently ongoing with soy supplementation during cisplatin chemotherapy and radiation therapy for head and neck cancer to decrease side effects caused by treatments.

Here, we demonstrated that daidzein is protective against cisplatin-induced nephrotoxicity. The protective effect was mediated by its antioxidant and anti-inflammatory properties.

2. Materials and Methods

2.1. Mouse Experiments. All protocols were approved by the Committee on the Ethics of Animal Experiments of the First Affiliated Hospital, College of Medicine, Zhejiang University, under the guidance of the Chinese Academy of Sciences. The mouse strain C57BL/6 was used as described before [9]. Male mice of ~8 weeks of age with weights of 18–22 g were used in all experiments. Mice were sacrificed under deep anesthesia with 5% isoflurane followed by cervical dislocation on the third day (72 hours) after a single injection of cisplatin (cis-diammineplatinum (II) dichloride, Sigma) at dose 25 mg/kg i.p. in 5% DMSO/saline vehicle. High-quality daidzein (>98% pure) was purchased from Nanjing Zelang Medical Technology Co. Ltd. Daidzein was dissolved in DMSO/saline and administered at 200 mg/kg, i.p., for two days, starting 1 h after the cisplatin administration. Daidzein and vehicle were also administered alone (without cisplatin treatment) as a separate group.

2.2. Kidney Function. Serum levels of blood urea nitrogen (BUN) and creatinine were measured as described earlier [10]. Serum NGAL and urinary KIM-1 were measured from serum using Mouse NGAL Quantikine ELISA Kit and Mouse KIM-1 Quantikine ELISA Kit (R&D Systems China Co. Ltd., Changning, China) according to the manufacturer's instruction.

2.3. Histology. Periodic acid-Schiff (PAS) staining for histological examination was performed as described earlier [10]. Slides with PAS staining were examined based on the following four histological criteria and scored. Tubular damage in PAS-stained sections was examined under the microscope and scored based on the percentage of cortical tubules showing epithelial necrosis: 0—normal, 1—<10%, 2—10 to 25%, 3—26 to 75%, and 4—>75%. Tubular necrosis was defined as the loss of the proximal tubular brush border, blebbing of apical membranes, tubular epithelial cell detachment from the basement membrane, or intraluminal aggregation of cells and proteins. The morphometric examinations were performed in a blinded manner.

Protein nitrotyrosine staining using monoclonal anti-nitrotyrosine antibody (Cayman Chemical, NeoBioscience Technology, Shenzhen, China) was performed as described earlier [10].

2.4. Fluorescence Microscopy. Kidneys were sectioned with a microtome, deparaffinized, and stained as provided below with a fluorescence microscope. Apoptosis was detected in the kidneys by the TUNEL assay (Roche Diagnostics, Indianapolis, IN, USA) along with nuclear staining using Hoechst 33342 (Solarbio, China) as described earlier [10]. CD11b-conjugated FITC (BD Biosciences, USA) for neutrophils/monocytes (leukocytes) and nuclear stain Hoechst 33342 (Solarbio, China) were used in kidney sections.

2.5. Renal Apoptosis. Caspase-3/7 activity of the lysate was measured using Apo-ONE Homogenous Caspase-3/7 Assay Kit (Promega Corp., Madison, WI, USA) as described earlier [9]. Caspase-3/7 activity was presented as caspase-3 activity in the figure and text. The activity was expressed as fold change.

2.6. Renal HNE Protein Adducts and Protein Nitration. Nitrotyrosine content was evaluated by ELISA as described [9] HNE adducts were determined using OxiSelect™ HNE Adduct ELISA Kit (Cell Biolabs, Genetimes Technology Inc., Shanghai, China) as described earlier [9].

2.7. Quantitative Determination of SOD Activity. SOD activity was determined from tissue lysates using an SOD activity kit (Enzo Life Sciences International Inc., Plymouth Meeting, PA, USA) as described before [9].

2.8. Glutathione Peroxidase Assay. Glutathione peroxidase was measured using a Glutathione Peroxidase (GPX) Assay Kit (Abcam Trading Company Ltd., Shanghai, China) according to the manufacturer's instruction.

2.9. Glutathione Content. Glutathione (GSH) was determined by using a colorimetric kit (Jiancheng Bioengineering Institute, China) according to the manufacturer's instructions.

2.10. Real-Time PCR. Isolation of RNA and real-time PCR were carried out as described earlier [9, 10]. The primer sets for TNFα (PPM03113G), IL-18 (PPM03112B), IL-10 (PPM03017C), MCP-1 (PPM03151G), NOX2 (PPM32951A), and β-actin (PPM02945B) were purchased from Qiagen (Pudong, Shanghai, China).

2.11. Renal Western Blot. Western blot was performed as described previously [11].

2.12. Cell Culture and Flow Cytometry Analyses. HK-2 cells were grown and processed as described earlier [9].

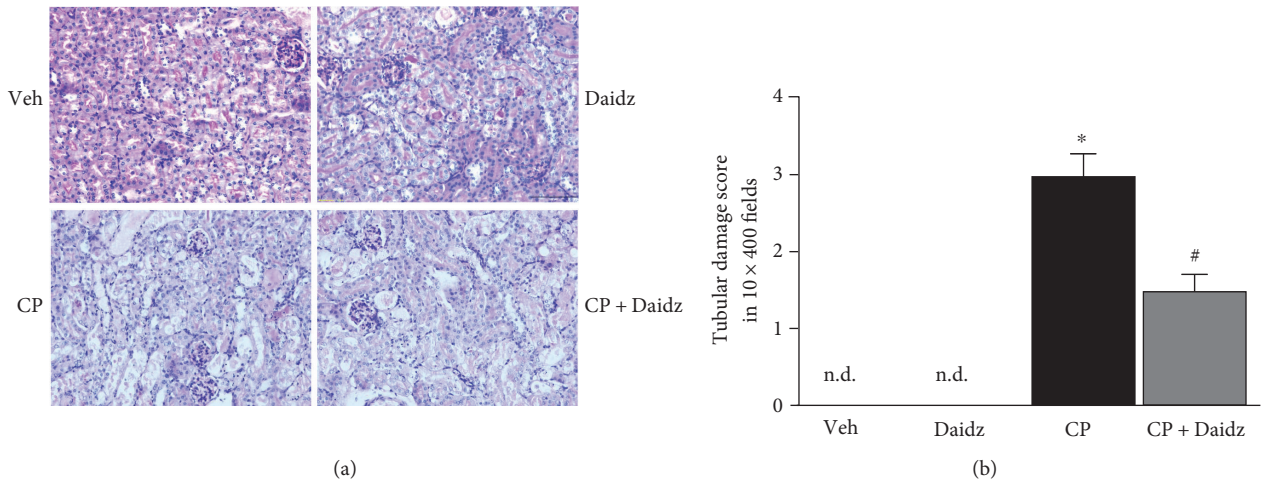

Figure 1: Effect of daidzein on cisplatin-induced kidney tubular damage in mice. (a) Cisplatin induced tubular damage as shown by PAS staining. The damage was attenuated by daidzein (daidz) treatment at dose 200 mg/kg. (b) Quantification of the tubular damage score from PAS-stained slide. Results are mean ± SEM ($n = 6$/group). $^{*}p < 0.05$ versus vehicle and $^{\#}p < 0.05$ versus cisplatin.

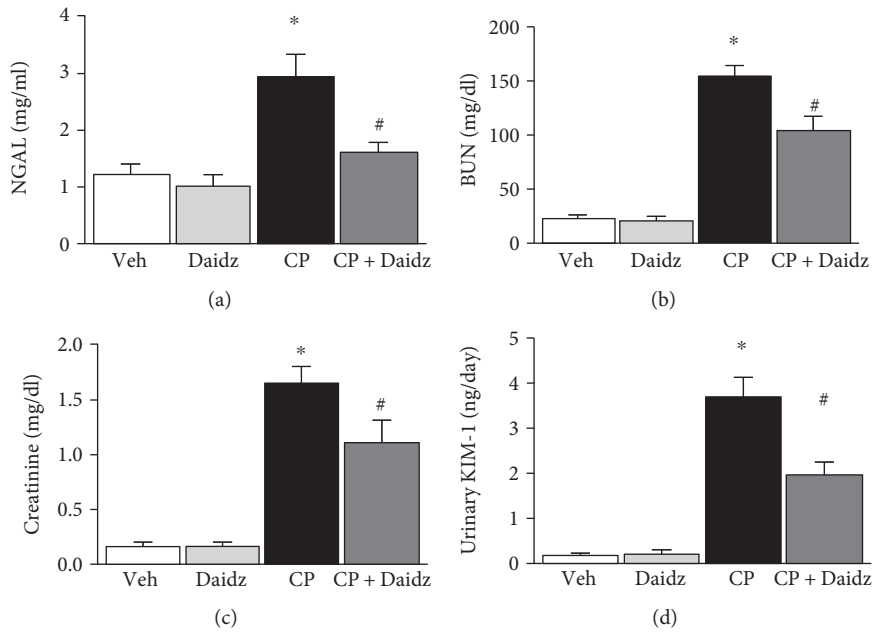

Figure 2: Effect of daidzein on cisplatin-induced renal dysfunction in mice. Cisplatin caused significant renal dysfunction as determined by the levels of NGAL (a), BUN (b), creatinine (c), and urinary KIM-1 at 72 hours (d). Cisplatin induced kidney injury which was attenuated by daidzein treatment. Results are mean ± SEM ($n = 6$/group). $^{*}p < 0.05$ versus vehicle and $^{\#}p < 0.05$ versus cisplatin.

Cisplatin was added at 50 μM and vehicle or daidzein at 30 μM after a 30 min delay to cisplatin addition for 24 hours. Flow cytometry experiments were performed as described earlier [9].

2.13. Statistical Analysis. All data were presented as the means ± SEMs. Multiple comparisons (Tukey) were performed using one-way ANOVA. The analyses were performed with GraphPad Prism software (GraphPad Software Inc., CA, USA). A p value <0.05 was considered statistically significant.

3. Results and Discussion

3.1. Effect of Daidzein on Cisplatin-Induced Tubular Damage, Kidney Injury, and Cell Death. Cisplatin administration to C57BL6 mice led to significant tubular damage at 72 hours as observed in PAS staining (Figure 1). Histological examination and quantification revealed vacuolation, protein cast formation, and desquamation of epithelial cells in the renal tubules. The damage was significantly attenuated by daidzein treatment in mice. Cisplatin also induced renal dysfunction as found by the kidney injury parameters such as NGAL,

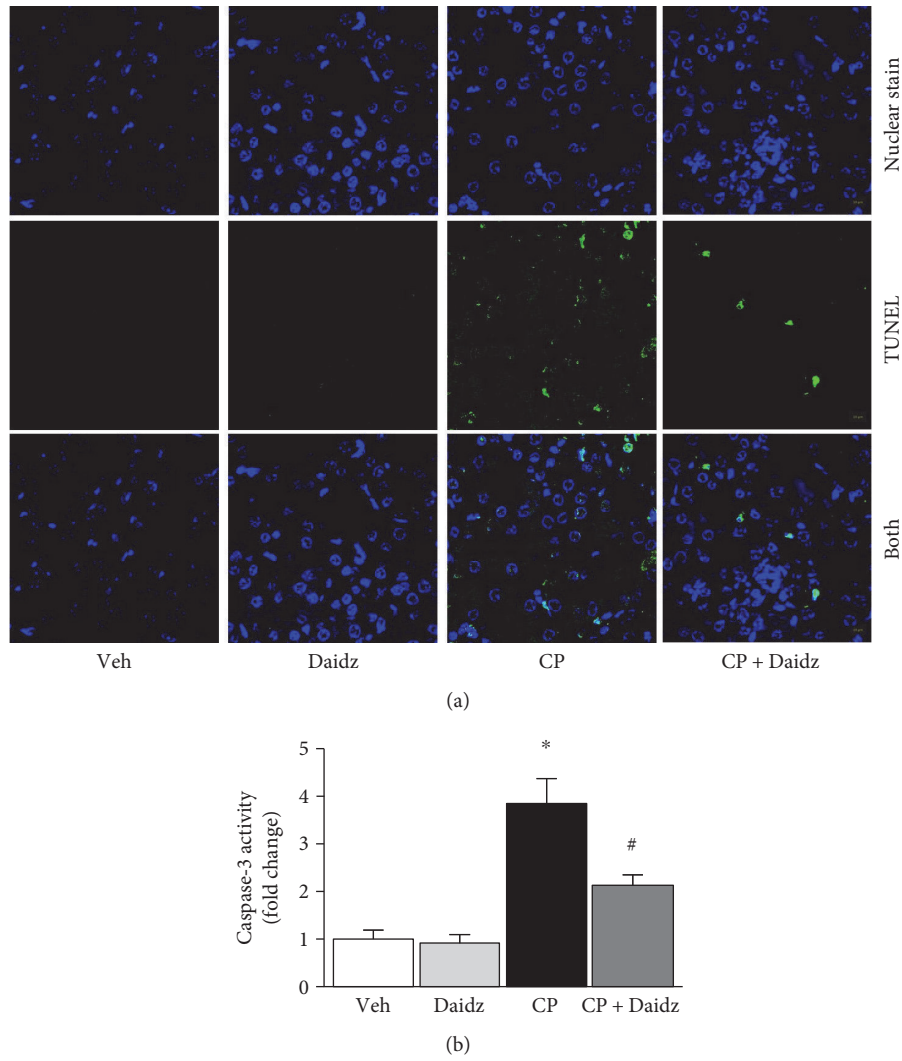

Figure 3: Effects of daidzein on cisplatin-induced cell death. Histological examination (a) demonstrated cisplatin-induced TUNEL staining (green) in the kidney and TUNEL staining was significantly attenuated with daidzein administration. Nuclei were stained with Hoechst 33342 (blue). (b) Caspase-3 activities were determined and daidzein attenuated cisplatin-induced caspase-3 activity. Results are mean ± SEM ($n = 6$/group). $^{*}p < 0.05$ versus vehicle and $^{\#}p < 0.05$ versus cisplatin.

BUN, creatinine, and urinary KIM-1 (Figure 2). Cisplatin administration resulted in a 2.46-, 6.92-, 9.93-, and 20-fold increase in NGAL, BUN, creatinine, and KIM-1, respectively. Daidzein attenuated all kidney injury markers. Daidzein at 200 mg/kg reduced cisplatin-induced kidney injury as shown by a decrease in serum levels of NGAL (2.93 to 1.60), BUN (153.5 to 103.6), creatinine (1.65 to 1.11), and urinary KIM-1 (3.7 to 1.98). Cisplatin is known to cause apoptotic cell death in the kidney. We have observed a significant increase in TUNEL staining in cisplatin kidney, and the number reduced after daidzein treatment (Figure 3(a)). Quantitative determination of caspase-3/7 activity demonstrated that cisplatin induced 3.86-fold increases and daidzein treatment reduced 43.9% of caspase-3/7 activity (Figure 3(b)).

Nephrotoxic drug-related acute kidney injury in hospital was approximately 20% and increased to 66% for the elderly [5]. Cisplatin accumulated at high concentration in the kidneys by the renal transport system, and its toxicity is dose dependent [12]. Whole soy and its constituent daidzein have a positive effect on renal function in a clinical trial [7]. Pharmacokinetics of daidzein in human, mouse, and rat demonstrates its presence as glucuronides [13, 14]. Comparative pharmacokinetics of traditional Chinese medicine Nao Mai Tong in a rat study also demonstrates the presence of daidzein [15]. In our study, daidzein significantly reduced cisplatin-induced acute kidney injuries by improving kidney function and prevented tubular cell death.

3.2. Effect of Daidzein on Cisplatin-Induced Oxidative Stress and Impaired Antioxidant Defense. Cisplatin-induced nephrotoxicity is mediated by oxidative stress [16]. We evaluated the effect of daidzein on cisplatin-induced oxidative footprints such as HNE protein adducts and protein nitration. Both oxidative stress markers HNE protein adducts and protein nitration were increased 2.6- and 2.9-fold in

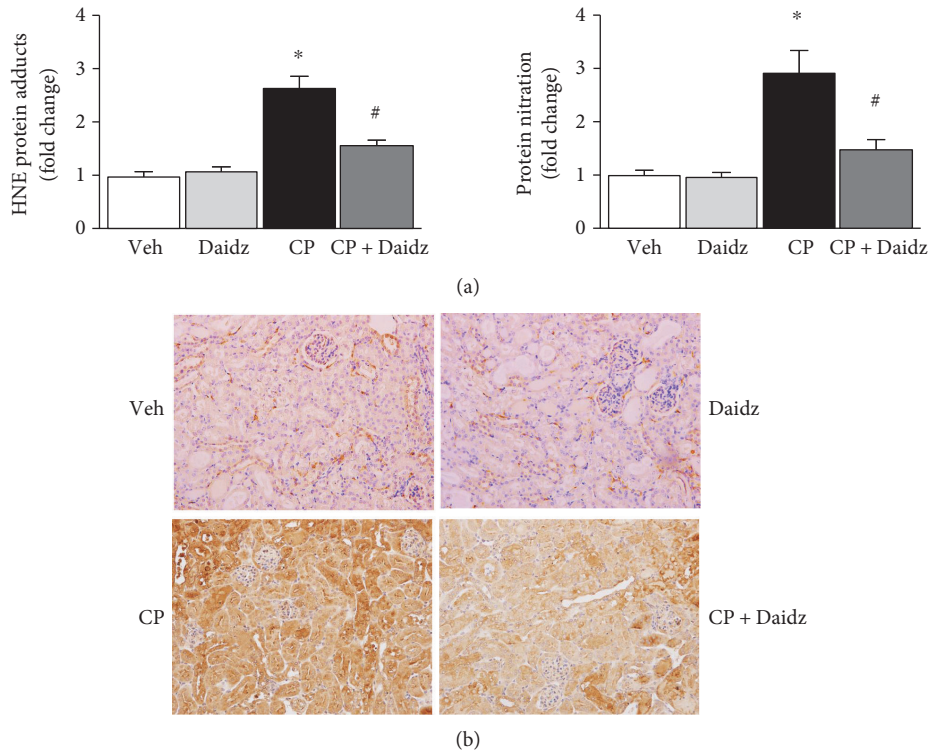

Figure 4: Effect of daidzein on cisplatin-induced oxidative/nitrative stress. (a) Quantitative measurement of HNE adducts and protein nitration by ELISA demonstrated cisplatin-induced lipid peroxidation and protein nitration. Daidzein attenuated both cisplatin-induced oxidative/nitrative stress markers. (b) Histological staining of protein nitration. A trend similar to quantitative protein nitration was observed. Results are mean ± SEM ($n = 6$/group). $^{*}p < 0.05$ versus vehicle and $^{\#}p < 0.05$ versus cisplatin.

cisplatin-treated mice (Figure 4(a)). Treatment with daidzein reduced 39.9% and 48.7% of HNE protein adducts and protein nitration, respectively. We also examined protein nitration by histological staining, and daidzein significantly reduced cisplatin-induced protein nitration (Figure 4(b)). In all above experiments, daidzein did not change any oxidative stress marker when administered alone.

The balance of reactive oxygen species- (ROS-) generating enzymes and antioxidant defense enzymes is critical for cisplatin nephrotoxicity [10, 17]. We found that cisplatin-induced gene expression of the ROS-generating enzyme NOX2 is significantly attenuated by daidzein (3.8- to 2.3-fold, Figure 5(a)). Glutathione plays a critical role in cisplatin-induced kidney injury [18]. Daidzein also improved up to 66% of cisplatin-mediated depletion of reduced glutathione in mouse kidney (Figure 5(b)). In addition to that, daidzein enhanced a cisplatin-mediated reduction in glutathione peroxidase activity and total SOD activity up to 49% and 55%, respectively (Figures 5(c) and 5(d)).

Oxidative stress plays a critical role in cisplatin-induced acute kidney injury [16, 19, 20]. Previous studies show that cisplatin mediated an increase in lipid peroxidation (one oxidative stress marker) and is attenuated by flavonoids and antioxidants [21–23]. Protein nitration is mediated by peroxynitrite and another hallmark of cisplatin-induced oxidative stress in the kidney [9]. Here, we demonstrated that daidzein attenuated cisplatin-induced protein nitration and lipid peroxidation (HNE adducts). NOX2 is one among several sources for oxidative stress [24, 25]. Daidzein attenuated cisplatin-induced NOX2 expression. Antioxidant defense is also critical in cisplatin-induced nephropathy [9, 26]. Cisplatin reduces the reserve of reduced glutathione, SOD activity, and glutathione peroxidase activity in kidneys [27–29]. Consistent with earlier studies, cisplatin impaired reduced glutathione reserve and decreased glutathione peroxidase activity and SOD activity. Daidzein improved all three antioxidant defense mechanisms and thus ameliorated cisplatin-induced oxidative stress.

3.3. Effect of Daidzein on Cisplatin-Induced Leukocyte Infiltration and Inflammatory Cytokines in the Kidney. Cisplatin-induced inflammatory response followed by infiltration of neutrophils and macrophages has been reported earlier [10, 19, 24]. Consistent with earlier findings, we observed CD11b-positive cells in cisplatin-induced kidney injury and daidzein significantly reduced CD11b-positive cells (Figure 6). Cisplatin induces several cytokines such as TNFα, IL-10, IL-18, and MCP-1 in kidney injury [30–32]. Cisplatin induced TNFα, IL-10, IL-18, and MCP-1 mRNA expression to 4.3-, 3.5-, 3.4-, and 2.98-fold, respectively (Figure 7(a)). Daidzein treatment attenuated 39.9%, 46.2%, 47%, and 43.2% of TNFα, IL-10, IL-18, and MCP-1 mRNA expression, respectively. We further verified one of the cytokines TNFα by Western blot analyses (Figure 7(b)), and the result was consistent with mRNA level. GAPDH was used as a loading control.

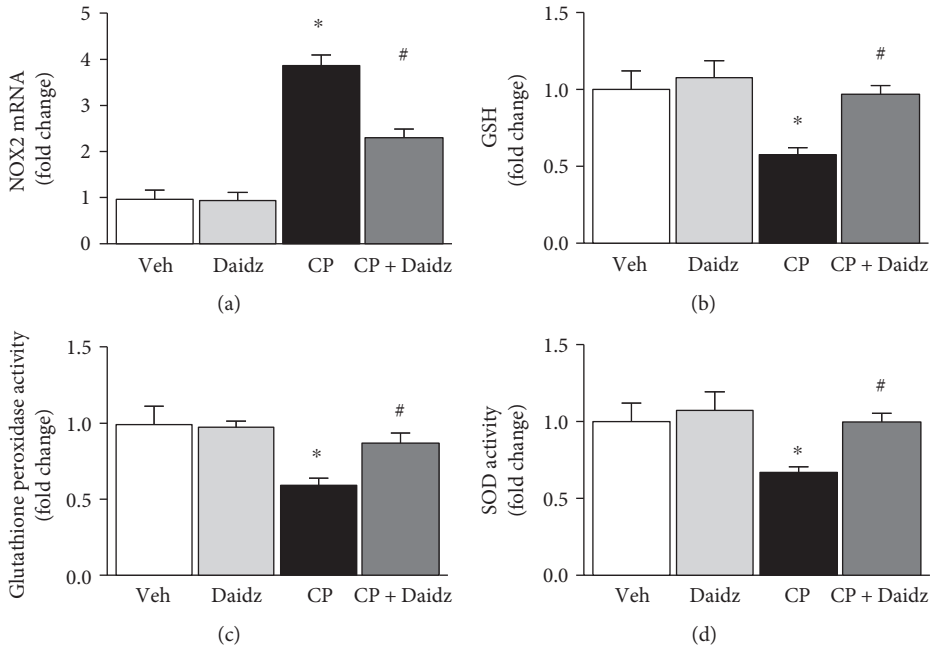

Figure 5: Effect of daidzein on cisplatin-induced changes in the ROS-generating enzyme NOX2 and antioxidant defense in mice. (a) Cisplatin induced the ROS-generating enzyme NOX2 mRNA as determined by real-time PCR, and daidzein attenuated cisplatin-reduced reduced glutathione reserve, glutathione peroxidase activity, and SOD activity. Daidzein administration restored those antioxidant defenses close to the control group. Results are mean ± SEM ($n = 6$/group). $^{*}p < 0.05$ versus vehicle and $^{\#}p < 0.05$ versus cisplatin.

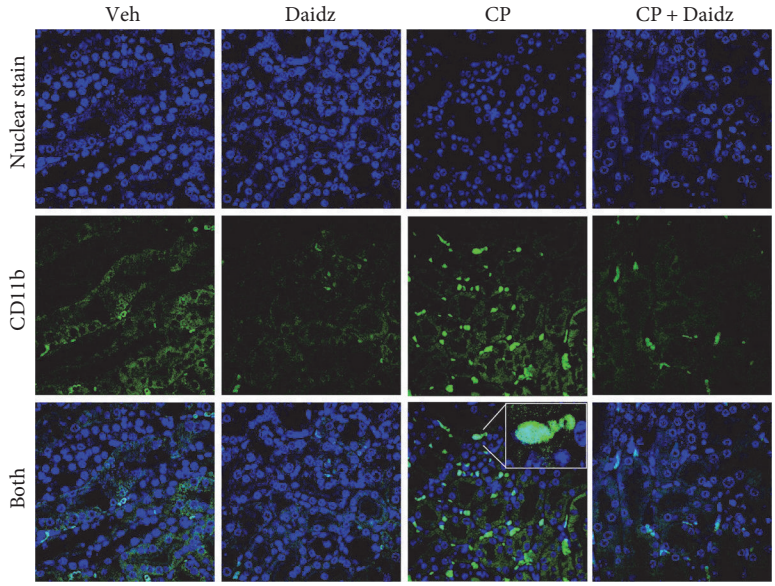

Figure 6: Effect of daidzein on cisplatin-induced CD11b-positive monocyte/macrophage in mice. Immunofluorescence examination revealed significant CD11b-positive cells (yellow) of the cisplatin-treated group. Nuclear staining (blue) was carried out using Hoechst 33342. In the cisplatin group, a zoom image of single cells was provided as an inset to demonstrate that staining covers surface staining and a larger area than nuclear staining. Daidzein treatment reduced the number of CD11b-positive cells. Either vehicle (Veh) or daidzein (daidz) control group does not have any CD11b-positive cells.

In the pathogenesis of cisplatin-induced nephrotoxicity, inflammation plays another major role [12, 33]. Different immune cells, namely, neutrophils, macrophages, T cells, and dendritic cells, play their role during the inflammatory response [12]. Neutrophils and monocyte-derived macrophages are myeloid cells which pursue common goals to neutralize danger in cisplatin-mediated nephropathy [32, 34]. CD11b is a αM integrin, a member of the integrin family,

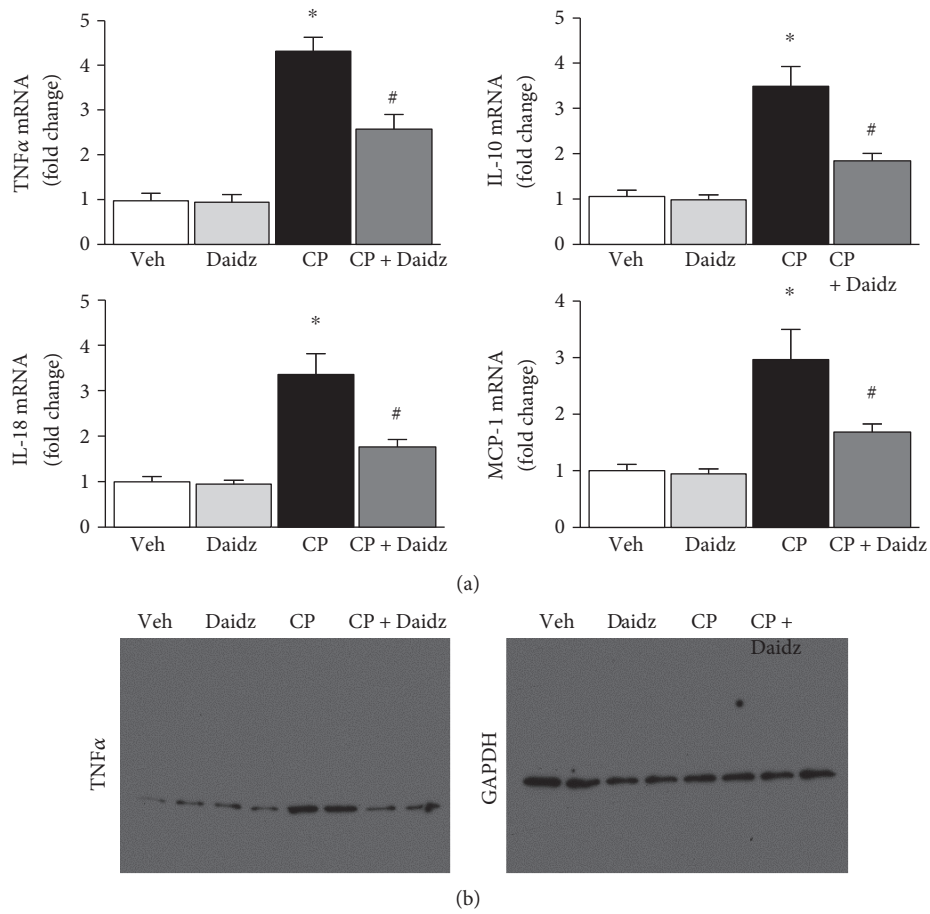

Figure 7: Effect of daidzein on cisplatin-induced proinflammatory cytokines in mice. (a) Real-time PCR-based analyses of proinflammatory cytokines TNFα, IL-10, IL-18, and MCP-1 indicated a profound increase in cisplatin-treated mice. Daidzein treatment attenuated cisplatin-induced cytokine MRNA expression. Results are mean ± SEM ($n = 6$/group). $^{*}p < 0.05$ versus vehicle and $^{\#}p < 0.05$ versus cisplatin. (b) Western blot analyses of TNFα and control GAPDH.

primarily expressed on monocytes/macrophages. Consistent with earlier data, we also observed a significant increase in a CD11b-positive macrophage in cisplatin-induced kidney injury [35]. Daidzein reduced cisplatin-induced macrophage accumulation in the kidneys. Daidzein inhibits production of nitric oxide and IL-6 in a lipopolysaccharide-induced macrophage [36].

Cisplatin activates the NF-κB pathway, thus facilitating inflammatory cytokines such as TNFα. Daidzein attenuated cisplatin-induced TNFα, and consistent with previous findings, berberine, curcumin, and chlorogenic acid mediated a renoprotective effect [21, 37, 38]. IL-18 is also crucial in cisplatin-mediated toxicity [39]. Genetic deletion of caspase-1, which cleaved IL-18 to make it active, reduced cisplatin kidney injury and neutrophil infiltration [40]. IL-18 was induced by cisplatin and attenuated with daidzein treatment in our study. IL-10 and MCP-1 also play a role in cisplatin-induced kidney injury [31, 41, 42]. We also observed that cisplatin induced both IL-10 and MCP-1 mRNA and those were attenuated by daidzein. Dendritic cells produce IL-10, and the modulation of dendritic cells by daidzein in cisplatin nephropathy cannot be excluded.

3.4. Effect of Daidzein on Cisplatin-Induced Cell Death of Proximal Tubular Cell Line In Vitro. Daidzein reduced both oxidative stress and inflammation. We also examined its effect on cell death under *in vitro* condition using HK-2 proximal tubular cell line. Cisplatin induced both apoptotic and necrotic cell death at 50 μM for 24 hours (Figure 8(a)). Daidzein addition at 30 μM attenuated cell death by 28.29% (Figure 8(b)). There was no effect of daidzein on HK-2 cell death when added without cisplatin.

Daidzein-mediated protection of cisplatin-induced proximal tubular cell death demonstrated its direct role. Cisplatin-induced nephrotoxicity is a far more complex situation where interplay of oxidative stress, inflammation, and cell death is partially correlated. Because anti-inflammatory properties of daidzein is reported earlier and our data demonstrated its direct role in inflammatory cytokines, we concluded that daidzein had anti-inflammatory properties in addition to its function to prevent cell death. It is also important to note that daidzein has antiestrogenic properties [43]. However, these specific properties of daidzein had no effect on our study as we have used male mice.

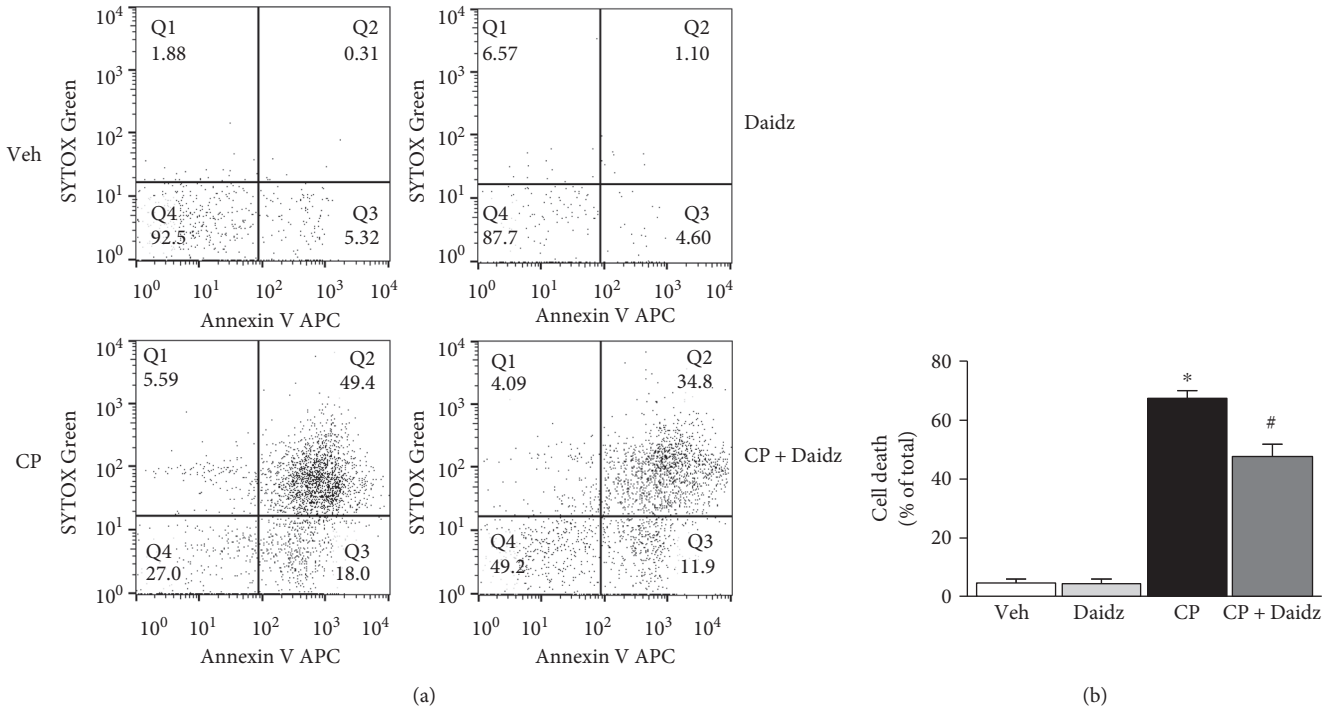

Figure 8: Effect of daidzein on cisplatin-induced cell death *in vitro*. (a) Representative dot plot of flow cytometric data of an HK-2 cell treated with either saline or daidzein in the presence or absence of cisplatin. *x*-axis represented the apoptotic cell death marker Annexin V whereas *y*-axis represented the dead cell marker SYTOX Green. (b) Quantitative determination of cell death (combined Q2 and Q3) among different groups. Results are mean ± SEM ($n = 3$/group). $^{*}p < 0.05$ versus vehicle and $^{\#}p < 0.05$ versus cisplatin.

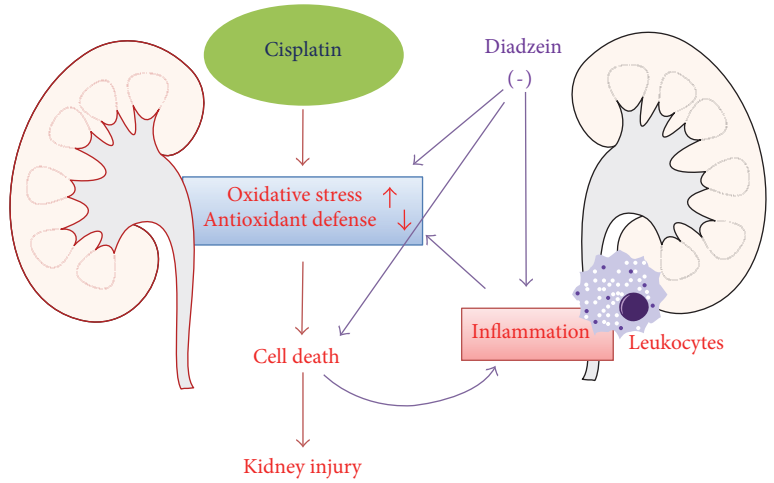

Figure 9: Schematic diagram of the protection mechanism of daidzein in cisplatin-induced kidney injury. EGCG inhibit cisplatin-induced ROS by attenuating ROS-generating enzymes and improving cisplatin-impaired antioxidant defense mechanisms in the renal tubular cells which caused cell death. Cell death also leads to proinflammatory response with cytokines and infiltrating leukocytes with the additional release of ROS. Daidzein attenuates cell death directly. Daidzein also neutralize cytokines and infiltrating leukocytes. Both antioxidant and anti-inflammatory effects leads to reduced cell death, thus protecting against cisplatin-induced kidney injury.

4. Conclusions

Cisplatin-induced tubular cell damage, cell death, and associated kidney injury were significantly attenuated with the administration of daidzein in mice. The molecular mechanism of protection is mediated through the interplay of oxidative stress and inflammation (Figure 9). Daidzein modulated cisplatin-induced lipid peroxidation, protein nitration, and NOX2 mRNA. Daidzein also improved cisplatin-impaired antioxidant defense such as reduced glutathione reserve,

GPX activity, and SOD activity. Cisplatin-induced macrophage accumulation and proinflammatory cytokine production were attenuated by daidzein.

Disclosure

The funding agency has no role in the study design or conclusion.

Conflicts of Interest

All authors hereby declare that no conflict of interest existed in this study.

Authors' Contributions

Hongzhou Meng, Guanghou Fu, and Jie Shen contributed equally to this work.

Acknowledgments

This work was supported by grants from the National Natural Science Foundation of China (no. 81000302), Science and Technology Department of Zhejiang Province (no. 2015C33214), and Zhejiang Medical and Health Science and Technology Plan Project (2014KYA070).

References

[1] M. H. Hanigan and P. Devarajan, "Cisplatin nephrotoxicity: molecular mechanisms," *Cancer Therapy*, vol. 1, pp. 47–61, 2003.

[2] G. Ciarimboli, D. Deuster, A. Knief et al., "Organic cation transporter 2 mediates cisplatin-induced oto- and nephrotoxicity and is a target for protective interventions," *The American Journal of Pathology*, vol. 176, pp. 1169–1180, 2010.

[3] N. A. Santos, C. S. Bezerra, N. M. Martins, C. Curti, M. L. Bianchi, and A. C. Santos, "Hydroxyl radical scavenger ameliorates cisplatin-induced nephrotoxicity by preventing oxidative stress, redox state unbalance, impairment of energetic metabolism and apoptosis in rat kidney mitochondria," *Cancer Chemotherapy and Pharmacology*, vol. 61, pp. 145–155, 2008.

[4] K. Hosohata, "Role of oxidative stress in drug-induced kidney injury," *International Journal of Molecular Sciences*, vol. 17, 2016.

[5] L. A. Peres and A. D. da Cunha Jr., "Acute nephrotoxicity of cisplatin: molecular mechanisms," *Jornal Brasileiro de Nefrologia*, vol. 35, pp. 332–340, 2013.

[6] S. J. Chinta, A. Ganesan, P. Reis-Rodrigues, G. J. Lithgow, and J. K. Andersen, "Anti-inflammatory role of the isoflavone diadzein in lipopolysaccharide-stimulated microglia: implications for Parkinson's disease," *Neurotoxicity Research*, vol. 23, pp. 145–153, 2013.

[7] Z. M. Liu, S. C. Ho, Y. M. Chen, N. Tang, and J. Woo, "Effect of whole soy and purified isoflavone daidzein on renal function–a 6-month randomized controlled trial in equol-producing postmenopausal women with prehypertension," *Clinical Biochemistry*, vol. 47, pp. 1250–1256, 2014.

[8] M. Hamalainen, R. Nieminen, P. Vuorela, M. Heinonen, and E. Moilanen, "Anti-inflammatory effects of flavonoids: genistein, kaempferol, quercetin, and daidzein inhibit STAT-1 and NF-kappaB activations, whereas flavone, isorhamnetin, naringenin, and pelargonidin inhibit only NF-kappaB activation along with their inhibitory effect on iNOS expression and NO production in activated macrophages," *Mediators of Inflammation*, vol. 2007, Article ID 45673, 10 pages, 2007.

[9] H. Pan, J. Chen, K. Shen et al., "Mitochondrial modulation by epigallocatechin 3-gallate ameliorates cisplatin induced renal injury through decreasing oxidative/nitrative stress, inflammation and NF-kB in mice," *PLoS One*, vol. 10, no. 4, article e0124775, 2015.

[10] H. Pan, K. Shen, X. Wang, H. Meng, C. Wang, and B. Jin, "Protective effect of metalloporphyrins against cisplatin-induced kidney injury in mice," *PLoS One*, vol. 9, article e86057, 2014.

[11] H. Pan, Z. Shen, P. Mukhopadhyay et al., "Anaphylatoxin C5a contributes to the pathogenesis of cisplatin-induced nephrotoxicity," *American Journal of Physiology-Renal Physiology*, vol. 296, pp. F496–F504, 2009.

[12] R. P. Miller, R. K. Tadagavadi, G. Ramesh, and W. B. Reeves, "Mechanisms of cisplatin nephrotoxicity," *Toxins (Basel)*, vol. 2, pp. 2490–2518, 2010.

[13] J. Rodriguez-Morato, M. Farre, C. Perez-Mana et al., "Pharmacokinetic comparison of soy isoflavone extracts in human plasma," *Journal of Agricultural and Food Chemistry*, vol. 63, pp. 6946–6953, 2015.

[14] S. T. Soukup, J. Helppi, D. R. Muller et al., "Phase II metabolism of the soy isoflavones genistein and daidzein in humans, rats and mice: a cross-species and sex comparison," *Archives of Toxicology*, vol. 90, pp. 1335–1347, 2016.

[15] C. Wu, L. Zhao, Y. Rong, G. Zhu, S. Liang, and S. Wang, "The pharmacokinetic screening of multiple components of the Nao Mai Tong formula in rat plasma by liquid chromatography tandem mass spectrometry combined with pattern recognition method and its application to comparative pharmacokinetics," *Journal of Pharmaceutical and Biomedical Analysis*, vol. 131, pp. 345–354, 2016.

[16] S. Ojha, B. Venkataraman, A. Kurdi, E. Mahgoub, B. Sadek, and M. Rajesh, "Plant-derived agents for counteracting cisplatin-induced nephrotoxicity," *Oxidative Medicine and Cellular Longevity*, vol. 2016, Article ID 4320374, 27 pages, 2016.

[17] R. Gonzalez, C. Romay, A. Borrego et al., "Lipid peroxides and antioxidant enzymes in cisplatin-induced chronic nephrotoxicity in rats," *Mediators of Inflammation*, vol. 2005, pp. 139–143, 2005.

[18] D. Appenroth and K. Winnefeld, "Role of glutathione for cisplatin nephrotoxicity in young and adult rats," *Renal Failure*, vol. 15, pp. 135–139, 1993.

[19] A. Ozkok and C. L. Edelstein, "Pathophysiology of cisplatin-induced acute kidney injury," *BioMed Research International*, vol. 2014, Article ID 967826, 17 pages, 2014.

[20] Y. I. Chirino and J. Pedraza-Chaverri, "Role of oxidative and nitrosative stress in cisplatin-induced nephrotoxicity," *Experimental and Toxicologic Pathology*, vol. 61, pp. 223–242, 2009.

[21] R. Domitrovic, O. Cvijanovic, V. Susnic, and N. Katalinic, "Renoprotective mechanisms of chlorogenic acid in cisplatin-induced kidney injury," *Toxicology*, vol. 324, pp. 98–107, 2014.

[22] Y. Wang, X. Luo, H. Pan et al., "Pharmacological inhibition of NADPH oxidase protects against cisplatin induced nephrotoxicity in mice by two step mechanism," *Food and Chemical Toxicology*, vol. 83, pp. 251–260, 2015.

[23] B. D. Sahu, J. Mahesh Kumar, and R. Sistla, "Baicalein, a bioflavonoid, prevents cisplatin-induced acute kidney injury by up-regulating antioxidant defenses and down-regulating the MAPKs and NF-kappaB pathways," *PLoS One*, vol. 10, article e0134139, 2015.

[24] B. D. Sahu, A. K. Kalvala, M. Koneru et al., "Ameliorative effect of fisetin on cisplatin-induced nephrotoxicity in rats via modulation of NF-kappaB activation and antioxidant defence," *PLoS One*, vol. 9, article e105070, 2014.

[25] P. Mukhopadhyay, H. Pan, M. Rajesh et al., "CB1 cannabinoid receptors promote oxidative/nitrosative stress, inflammation and cell death in a murine nephropathy model," *British Journal of Pharmacology*, vol. 160, pp. 657–668, 2010.

[26] M. A. Rodrigues, J. L. Rodrigues, N. M. Martins et al., "Carvedilol protects against cisplatin-induced oxidative stress, redox state unbalance and apoptosis in rat kidney mitochondria," *Chemico-Biological Interactions*, vol. 189, pp. 45–51, 2011.

[27] M. A. Darwish, A. M. Abo-Youssef, M. M. Khalaf, A. A. Abo-Saif, I. G. Saleh, and T. M. Abdelghany, "Vitamin E mitigates cisplatin-induced nephrotoxicity due to reversal of oxidative/nitrosative stress, suppression of inflammation and reduction of total renal platinum accumulation," *Journal of Biochemical and Molecular Toxicology*, vol. 31, pp. 1–9, 2017.

[28] S. M. Hassan, M. M. Khalaf, S. A. Sadek, and A. M. Abo-Youssef, "Protective effects of apigenin and myricetin against cisplatin-induced nephrotoxicity in mice," *Pharmaceutical Biology*, vol. 55, pp. 766–774, 2017.

[29] X. He, C. Li, Z. Wei et al., "Protective role of apigenin in cisplatin-induced renal injury," *European Journal of Pharmacology*, vol. 789, pp. 215–221, 2016.

[30] G. Ramesh and W. B. Reeves, "TNF-alpha mediates chemokine and cytokine expression and renal injury in cisplatin nephrotoxicity," *The Journal of Clinical Investigation*, vol. 110, pp. 835–842, 2002.

[31] R. K. Tadagavadi and W. B. Reeves, "Endogenous IL-10 attenuates cisplatin nephrotoxicity: role of dendritic cells," *Journal of Immunology*, vol. 185, pp. 4904–4911, 2010.

[32] S. Faubel, E. C. Lewis, L. Reznikov et al., "Cisplatin-induced acute renal failure is associated with an increase in the cytokines interleukin (IL)-1beta, IL-18, IL-6, and neutrophil infiltration in the kidney," *The Journal of Pharmacology and Experimental Therapeutics*, vol. 322, pp. 8–15, 2007.

[33] B. H. Ali and M. S. Al Moundhri, "Agents ameliorating or augmenting the nephrotoxicity of cisplatin and other platinum compounds: a review of some recent research," *Food and Chemical Toxicology*, vol. 44, pp. 1173–1183, 2006.

[34] P. Chauhan, A. Sodhi, and A. Shrivastava, "Cisplatin primes murine peritoneal macrophages for enhanced expression of nitric oxide, proinflammatory cytokines, TLRs, transcription factors and activation of MAP kinases upon co-incubation with L929 cells," *Immunobiology*, vol. 214, pp. 197–209, 2009.

[35] L. H. Lu, D. J. Oh, B. Dursun et al., "Increased macrophage infiltration and fractalkine expression in cisplatin-induced acute renal failure in mice," *The Journal of Pharmacology and Experimental Therapeutics*, vol. 324, pp. 111–117, 2008.

[36] E. Y. Choi, J. Y. Jin, J. Y. Lee, J. I. Choi, I. S. Choi, and S. J. Kim, "Anti-inflammatory effects and the underlying mechanisms of action of daidzein in murine macrophages stimulated with Prevotella intermedia lipopolysaccharide," *Journal of Periodontal Research*, vol. 47, pp. 204–211, 2012.

[37] R. Domitrovic, O. Cvijanovic, E. Pernjak-Pugel, M. Skoda, L. Mikelic, and Z. Crncevic-Orlic, "Berberine exerts nephroprotective effect against cisplatin-induced kidney damage through inhibition of oxidative/nitrosative stress, inflammation, autophagy and apoptosis," *Food and Chemical Toxicology*, vol. 62, pp. 397–406, 2013.

[38] M. Ueki, M. Ueno, J. Morishita, and N. Maekawa, "Curcumin ameliorates cisplatin-induced nephrotoxicity by inhibiting renal inflammation in mice," *Journal of Bioscience and Bioengineering*, vol. 115, pp. 547–551, 2013.

[39] Y. Nozaki, K. Kinoshita, T. Yano et al., "Signaling through the interleukin-18 receptor alpha attenuates inflammation in cisplatin-induced acute kidney injury," *Kidney International*, vol. 82, pp. 892–902, 2012.

[40] S. Faubel, D. Ljubanovic, L. Reznikov, H. Somerset, C. A. Dinarello, and C. L. Edelstein, "Caspase-1-deficient mice are protected against cisplatin-induced apoptosis and acute tubular necrosis," *Kidney International*, vol. 66, pp. 2202–2213, 2004.

[41] M. G. Kim, H. N. Yang, H. W. Kim, S. K. Jo, W. Y. Cho, and H. K. Kim, "IL-10 mediates rosiglitazone-induced kidney protection in cisplatin nephrotoxicity," *Journal of Korean Medical Science*, vol. 25, pp. 557–563, 2010.

[42] G. Ramesh and W. B. Reeves, "Salicylate reduces cisplatin nephrotoxicity by inhibition of tumor necrosis factor-alpha," *Kidney International*, vol. 65, pp. 490–499, 2004.

[43] J. M. Guo, B. X. Xiao, D. J. Dai, Q. Liu, and H. H. Ma, "Effects of daidzein on estrogen-receptor-positive and negative pancreatic cancer cells in vitro," *World Journal of Gastroenterology*, vol. 10, pp. 860–863, 2004.

Hindawi
Oxidative Medicine and Cellular Longevity
Volume 2017, Article ID 2302896, 10 pages
https://doi.org/10.1155/2017/2302896

Research Article

Apigenin Alleviates Endotoxin-Induced Myocardial Toxicity by Modulating Inflammation, Oxidative Stress, and Autophagy

Fang Li,[1] Fangfang Lang,[2] Huilin Zhang,[3] Liangdong Xu,[4] Yidan Wang,[4] Chunxiao Zhai,[4] and Enkui Hao[4]

[1]*Department of Health, Jinan Central Hospital Affiliated to Shandong University, Jinan, China*
[2]*Department of Obstetrics and Gynecology, Jinan Central Hospital Affiliated to Shandong University, Jinan, China*
[3]*Central Laboratory, Jinan Central Hospital Affiliated to Shandong University, Jinan, China*
[4]*Department of Cardiology, Qianfoshan Hospital Affiliated to Shandong University, Jinan, China*

Correspondence should be addressed to Enkui Hao; haoenkui@sdu.edu.cn

Received 12 April 2017; Revised 8 June 2017; Accepted 15 June 2017; Published 30 July 2017

Academic Editor: Aditya Sen

Apigenin, a component in daily diets, demonstrates antioxidant and anti-inflammatory properties. Here, we intended to explore the mechanism of apigenin-mediated endotoxin-induced myocardial injury and its role in the interplay among inflammation, oxidative stress, and autophagy. In our lipopolysaccharide- (LPS-) induced myocardial injury model, apigenin ameliorated cardiac injury (lactate dehydrogenase (LDH) and creatine kinase (CK)), cell death (TUNEL staining, DNA fragmentation, and PARP activity), and tissue damage (cardiac troponin I (cTnI) and cardiac myosin light chain-1 (cMLC1)) and improved cardiac function (ejection fraction (EF) and end diastolic left ventricular inner dimension (LVID)). Apigenin also alleviated endotoxin-induced myocardial injury by modulating oxidative stress (nitrotyrosine and protein carbonyl) and inflammatory cytokines (TNF-α, IL-1β, MIP-1α, and MIP-2) along with their master regulator NFκB. Apigenin modulated redox homeostasis, and its anti-inflammatory role might be associated with its ability to control autophagy. Autophagy (determined by LAMP1, ATG5, and p62), its transcriptional regulator transcription factor EB (TFEB), and downstream target genes including vacuolar protein sorting-associated protein 11 (Vps11) and microtubule-associated proteins 1A/1B light chain 3B (Map1lc3) were modulated by apigenin. Thus, our study demonstrated that apigenin may lead to potential development of new target in sepsis treatment or other myocardial oxidative and/or inflammation-induced injuries.

1. Introduction

Sepsis affects significant number of people worldwide and has significant cost in emergency care and stunning high mortality rate [1]. Mortality rate is even higher in patients who have sepsis in past several years [2]. Cardiovascular risk is much higher among patients who have survived from severe sepsis [3]. Sepsis is attributed to a component of the cell wall of Gram negative bacteria: lipopolysaccharide (LPS). Cardiac dysfunction is one of the key factors in sepsis-related complications [4, 5]. The significant role of inflammation and associated activation of NFκB in LPS-induced sepsis have been reported in the literature [6–8]. Oxidative stress in sepsis is well documented [9, 10]. The role of autophagy in sepsis is crucial but the relevant research is very limited [11, 12].

Incident of cardiovascular disease is rising due to epidemic of obesity, diabetes, and hypertension [13]. Increase of oxidative stress and chronic low-grade inflammation occurs in all these health disorders in addition to aging [14, 15]. Low-grade inflammation leads to circulating immune cells and platelets, which generate superoxide as byproduct of mitochondrial respiration or by enzymatic reactions such as lipoxygenases, myeloperoxidase, NADPH oxidases, and xanthine oxidase [16]. Thus, interplay of inflammation and oxidative stress plays critical role in cardiovascular disease.

Flavonoids, present in fruits and vegetables, are polyphenols and have great potential against cardiovascular

complications including sepsis [17–19]. Apigenin, a flavonoid, is a traditional Chinese medicine isolated from celery *Apium graveolens*. Apigenin is also present in parsley and chamomile. Various researches have demonstrated that apigenin is anticancer, antioxidant, and anti-inflammatory [20–22]. Cardioprotective effects of apigenin have been reported in numerous studies. Apigenin ameliorates myocardial ischemia/reperfusion injury via the inactivation of p38 mitogen-activated protein kinase [23]. Apigenin reduces the blood pressure, heart weight, heart weight index, cardiomyocyte cross-sectional area, and serum angiotensin II in a cardiac hypertrophy model via HIF-1 and PPARα pathways [24]. In an autoimmune myocarditis model of mice, apigenin mediates protection by inhibiting lymphocyte proliferation [25]. Apigenin attenuated proinflammatory cytokine expression by inactivating NF-kappaB through the suppression of p65 phosphorylation in vitro study of human monocytes and reduced LPS-induced mortality in mice [26]. In a LPS-induced endotoxemic rat model, apigenin attenuates heart injury by suppressing sphingosine kinase 1/sphingosine 1-phosphate signaling pathway [27]. We have shown earlier the role of autophagy, inflammation, and oxidative stress in sepsis model [28] and the cardioprotective role of resveratrol in LPS-induced myocardial toxicity via NRF2 [29].

In this study, we demonstrated that apigenin protected against LPS-induced cardiac tissue damage, cardiac injury, cardiomyocyte cell death, and cardiac dysfunction. Cardioprotection by apigenin was mediated by its anti-inflammatory and antioxidant effect. Autophagy by apigenin also played a role in cardioprotection.

2. Methods

2.1. Animal Experiments. Male C57BL/6 mice that are 4–6 weeks old were obtained from the Experimental Animal Center of Shandong University (Jinan, Shandong, China). LPS was purchased from Sigma (Beijing, China). LPS was dissolved in saline and administered intraperitoneally (i.p.) as described earlier [29]. The mice were given 4 mg/kg dose of LPS and kept for 18 hours for endpoint analyses. Apigenin (>98 purity) was purchased from Shanghai Winherb Medical S&T Development Co. Ltd. (China) and administered at 50 mg/kg of body weight intraperitoneally (i.p.) 1 hour post challenge of LPS. Vehicle for drug was 5% dimethyl sulfoxide (DMSO) in sterile saline. Mice experimental protocols were approved by the Institutional Animal Care and Use Committee of Shandong University and were in compliance with the Health Ministry of the People's Republic of China. Mice were sacrificed under deep anesthesia after completion of echocardiography.

2.2. Cardiac Injury and Tissue Damage Markers. Plasma CK and LDH levels were determined using an automated analyzer (Abbott Architect, Abbot Park, Illinois, USA) as described earlier [11]. Plasma cTnI concentrations were measured by ELISA-based assay according to the manufacturer's protocol (Abnova, Taiwan). Plasma cardiac myosin light chain-1 (cMLC1) was determined by ELISA (Life Diagnostics Inc., USA) according to the manufacturer's protocol. Both were described earlier [28].

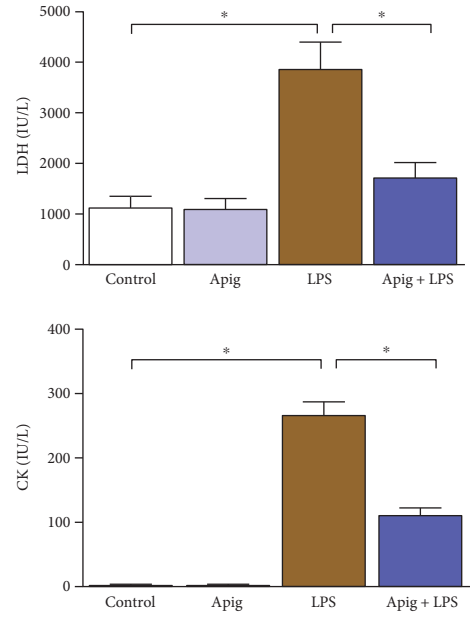

Figure 1: Apigenin attenuates LPS-induced cardiac injuries. Cardiac injuries were measured by plasma LDH and CK. LDH and CK plasma levels were increased in LPS-treated mice. Increase of LPS-induced cardiac injury was significantly attenuated by apigenin treatment. Values represented as means ± SD; $^*P < 0.05$ and $n = 6$/group. Control was a vehicle-treated group where Apig was apigenin-treated group. LPS and Apig + LPS were administered with LPS along with posttreatment of vehicle or apigenin. Same nomenclature was used in all other figures.

2.3. Echocardiography. Echocardiographic cardiac parameters were determined as described earlier [29, 30].

2.4. Real-Time PCR. Total RNA was isolated by QIAzol method and reverse transcribed by OneStep Ahead RT-PCR Kit (Qiagen). All predesigned primers were purchased from Qiagen. mRNA level of TNF-α (tumor necrosis factor), IL-1β (interleukin 1 beta), MIP-2 (macrophage inflammatory protein-2), MCP1 (CD46), MAP1lc3 (microtubule-associated protein 1 light chain 3), VPS11 (vacuolar protein sorting-associated protein 11), or β-actin was detected by real-time PCR. The fold changes were determined by relative quantification method as described earlier [29].

2.5. Western Blot. Heart tissues were homogenized in lysis buffer, and protein concentration was determined as described earlier [29]. Nuclear and cytoplasmic fractions were isolated as described earlier [29]. PVDF membranes were incubated with TNF-α (1 : 200, Santa Cruz Biotechnology), MIP-2 (1 : 100, Abcam China), tubulin, NFκB p65 antibody, anti-TFEB antibody, LAMP1, ATG5, p62, and histone H3 (1 : 200, Santa Cruz Biotechnology) overnight at 4°C. After three repeated washes, the membranes were probed with corresponding HRP-conjugated secondary antibody (1 : 2000, Rockland, Gilbertsville) for 1 h at room temperature. After three repeated washes, the membranes were

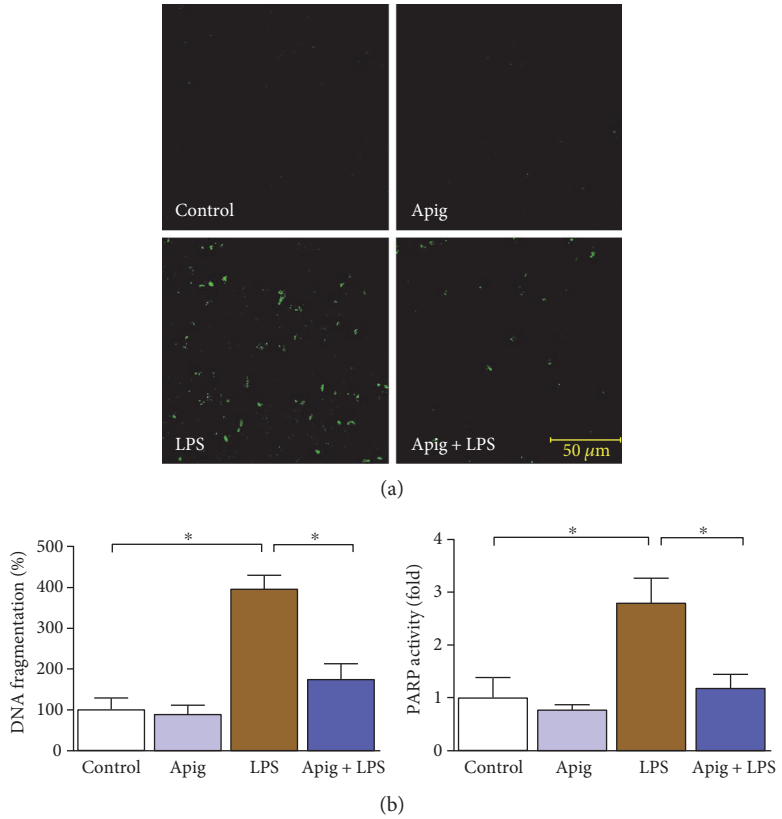

Figure 2: Apigenin attenuates LPS-induced cardiac cell death. (a) TUNEL staining performed on paraffin section of mice heart in each group and representative fluorescent images were provided. Green color demonstrated TUNEL-positive nuclei. Scale bar was provided in representative Apig + LPS image. (b) Cardiac cell death markers DNA fragmentation and PARP activity assay were examined. Both DNA fragmentation and PARP activity were significantly increased in LPS-treated mice, and apigenin treatment ameliorated those elevated level. Values represented as means ± SD; $^*P < 0.05$ and $n = 6$/group.

detected by chemiluminescence and were exposed on an X-ray film for autoradiography.

2.6. Cardiac Cell Death Markers. DNA fragmentation was measured by ELISA-based kit (Roche) as described earlier [29]. For PARP activity, we used the HT Universal Colorimetric PARP assay kit from Trevigen as described earlier [31].

2.7. Cardiac TUNEL Staining. All TUNEL staining were performed with the In Situ Cell Death Detection Kit (Roche Applied Science) according to the manufacturer's instructions and published earlier [32].

2.8. Cardiac Glutathione Level. Cardiac glutathione levels from tissue lysates were determined by GSR-DTNB recycling assay and used in previous publication [33].

2.9. Cardiac Oxidative Stress Markers. Protein nitrotyrosine nitration was determined using OxiSelect™ Nitrotyrosine ELISA Kit (Cell Biolabs) as described earlier [12]. Carbonyl content in protein from tissue lysate was determined by Protein Carbonyl Colorimetric Assay Kit (Cayman Chemical) as described earlier [28].

2.10. Statistical Analysis. Data were expressed as mean ± standard deviation (SD), and statistical analysis was done by using GraphPad Prism software. Paired *t*-test or one-way analysis of variance followed by Tukey's posttest was performed and considered statistically significant.

3. Results and Discussion

3.1. Apigenin Attenuates Endotoxin-Induced Myocardial Injury and Cell Death of Cardiomyocytes in Mice. To examine cardioprotective effect of apigenin, we administered 4 mg/kg of LPS for 18 hours in C57BL/6 mice posttreated with either vehicle (control) or apigenin. LPS-induced myocardial injury was evident by increase in LDH and CK (Figure 1). Aginenin treatment significantly reduced LPS-induced myocardial injury. Cell death including apoptotic cell death markers were determined by TUNEL staining (Figure 2(a)). Quantitative cell death markers DNA fragmentation and PARP activity were determined and both were induced at 398% and 2.8-fold in response to LPS, respectively. Both markers, DNA fragmentation and PARP activity, were reduced to 55% and 57%, respectively, by apigenin treatment (Figure 2(b)). Cardiac troponin I (cTnI) and cardiac myosin light chain-1 (cMLC1) are proficient markers of acute heart disorders specifically for heart muscle cell death. cTnI and cMLC1 were induced by LPS administration to 6.3 ng/ml and 0.89 ng/ml in mice serum

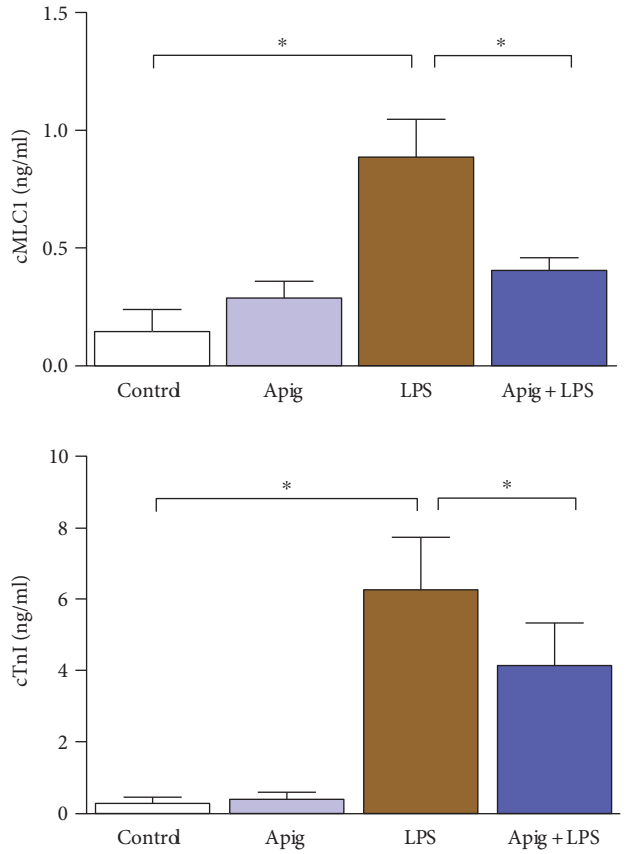

Figure 3: Apigenin attenuates LPS-induced cardiac damage. Cardiac damage was measured by plasma cTnI and cMLC1, which were secreted by damaged cardiomyocytes from the heart. Both of them were significantly increased in LPS-treated mice and were significantly attenuated by apigenin treatment. Values represented as means ± SD; $^*P < 0.05$ and $n = 6$/group.

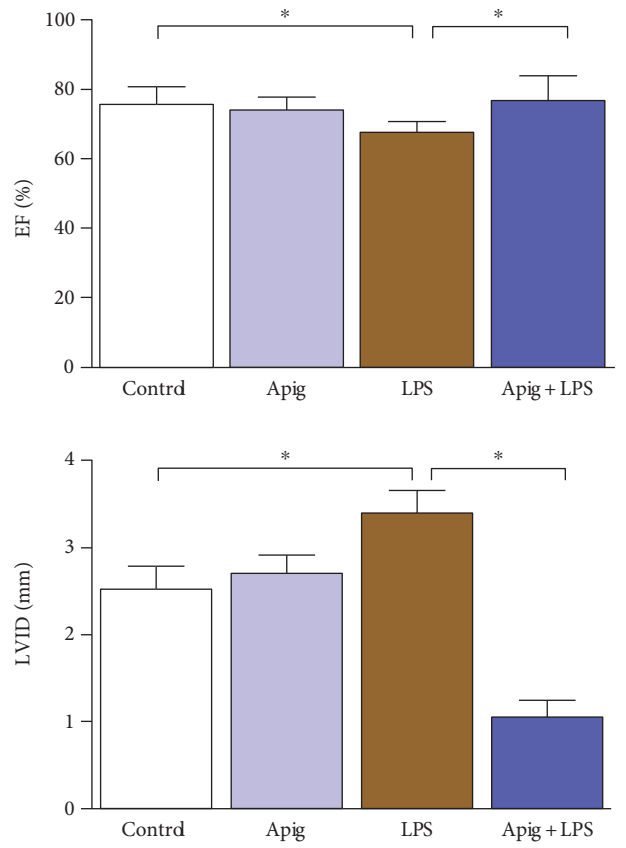

Figure 4: Apigenin improves LPS-induced cardiac dysfunction. Cardiac function parameters ejection fraction (EF) and left ventricular internal dimension (LVID) were measured by echocardiography. LVID was significantly increased whereas EF was decreased in LPS-treated mice. Apigenin reversed those changes and improved function. Values represented as means ± SD; $^*P < 0.05$ and $n = 6$/group.

from 0.34 ng/ml and 0.14 ng/ml in the control group, respectively (Figure 3). Treatment with apigenin significantly attenuated LPS-induced serum cTnI and cMLC1 to 4.22 and 0.42, respectively. Cardiac function parameters such as left ventricular (LV) structure and function were assessed by echocardiography. LPS administration cause a decrease in ejection fraction (EF) and an increase of end diastolic left ventricular inner dimension (LVID), which was significantly attenuated by apigenin administration (Figure 4). The heart rates of the mice among all the four treatment groups were not statistically different. Treatment with apigenin alone did not alter any cardiac injury markers or function in the above experiments.

Multiple factors have been demonstrated to be involved in the endotoxin-mediated myocardial injury and cardiac dysfunction [5, 34–36]. Consistent with previous findings, our in vivo experiments indicated that LPS dramatically increased the plasma level of LDH, CK, cMLC1, cTnI, and cell death markers TUNEL staining, DNA fragmentation, and PARP activity. Apigenin treatment significantly reduced all the above markers. Primary mechanism of cell death in sepsis is by both apoptosis and necrosis with overlapping signaling pathways. In apoptosis, cell shrinkage and associated loss of myocardial structure leads to cardiac dysfunction [37]. In necrosis, an inflammatory response occurs, which also cause cardiac dysfunction [37]. We observed both types of cell death and apigenin-reduced cell death and cardiac dysfunction.

Pharmacokinetics study of apigenin in a rat model demonstrated that apigenin can be available in the system up to 10 days [38]. Apigenin can be found in human red blood cells after parsley consumption and thus increase its distribution and bioavailability [39]. We also observed that apigenin treatment improved LPS-induced cardiac dysfunction. In a long-term study of diabetic cardiomyopathy in mice, apigenin administration improves left ventricular functions in the heart [40]. Apigenin also improves the recovery of cardiac function during ischemia/reperfusion injury of isolated rat heart using Langedorff system [23]. Thus, our data on apigenin-mediated recovery of myocardial injury and cardiac dysfunction may lead to potential therapeutic development in sepsis.

3.2. Apigenin Suppresses Endotoxin-Induced Production of Proinflammatory Cytokines, NFκB, and Oxidative Stress.

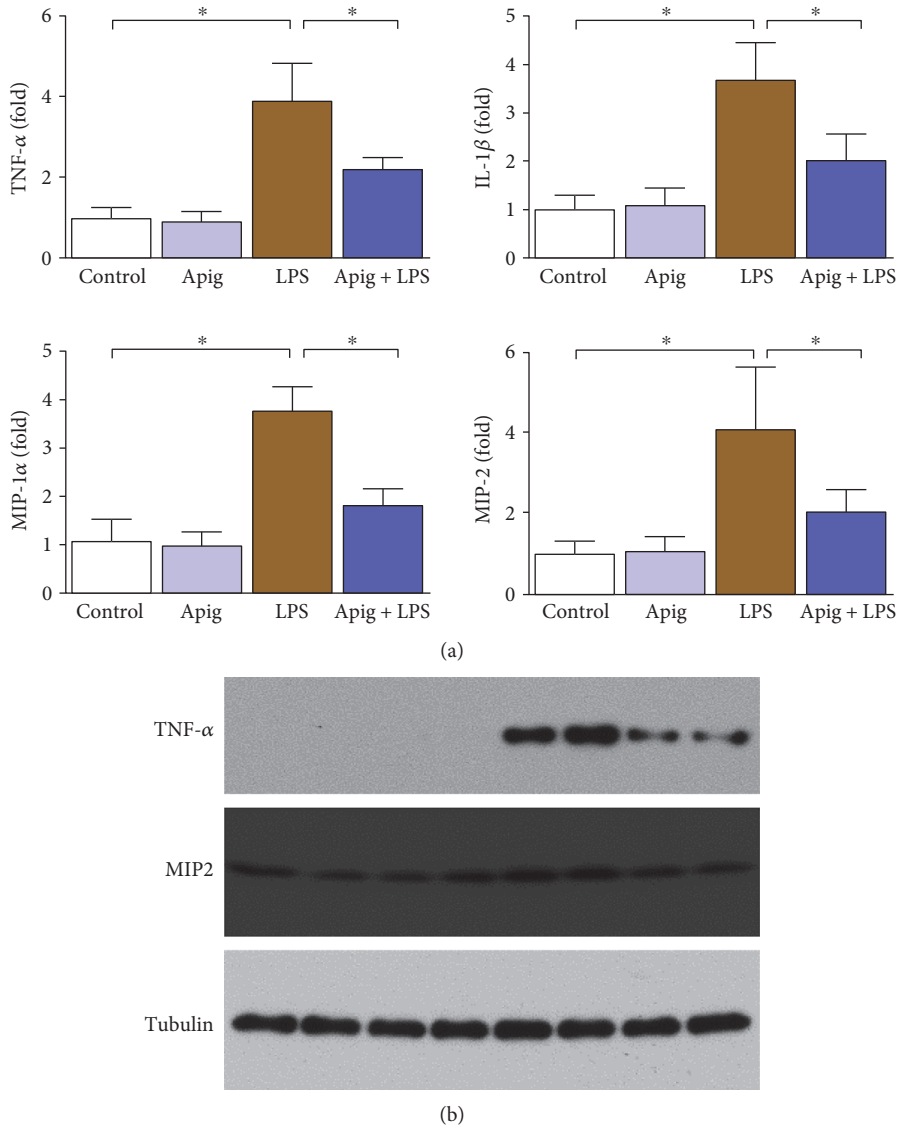

Figure 5: Apigenin attenuates LPS-induced cardiac proinflammatory cytokines. (a) Cardiac inflammation markers TNF-α, IL-1β, MIP-1?, and MIP-2 were measured by real-time PCR, and apigenin treatment significantly attenuated LPS-induced proinflammatory cytokines. Values represented as means ± SD; $^*P < 0.05$ and $n = 6$/group. (b) Protein level verification of TNF-α and MIP-2 performed by Western blot analyses where tubulin was used as a loading control.

Real-time PCR analyses of proinflammatory cytokines demonstrated induction of TNF-α, IL-1β, MIP-1α, and MIP-2 by LPS administration up to 3.9, 3.7, 3.8, and 4.1, respectively. Apigenin treatment reduced LPS-induced cytokine gene expression by 43%, 45%, 51%, and 48% for TNF-α, IL-1β, MIP-1α, and MIP-2, respectively (Figure 5(a)). Two proinflammatory cytokines were verified at protein level, and it was consistent with mRNA level (Figure 5(b)). Western blot analyses demonstrated that NFκB p65 was increased in nuclear fraction in heart lysate from LPS-treated mice and such increase was significantly reduced with apigenin treatment (Figure 6(a)). Similar analyses with cytoplasmic fraction also demonstrated that the cytoplasmic level of p65 was decreased by endotoxin and apigenin treatment restored to normal. NFκB pathway is considered a conventional proinflammatory signaling pathway [41]. NFκB is implicated in the expression of proinflammatory sources including cytokines, chemokines, and adhesion molecules. In sepsis, canonical pathways of NFκB activation occurs [42]. Role of NFκB activation is critical in inhibition of lipopolysaccharide-induced shock [43]. Thus, inhibition of p65 nuclear localization by apigenin in endotoxin-induced sepsis was beneficial.

Quantitative determination of oxidative stress markers protein nitrotyrosine and protein carbonyl by ELISA demonstrated significant increase 3.6 and 5.1, respectively. Apigenin attenuated LPS-induced protein nitrotyrosine and protein carbonyl by 61% and 515, respectively (Figure 6(b)). We also determined glutathione level in both oxidized (GSSG) and reduced (GSH) form. Endotoxin induced oxidized

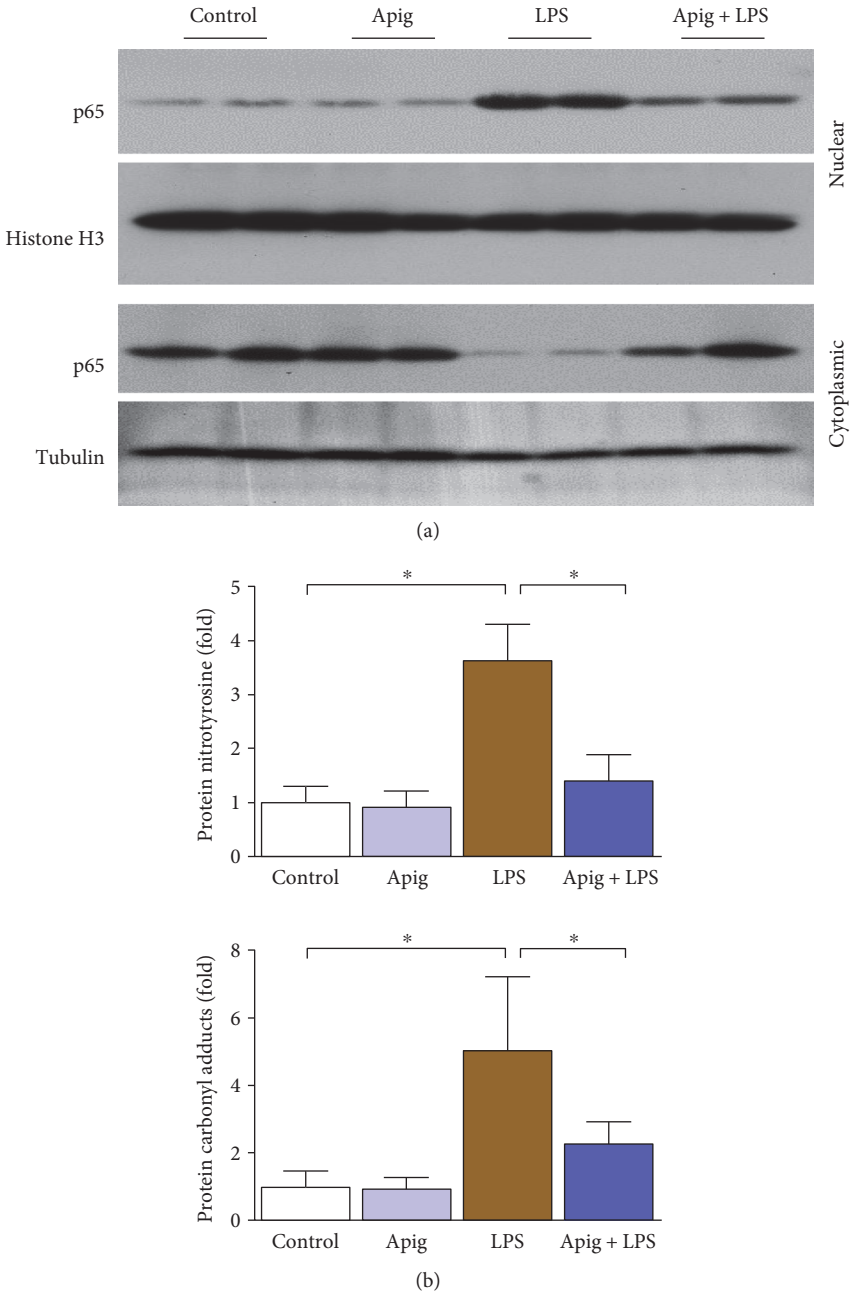

Figure 6: Apigenin attenuates LPS-induced cardiac NFκB nuclear translocation and oxidative damage. (a) Western blot analyses of NFκB (p65) in nuclear and cytoplasmic fractions from heart lysates. Histone H3 was used as a nuclear control whereas tubulin was used as a cytoplasmic control. (b) Cardiac oxidative markers protein nitration and carbonyl content measured by quantitative ELISA. All markers were significantly increased in LPS-treated mice. Apigenin significantly reduced LPS-induced oxidative stress markers. Values represented as means ± SD; $^*P < 0.05$ and $n = 6$/group.

glutathione level and decreased reduced glutathione level, which were reversed by apigenin treatment (Figure 7).

Endotoxin-induced myocardial injury is associated with defects in redox balance and antioxidant enzymes, which leads to inflammation [44]. We have shown earlier the role of NRF2 in the sepsis and the protective effect by resveratrol [29]. In consistent with earlier literatures, we found increase in oxidative stress markers nitrotyrosine and protein carbonyl by LPS. LPS also induced inflammatory cytokines. Apigenin treatment significantly reduced both oxidative stress and inflammatory response. In a rat model of sepsis, cecal ligation and puncture induces oxidative stress and inflammatory response in the spleen and is attenuated by apigenin [45]. In another rat model of LPS-induced sepsis, apigenin ameliorates inflammatory response by suppressing sphingosine kinase 1 pathway, known as modulator of transcription factor NFκB [27]. We also observed in this study that LPS-induced nuclear translocation of NFκB was attenuated by apigenin. Apigenin inhibits the release of cytokines and suppresses NFκB activity in LPS-stimulated

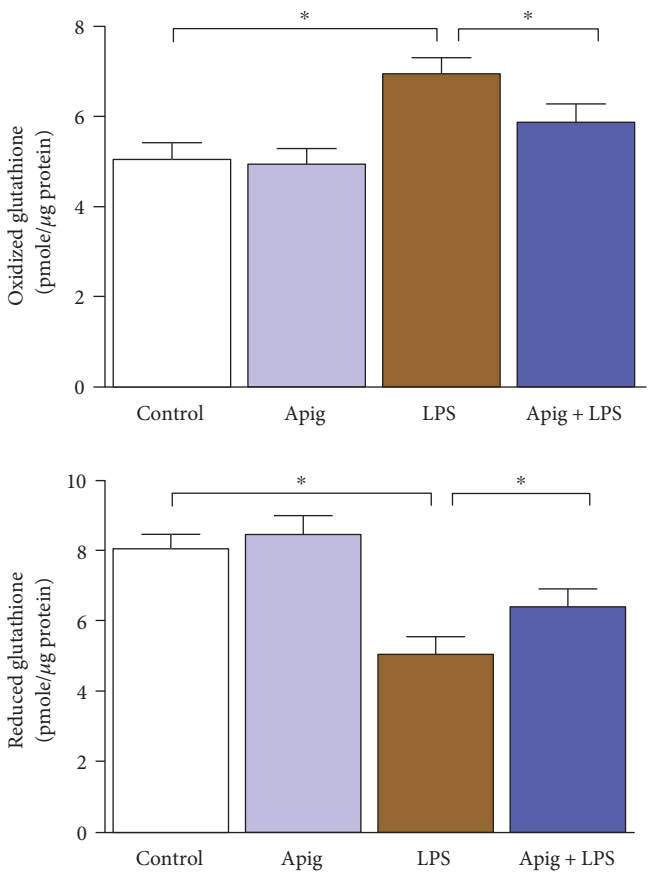

Figure 7: Apigenin restores LPS-induced redox status of glutathione. Apigenin restores LPS-induced oxidized glutathione. LPS downregulated reduced glutathione, which was restored by apigenin. Values represented as means ± SD; $^*P < 0.05$ and $n = 6$/group.

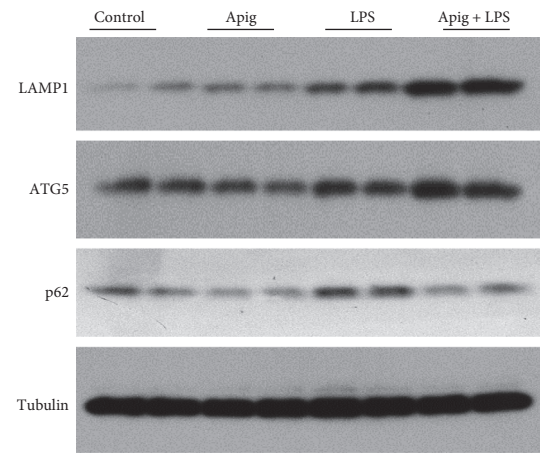

Figure 8: Effect of apigenin on autophagy pathway. Western blot analyses of three autophagy markers LAMP1, ATG5, and p62 along with control protein tubulin. Apigenin induces autophagy protein in LPS-treated mice where p62 is downregulated in the same samples.

monocytes isolated from human donor [26]. In a recent report, apigenin reduces NFκB-associated neuroinflammation in a diet-induced obesity model of rat [46]. Thus, our study demonstrating apigenin as antioxidant and anti-inflammatory modulator via NFκB in endotoxin-induced myocardial injury may be effective to other inflammatory heart injury models such as myocarditis.

3.3. Apigenin Modulates Autophagy in Endotoxin-Induced Cardiac Injury. In animal model of sepsis and in clinical setting of sepsis, cardiac autophagy is increased [47]. Autophagy is also beneficial for cardioprotection during sepsis [48]. We examined autophagy by Western blot analyses of LAMP1, ATG5, and p62 (Figure 8). All three autophagy markers were increased in endotoxin-induced cardiac injury. Apigenin enhanced LAMP1 and ATG5 protein levels whereas p62 level was decreased by apigenin. These findings were in consistent with the fact that apigenin induced autophagy as p62 level was decreased and is a marker of autophagy induction in addition to be degraded by autophagy linking ubiquitinated proteins to the autophagic machinery in the lysosome [49]. Western blot analyses of nuclear fraction demonstrated that TFEB, a major modulator of autophagy and associated CLEAR pathway, was increased by both LPS and apigenin alone. Apigenin treatment along with LPS significantly enhanced nuclear localization (Figure 9(a)). To understand the functional role of nuclear translocation of TFEB, we determined two of its target genes Vps11 and Map1lc3 by real-time PCR (Figure 9(b)). LPS induced Vps11 and Map1lc3 gene expression by 1.53- and 1.83-fold, respectively. Apigenin treatment enhanced further LPS-induced gene expression to 2.6- and 2.9-fold for Vps11 and Map1lc3, respectively.

Flavonoids are known to modulate autophagy in a variety of pathological condition or physiological processes in animal models [50–53]. We have shown earlier that TFEB-mediated autophagy is modulated during aging [28]. In this study, we found that apigenin modulated autophagy pathway during sepsis. Curcumin, a flavonoid, also targets TFEB for induction of autophagy [54]. Recent literatures demonstrate the link of flavonoids with TFEB and/or autophagy [55–57]. Autophagy is also regulator for cardiovascular redox homeostasis and thus interplay of oxidative stress, autophagy, and inflammation is crucial in apigenin-mediated cardioprotection [58, 59]. We observed the protective role of TFEB and its downstream targets in LPS-induced myocardial injury and its modulation by apigenin. In doxorubicin-induced cardiomyopathy, TFEB is also modulated [60]. However, activation of autophagy has been identified as cardioprotective in some settings, but in other cases, sustained autophagy has been linked with cardiopathology [61]. Autophagy is thus known for its function as a double-edged sword [62, 63]. In this study, autophagy may work as redox homeostasis, enhancing the lysomal degradation of LPS-induced myocardial injury. Both are important for apigenin-mediated cardioprotection.

Our study on apigenin-mediated protection of endotoxin-induced myocardial injury demonstrated interplay of oxidative stress, inflammation, and autophagy. Increased cell death lead to increased inflammation, which

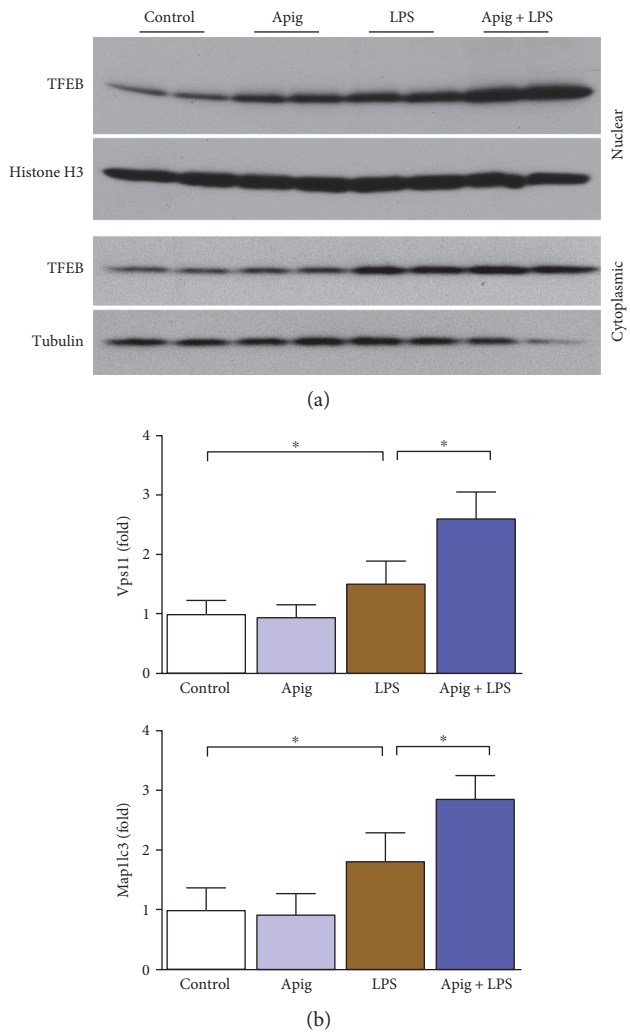

Figure 9: Apigenin enhances LPS-induced TFEB nuclear localization and its downstream genes Vps11 and Map1lc3. (a) Western blot analyses of TFEB in nuclear and cytoplasmic fraction from heart lysates. Histone H3 was used as a nuclear control whereas tubulin was used as a cytoplasmic control. (b) TFEB-regulated genes Map1lc3 and Vps11 were examined at mRNA level by real-time PCR. LPS induced mRNA level in both genes whereas apigenin further enhanced those mRNA expression. Values represented as means ± SD; $^*P < 0.05$ and $n = 6$/group.

is linked to increased oxidative stress. This process goes in cycle and thus enhances the damaging effect of endotoxin. Autophagy and antioxidant defense are also linked [64]. Autophagy regulates both redox balance and ROS formation, and autophagy plays a major role in the degradation of oxidized proteins [65].

4. Conclusion

We demonstrated that apigenin protects against LPS-induced cardiac injury, tissue damage, and cardiomyocyte cell death. Apigenin improves LPS-induced cardiac dysfunction. Apigenin-mediated protection against LPS-induced myocardial toxicity is mediated by multiple mechanisms where inflammation and oxidative stress were modulated

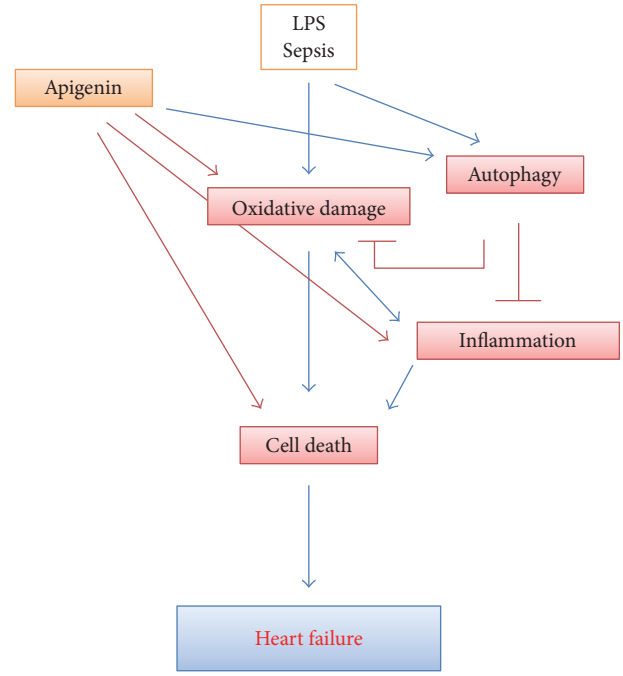

Figure 10: Schematic diagram of apigenin-mediated protection in LPS-induced myocardial toxicity and heart failure. Interplay of autophagy with oxidative damage and inflammation plays a critical role in pathophysiology of sepsis-induced cardiac dysfunction which results in heart failure. By enhancing autophagy, apigenin reduces oxidative damage, which also leads to inflammation and cell death.

by apigenin along with their master regulator NFκB. In addition to that, autophagic pathway regulator TFEB was enhanced by apigenin. Due to autophagy enhancement, apigenin reduced LPS-induced inflammation and oxidative stress (Figure 10). Thus, the interplay of autophagy, inflammation, and oxidative stress and its modulation by apigenin played important role in cardioprotection.

Conflicts of Interest

The authors declare that they have no competing interests.

Acknowledgments

This study was supported by the Science and Technology Project of Shandong Province (Grant no. 2014GSF118187).

References

[1] E. Papathanassoglou, N. Middleton, J. Benbenishty, G. Williams, M. D. Christofi, and K. Hegadoren, "Systematic review of gender-dependent outcomes in sepsis," *Nursing in Critical Care*, 2017.

[2] S. Yende, T. J. Iwashyna, and D. C. Angus, "Interplay between sepsis and chronic health," *Trends in Molecular Medicine*, vol. 20, no. 4, pp. 234–238, 2014.

[3] S. Yende, W. Linde-Zwirble, F. Mayr, L. A. Weissfeld, S. Reis, and D. C. Angus, "Risk of cardiovascular events in survivors

of severe sepsis," *American Journal of Respiratory and Critical Care Medicine*, vol. 189, no. 9, pp. 1065–1074, 2014.

[4] K. Drosatos, A. Lymperopoulos, P. J. Kennel, N. Pollak, P. C. Schulze, and I. J. Goldberg, "Pathophysiology of sepsis-related cardiac dysfunction: driven by inflammation, energy mismanagement, or both?" *Current Heart Failure Reports*, vol. 12, no. 2, pp. 130–140, 2015.

[5] K. E. Fenton and M. M. Parker, "Cardiac function and dysfunction in sepsis," *Clinics in Chest Medicine*, vol. 37, no. 2, pp. 289–298, 2016.

[6] C. V. Rosadini and J. C. Kagan, "Early innate immune responses to bacterial LPS," *Current Opinion in Immunology*, vol. 44, pp. 14–19, 2016.

[7] X. Lv and H. Wang, "Pathophysiology of sepsis-induced myocardial dysfunction," *Military Medical Research*, vol. 3, p. 30, 2016.

[8] Y. Kakihana, T. Ito, M. Nakahara, K. Yamaguchi, and T. Yasuda, "Sepsis-induced myocardial dysfunction: pathophysiology and management," *Journal of Intensive Care*, vol. 4, p. 22, 2016.

[9] D. Bar-Or, M. M. Carrick, C. W. Mains, L. T. Rael, D. Slone, and E. N. Brody, "Sepsis, oxidative stress, and hypoxia: are there clues to better treatment?" *Redox Report*, vol. 20, no. 5, pp. 193–197, 2015.

[10] M. Rajesh, L. Cai, P. Mukhopadhyay, and S. Vedantham, "Redox signaling and myocardial cell death: molecular mechanisms and drug targets," *Oxidative Medicine and Cellular Longevity*, vol. 2016, Article ID 3190753, 2 pages, 2016.

[11] A. J. Lewis, T. R. Billiar, and M. R. Rosengart, "Biology and metabolism of sepsis: innate immunity, bioenergetics, and autophagy," *Surgical Infections (Larchmt)*, vol. 17, no. 3, pp. 286–293, 2016.

[12] Y. Mejias-Pena, B. Estebanez, P. Rodriguez-Miguelez et al., "Impact of resistance training on the autophagy-inflammation-apoptosis crosstalk in elderly subjects," *Aging (Albany NY)*, vol. 9, no. 2, pp. 408–418, 2017.

[13] J. Wu, S. Xia, B. Kalionis, W. Wan, and T. Sun, "The role of oxidative stress and inflammation in cardiovascular aging," *BioMed Research International*, vol. 2014, Article ID 615312, 13 pages, 2014.

[14] C. Franceschi, M. Bonafe, S. Valensin et al., "Inflamm-aging. An evolutionary perspective on immunosenescence," *Annals of the new York Academy of Sciences*, vol. 908, pp. 244–254, 2000.

[15] N. Garcia, C. Zazueta, and L. Aguilera-Aguirre, "Oxidative stress and inflammation in cardiovascular disease," *Oxidative Medicine and Cellular Longevity*, vol. 2017, Article ID 5853238, 2 pages, 2017.

[16] J. A. Leopold and J. Loscalzo, "Oxidative risk for atherothrombotic cardiovascular disease," *Free Radical Biology and Medicine*, vol. 47, no. 12, pp. 1673–1706, 2009.

[17] P. Mukhopadhyay, S. Mukherjee, K. Ahsan, A. Bagchi, P. Pacher, and D. K. Das, "Restoration of altered microRNA expression in the ischemic heart with resveratrol," *PLoS One*, vol. 5, no. 12, article e15705, 2010.

[18] H. Shapiro, S. Lev, J. Cohen, and P. Singer, "Polyphenols in the prevention and treatment of sepsis syndromes: rationale and pre-clinical evidence," *Nutrition*, vol. 25, no. 10, pp. 981–997, 2009.

[19] D. S. Wheeler, P. M. Lahni, P. W. Hake et al., "The green tea polyphenol epigallocatechin-3-gallate improves systemic hemodynamics and survival in rodent models of polymicrobial sepsis," *Shock*, vol. 28, no. 3, pp. 353–359, 2007.

[20] B. Sung, H. Y. Chung, and N. D. Kim, "Role of apigenin in cancer prevention via the induction of apoptosis and autophagy," *Journal of Cancer Prevention*, vol. 21, no. 4, pp. 216–226, 2016.

[21] M. Venigalla, E. Gyengesi, and G. Munch, "Curcumin and apigenin - novel and promising therapeutics against chronic neuroinflammation in Alzheimer's disease," *Neural Regeneration Research*, vol. 10, no. 8, pp. 1181–1185, 2015.

[22] N. Leyva-Lopez, E. P. Gutierrez-Grijalva, D. L. Ambriz-Perez, and J. B. Heredia, "Flavonoids as cytokine modulators: a possible therapy for inflammation-related diseases," *International Journal of Molecular Sciences*, vol. 17, no. 6, 2016.

[23] X. Yang, J. Yang, J. Hu, X. Li, X. Zhang, and Z. Li, "Apigenin attenuates myocardial ischemia/reperfusion injury via the inactivation of p38 mitogen activated protein kinase," *Molecular Medicine Reports*, vol. 12, no. 5, pp. 6873–6878, 2015.

[24] Z. Y. Zhu, T. Gao, Y. Huang, J. Xue, and M. L. Xie, "Apigenin ameliorates hypertension-induced cardiac hypertrophy and down-regulates cardiac hypoxia inducible factor-lalpha in rats," *Food & Function*, vol. 7, no. 4, pp. 1992–1998, 2016.

[25] S. Zhang, X. Liu, C. Sun et al., "Apigenin attenuates experimental autoimmune myocarditis by modulating Th1/Th2 cytokine balance in mice," *Inflammation*, vol. 39, no. 2, pp. 678–686, 2016.

[26] C. Nicholas, S. Batra, M. A. Vargo et al., "Apigenin blocks lipopolysaccharide-induced lethality in vivo and proinflammatory cytokines expression by inactivating NF-kappaB through the suppression of p65 phosphorylation," *Journal of Immunology*, vol. 179, no. 10, pp. 7121–7127, 2007.

[27] T. Zhang, T. Yan, J. Du, S. Wang, and H. Yang, "Apigenin attenuates heart injury in lipopolysaccharide-induced endotoxemic model by suppressing sphingosine kinase 1/sphingosine 1-phosphate signaling pathway," *Chemico-Biological Interactions*, vol. 233, pp. 46–55, 2015.

[28] F. Li, F. Lang, H. Zhang, L. Xu, Y. Wang, and E. Hao, "Role of TFEB mediated autophagy, oxidative stress, inflammation, and cell death in endotoxin induced myocardial toxicity of young and aged mice," *Oxidative Medicine and Cellular Longevity*, vol. 2016, Article ID 5380319, 10 pages, 2016.

[29] E. Hao, F. Lang, Y. Chen et al., "Resveratrol alleviates endotoxin-induced myocardial toxicity via the Nrf2 transcription factor," *PLoS One*, vol. 8, no. 7, article e69452, 2013.

[30] M. K. ElZarrad, P. Mukhopadhyay, N. Mohan et al., "Trastuzumab alters the expression of genes essential for cardiac function and induces ultrastructural changes of cardiomyocytes in mice," *PLoS One*, vol. 8, no. 11, article e79543, 2013.

[31] P. Mukhopadhyay, M. Rajesh, Z. Cao et al., "Poly (ADP-ribose) polymerase-1 is a key mediator of liver inflammation and fibrosis," *Hepatology*, vol. 59, no. 5, pp. 1998–2009, 2014.

[32] L. An, X. Zhao, J. Wu et al., "Involvement of autophagy in cardiac remodeling in transgenic mice with cardiac specific over-expression of human programmed cell death 5," *PLoS One*, vol. 7, no. 1, article e30097, 2012.

[33] I. H. Dias, I. L. Chapple, M. Milward et al., "Sulforaphane restores cellular glutathione levels and reduces chronic periodontitis neutrophil hyperactivity in vitro," *PLoS One*, vol. 8, no. 6, article e66407, 2013.

[34] L. Liaudet, N. Rosenblatt-Velin, and P. Pacher, "Role of peroxynitrite in the cardiovascular dysfunction of septic

shock," *Current Vascular Pharmacology*, vol. 11, no. 2, pp. 196–207, 2013.

[35] P. Bentzer, J. A. Russell, and K. R. Walley, "Advances in sepsis research," *Clinics in Chest Medicine*, vol. 36, no. 3, pp. 521–530, 2015.

[36] D. N. Mannel, "Advances in sepsis research derived from animal models," *International Journal of Medical Microbiology*, vol. 297, no. 5, pp. 393–400, 2007.

[37] K. Konstantinidis, R. S. Whelan, and R. N. Kitsis, "Mechanisms of cell death in heart disease," *Arteriosclerosis, Thrombosis, and Vascular Biology*, vol. 32, no. 7, pp. 1552–1562, 2012.

[38] A. Gradolatto, J. P. Basly, R. Berges et al., "Pharmacokinetics and metabolism of apigenin in female and male rats after a single oral administration," *Drug Metabolism and Disposition*, vol. 33, no. 1, pp. 49–54, 2005.

[39] H. Meyer, A. Bolarinwa, G. Wolfram, and J. Linseisen, "Bioavailability of apigenin from apiin-rich parsley in humans," *Annals of Nutrition & Metabolism*, vol. 50, no. 3, pp. 167–172, 2006.

[40] H. J. Liu, Y. L. Fan, H. H. Liao et al., "Apigenin alleviates STZ-induced diabetic cardiomyopathy," *Molecular and Cellular Biochemistry*, vol. 428, no. 1-2, pp. 9–21, 2017.

[41] T. Lawrence, "The nuclear factor NF-kappaB pathway in inflammation," *Cold Spring Harbor Perspectives in Biology*, vol. 1, no. 6, article a001651, 2009.

[42] S. Ghosh and M. Karin, "Missing pieces in the NF-kappaB puzzle," *Cell*, vol. 109, pp. S81–S96, 2002.

[43] M. Gadjeva, M. F. Tomczak, M. Zhang et al., "A role for NF-kappa B subunits p50 and p65 in the inhibition of lipopolysaccharide-induced shock," *Journal of Immunology*, vol. 173, no. 9, pp. 5786–5793, 2004.

[44] M. Bosmann and P. A. Ward, "The inflammatory response in sepsis," *Trends in Immunology*, vol. 34, no. 3, pp. 129–136, 2013.

[45] M. Karamese, H. S. Erol, M. Albayrak, G. Findik Guvendi, E. Aydin, and K. S. Aksak, "Anti-oxidant and anti-inflammatory effects of apigenin in a rat model of sepsis: an immunological, biochemical, and histopathological study," *Immunopharmacology and Immunotoxicology*, vol. 38, no. 3, pp. 228–237, 2016.

[46] J. Kalivarathan, S. P. Chandrasekaran, K. Kalaivanan, V. Ramachandran, and V. A. Carani, "Apigenin attenuates hippocampal oxidative events, inflammation and pathological alterations in rats fed high fat, fructose diet," *Biomedicine & Pharmacotherapy*, vol. 89, pp. 323–331, 2017.

[47] Q. S. Zang, S. E. Wolf, and J. P. Minei, "Sepsis-induced cardiac mitochondrial damage and potential therapeutic interventions in the elderly," *Aging and Disease*, vol. 5, no. 2, pp. 137–149, 2014.

[48] C. H. Hsieh, P. Y. Pai, H. W. Hsueh, S. S. Yuan, and Y. C. Hsieh, "Complete induction of autophagy is essential for cardioprotection in sepsis," *Annals of Surgery*, vol. 253, no. 6, pp. 1190–1200, 2011.

[49] G. Bjorkoy, T. Lamark, S. Pankiv, A. Overvatn, A. Brech, and T. Johansen, "Monitoring autophagic degradation of p62/SQSTM1," *Methods in Enzymology*, vol. 452, pp. 181–197, 2009.

[50] M. Reinisalo, A. Karlund, A. Koskela, K. Kaarniranta, and R. O. Karjalainen, "Polyphenol stilbenes: molecular mechanisms of defence against oxidative stress and aging-related diseases," *Oxidative Medicine and Cellular Longevity*, vol. 2015, Article ID 340520, 24 pages, 2015.

[51] N. K. Zenkov, A. V. Chechushkov, P. M. Kozhin, N. V. Kandalintseva, G. G. Martinovich, and E. B. Menshchikova, "Plant phenols and autophagy," *Biochemistry (Mosc)*, vol. 81, no. 4, pp. 297–314, 2016.

[52] K. Pallauf and G. Rimbach, "Autophagy, polyphenols and healthy ageing," *Ageing Research Reviews*, vol. 12, no. 1, pp. 237–252, 2013.

[53] N. Ferrari, F. Tosetti, S. De Flora et al., "Diet-derived phytochemicals: from cancer chemoprevention to cardio-oncological prevention," *Current Drug Targets*, vol. 12, no. 13, pp. 1909–1924, 2011.

[54] J. Zhang, J. Wang, J. Xu et al., "Curcumin targets the TFEB-lysosome pathway for induction of autophagy," *Oncotarget*, vol. 7, no. 46, pp. 75659–75671, 2016.

[55] M. Moskot, S. Montefusco, J. Jakobkiewicz-Banecka et al., "The phytoestrogen genistein modulates lysosomal metabolism and transcription factor EB (TFEB) activation," *The Journal of Biological Chemistry*, vol. 289, no. 24, pp. 17054–17069, 2014.

[56] L. S. Gan, L. W. Zeng, X. R. Li, C. X. Zhou, and J. Li, "New homoisoflavonoid analogues protect cells by regulating autophagy," *Bioorganic & Medicinal Chemistry Letters*, vol. 27, no. 6, pp. 1441–1445, 2017.

[57] P. W. Zhang, C. Tian, F. Y. Xu et al., "Green tea polyphenols alleviate autophagy inhibition induced by high glucose in endothelial cells," *Biomedical and Environmental Sciences*, vol. 29, no. 7, pp. 524–528, 2016.

[58] Y. Yan and T. Finkel, "Autophagy as a regulator of cardiovascular redox homeostasis," *Free Radical Biology and Medicine*, vol. 109, pp. 108–113, 2017.

[59] S. Lavandero, M. Chiong, B. A. Rothermel, and J. A. Hill, "Autophagy in cardiovascular biology," *The Journal of Clinical Investigation*, vol. 125, no. 1, pp. 55–64, 2015.

[60] J. J. Bartlett, P. C. Trivedi, and T. Pulinilkunnil, "Autophagic dysregulation in doxorubicin cardiomyopathy," *Journal of Molecular and Cellular Cardiology*, vol. 104, pp. 1–8, 2017.

[61] L. M. Delbridge, K. M. Mellor, D. J. Taylor, and R. A. Gottlieb, "Myocardial stress and autophagy: mechanisms and potential therapies," *Nature Reviews Cardiology*, vol. 14, no. 7, pp. 412–425, 2017.

[62] T. Shintani and D. J. Klionsky, "Autophagy in health and disease: a double-edged sword," *Science*, vol. 306, no. 5698, pp. 990–995, 2004.

[63] A. Thorburn, "Autophagy and its effects: making sense of double-edged swords," *PLoS Biology*, vol. 12, no. 10, article e1001967, 2014.

[64] J. Lee, S. Giordano, and J. Zhang, "Autophagy, mitochondria and oxidative stress: cross-talk and redox signalling," *The Biochemical Journal*, vol. 441, no. 2, pp. 523–540, 2012.

[65] R. Scherz-Shouval and Z. Elazar, "Regulation of autophagy by ROS: physiology and pathology," *Trends in Biochemical Sciences*, vol. 36, no. 1, pp. 30–38, 2011.

Hindawi
Oxidative Medicine and Cellular Longevity
Volume 2017, Article ID 6169128, 11 pages
https://doi.org/10.1155/2017/6169128

Research Article

Baicalin Ameliorates Experimental Liver Cholestasis in Mice by Modulation of Oxidative Stress, Inflammation, and NRF2 Transcription Factor

Kezhen Shen,[1,2] Xiaowen Feng,[1,2] Hao Pan,[3] Feng Zhang,[1,2] Haiyang Xie,[1,2] and Shusen Zheng[1,2,4]

[1]*Key Laboratory of Combined Multi-Organ Transplantation, Ministry of Public Health, the First Affiliated Hospital, College of Medicine, Zhejiang University, Hangzhou, Zhejiang 310003, China*
[2]*Collaborative Innovation Center for Diagnosis and Treatment of Infectious Diseases, the First Affiliated Hospital, College of Medicine, Zhejiang University, Hangzhou, Zhejiang 310003, China*
[3]*Department of Urology, the First Affiliated Hospital, College of Medicine, Zhejiang University, Hangzhou, Zhejiang 310003, China*
[4]*Division of Hepatobiliary and Pancreatic Surgery, the First Affiliated Hospital, Zhejiang University School of Medicine, Hangzhou, Zhejiang 310003, China*

Correspondence should be addressed to Shusen Zheng; shusenzheng@zju.edu.cn

Received 25 March 2017; Revised 18 May 2017; Accepted 28 May 2017; Published 5 July 2017

Academic Editor: Aditya Sen

Experimental cholestatic liver fibrosis was performed by bile duct ligation (BDL) in mice, and significant liver injury was observed in 15 days. Administration of baicalin in mice significantly ameliorates liver fibrosis. Experimental cholestatic liver fibrosis was associated with induced gene expression of fibrotic markers such as collagen I, fibronectin, alpha smooth muscle actin (SMA), and connective tissue growth factor (CTGF); increased inflammatory cytokines (TNFα, MIP1α, IL1β, and MIP2); increased oxidative stress and reactive oxygen species- (ROS-) inducing enzymes (NOX2 and iNOS); dysfunctional mitochondrial electron chain complexes; and apoptotic/necrotic cell death markers (DNA fragmentation, caspase 3 activity, and PARP activity). Baicalin administration on alternate day reduced fibrosis along with profibrotic gene expression, proinflammatory cytokines, oxidative stress, and cell death whereas improving the function of mitochondrial electron transport chain. We observed baicalin enhanced NRF2 activation by nuclear translocation and induced its target genes HO-1 and GCLM, thus enhancing antioxidant defense. Interplay of oxidative stress/inflammation and NRF2 were key players for baicalin-mediated protection. Stellate cell activation is crucial for initiation of fibrosis. Baicalin alleviated stellate cell activation and modulated TIMP1, SMA, collagen 1, and fibronectin in vitro. This study indicates that baicalin might be beneficial for reducing inflammation and fibrosis in liver injury models.

1. Introduction

Chronic liver disease prevalence is increasing globally, and liver fibrosis associated with such chronic liver disease is an important cause of morbidity and mortality in the world [1]. Due to repetitive injury and inflammation in chronic liver disease, significant extracellular matrix is deposited and causes severe liver damage and organ failure. This liver fibrosis can also lead to cirrhosis and hepatocellular carcinoma [1]. Chronic cholestatic liver disease is also observed after liver transplantation [2]. Unfortunately limited antifibrotic therapies are available to treat patients with liver fibrosis [3, 4]. Many plant-derived flavonoids including baicalin show antifibrotic properties in the liver of animal models, but the mechanistic studies are limited.

The proposed mechanism of liver fibrosis includes oxidative tissue injury, mitochondrial dysregulation, and inflammation, which lead to apoptotic and necrotic cell death [5, 6]. Liver fibrogenic cells (myofibroblasts), mainly derived from hepatic stellate cells (HSC), play a central role during

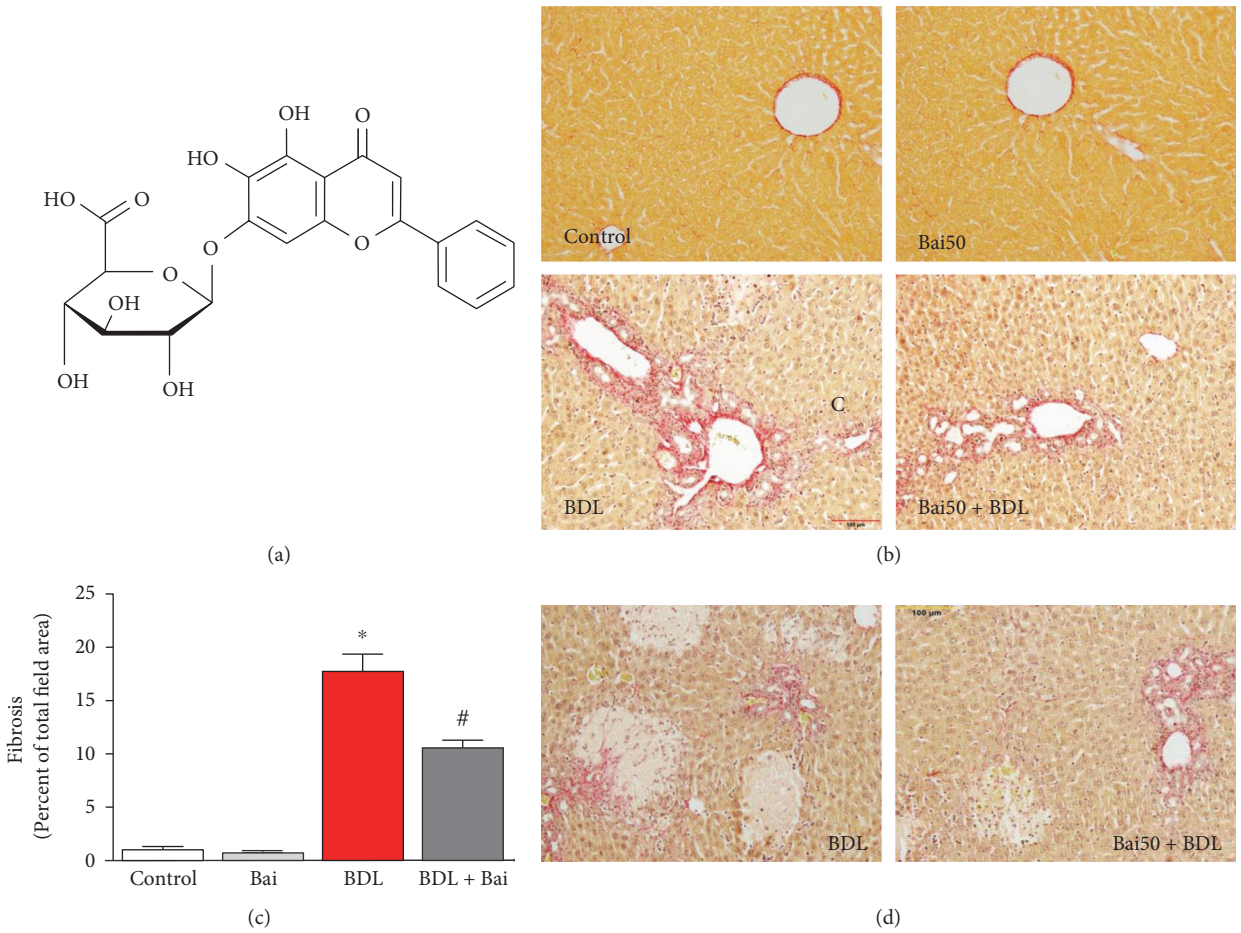

Figure 1: Baicalin significantly attenuated BDL-induced liver fibrosis in mice. (a) Chemical structure of baicalin. (b) BDL-induced liver fibrosis as measured by picrosirius red staining. The images were quantified in a blinded manner by ImageJ software (c). BDL resulted in severe liver fibrosis which was attenuated by baicalin treatment. Results are mean ± S.E.M. $n = 6$ for each group. $^{*}p < 0.05$ versus control and $^{\#}p < 0.05$ versus BDL. (d) Representative images for highlighting necrosis area in BDL and BDL samples pretreated with baicalin.

liver fibrosis [7]. At early stage of tissue injury, all surrounding cells to HSC contribute to its activation. Inflammation-mediated hepatocyte cell death and its engulfment by HSC result in a profibrogenic response and also activate Kupffer cells [8, 9].

Flavonoids are natural compounds and are of considerable interest in the field of drug discovery as well as food supplement industry [10]. Baicalin is one such flavonoid and derived from the roots of *Scutellaria baicalensis* Georgi, and these plants are mainly cultivated in China, Siberia, Russia, and Mongolia [11]. The chemical nomenclature (IUPAC) is 5,6-dihydroxy-4-oxo-2-phenyl-4H-chromen-7-yl β-D-glucopyranosiduronic acid (Figure 1(a)). Protective effects of baicalin in many liver disease animal models have been reported. In a rat ischemia/reperfusion injury model, baicalin protects the liver by antioxidant and anti-inflammatory properties [12]. In concanavalin A-induced mouse liver injury, baicalin protects by modulating cytokine production [13]. Baicalin attenuates alcoholic liver injury involving sonic hedgehog pathway in addition to its antioxidant and anti-inflammatory properties [14]. In a high-fat diet-induced obesity model of mice, baicalin attenuates liver dysfunction by inhibiting CaMKK/AMPK/ACC pathway and protein kinase B/glycogen synthase kinase 3 beta pathway [15, 16]. Recently, baicalin is shown to protect the carbon tetrachloride-induced liver injury model of the rat by activating PPARγ and inhibiting TGFβ1 [17]. Here, we demonstrated the protective effect of baicalin in a cholestatic mice model was mediated via NRF2 transcription factor and its downstream target in addition to modulation of oxidative stress-generating enzymes and inflammation.

2. Materials and Methods

2.1. Mice Surgeries and Baicalin Treatment. Animal Ethics Review Committees of Zhejiang University approved the animal study protocol. Male inbred C57BL/6 (H2b) mice at 6–8 weeks old were obtained from the Animal Research Institution of Zhejiang Province (Hangzhou). BDL surgeries were performed under anesthesia as described earlier [5]. To determine the effect of baicalin on liver fibrosis, mice received one dose of preoperative (2 hours) IP injection of baicalin and alternate day postoperative IP injection of

baicalin (50 mg/kg/day) for additional 14 days. For all animal experiments, we used 12 mice/group.

2.2. Liver Fibrosis Marker. Quantitative determination of liver fibrosis was performed with Picrosirius Red Stain kit (Abcam Company Ltd., China) as described earlier [5]. The quantification of collagen staining (red) was analyzed from images using ImageJ software (NIH, USA).

2.3. mRNA Quantification. RNA isolation and reverse transcription were carried out according to the previously published method [5]. Fold change was calculated as described earlier [18]. The gene-specific primers were purchased from Qiagen (USA).

2.4. Mitochondrial Electron Transport Chain Complexes. Activities of mitochondrial electron transport chain complex I, complex II, and complex IV were performed (Mitosciences, USA), and activities were expressed as fold change as described earlier [5]. Activities were determined from total tissue lysates as recommended by the manufacturer.

2.5. Liver Oxidative Stress Markers. Liver 3-NT levels were determined with ELISA kit from Hycult Biotechnology, Cell Sciences, Canton, USA, as described earlier [5].

HNE adducts were determined using the OxiSelect™ HNE Adduct ELISA Kit according to manufacturer's instruction (Cell Biolabs, Genetimes Technology Inc., Shanghai, China) as described earlier [19].

2.6. Nuclear and Cytoplasmic Fractionation. Nuclear and cytoplasmic fractions were separated from the same set of samples by commercial kit (NE-PER Nuclear and Cytoplasmic Extraction Reagents, Thermo Fisher Scientific, USA).

2.7. Mitochondria Isolation. Mitochondria were isolated using commercial tissue mitochondria isolation kit (Pierce, USA) as described earlier [5].

2.8. Immunoblot Analyses. The protein contents were determined according to the Bradford method. Aliquots of 40 micrograms of protein were analyzed by SDS-PAGE. Western blots were carried out using antibodies for TNFα, GAPDH, NRF2, and lamin A (Abcam Company Ltd., China), Secondary antibodies were purchased from Fazendo Media (Beijing, China).

2.9. Liver PARP Activity. Liver PARP activities were determined using the commercial assay kit (Trevigen Inc.) as described earlier [5]. The quantitative values were expressed as fold change compared to those of the sham control.

2.10. Liver Apoptotic Markers. Caspase 3 activities were measured by using colorimetric caspase 3 activity assay kit (Beyotime Biotech, China) according to the manufacturer's instruction and expressed as fold change. DNA fragment quantifications were performed with the DNA fragmentation kit (Takara, China) according to the manufacturer's protocol.

2.11. Stellate Cell Isolation and Culture. Primary stellate cells from mice were isolated based on our earlier published method [5]. Primary stellate cells were grown for 8 days. Baicalin was added at 20 μM every day after replacing with fresh media. RNA was extracted either from fresh culture (day 0) or after 8 days (day 8), and real-time PCR was performed after reverse transcription.

2.12. Statistical Analysis. All graphical data were shown as the means ± SEMs. Multiple comparisons were performed using one-way ANOVA using Graph Pad Prism software (USA). A p value less than 0.05 was considered statistically significant.

3. Results and Discussions

3.1. Baicalin Attenuates BDL-Induced Liver Fibrosis in Mice. BDL for 15 days induced significant fibrosis based on picosirius red staining, which stains collagen proteins in parenchymal cells (Figure 1(b)). Treatment with baicalin at 200 mg/kg dose on alternate day reduced fibrosis. Image quant analysis of the images demonstrated that 17.9-fold increased in fibrotic area was observed due to BDL and baicalin attenuated up to 40.3% (Figure 1(c)). In addition to fibrosis, significant increase of hepatocyte necrosis was observed and baicalin treatment attenuated those necrosis incidents (Figure 1(d)). To understand the molecular basis of fibrosis, we determined mRNA level of genes associated with fibrosis by real-time PCR. Collagen I, fibronectin, SMA, and CTGF were induced to 7.3-, 6.8-, 7.5-, and 8.3-fold, respectively, in BDL model (Figure 2). Alternate day of baicalin treatment attenuated BDL-induced mRNA of collagen I, fibronectin, SMA, and CTGF to 58%, 55%, 42%, and 65% of BDL level, respectively.

We demonstrated that baicalin protected against liver fibrosis in a well-established mice of BDL. Baicalin is the glucuronide of baicalein, which is obtained through the binding of glucuronic acid to baicalein. Baicalin has both antioxidant and anti-inflammatory properties [20, 21]. The metabolism of baicalin was studied in rodent model and no toxicity was observed [22, 23]. Liver fibrosis induced by BDL has the deposition of connective tissue elements and formation of ductular followed by necrosis [24]. Role of hepatocytes are crucial in development of liver fibrosis. Cell death of hepatocytes leads to a series of proinflammatory response [25]. Hepatocyte has complex role in liver injuries and multiple factors regulate the process including retinoic acid [26]. It is also known that biliary epithelial cells and hepatocytes can undergo epithelial–mesenchymal transition during liver fibrosis [27]. Expression of profibrotic markers such as collagen I, fibronectin, SMA and CTGF in response to BDL has been reported earlier [5, 18]. We demonstrated that all profibrotic markers were attenuated by alternate day treatment of baicalin. Consistent with our study, the protective effect of baicalin in other mouse models of liver fibrosis has been reported [28].

3.2. Baicalin Ameliorates BDL-Induced Liver Inflammation in Mice. BDL induced fibrosis, which is initiated by cell death-associated inflammatory stimuli. We determined

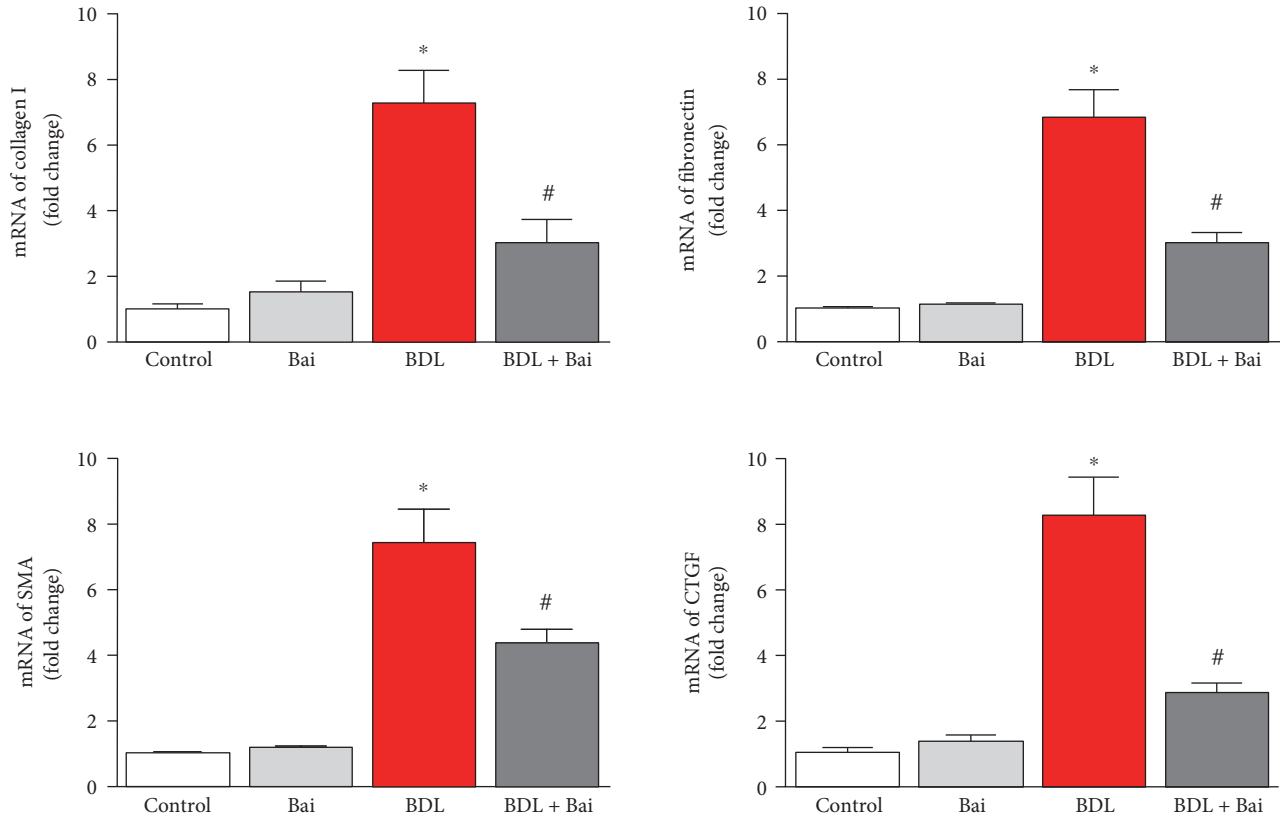

Figure 2: Baicalin markedly attenuated BDL-induced fibrotic gene expression. BDL induced liver profibrotic genes at mRNA level. Real-time PCR analyses were performed for collagen I, fibronectin, alpha smooth muscle actin (SMA), and CTGF genes. BDL-induced increases in all four gene expressions and the inductions were significantly reduced by baicalin treatment. Results are mean ± S.E.M. $n = 6$ for each group. $^{*}p < 0.05$ versus control and $^{\#}p < 0.05$ versus BDL.

proinflammatory cytokines TNFα, MIP1α, IL1β, and MIP2 by real-time PCR. The result demonstrated induced TNFα, MIP1α, IL1β, and MIP2 mRNA levels to 6.29-fold, 4.51-fold, 5.32-fold, and 4.83-fold, respectively (Figure 3(a)). Administration of baicalin on alternate day for 15 days reduced BDL-induced proinflammatory cytokines TNFα, MIP1α, IL1β, and MIP2 to 63%, 47%, 47%, and 49% respectively. To verify the mRNA signal to protein level, we examined one marker TNFα by immunoblot analyses and BDL increased TNFα protein level and was attenuated by baicalin, which is consistent with the mRNA expression pattern.

Our study demonstrated that baicalin prevents fibrosis by attenuating BDL-induced proinflammatory cytokines and inflammation. Modulation of inflammatory signal by baicalin in the liver for hepato-protection is well known in other liver injuries induced by concanavalin A, D-galactosamine, and alcoholic fatty liver [13, 14, 29]. The resident macrophage, known as the Kupffer cell, plays critical role in this process [30].

3.3. Baicalin Ameliorates BDL-Induced Oxidative Stress Markers in Mice. Inflammatory response in BDL induces oxidative stress and reduces cellular antioxidant capability. Here, we determined oxidative/nitrative markers and their causes. HNE protein adducts increased significantly in the liver due to BDL (3.9-fold) and baicalin treatment reduced significantly to 47% (Figure 4(a)). Hepatic protein nitration is also increased to 3.5-fold and baicalin attenuated 45.7% from BDL (Figure 4(a)). The sources of oxidative stress were investigated by real-time PCR of NOX2 and iNOS. Both of them were induced in BDL and attenuated by baicalin. Treatment with baicalin in control group does not have any effect of oxidative stress and ROS-generating sources.

BDL induced significant oxidative stress through bile salt and other free radicals which causes damage to other organs such the kidney in addition to liver [31]. In liver injury, hepatocytes are primary parenchymal cells targeted by oxidative stress [32]. Consistent with our study in BDL, the antioxidant properties of baicalin are reported in many other liver injury models [28, 33].

3.4. Baicalin Improves BDL-Impaired Mitochondrial Membrane Complex Activities in Mice. Mitochondrial electron transport chain is one of the major sources for free radical generation and oxidative injury. We examined electron transport chain complex activities from isolated mitochondria of the liver. BDL surgeries in mice reduced complex I, complex II, and complex IV activities to 45%, 35%, and 37%, respectively (Figure 5). Administration of baicalin every day during two weeks BDL improved complex I activity to 40%, complex II to 31%, and complex IV to 33%. Thus, baicalin administration significantly ameliorates BDL-

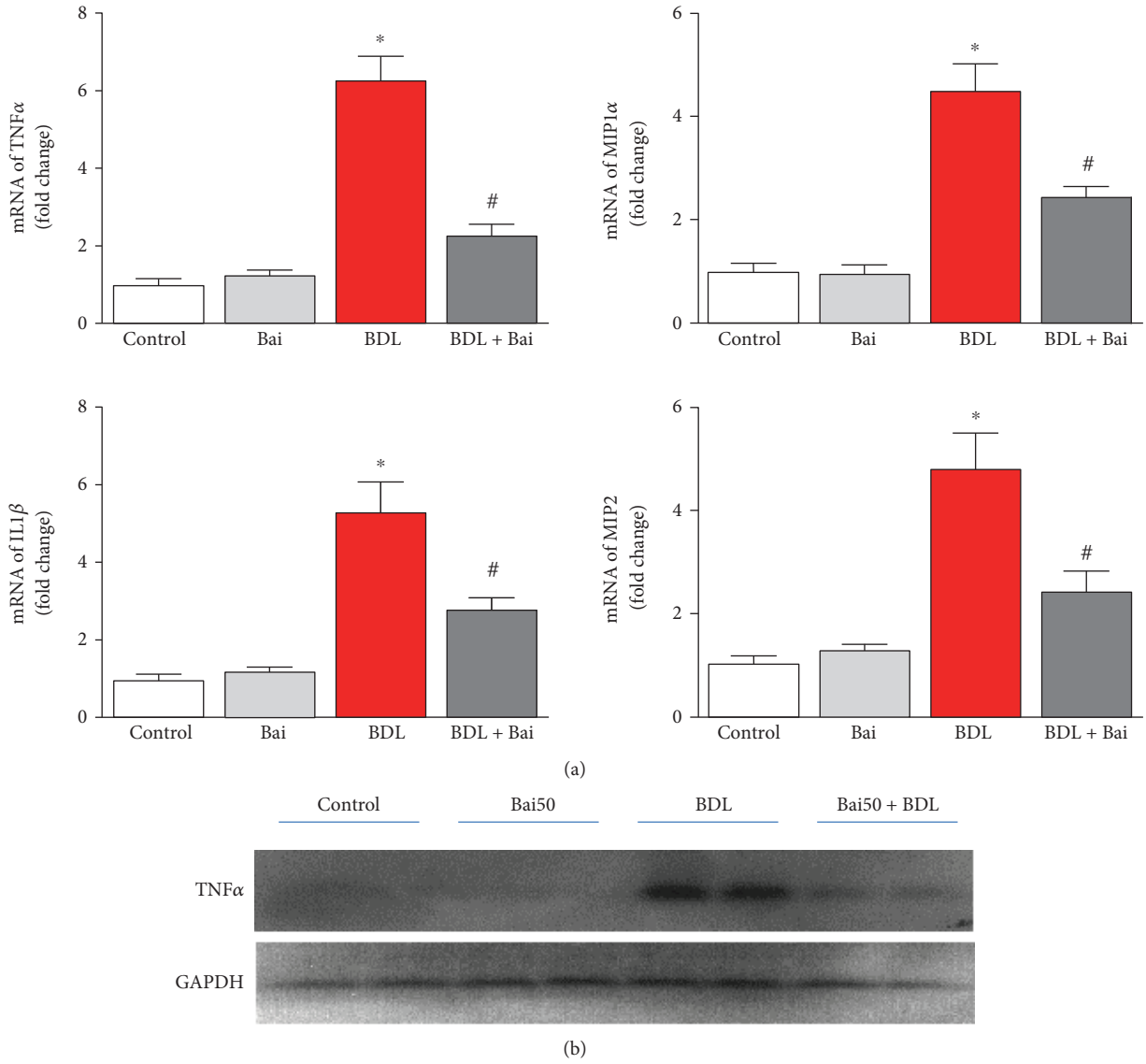

Figure 3: Effect of baicalin on BDL-induced proinflammatory cytokines in mice liver. (a) BDL-induced proinflammatory cytokines as measured by real-time PCR analyses for TNFα, MIP1α, IL1β, and MIP2 genes. BDL-induced proinflammatory cytokine mRNA was attenuated by alternate day baicalin treatment. Results are mean ± S.E.M. $n = 6$ for each group. $^{*}p < 0.05$ versus control and $^{\#}p < 0.05$ versus BDL. (b) Protein level of TNFα was verified by immunoblot analyses, and GAPDH was used as the loading control.

induced mitochondrial dysfunction and associated oxidative injury in the liver.

Mitochondria play a bigger role in BDL-induced liver injury [34, 35]. The dysfunctional electron transport chain in mitochondria is one of the major sources of ROS [36]. We observed dysfunctional electron transport chain in BDL mouse liver, and baicalin improved those functions of electron chain complexes. Baicalin ameliorates mitochondrial damage in streptozotocin-induced diabetic rats, and its beneficial effects on mitochondria are reported [37–39]. Baicalin has a beneficial effect on mitochondrial function [38].

3.5. Baicalin Enhances BDL-Induced Nuclear Translocation of Nrf2 and Increases HO-1 and GCLM Expression. NRF2 is key transcriptional regulator for antioxidant defense in many liver diseases [40]. Baicalin significantly enhanced nuclear localization of NRF2 (Figure 6(a), top panel) in BDL mice. An increase in BDL-induced NRF2 nuclear localization may be due to induction of endogenous antioxidant defense in response to oxidative stress but not sufficient to protect against injury. In addition, we also observed little increase of NRF2 in cytoplasmic fractions of BDL mice pretreated with baicalin (Figure 6(a), bottom panel). These results indicated baicalin mediated upregulation of NRF2 in fibrotic liver. Nuclear translocation of NRF2 is also associated with transcriptional activation as evident by the fact that the target genes (HO-1 and GCLM) also induced in the same pattern as nuclear translocation (Figure 6(b)).

The hepatoprotective effect of many naturally occurring compounds is mediated by NRF2 [41]. NRF2 is also is a

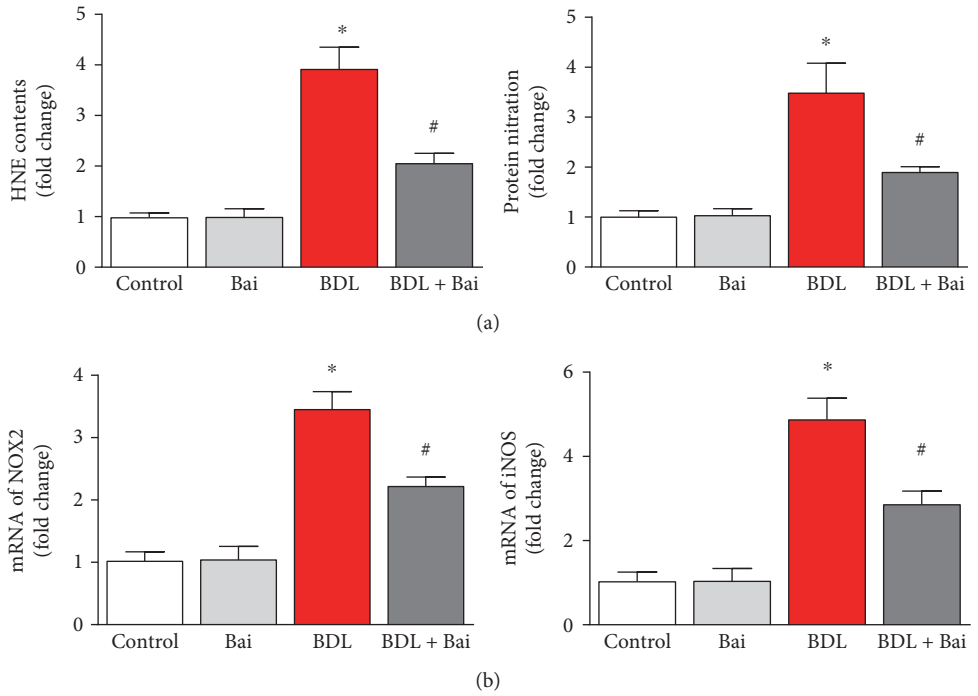

Figure 4: Baicalin significantly reduced BDL-induced oxidative/nitrative stress in mouse liver. BDL caused significant increase in oxidative and nitrative stress as measured by HNE protein adducts and protein nitration using commercial ELISA kits. BDL induced nitrative stress and oxidative stresses (a) and was attenuated by baicalin treatment. Results are mean ± S.E.M. $n = 6$ for each group. $^{*}p < 0.05$ versus control and $^{\#}p < 0.05$ versus BDL. Real-time PCR analyses were performed for NOX2 and iNOS genes (b). BDL induced both gene expression, and the inductions were significantly reduced by baicalin treatment. Results are mean ± S.E.M. $n = 6$ for each group. $^{*}p < 0.05$ versus control and $^{\#}p < 0.05$ versus BDL.

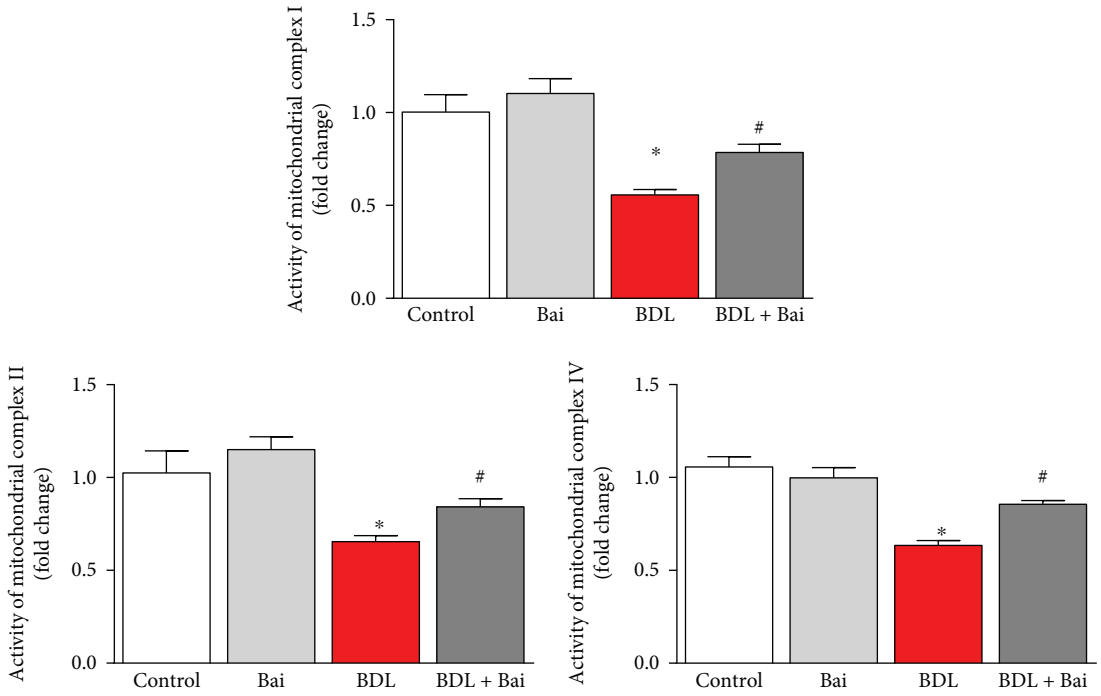

Figure 5: Baicalin improved BDL-induced decrease of mitochondrial membrane complex activities in mouse liver. BDL caused decrease in mitochondrial membrane complexes as measured from enzyme activities of electron transport chain complex I, complex II, and complex IV. BDL mediated decrease of mitochondrial complex activities were improved level by alternate day of baicalin treatment. Results are mean ± S.E.M. $n = 6$ for each group. $^{*}p < 0.05$ versus control and $^{\#}p < 0.05$ versus BDL.

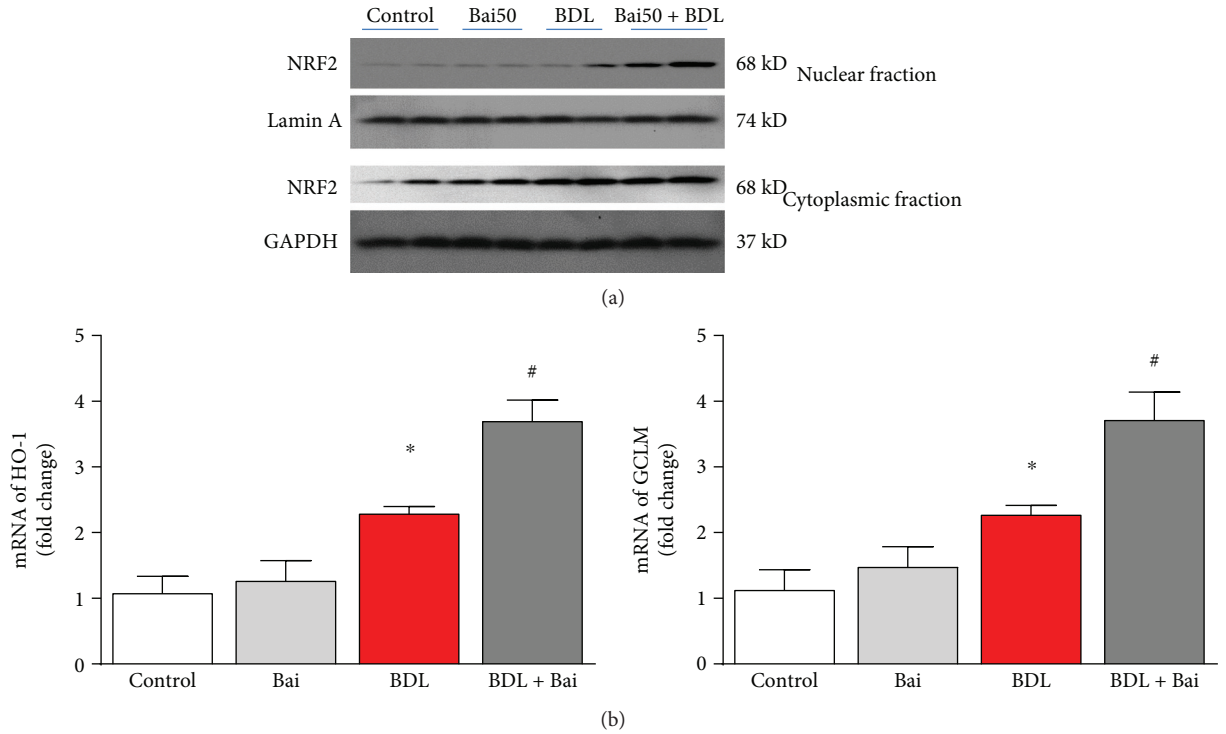

Figure 6: Baicalin enhanced nuclear translocation of NRF2 in BDL mice and increased transcription of its target genes HO-1 and GCLM. (a) Western blot images showing BDL-induced nuclear localization of NRF2 were further enhanced significantly by baicalin treatment. Western blot analyses of cytoplasmic fraction showing increased expression of NRF2 in samples with BDL pretreated with baicalin. (b) Real-time PCR analyses were performed for HO-1 and GCLM genes. BDL induced both gene expressions, and the inductions were significantly enhanced by baicalin treatment. Results are mean ± S.E.M. $n = 6$ for each group. $^{*}p < 0.05$ versus control and $^{\#}p < 0.05$ versus BDL.

key regulator of oxidative stress in numerous cell types [42, 43]. In BDL, Nrf2-deficient mice show reduced elimination of bile acids leading to liver injury [44]. Consistent with the key role of NRF2 in BDL, we also demonstrated that baicalin modulates NFR2 and its increased nuclear translocation led to protective effect. The induction of antioxidant defense such as HO-1 by baicalin-induced NRF2 translocation may be responsible for hepatoprotection. NRF2 translocation by baicalin is not mediated by any prooxidant properties, but the modulation is at the molecular level. This hypothesis is further supported by the fact that baicalin did not induce NRF2 in the control group.

3.6. Baicalin Ameliorates BDL-Induced Cell Death Pathway in Mouse Liver. BDL induces significant apoptotic and necrotic cell death in liver [5]. We examined three cell death markers DNA fragmentation, PARP activity, and caspase 3 activity. BDL induced 3.6-fold and 3.7-fold increase in apoptotic cell death markers DNA fragmentation and caspase 3 activity. Baicalin administration reduced BDL-induced DNA fragmentation and caspase 3 activity up to 40% and 42%, respectively (Figure 7(a)). We also investigated another cell death marker PARP activity which represents necrotic pathway and apoptotic pathways in liver injury [6]. BDL induced 3-fold increase in PARP activity, and baicalin administration significantly reduced BDL-induced PARP activity (44.5%) (Figure 7(b)).

Oxidative stress is major source for cell death in BDL [45, 46]. Intervention of PARP is shown to ameliorate liver fibrosis in BDL [4]. Baicalin prevented BDL-induced apoptotic and necrotic cell death. The effect may be due to reducing oxidative stress, promoting antioxidant defense, and attenuating inflammation.

3.7. Mechanistic Role of Stellate Cells in Baicalin-Mediated Antifibrotic Action. Hepatic stellate cells contribute to liver fibrosis through various steps including extracellular matrix homeostasis [47]. As we observed significant drop in liver fibrosis by baicalin, an in vitro study with stellate cells was essential. We used a natural phenomenon where spontaneous activation occurs at day 8 when stellate cells grow under in vitro condition [5]. To elucidate the inhibitory role of baicalin in the activation of stellate cell process and its effect on profibrotic marker production, we examined using real-time PCR analyses. The data demonstrated that baicalin treatment at 20 μM significantly reduced profibrotic genes such as SMA, collagen 1, and fibronectin (Figure 8).

After liver injury, stellate cell activation plays central role in initiation and propagation of liver fibrosis [48]. Kupffer cell activation facilitates stellate cell activation by secretion of TGFβ and ROS in the extracellular environment [30]. We observed modulation of stellate cell activation by baicalin in vitro. This is significant because of the fact that baicalin

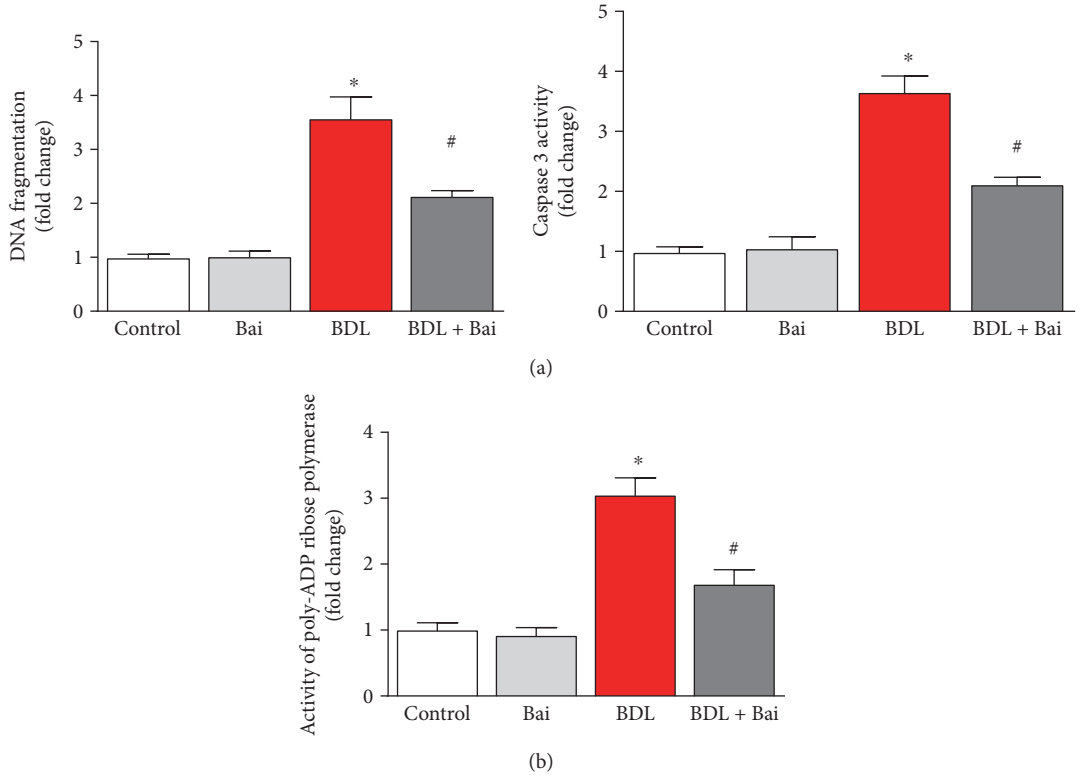

Figure 7: Baicalin markedly attenuated BDL-induced apoptotic and necrotic cell death markers DNA fragmentation, caspase 3 activity, and PARP activity in mouse liver. BDL induced significant increases in liver DNA fragmentation and caspase 3 activity, both markers of apoptotic cell death (a). BDL induced significant increase in PARP activity, a marker of necrotic and apoptotic cell death (b). BDL-induced increases in all three cell death markers were attenuated by baicalin treatment. Results are mean ± S.E.M. $n = 6$/group. $^{*}p < 0.05$ versus control and $^{\#}p < 0.05$ versus BDL.

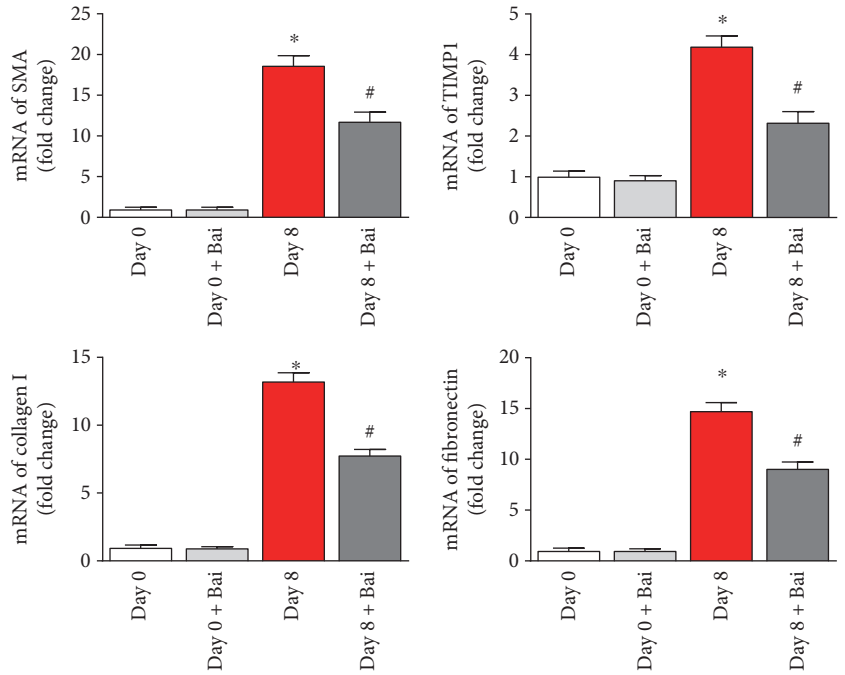

Figure 8: Baicalin attenuated profibrotic gene expression in isolated mouse stellate cells. Stellates were cultured for 8 days to stimulate activation in culture and compared with fresh isolated stellate cells (day 0). Real-time PCR analyses of profibrotic mRNA of smooth muscle actin alpha (SMA), TIMP1, collagen 1, and fibronectin were induced during fibrosis stimulation. Baicalin reversed mRNA expressions in all four genes. Results are mean ± S.E.M. $n = 4$ for each group. $^{*}p < 0.05$ versus day 0 and $^{\#}p < 0.05$ versus day 8.

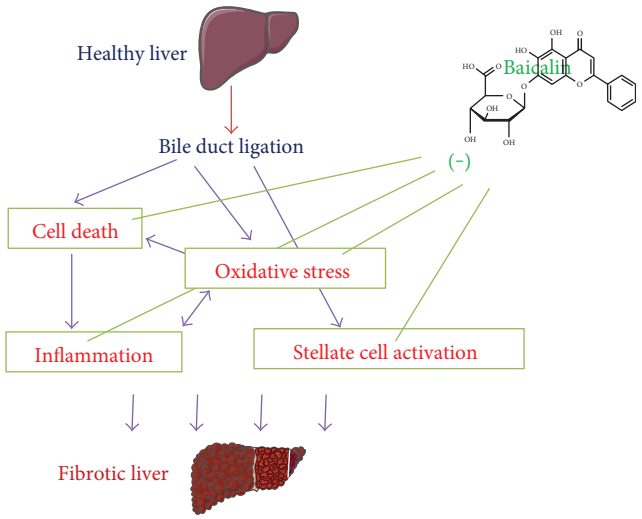

Figure 9: Schematic diagram of baicalin-mediated protection in experimental cholestatic liver injury. Bile duct ligation of healthy liver leads to hepatocyte cell death and oxidative stress. Both of these factors lead to proinflammatory responses, and significant inflammation occurs. Inflammation also leads to increased oxidative stress and thus interplay each other. Baicalin protects against cell death, oxidative stress, and inflammation. In addition to that, stellate cell activation occurs which leads to liver fibrosis. Under in vitro condition, baicalin attenuates stellate cell activation. All the above pathophysiological conditions lead to fibrotic liver.

can modulate liver fibrosis not only by reducing oxidative stress/inflammation/cell death but also by regulating stellate cell activation.

4. Conclusion

The complexities of liver fibrosis and lack of approved treatment to patients lead this subject to forefront to researchers and clinicians. In our study, baicalin partially protects against experimental liver cholestasis via multiple mechanisms (Figure 9). The complexities of cholestatic liver fibrosis are due to the involvement of different cells in the liver such as hepatocytes, stellate cells, and immune cells, and their interactions are real crucial. Reversal of such process is challenging. Thus, the limitation of baicalin-mediated protection is due to the additional challenging factors including bioavailability, selective transportation to hepatocytes or stellate cells, or targeting other cell types. Despite the above limitations, baicalin protects against experimental cholestatic liver fibrosis by reducing inflammation, oxidative stress, and cell death and enhancing antioxidant defense in addition to modulating stellate cell activation.

Conflicts of Interest

The authors declare that there is no conflict of interest regarding the publication of this paper.

Authors' Contributions

Kezhen Shen and Xiaowen Feng contributed equally to this work.

Acknowledgments

This work was supported by grants from the Major Program of National Natural Science Foundation of China (no. 91542205), Science and Technology Department of Zhejiang Province (no. 2015C33214), and Zhejiang Medical and Health Science and Technology Plan Project (nos. 2014KYA070 and 200815385).

References

[1] Y. S. Lim and W. R. Kim, "The global impact of hepatic fibrosis and end-stage liver disease," *Clinics in Liver Disease*, vol. 12, pp. 733–746, 2008, vii.

[2] T. E. Starzl, A. J. Demetris, and D. Van Thiel, "Liver transplantation (1)," *The New England Journal of Medicine*, vol. 321, pp. 1014–1022, 1989.

[3] M. A. Doyle, J. Singer, T. Lee, M. Muir, and C. Cooper, "Improving treatment and liver fibrosis outcomes with metformin in HCV-HIV co-infected and HCV mono-infected patients with insulin resistance: study protocol for a randomized controlled trial," *Trials*, vol. 17, p. 331, 2016.

[4] Y. Koyama, J. Xu, X. Liu, and D. A. Brenner, "New developments on the treatment of liver fibrosis," *Digestive Diseases*, vol. 34, pp. 589–596, 2016.

[5] K. Shen, X. Feng, R. Su, H. Xie, L. Zhou, and S. Zheng, "Epigallocatechin 3-gallate ameliorates bile duct ligation induced liver injury in mice by modulation of mitochondrial oxidative stress and inflammation," *PloS One*, vol. 10, article e0126278, 2015.

[6] P. Mukhopadhyay, M. Rajesh, Z. Cao et al., "Poly (ADP-ribose) polymerase-1 is a key mediator of liver inflammation and fibrosis," *Hepatology*, vol. 59, pp. 1998–2009, 2014.

[7] T. Kisseleva and D. A. Brenner, "Hepatic stellate cells and the reversal of fibrosis," *Journal of Gastroenterology and Hepatology*, vol. 21, Supplement 3, pp. S84–S87, 2006.

[8] A. Canbay, P. Taimr, N. Torok, H. Higuchi, S. Friedman, and G. J. Gores, "Apoptotic body engulfment by a human stellate cell line is profibrogenic," *Laboratory Investigation*, vol. 83, pp. 655–663, 2003.

[9] A. Canbay, A. E. Feldstein, H. Higuchi et al., "Kupffer cell engulfment of apoptotic bodies stimulates death ligand and cytokine expression," *Hepatology*, vol. 38, pp. 1188–1198, 2003.

[10] A. L. Harvey, R. Edrada-Ebel, and R. J. Quinn, "The re-emergence of natural products for drug discovery in the genomics era," *Nature Reviews Drug Discovery*, vol. 14, pp. 111–129, 2015.

[11] D. Wozniak, E. Lamer-Zarawska, and A. Matkowski, "Antimutagenic and antiradical properties of flavones from the roots of Scutellaria baicalensis georgi," *Die Nahrung*, vol. 48, pp. 9–12, 2004.

[12] S. J. Kim, Y. J. Moon, and S. M. Lee, "Protective effects of baicalin against ischemia/reperfusion injury in rat liver," *Journal of Natural Products*, vol. 73, pp. 2003–2008, 2010.

[13] L. L. Liu, L. K. Gong, H. Wang et al., "Baicalin protects mouse from concanavalin A-induced liver injury through inhibition of cytokine production and hepatocyte apoptosis," *Liver International*, vol. 27, pp. 582–591, 2007.

[14] H. Wang, Y. Zhang, R. Bai, M. Wang, and S. Du, "Baicalin attenuates alcoholic liver injury through modulation of hepatic oxidative stress, inflammation and sonic hedgehog pathway in rats," *Cellular Physiology and Biochemistry*, vol. 39, pp. 1129–1140, 2016.

[15] Y. L. Xi, H. X. Li, C. Chen et al., "Baicalin attenuates high fat diet-induced insulin resistance and ectopic fat storage in skeletal muscle, through modulating the protein kinase B/glycogen synthase kinase 3 beta pathway," *Chinese Journal of Natural Medicines*, vol. 14, pp. 48–55, 2016.

[16] Y. Xi, M. Wu, H. Li et al., "Baicalin attenuates high fat diet-induced obesity and liver dysfunction: dose-response and potential role of CaMKKbeta/AMPK/ACC pathway," *Cellular Physiology and Biochemistry*, vol. 35, pp. 2349–2359, 2015.

[17] H. Qiao, H. Han, D. Hong, Z. Ren, Y. Chen, and C. Zhou, "Protective effects of baicalin on carbon tetrachloride induced liver injury by activating PPARgamma and inhibiting TGFbeta1," *Pharmaceutical Biology*, vol. 49, pp. 38–45, 2011.

[18] F. Shi, Q. Sheng, X. Xu, W. Huang, and Y. J. Kang, "Zinc supplementation suppresses the progression of bile duct ligation-induced liver fibrosis in mice," *Experimental Biology and Medicine*, vol. 240, pp. 1197–1204, 2015.

[19] H. Pan, J. Chen, K. Shen et al., "Mitochondrial modulation by epigallocatechin 3-gallate ameliorates cisplatin induced renal injury through decreasing oxidative/nitrative stress, inflammation and NF-kB in mice," *PloS One*, vol. 10, article e0124775, 2015.

[20] D. E. Shieh, L. T. Liu, and C. C. Lin, "Antioxidant and free radical scavenging effects of baicalein, baicalin and wogonin," *Anticancer Research*, vol. 20, pp. 2861–2865, 2000.

[21] B. Q. Li, T. Fu, W. H. Gong et al., "The flavonoid baicalin exhibits anti-inflammatory activity by binding to chemokines," *Immunopharmacology*, vol. 49, pp. 295–306, 2000.

[22] Y. Wang, J. Yang, X. Li, and J. Wang, "The metabolism of baicalin in rat and the biological activities of the metabolites," *Evidence-Based Complementary and Alternative Medicine*, vol. 2012, Article ID 404529, 6 pages, 2012.

[23] M. Y. Lai, S. L. Hsiu, S. Y. Tsai, Y. C. Hou, and P. D. Chao, "Comparison of metabolic pharmacokinetics of baicalin and baicalein in rats," *The Journal of Pharmacy and Pharmacology*, vol. 55, pp. 205–209, 2003.

[24] S. Hinz, H. Franke, G. Machnik, A. Muller, and R. Dargel, "Histological and biochemical changes induced by total bile duct ligation in the rat," *Experimental and Toxicologic Pathology*, vol. 49, pp. 281–288, 1997.

[25] H. Malhi, M. E. Guicciardi, and G. J. Gores, "Hepatocyte death: a clear and present danger," *Physiological Reviews*, vol. 90, pp. 1165–1194, 2010.

[26] B. Mukhopadhyay, J. Liu, D. Osei-Hyiaman et al., "Transcriptional regulation of cannabinoid receptor-1 expression in the liver by retinoic acid acting via retinoic acid receptor-gamma," *The Journal of Biological Chemistry*, vol. 285, pp. 19002–19011, 2010.

[27] M. D. Gorrell, "Liver fibrosis: the hepatocyte revisited," *Hepatology*, vol. 46, pp. 1659–1661, 2007.

[28] S. W. Park, C. H. Lee, Y. S. Kim et al., "Protective effect of baicalin against carbon tetrachloride-induced acute hepatic injury in mice," *Journal of Pharmacological Sciences*, vol. 106, pp. 136–143, 2008.

[29] L. L. Liu, L. K. Gong, H. Wang et al., "Baicalin inhibits macrophage activation by lipopolysaccharide and protects mice from endotoxin shock," *Biochemical Pharmacology*, vol. 75, pp. 914–922, 2008.

[30] G. Kolios, V. Valatas, and E. Kouroumalis, "Role of Kupffer cells in the pathogenesis of liver disease," *World Journal of Gastroenterology*, vol. 12, pp. 7413–7420, 2006.

[31] M. Orellana, R. Rodrigo, L. Thielemann, and V. Guajardo, "Bile duct ligation and oxidative stress in the rat: effects in liver and kidney," *Comparative Biochemistry and Physiology Part C: Pharmacology, Toxicology and Endocrinology*, vol. 126, pp. 105–111, 2000.

[32] J. B. Hoek and J. G. Pastorino, "Ethanol, oxidative stress, and cytokine-induced liver cell injury," *Alcohol*, vol. 27, pp. 63–68, 2002.

[33] C. C. Liao, Y. J. Day, H. C. Lee, J. T. Liou, A. H. Chou, and F. C. Liu, "Baicalin attenuates IL-17-mediated acetaminophen-induced liver injury in a mouse model," *PloS One*, vol. 11, article e0166856, 2016.

[34] M. M. Tiao, T. K. Lin, P. W. Wang, J. B. Chen, and C. W. Liou, "The role of mitochondria in cholestatic liver injury," *Chang Gung Medical Journal*, vol. 32, pp. 346–353, 2009.

[35] N. Alptekin, G. Mehmetcik, M. Uysal, and G. Aykac-toker, "Evidence for oxidative stress in the hepatic mitochondria of bile duct ligated rats," *Pharmacological Research*, vol. 36, pp. 243–247, 1997.

[36] K. M. Holmstrom and T. Finkel, "Cellular mechanisms and physiological consequences of redox-dependent signalling," *Nature Reviews Molecular Cell Biology*, vol. 15, pp. 411–421, 2014.

[37] V. Y. Waisundara, A. Hsu, B. K. Tan, and D. Huang, "Baicalin reduces mitochondrial damage in streptozotocin-induced diabetic Wistar rats," *Diabetes/Metabolism Research and Reviews*, vol. 25, pp. 671–677, 2009.

[38] M. R. de Oliveira, S. F. Nabavi, S. Habtemariam, I. Erdogan Orhan, M. Daglia, and S. M. Nabavi, "The effects of baicalein and baicalin on mitochondrial function and dynamics: a review," *Pharmacological Research*, vol. 100, pp. 296–308, 2015.

[39] W. H. Chang, C. H. Chen, and F. J. Lu, "Different effects of baicalein, baicalin and wogonin on mitochondrial function, glutathione content and cell cycle progression in human hepatoma cell lines," *Planta Medica*, vol. 68, pp. 128–132, 2002.

[40] S. M. Shin, J. H. Yang, and S. H. Ki, "Role of the Nrf2-ARE pathway in liver diseases," *Oxidative Medicine and Cellular Longevity*, vol. 2013, Article ID 763257, 9 pages, 2013.

[41] R. N. Jadeja, K. K. Upadhyay, R. V. Devkar, and S. Khurana, "Naturally occurring Nrf2 activators: potential in treatment of liver injury," *Oxidative Medicine and Cellular Longevity*, vol. 2016, Article ID 3453926, 13 pages, 2016.

[42] H. Zhang, K. J. Davies, and H. J. Forman, "Oxidative stress response and Nrf2 signaling in aging," *Free Radical Biology & Medicine*, vol. 88, pp. 314–336, 2015.

[43] O. Al-Sawaf, T. Clarner, A. Fragoulis et al., "Nrf2 in health and disease: current and future clinical implications," *Clinical Science*, vol. 129, pp. 989–999, 2015.

[44] L. M. Aleksunes, A. L. Slitt, J. M. Maher et al., "Nuclear factor-E2-related factor 2 expression in liver is critical for induction of NAD(P)H:quinone oxidoreductase 1 during cholestasis," *Cell Stress & Chaperones*, vol. 11, pp. 356–363, 2006.

[45] F. J. Padillo, A. Cruz, C. Navarrete et al., "Melatonin prevents oxidative stress and hepatocyte cell death induced by experimental cholestasis," *Free Radical Research*, vol. 38, pp. 697–704, 2004.

[46] C. Ara, H. Kirimlioglu, A. B. Karabulut et al., "Protective effect of resveratrol against oxidative stress in cholestasis," *The Journal of Surgical Research*, vol. 127, pp. 112–117, 2005.

[47] J. E. Puche, Y. Saiman, and S. L. Friedman, "Hepatic stellate cells and liver fibrosis," *Comprehensive Physiology*, vol. 3, pp. 1473–1492, 2013.

[48] M. J. Arthur, D. A. Mann, and J. P. Iredale, "Tissue inhibitors of metalloproteinases, hepatic stellate cells and liver fibrosis," *Journal of Gastroenterology and Hepatology*, vol. 13, pp. S33–S38, 1998.